Technical Report SL-98-4
May 1998

US Army Corps of Engineers
Waterways Experiment Station

Earthquake Engineering Research Program

Roller-Compacted Concrete (RCC) Dams

Report 1
Laboratory Characterization of RCC Cores from Elk Creek Dam, Trail, Oregon

by Mark L. Green, Billy D. Neeley, Paul A. Reed, WES
Clayton T. Amundson, Portland District

Prepared for Headquarters, U.S. Army Corps of Engineers

The contents of this report are not to be used for advertising, publication, or promotional purposes. Citation of trade names does not constitute an official endorsement or approval of the use of such commercial products.

The findings of this report are not to be construed as an official Department of the Army position, unless so designated by other authorized documents.


PRINTED ON RECYCLED PAPER

Earthquake Engineering Research Program

Technical Report SL-98-4
May 1998

Roller-Compacted Concrete (RCC) Dams

Report 1
Laboratory Characterization of RCC Cores from Elk Creek Dam, Trail, Oregon

by Mark L. Green, Billy D. Neeley, Paul Reed

U.S. Army Corps of Engineers
Waterways Experiment Station
3909 Halls Ferry Road
Vicksburg, MS 39180-6199

Clayton T. Amundson

U.S. Army Engineer District, Portland
Geotechnical Engineering Branch
333 SW-First Avenue
Portland, OR 97208-2946

Report 1 of a series

Prepared for U.S. Army Corps of Engineers
Washington, DC 20314-1000

Under Work Unit Number 33018

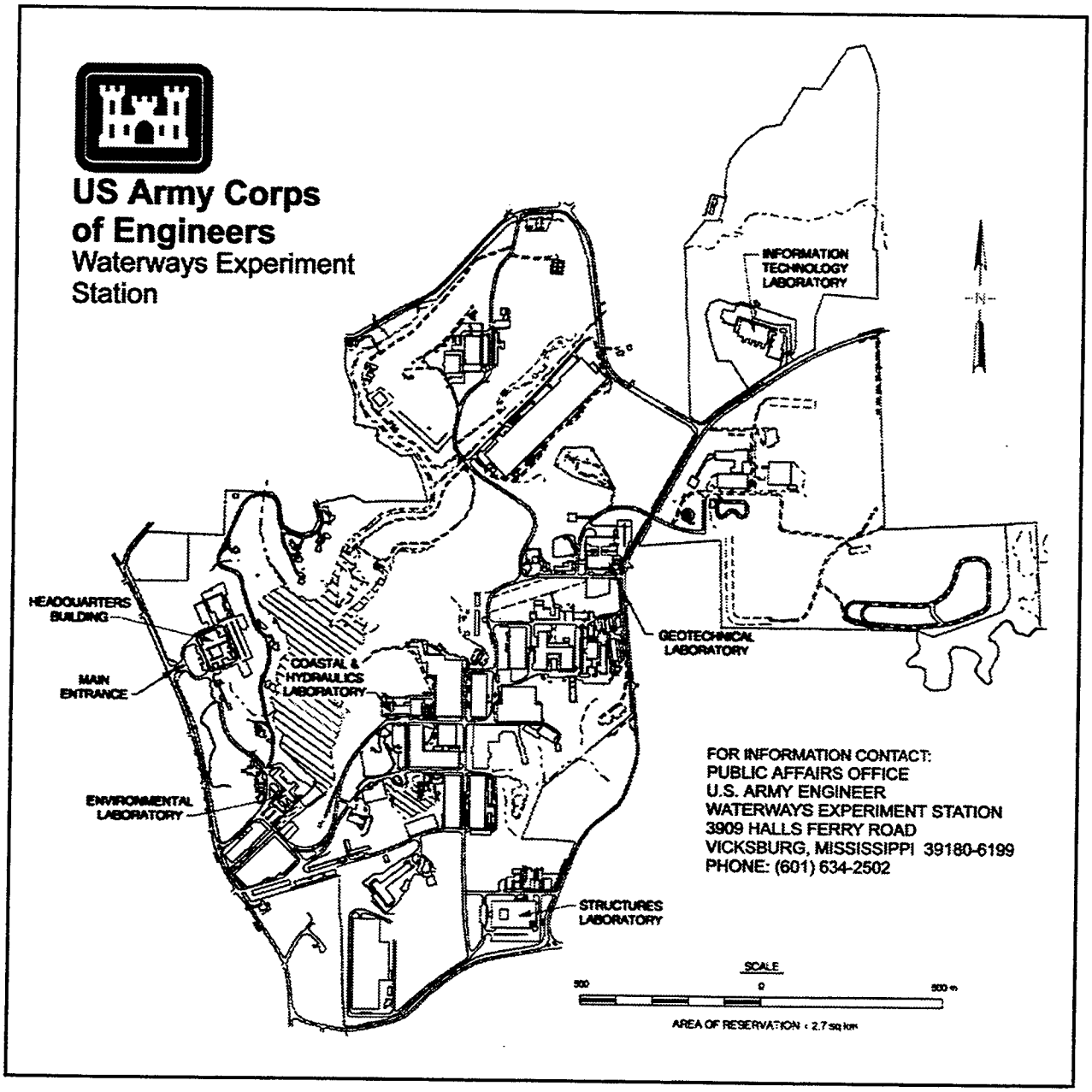

Waterways Experiment Station Cataloging-in-Publication Data

Roller-Compacted Concrete (RCC) Dams / by Mark L. Green ... [et al.] ; prepared for U.S. Army Corps of Engineers.
148 p. : ill. ; 28 cm. — (Technical report ; SL-98-4 rept.1)
Includes bibliographic references.
Report 1 of a series.
1. Elk Creek Dam (Or.) 2. Dams — Oregon. 3. Roller compacted concrete. I. Green, Mark L. II. United States. Army. Corps of Engineers. III. U.S. Army Engineer Waterways Experiment Station. IV. Structures Laboratory (U.S. Army Engineer Waterways Experiment Station) V. Earthquake Engineering Research Program (U.S.) VI. Series: Technical report (U.S. Army Engineer Waterways Experiment Station) ; SL-98-4 rept.1.
TA7 W34 no.SL-98-4 rept.1

Contents

Preface

This laboratory mechanical property investigation of roller-compacted concrete cores from Elk Creek Dam was conducted by the U.S. Army Engineer Waterways Experiment Station (WES) for Headquarters, U.S. Army Corps of Engineers (HQUSACE), under the Earthquake Engineering Research Program, Work Unit Number 33018, "Roller-Compacted Concrete Gravity Dam." Technical monitors for the project at HQUSACE were Messrs. Donald Dressler and Lucian Guthrie, Structures Branch, Engineering Division, Directorate of Civil Works. This study was conducted from February 1996 to September 1997 by members of the staff of the Structures Laboratory (SL), WES, under the direction of Dr. Bryant Mather, Director, and Mr. John Ehrgott, Assistant Director, and under the general supervision of Dr. Reed Mosher, Chief, Structural Mechanics Division, Dr. Robert Hall, Chief, Structural Analysis Group (SS-A), Mr. Andrew E. Jackson, Acting Chief, Geomechanics and Explosion Effects Division (GEED), and Dr. Paul Mlakar, Chief, Concrete and Materials Division (CMD).

The Principal Investigator for this project was Dr. Luis A. de Bẽjar, SS-A, SL. The laboratory characterization effort was coordinated by Mr. Mark L. Green, GEED. The laboratory characterization tests were performed by Mr. Jimmy Hall, CMD, Ms. Linda Mayfield, CMD, and Mr. Paul A. Reed, GEED, under the technical direction of Mr. Green and Mr. Billy D. Neeley, CMD. Instrumentation support was provided by Messrs. A. Leroy Peeples and John K. Rhodes, Instrumentation Services Development Division, Information Technology Laboratory. This report was written by Messrs. Green, Neeley, Reed, and Clayton T. Amundson, Geotechnical Engineering Branch, U.S. Army Engineer District, Portland, CENWP-PE-G.

During this investigation, Mr. Donald R. Chambers, Chief, Structural and Architectural Design Branch, U.S. Army Engineer District, Portland, CENWP-PE-DS, Messrs. James Griffiths and Dennis Hopmann, CENWP-PE-G, and Mr. James Hinds, Materials Laboratory, CENWP-PE-L, provided planning assistance and technical advice.

At the time of publication of this report, Director of WES was Dr. Robert W. Whalin. Commander was COL Robin R. Cababa, EN.

Conversion Factors, Non-SI to SI Units of Measurement

Non-SI units of measurement used in this report can be converted to SI units as follows:

Multiply	By	To Obtain
degrees (angle)	1.745 329 x E -2	radians
feet	3.048 000 x E -1	metres
gallons	3.785 412 x E -3	cubic metres
inches	2.540 000 x E +1	millimetres
pounds (force)	4.448 222 x E +0	kilonewtons

Most of the dimensions and measurements reported were obtained in non-SI units. All such values have been converted using the conversion factors given in ASTM E 380-91a (ASTM 1991).

1 Introduction

Background

The U. S. Army Engineer Waterways Experiment Station (WES) conducted a laboratory investigation to characterize the strength and constitutive property behavior of large-diameter, roller-compacted concrete (RCC) core samples obtained from the main Elk Creek Dam, located at Trail, Oregon. To accomplish this, WES conducted a total of 54 mechanical property tests consisting of 10 unconfined compression (UC) tests, 13 unconfined tension (UT; direct pull) tests, 8 triaxial compression (TXC) tests, 16 direct shear (DS) tests, and 7 splitting tensile strength (ST) tests. Fourteen of the tests were performed for the purpose of characterizing the strength properties of the interfaces between the RCC lifts. Specifically this included eight direct shear tests and six unconfined tension tests. In addition to the mechanical property tests, an extensive suite of nondestructive pulse velocity tests were performed on the cores to assess the degree of anisotropy in the RCC.

The large, 197-mm-diam core samples of the RCC were provided by the U.S. Army Engineer District (USAED), Portland. These core samples were obtained from four 8.6-m-deep boreholes drilled in the dam. Details of the equipment, methods, and procedures used to obtain these cores are provided in Appendix A. Station locations and offsets (distance from upstream edge of the dam) for the boreholes are provided in Table 1. A graphical summary of the recovered core is provided in Figure 1. In all, 25 m of core were obtained.

Table 1
Borehole Locations and Offsets

Borehole	CBL Station	Offset	
		(ft)	(m)
WDH1	131+62	37	11.28
WDH2	128+68	119	36.27
WDH3	127+17	116	35.36
WDH4	125+68	114	34.75

Purpose and Scope

The purpose of this report is to document the results from the series of pulse velocity and laboratory mechanical property tests performed on the RCC core.

Descriptions of the RCC, composition properties, test procedures, and test results are provided in Chapter 2. Comparative plots and analyses of the experimental results are presented in Chapter 3. A summary is provided in Chapter 4.

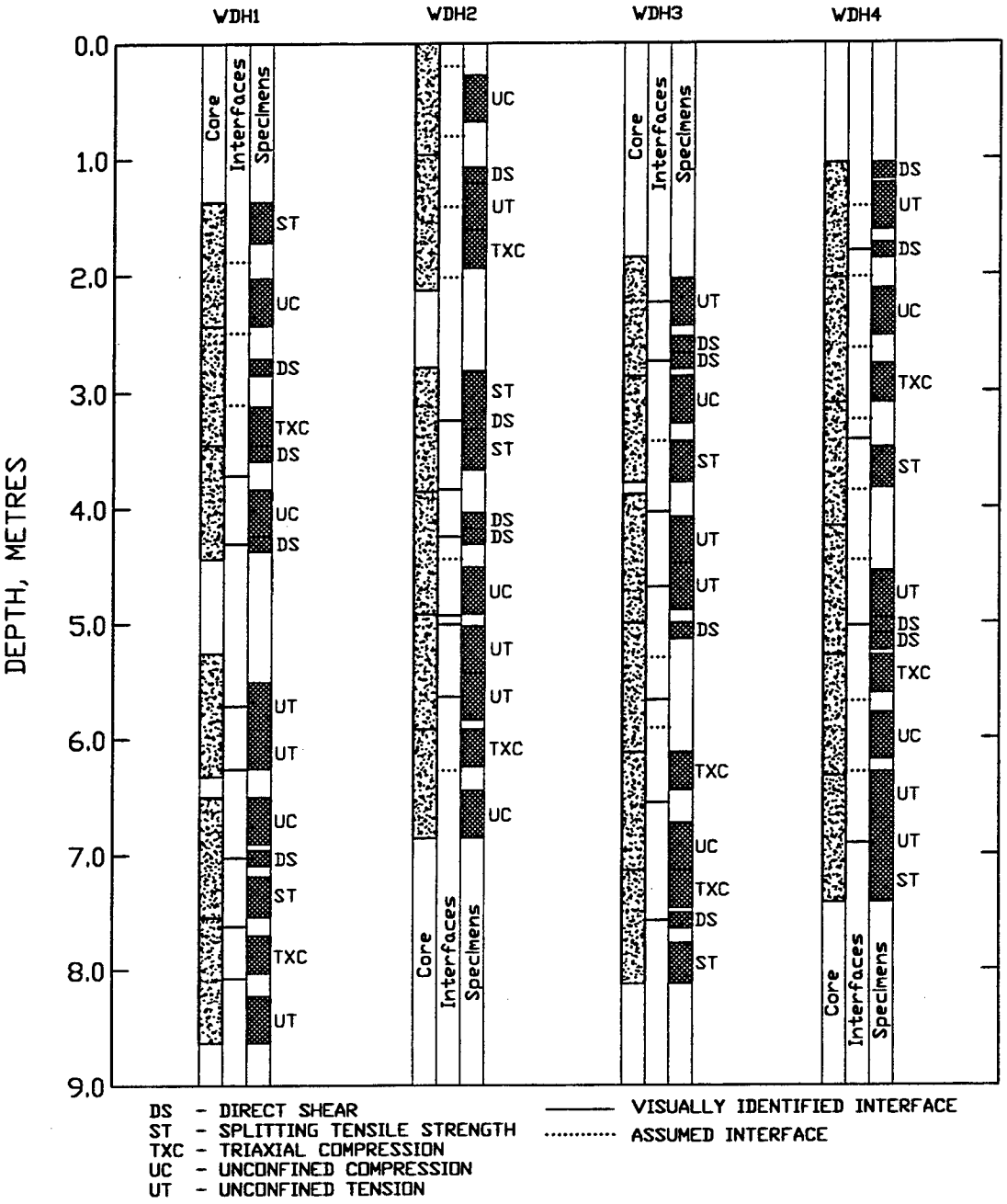

Figure 1. Graphical summary of recovered RCC cores, lift interfaces, and selected specimens

2 Laboratory Tests

Material Description

The RCC samples were shipped to WES in well-constructed, wooden core boxes. The core boxes were lined with sheets of Styrofoam, and the gaps between the cores and the Styrofoam sheets were filled with Styrofoam peanuts and expanding spray Styrofoam. The sides of the cores were marked to indicate the core orientation relative to the left or right dam abutment. Core depths were marked on the core boxes.

The RCC mixture contained Type II portland cement, natural sand fine aggregate, crushed basalt coarse aggregate, and Class F fly ash (Appendix A). The aggregate was angular to extremely angular in shape and had a nominal maximum size of approximately 75 mm. The RCC was placed in 610-mm-thick lifts. A sand and cement bedding mortar was placed between each lift. The bedding mortar was typically 6.4 mm thick but, due to local irregularities in the lift surfaces, varied from 0 to 50 mm in thickness.

Lift interfaces were identified by wetting and visually inspecting the cores. Distinguishing characteristics used to identify an interface were (a) a thin zone containing only bedding mortar, (b) a thin zone containing only small aggregate, i.e., less than 19 mm in length, or (c) a zone containing horizontally elongated aggregate. A graphical log of the interfaces is provided in Figure 1. Those interfaces that were visually observed are indicated in the figure by a thick horizontal line. In many instances, the interfaces were not evident but their location could be estimated using the nominal lift thickness of 610 mm as a gauge. These location estimates or assumed interfaces are indicated in Figure 1.

Composition Property Tests

Prior to performing the mechanical property tests, the height, diameter, and mass for most of the test specimens were determined. These measurements, along with the specimen's posttest moisture content, w, were used to compute the specimen's bulk or "as-tested" density, ρ, and dry density, ρ_d. Results from these determinations are provided in Table 2. The RCC had a nominal dry density of 2.26 Mg/m^3.

Ultrasonic Velocity Determinations

Prior to performing the mechanical property tests, an extensive suite of radial (cross-axis) ultrasonic pulse velocity tests were conducted on every core sample to assess the degree of anisotropy in the RCC. This involved measuring the transit distance and time for each P (compressional) or S (shear) pulse to propagate through a given sample. The velocity was then computed by dividing the transit distance by the transit time. A matching pair of 54-kHz piezoelectric transducers was used to transmit and receive the ultrasonic P waves. A pair of 500-kHz piezoelectric transducers was used to transmit and receive the ultrasonic S waves. The transit time was measured with a 100-MHz digital oscilloscope and the transit distance with a digital micrometer. All of these wave speed determinations were made under atmospheric conditions, i.e., no prestress of any kind was applied to the specimens. The tests were conducted in accordance with procedures provided in American Society for Testing and Materials (ASTM) C 597 (ASTM 1996d).

For a given depth, the P- and S-wave speeds were measured radially through the core with propagation directions oriented 0, 45, 90, and 135 deg from the right-abutment side of the core. At each location, one compressional wave speed and two shear wave speeds were determined, i.e., shear waves vibrating in the radial plane (Sr) and in the axial plane (Sa). This yielded a total of 12 wave speed measurements at each depth. This suite of measurements was repeated every 152 mm along the length of each core sample from all boreholes. These wave speed determinations are provided in Appendix B.

In addition, P- and S-wave speeds were determined for each mechanical property test specimen prior to being mechanically deformed (crushed or sheared). One compressional and two shear wave speeds were determined axially through the core. One shear wave vibrated in an axial plane oriented in the left-right (0 to 180 deg) abutment direction and the other in an axial plane oriented in the upstream-downstream direction (90 to 270 deg). This latter shear wave speed was not measured for the direct shear test specimens. Radial P- and S-wave speeds were also determined for each specimen. For the UC, UT, TXC, and ST test specimens, six radial P-, Sa-, and Sr-wave speeds (total of 18 velocities) were determined, two transverse to each other at elevations of one fourth, one half, and three forths the specimen height. For the DS test specimens, four radial P-, Sa-, and Sr-wave speeds were measured with two measurements transverse to each other at elevations of one third and two thirds of the specimen height. The various P- and S-wave speeds determined for the test specimens are provided in Table 2. The radial wave speeds listed in Table 2 are the average values.

Mechanical Property Tests

A total of 54 mechanical property tests were performed on air-dry specimens of the RCC to characterize the strength and constitutive properties of the RCC. All of the tests were conducted quasi-statically with times to peak load on the order of 5 to 15 min. The test matrix consisted of 10 UC, 13 UT tests, 8 TXC,

16 DS, and 7 ST tests. Four of the ST tests were performed with the applied loading oriented in the upstream-downstream direction of the core. For the remaining three tests, the loading was oriented in the left-right abutment direction of the core. Likewise, half of the direct shear specimens were sheared in the upstream-downstream direction and half in the left-right abutment direction. To determine the interface strength properties between the RCC lifts, half of the DS tests and six UT tests were performed on core specimens that contained a lift interface at about the specimen's midheight. A graphical log is provided in Figure 1 to illustrate the location, i.e., boring and depth, for each specimen.

Test description

A TXC test is conducted in two phases. During the first phase, the isotropic compression (IC) phase, the cylindrical test specimen is subjected to an increase in hydrostatic pressure loading while measurements of the specimen's height and diameter changes are made. The data are typically plotted as pressure versus volumetric strain, the slope of which, assuming elastic behavior, is termed the bulk modulus, K. The second phase of the TXC test, the shear phase, is conducted after the desired confining pressure has been applied during the IC phase. While holding the desired confining pressure constant, axial load is increased, and measurements of the specimen's height and diameter changes are made. The axial (compressive) load is increased until the specimen fails. The shear data are generally plotted as curves of principal stress difference (PSD) versus axial strain, the slope of which represents Young's modulus, E. The maximum PSD which a given specimen can support, or the PSD at 15 percent axial strain during the shear loading, is defined as the peak strength.

Note that the UC test is a TXC test in which no confining pressure is applied. The maximum PSD observed during a UC test is defined as the unconfined compressive strength, q_u, of the material.

A UT test is conducted by applying a tensile axial load to the cylindrical specimen while monitoring changes in the specimen's height and diameter. No confining pressure is applied during the test. The tensile load is increased until the specimen fails in tension. The data are generally plotted as curves of PSD versus axial strain. The PSD at specimen failure is defined as the unconfined tensile strength, q_t, of the material.

A DS test is also conducted in two phases. Initially, the cylindrical specimen is subjected to an axial (compressive) normal load. After a desired normal load has been applied, a radial shearing force is applied at the midheight of the specimen. The shearing force is increased until the specimen fails in shear. During the test, the specimen's axial (normal) and shear displacements and shear and normal loads are measured. The maximum shear stress that the specimen can support is defined as the peak shear strength.

The ST test is conducted by applying a diametral compressive loading along the length of a cylindrical specimen. This loading induces compressive stresses in the direction of loading and tensile stresses normal to the plane of loading. The tensile stress at failure is defined as the splitting tensile strength.

Definition of stresses and strains

During the UC, UT, and TXC tests, measurements are made of the axial and radial deformations of the specimen as confining pressure and/or axial load is applied or removed. These measurements along with the pretest measurements of the initial height and diameter of the specimen are used to convert the measured test data to stresses and strains.[1]

Axial strain, ϵ_a, is computed by dividing the measured axial deformation, Δh (change in height), by the original height, i.e., $\epsilon_a = \Delta h/h_o$. Similarly, radial strain, ϵ_r, is computed by dividing the measured radial deformation, Δd (change in diameter), by the original diameter, i.e., $\epsilon_r = \Delta d/d_o$. For this report, the volumetric strain is assumed to be the sum of the axial strain and twice the radial strain, $\epsilon_v = \epsilon_a + 2\epsilon_r$.

By definition, the confining pressure, σ_c, is equal to the radial stress, σ_r. The principal stress difference, q, is calculated by dividing the axial load by the original cross-sectional area of the specimen, A_o. In equation form:

$$q = \left(\sigma_a - \sigma_r\right) = \frac{Axial\ Load}{A_o} \tag{1}$$

where σ_a is the axial stress. The axial stress is related to the confining pressure and the principal stress difference by:

$$\sigma_a = q + \sigma_r \tag{2}$$

The mean normal stress, p, is the average of the applied principal stresses. In cylindrical geometry,

$$p = \frac{\left(\sigma_a + 2\sigma_r\right)}{3} \tag{3}$$

For the direct shear tests, the shear stress, τ, is computed by dividing the shear load by the cross-sectional area, A_o, of the specimen.

The ST strength of a specimen can be estimated from the applied line load, F, acting along the diameter of the specimen and its dimensions. Assuming that the

---

[1] Compressive stresses and strains (i.e., shortening) are assumed to be positive.

material is elastic, the tensile stress, T, along the center axis of the specimen, normal to the plane of loading is (Al-Hussaini and Townsend 1973)

$$T = -\frac{2F}{\pi l d_o} \tag{4}$$

and the compressive stresses, C, along the center axis of the specimen acting in the direction of loading, normal to T, is

$$C = \frac{6F}{\pi l d_o} \tag{5}$$

where l is the length of the specimen.

Specimen preparation

The mechanical property test specimens were cut from the desired sections of the large 197-mm-diam RCC core samples approximately 50 mm longer than their final desired length. Then, due to physical constraints of the test device, each specimen was recored to a diameter of 152 mm using a diamond-bit core barrel and following the procedures provided in ASTM C 42 (ASTM 1996b). The ends of the specimens were recut to the correct length. For the UC, UT, and TXC test specimens, the ends were ground flat, parallel to each other, and perpendicular to the sides of the core. The UC, UT, TXC, and ST test specimens had a height of approximately 305 mm. The DS test specimens were approximately 152 mm in height. Prior to testing, the prepared specimens were measured for height and diameter, weighed, and ultrasonically pulsed to determine the composition properties and wave speeds of the specimen.

Procedures

The UC and TXC tests were performed in accordance with ASTM C 39 and ASTM C 801, respectively (ASTM 1996a, e). Each specimen was placed between hardened steel top and base caps. A 0.6-mm-thick latex rubber membrane was placed around the specimen with the aid of a membrane stretcher (thin-walled steel tube). The membrane was positioned inside the membrane stretcher, and a vacuum was applied through the side of the stretcher to pull the membrane against the stretcher's inner side. The stretcher and membrane were lowered past the top cap/specimen/base cap assembly, and the vacuum was removed, thereby causing the membrane to collapse around the assembly encasing the specimen. The membrane stretcher was then removed. For the TXC specimens, a second 0.6-mm-thick membrane was placed around the specimen, and the exterior of the outside membrane was coated with a liquid synthetic rubber to inhibit deterioration caused by the confining-pressure fluid. The fluid was a mixture of kerosene and hydraulic oil. Finally, the specimen,

along with its top cap and base cap assembly, was placed into the pressure chamber of the test apparatus, and the instrumentation setup was commenced.

During testing, the axial and radial deformations of the specimen, applied confining pressure (for the TXC tests only), and axial load were continuously monitored. The outputs from the various instrumentation sensors were electronically amplified and filtered, and the conditioned signals were recorded by a computer-controlled 16-bit analog-to-digital converter. This data acquisition system was programmed to sample the data channels every 3 to 5 sec, convert the measured voltages to engineering units, and store the data for posttest processing.

The vertical deflection measurement system consisted of two linear variable differential transformers (LVDTs) mounted vertically on top of the specimen and positioned 180 deg apart. They were oriented to measure the displacement between the top and base caps, thus providing a measure of the axial deformation of the specimen. In addition, a film potentiometer (film pot) was mounted externally to the pressure chamber to measure the displacement of the piston through which axial loads are applied. This provided a backup to the vertical LVDTs in case they exceeded their calibrated range. Four strain gauges with a 50.8-mm gauge length were glued to the sides of the specimen at mid-height. Two of the strain gauges were oriented to measure axial strain and two to measure radial strain. Each pair of strain gauges was mounted diametrically opposite on the specimen.

Axial load was measured by a load cell mounted inside the pressure chamber in the base of the specimen pedestal. For the TXC tests, a pressure transducer mounted external to the pressure chamber in the confining fluid line was used to measure confining pressure.

The UT tests were conducted in general accordance with CRD-C 164 (USAEWES 1949). The ends of the these specimens were glued to hardened steel end caps using a high-strength epoxy adhesive. The glue was allowed to dry for a minimum of 24 hours. Then, the specimen/end cap assembly was placed into the direct-pull tension apparatus and carefully aligned with the axial pull-rods used to apply the axial tensile loading. Both end caps were connected to the top and bottom pull-rods using a ball-and-socket type connection (exception to CRD-C 164). The socket was coated with an antiseize lubricant to ensure unimpeded rotation of the ball and socket. During the test, the axial and radial deformations of the specimen and applied tensile load were continuously monitored. Two strain gauges were used to measure axial strain and two to measure radial strain. Like the UC and TXC test specimens, all four strain gauges were mounted at the midheight of the specimen with each pair diametrically opposite each other. A load cell mounted in line with the bottom pull-rod was used to measure the tensile loads. The same data acquisition and signal conditioning systems described above were used for the UT tests.

To conduct a DS test, the specimen was first centered inside a 6.35-mm-thick steel ring that had a diameter of 178 mm and a height of 63.5 mm. The annulus

between the specimen and ring was filled with a hydrated gypsum cement to bond the specimen to the ring. After the cement hardened, a 3.2-mm-high spacer ring, a 76-mm-high steel ring, and a 12-mm-high cap extender ring were placed on top of the first steel ring. The spacer ring was placed between the two steel rings. The extender ring was placed on top of the second steel ring. The second steel ring had the same diameter and thickness as the bottom steel ring. The annulus between the top ring and specimen was then filled with the gypsum cement. The gypsum cement completely covered the top of the RCC specimen. After hardening, the top of the gypsum was ground flat with the top of the cap extender ring. The spacer ring and the cap extender ring were removed and a set of two aluminum rings were placed over the steel rings. The ring/specimen assembly was placed inside the direct shear apparatus and the instrumentation setup. The two aluminum rings were pinned on one side to a load cell for measuring the shear load and on the opposite side to a screw driven loader. Finally, an aluminum platen was placed on top of the specimen through which the normal load was applied. The procedures used to conduct this test were in accordance with U.S. Bureau of Reclamation 4915 (USBR 1992).

During the test, the applied normal and shear loadings and the normal and shear displacements were recorded by a computer-controlled, 20-bit analog-to-digital converter. A steel piston with a spherical seat was used to apply the axial load to the top of the aluminum platen. A gas pressure was applied to the top of the piston to generate the axial loading. The magnitude of the normal load was determined by measuring the gas pressure that was applied to the top of the loading piston and multiplying the pressure by the cross-sectional area of the piston. A load cell was used to measure the applied shear loading. Both the shear and normal displacements were measured with LVDTs.

The ST tests were conducted in accordance with ASTM C 496 (ASTM 1996c). To conduct this test, the cylindrical specimen was placed on its side in an aligning jig like the one detailed in ASTM C 496. The aligning jig contained top and bottom steel bearing bars to transmit the applied loading to the sides of the specimen. Wooden bearing strips, 3.2-mm-thick by 25-mm-wide, were placed between the bearing bars and the specimen. The aligning jig containing the specimen was then placed between two steel platens of the load frame. During the test, the applied diametral loading and the specimen's change in diameter in the plane of the loading were measured.

Results

Results from the UC, UT, TXC, and DS mechanical property tests are presented in Plates 1-55. No data plates are provided for the ST tests. Results from all tests are summarized in Tables 3-7.

One data plate is presented for each UC and UT test. Each plate displays four plots: principal stress difference versus (a) mean normal stress, (b) volumetric strain, (c) axial strain, and (d) radial strain. For the UC tests (Plates 1-10), two axial strain responses are plotted, one from the LVDT measurements and one

from the axial strain gauges. The radial strains measured for most of the UT tests (Plates 43-55) were of very low amplitude. As a result, these signals are very "noisy." The radial strains for specimens 9604A19, 9604A23, and 9604A30 are suspect. These data and the computed volumetric strains for these specimens should be disregarded.

Two data plates are provided to display the results of each TXC test. These plates (Plates 11-26) contain plots of principal stress difference versus mean normal stress and principal stress difference and mean normal stress versus axial strain, radial strain, and volumetric strain. As before, two axial strain responses are provided for each TXC test, i.e., one from the axial strain gauges and one from the LVDT measurements. Specimen 9604A10 experienced a seating "instability" at the start of the shear loading phase, causing the "soft" initial shear response.

One data plate is provided for each direct shear test. These data are shown in Plates 27-42 as plots of shear stress versus normal stress and shear displacement. At peak shear strength, the specimens failed abruptly, causing the pronounced decrease in shear stress and increase in shear displacement. Due to the rapid failure, the normal stresses during this initial postpeak portion of the tests increased. Shortly thereafter, the normal stresses decreased to their prefailure level and maintained that level for the remainder of the test.

Table 2
Composition Properties and Ultrasonic P- and S-Wave Velocities for Air-Dry RCC Laboratory Mechanical Property Test Specimens

Test Number	Boring Number	Sample Number	Depth (m)	Moisture Content (%)	Wet Density (Mg/m³)	Dry Density (Mg/m³)	S-Wave Velocity, (km/s)				P-Wave Velocity (km/s)	
							Axial		Radial			
							0°-180°	90°-270°	Sr	Sa	Axial	Radial
Unconfined Compression Tests												
9604A01	WDH4	11	5.97	4.35	2.374	2.275	2.451	2.499	2.579	2.515	4.180	4.424
9604A02	WDH3	4	3.05	3.83	2.347	2.260	2.546	2.500	2.495	2.437	4.122	4.211
9604A03	WDH2	14	6.65	4.76	2.356	2.249	2.591	2.560	2.597	2.583	4.399	4.444
9604A04	WDH2	1	0.48	4.33	2.368	2.270	2.532	2.536	2.506	2.519	4.325	4.279
9604A05	WDH3	10	6.93	3.63	2.369	2.286	2.477	2.518	2.586	2.521	4.123	4.342
9604A06	WDH1	6	4.05	3.66	2.371	2.287	2.569	2.565	2.526	2.527	4.338	4.409
9604A07	WDH2	10	4.72	4.66	2.367	2.262	2.542	2.425	2.543	2.467	4.254	4.339
9604A08	WDH1	2	2.26	4.89	2.348	2.239	2.462	2.462	2.556	2.493	4.159	4.542
9604A09	WDH1	10	6.74	3.88	2.390	2.301	2.613	2.604	2.644	2.634	4.496	4.701
9604A18	WDH4	4	2.32	4.69	2.322	2.218	2.296	2.543	2.491	2.533	3.887	4.245
Triaxial Compression Tests												
9604A10	WDH1	13	7.83	4.17	2.341	2.247	2.455	2.482	2.442	2.440	4.164	4.449
9604A11	WDH4	5	2.91	3.42	2.346	2.268	2.453	2.474	2.548	2.511	--	--
9604A12	WDH3	9	6.31	4.36	2.336	2.238	2.562	2.447	2.521	2.404	4.039	4.377
9604A13	WDH4	10	5.46	3.95	2.361	2.271	2.482	2.571	2.483	2.428	--	--
9604A14	WDH1	4	3.26	4.12	2.340	2.247	2.500	2.393	2.534	2.489	4.290	4.371
9604A15	WDH2	4	1.83	3.74	2.319	2.235	2.417	2.417	2.480	2.449	4.241	4.266
9604A16	WDH3	11	7.28	4.22	2.363	2.267	2.647	2.561	2.618	2.538	4.339	4.463
9604A17	WDH2	13	6.04	3.64	2.354	2.271	2.580	2.559	2.566	2.541	4.371	4.394

(Sheet 1 of 3)

Table 2
(Continued)

Test Number	Boring Number	Sample Number	Depth (m)	Moisture Content (%)	Wet Density (Mg/m^3)	Dry Density (Mg/m^3)	S-Wave Velocity, (km/s)				P-Wave Velocity (km/s)	
							Axial		Radial			
							0°-180°	90°-270°	Sr	Sa	Axial	Radial
Direct Shear Tests												
9604Y01	WDH1	3	2.77	--	--	--	2.666	--	2.619	2.676	4.610	4.644
9604Y02	WDH1	5	3.60	--	--	--	2.522	--	2.440	2.565	4.357	4.250
9604Y03	WDH1	7	4.30	--	--	--	2.552	--	2.562	2.503	4.464	4.480
9604Y04	WDH1	11	7.01	--	--	--	2.540	--	2.497	2.395	4.168	4.363
9604Y05	WDH2	2	1.16	--	--	--	2.604	--	2.707	2.661	4.436	4.546
9604Y06	WDH2	6	3.29	--	--	--	2.541	--	2.724	2.594	4.382	4.491
9604Y07	WDH2	8	4.11	--	--	--	2.613	--	2.725	2.689	4.552	4.707
9604Y08	WDH2	9	4.33	--	--	--	2.574	--	2.686	2.599	4.307	4.501
9604Y09	WDH3	2	2.62	--	--	--	2.465	--	2.539	2.426	4.498	4.377
9604Y10	WDH3	3	2.74	--	--	--	2.463	--	2.561	2.485	4.189	4.499
9604Y11	WDH3	8	5.09	--	--	--	2.434	--	2.564	2.488	4.227	4.510
9604Y12	WDH3	12	7.58	--	--	--	2.379	--	2.580	2.460	4.197	4.586
9604Y13	WDH4	1	1.13	--	--	--	2.277	--	2.345	2.403	3.940	4.198
9604Y14	WDH4	3	1.80	--	--	--	2.561	--	2.484	2.455	4.339	4.363
9604Y15	WDH4	8	5.04	--	--	--	--	--	--	--	--	--
9604Y16	WDH4	9	5.17	--	--	--	--	--	--	--	--	--
Unconfined (direct pull) Tension Tests												
9604A19	WDH1	8	5.68	4.03	2.324	2.234	2.516	2.663	2.477	2.468	4.094	4.265
9604A20	WDH2	12	5.64	4.53	2.347	2.245	2.471	2.483	2.516	2.456	4.159	4.345
9604A21	WDH1	9	6.07	3.93	2.339	2.251	2.443	2.389	2.532	2.458	4.031	4.463
9604A22	WDH2	11	5.23	2.91	2.337	2.271	2.437	2.449	2.546	2.464	4.181	4.342
9604A23	WDH3	6	4.33	3.18	2.372	2.299	2.607	2.620	2.611	2.484	4.403	4.361
9604A24	WDH4	7	4.72	2.75	2.357	2.294	2.550	2.517	2.580	2.477	4.265	4.354
9604A25	WDH4	12	6.52	3.09	2.351	2.281	2.488	2.428	2.612	2.580	--	--
9604A26	WDH1	14	8.32	2.69	2.341	2.280	2.551	2.527	2.516	2.484	4.310	4.484
9604A27	WDH3	7	4.69	3.54	2.237	2.161	2.472	2.443	2.562	2.434	--	--
9604A28	WDH4	2	1.40	3.46	2.320	2.242	2.479	2.436	2.445	2.461	4.036	4.137
9604A29	WDH4	13	6.89	3.69	2.327	2.244	2.386	2.409	2.467	2.373	4.033	4.307
9604A30	WDH3	1	2.29	3.04	2.335	2.266	2.522	2.560	2.535	2.417	4.169	3.858
9604A31	WDH2	3	1.46	3.18	2.323	2.251	2.613	2.507	2.464	2.473	4.279	4.353

(Sheet 2 of 3)

Table 2
(Concluded)

Test Number	Boring Number	Sample Number	Depth (m)	Moisture Content (%)	Wet Density (Mg/m^3)	Dry Density (Mg/m^3)	S-Wave Velocity, (km/s)				P-Wave Velocity (km/s)	
							Axial		Radial			
							0°-180°	90°-270°	Sr	Sa	Axial	Radial
Splitting Tensile Tests												
--	WDH2	5	2.93	--	--	--	2.542	2.559	2.570	2.509	4.098	4.479
9604Z01	WDH1	1	1.59	--	--	--	2.442	2.450	2.512	2.460	4.200	4.441
9604Z02	WDH1	12	7.38	--	--	--	2.404	2.451	2.524	2.499	4.001	4.468
9604Z03	WDH2	7	3.51	--	--	--	2.620	2.518	2.614	2.548	4.203	4.416
9604Z04	WDH3	5	3.60	--	--	--	2.495	2.515	2.562	2.501	4.243	4.351
9604Z05	WDH3	13	7.96	--	--	--	2.576	2.558	2.610	2.584	4.319	4.406
9604Z06	WDH4	6	3.66	--	--	--	2.574	2.574	2.623	2.569	4.348	4.476
9604Z07	WDH4	14	7.25	--	--	--	2.464	2.479	2.474	2.383	4.153	4.220

(Sheet 3 of 3)

Table 3
Summary of Unconfined Compression Tests Performed for Air-Dry Specimens of RCC

Plate Number	Test Number	Boring Number	Sample Number	Depth (m)	Stress at Failure, (MPa)		Young's Modulus (MPa)	Poisson's Ratio
					Mean Normal Stress	Principal Stress Difference		
1	9604A01	WDH4	11	5.97	5.3	15.9	15,920	0.230
2	9604A02	WDH3	4	3.05	6.2	18.6	15,970	0.133
3	9604A03	WDH2	14	6.65	11.6	34.9	34,600	0.210
4	9604A04	WDH2	1	0.48	5.9	17.8	20,240	0.225
5	9604A05	WDH3	10	6.93	6.7	20.2	23,810	0.143
6	9604A06	WDH1	6	4.05	7.5	22.4	22,370	0.182
7	9604A07	WDH2	10	4.72	7.1	21.3	20,270	0.231
8	9604A08	WDH1	2	2.26	7.2	21.7	26,670	0.180
9	9604A09	WDH1	10	6.74	8.9	26.8	22,000	0.239
10	9604A18	WDH4	4	2.32	4.2	12.6	13,890	0.160

Note: To convert stresses from MPa to psi multiply by 145.

Table 4
Summary of Triaxial Compression Tests for Air-Dry Specimens of RCC

Plate Numbers	Test Number	Boring Number	Sample Number	Depth (m)	Confining Pressure (MPa)	Stress at Failure, (MPa)		Young's Modulus (MPa)	Poisson's Ratio
						Mean Normal Stress	Principal Stress Difference		
11, 12	9604A10	WDH1	13	7.83	0.70	7.9	21.7	24,510	0.187
13, 14	9604A11	WDH4	5	2.91	0.70	9.1	25.4	26,320	0.185
15, 16	9604A12	WDH3	9	6.31	3.46	16.0	37.6	20,000	0.091
17, 18	9604A13	WDH4	10	5.46	3.43	15.6	36.3	25,810	0.159
19, 20	9604A14	WDH1	4	3.26	3.51	15.2	35.2	13,300	0.130
21, 22	9604A15	WDH2	4	1.83	0.70	12.4	35.1	13,740	0.050
23, 24	9604A16	WDH3	11	7.28	0.71	9.0	24.8	23,590	0.186
25, 26	9604A17	WDH2	13	6.04	0.69	9.9	27.6	27,780	0.184

Note: To convert stresses from MPa to psi multiply by 145.

Table 5
Summary of Direct Shear Tests Performed on Air-Dry Specimens of RCC

Plate Number	Test Number	Boring Number	Sample Number	Depth (m)	Layer Interface (Y or N)	Direction of Shear (LR or UD)[1]	Stress at Failure, (MPa)	
							Normal Stress	Shear Stress
27	9604Y01	WDH1	3	2.77	N	LR	0.553	4.198
28	9604Y02	WDH1	5	3.60	N	UD	0.139	3.044
29	9604Y03	WDH1	7	4.30	Y	LR	0.140	3.324
30	9604Y04	WDH1	11	7.01	Y	UD	0.278	2.804
31	9604Y05	WDH2	2	1.16	N	UD	0.277	3.224
32	9604Y06	WDH2	6	3.29	Y	UD	0.139	2.487
33	9604Y07	WDH2	8	4.11	N	LR	0.281	3.318
34	9604Y08	WDH2	9	4.33	Y	LR	0.552	3.306
35	9604Y09	WDH3	2	2.62	N	LR	0.138	2.908
36	9604Y10	WDH3	3	2.74	Y	LR	0.555	3.952
37	9604Y11	WDH3	8	5.09	N	UD	0.276	3.111
38	9604Y12	WDH3	12	7.58	Y	UD	0.276	3.256
39	9604Y13	WDH4	1	1.13	N	UD	0.139	3.505
40	9604Y14	WDH4	3	1.80	Y	UD	0.552	5.001
41	9604Y15	WDH4	8	5.04	Y	LR	0.138	3.100
42	9604Y16	WDH4	9	5.17	N	LR	0.278	3.855

Note: To convert stresses from MPa to psi multiply by 145.
[1] LR = Shear in direction of left-right abutment.
UD = Shear in upstream-downstream direction.

Table 6
Summary of Unconfined Tension (Direct Pull) Tests for Air-Dry Specimens of RCC

Plate Number	Test Number	Boring Number	Sample Number	Depth (m)	Layer Interface (Y or N)	Stress at Failure, (MPa)		Young's Modulus (MPa)
						Mean Normal Stress	Principal Stress Difference	
43	9604A19	WDH1	8	5.68	Y	-0.09	-0.28	7,500
44	9604A20	WDH2	12	5.64	N	-0.18	-0.55	17,650
45	9604A21	WDH1	9	6.07	N	-0.20	-0.59	19,360
46	9604A22	WDH2	11	5.23	N	-0.37	-1.10	19,230
47	9604A23	WDH3	6	4.33	N	-0.43	-1.28	21,430
48	9604A24	WDH4	7	4.72	N	-0.42	-1.27	27,830
49	9604A25	WDH4	12	6.52	N	-0.24	-0.72	19,740
50	9604A26	WDH1	14	8.32	N	-0.41	-1.23	25,000
51	9604A27	WDH3	7	4.45	Y	-0.12	-0.36	21,050
52	9604A28	WDH4	2	1.40	Y ?	-0.24	-0.72	17,650
53	9604A29	WDH4	13	6.89	Y	-0.18	-0.53	21,050
54	9604A30	WDH3	1	2.29	Y	-0.26	-0.78	13,330
55	9604A31	WDH2	3	1.46	Y?	-0.25	-0.76	17,780

Note: To convert stresses from MPa to psi multiply by 145.

Table 7
Summary of Splitting Tensile (Brazilian) Tests for Air-Dry Specimens of RCC

Test Number	Boring Number	Sample Number	Depth (m)	Direction of Loading (LR or UD)[1]	Tensile Strength (MPa)
9604Z01	WDH1	1	1.59	LR	2.85
9604Z02	WDH1	12	7.38	UD	2.25
9604Z03	WDH2	7	3.51	UD	3.00
9604Z04	WDH3	5	3.60	LR	3.00
9604Z05	WDH3	13	7.96	UD	3.35
9604Z06	WDH4	6	3.66	UD	3.70
9604Z07	WDH4	14	7.25	LR	4.80

Note: To convert stresses from MPa to psi multiply by 145.
[1]LR = Loading appled in direction of left-right abutment.
UD = Loading applied in upstream-downstream direction.

3 Test Results

Pulse Velocity Results

In order to assess the degree of anisotropy in the RCC, an extensive suite of nondestructive pulse velocity tests were conducted on core samples obtained from the dam. Results from these tests are provided in Tables B1-B12 and Plates B1-B12. Details of the procedures and equipment used to conduct these tests are provided in Chapter 2.

Table B1 lists the measured radial P-wave velocities obtained for each core acquired from borehole WDH1. As indicated in the table, four P-wave speeds were determined for each depth. The angle listed at the top of each column corresponds to the propagation direction of the P-wave relative to the right abutment side of the dam. Therefore, for the 0-deg direction, the wave propagates from the right abutment side of the core to the left abutment side, and for the 90-deg direction, the wave propagates from the downstream side to the upstream side. By comparing the velocities for different propagation paths within the same radial plane, the degree of anisotropy in the radial plane can be assessed.

The wave speeds listed in Table B1 are plotted in Plate B1. For each orientation, the velocities appear to be independent of depth and randomly distributed about a mean value. Mean and standard deviations for each orientation were computed and are listed in Table B1. Occasionally, and for no apparent reason, an unusually low or high wave speed was detected in the velocity profile. These outliers could have been due to large voids or large aggregate hidden within the concrete. Therefore, to determine whether these readings were outliers, a statistical technique known as Chauvenet's criterion was used to define the acceptable deviation band about the mean. A concise description of this technique is provided in Coleman and Steele (1989). This procedure assumes that the acceptable band about the mean value corresponds to a probability of 1-1/(2N), where N is the number of readings in the sample set. For this probability, the nondimensional deviation, τ, can be determined using a Gaussian probability curve as illustrated in Figure 2. The maximum acceptable deviation from the mean velocity, ΔV_{max}, can be computed by

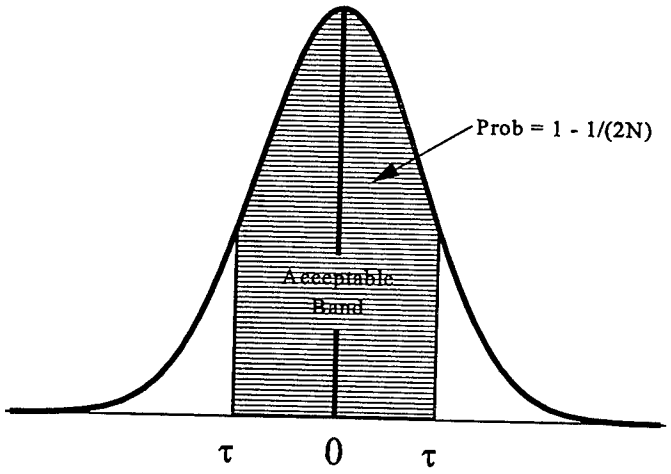

Figure 2. Illustration of Chauvenet's criterion

$$\Delta V_{\max} = \tau S_{dev} \tag{6}$$

where S_{dev} is the standard deviation of the velocity data set. Therefore, points that fall outside the band

$$\left(V_{avg} - \Delta V_{\max}\right) \leq V_i \leq \left(V_{avg} + \Delta V_{\max}\right) \tag{7}$$

should be rejected as an outlier, and a new mean and standard deviation should be calculated.

Using this technique, upper and lower bounds were calculated, outliers were rejected, and a new mean and standard deviation were determined for each orientation. These new means and standard deviations are listed at the bottom of Table B1.

Similarly, means and standard deviations were calculated for the shear wave velocities listed in Tables B2 and B3 and plotted in Plates B2 and B3 for borehole WDH1. Tables B2 and B3 list the Sa-wave speeds (shear waves vibrating in the axial plane) and Sr-wave speeds (shear waves vibrating in the radial plane), respectively. These average shear wave speeds along with the mean P-wave velocities for the same borehole are plotted versus propagation direction in Figure 3. Plus and minus one standard deviation bands are also plotted in the figure. As shown, the mean values for each type of velocity appear to be independent of orientation. To test this observation, each of the three velocity sets were analysed using a one-way analysis of variance. At the 0.05 significance level, the mean velocities for each orientation were from the same population. Therefore, the velocity data from borehole WDH1 appear to be isotropic in the radial plane.

The velocity data acquired for boreholes WDH2, WDH3, and WDH4 are listed in Tables B4-B12 and plotted in Plates B4-B12. Mean velocities (with +/-

one S_{dev} bands) are plotted versus orientation in Figures 4-6. Applying the same analysis techniques to these data revealed that, for each borehole, the shear and compressional wave-speed data were independent of propagation direction, and it is concluded that the shear and compressional wave speeds are isotropic in the radial plane. Since wave speeds and elastic mechanical response are related through the following relations,

$$M = \rho P^2 \tag{8}$$

$$G = \rho S^2 \tag{9}$$

where M and G are the constrained and shear modulus, respectively, the wave-speed data suggest that the compressibility and shear responses of the material are unaffected by orientation in the radial plane.

Since pulse velocity was determined to be direction independent in the radial plane, the data from all four orientations were used to compute mean P-, Sa-, and Sr-wave speeds for each borehole. These mean and standard deviation values are listed in the last columns of Tables B1-B12. The data used to compute these statistics are plotted in the velocity profiles shown in Figures 7-10. As before, Chauvenet's criterion was used to reject the outliers. Mean velocities are plotted versus borehole in Figure 11. On average, the RCC has radial P, Sa, and Sr velocities of 4.416, 2.489, and 2.548 km/s, respectively.

Closer examination of the shear wave-speed data plotted in Figure 11 suggests a slight degree of anisotropy in the Sa and Sr data. The average values of Sr and Sa were ratioed for each borehole and are plotted in Figure 12. In all cases, the velocity ratio is greater than 1. This means that a shear wave vibrating in the radial plane (Sr) will propagate, on average, 2.4 percent faster radially through the core than will a shear wave vibrating in the axial plane.

Similar results are obtained from the P-wave speed data collected for the mechanical property test specimens. These data are listed in Table 2. From these data, mean axial and radial P-wave speeds were determined for each borehole and are plotted in Figure 13. Average radial and axial P-wave velocity pairs were ratioed and are plotted in Figure 14. Again, in all cases, the radial P-waves propagated faster, 3.4 percent on average, than did the axial P-waves. Based on Equations 8 and 9, the 2.4-percent increase in shear wave speed will yield a 4.9-percent increase in shear modulus, and the 3.4-percent increase in compressional wave speed will yield a 6.9-percent increase in constrained modulus.

Unconfined Compression Tests

Ten unconfined compression tests were performed on the RCC specimens. Results from these tests are presented in Plates 1-10 and are summarized in Table 3. As previously mentioned in Chapter 2, two axial strain responses are presented for each test; one determined from the LVDT measurements and one

from the axial strain gauges bonded to the sides of the specimen. In all cases, the LVDT-derived strains displayed an initial nonlinear shear response concave to the principal stress difference axis (see Plates 1-10). This nonlinearity is due to "seating" errors introduced by the specimen's contact with the top and bottom steel end caps. With additional shear loading, these shear responses became linear and generally paralleled the strain gauge responses. As the shear loading increased, both axial strain responses became nonlinear but concave to the axial strain axis. This behavior indicates specimen yielding. At peak strength, the specimen failed causing the apparent "softening" behavior (decrease in stress difference with increasing axial deformation). At peak strength, the strain gauges either failed or displayed erratic results. Therefore, these records were terminated at peak strength.

To obtain the most accurate representation of the specimen's axial strain response, both the strain gauge and LVDT data were used. For all tests, the most representative curve was constructed as follows. Initially the strain gauge data were used. Then, at a stress difference where the strain gauge and LVDT data paralleled each other, the LVDT curve was shifted and merged with the strain gauge record. The LVDT data were used for the remainder of the shear response. These representative shear responses are provided in Figures 15 and 16. Young's moduli from the slope of the linear, elastic portion of the tests are listed in Table 3. On average, the RCC had a Young's modulus of 21.6 GPa.

Radial strain responses for these tests are also plotted Figures 15 and 16. These responses were obtained from the radial strain gauges bonded to the side of the specimens. Like the axial strain gauges, the radial gauges failed or became erratic at peak stress. Therefore, these records were terminated at peak strength. The slope of the elastic portion of each curve was determined and used with the specimen's Young's modulus to compute the Poisson's ratio for each specimen. The values for each test are listed in Table 3 and averaged 0.19.

The axial and radial strains shown in these figures were used to compute volumetric responses for each test. These responses are plotted in Figure 17. These volumetric responses initially show compaction (positive volumetric strain), but, with increasing shear loading, the specimens dilated (volume expansion), presumably due to microcrack growth and coalescence, up to specimen failure.

Peak strengths were determined for each test. These strength values are listed in Table 3 and plotted in Figure 18. As shown, the unconfined compressive strengths of the test specimens ranged from a low of 12.6 MPa to a high of 34.9 MPa. On average, the RCC has an unconfined compressive strength of 21.2 MPa.

Triaxial Compression Tests

Results from the eight triaxial compression tests performed on the RCC specimens are provided in Plates 11-26. The results from these tests are summarized in Figures 19-21 and Table 4. Like the UC results, the axial strain

responses shown in Figure 19 were derived from both strain gauges and LVDT data. The strain gauge data were used for the isotropic compression phase and the elastic portion and part of the yield portion of the shear phase. The LVDT data were then merged with the strain gauge responses and used for the remainder of the test. Five test specimens were sheared at a nominal confining pressure of 0.70 MPa. These specimens exhibited a brittle failure characterized by faulting and subsequent strain softening. The three specimens sheared at a nominal 3.46-MPa confining pressure displayed a ductile failure response. That is, after an initial elastic loading, the specimens yielded causing them to loss their resistance to the shear loading as evidenced by the decreasing modulus with continued axial deformation. At about 2.0- to 2.5-percent axial strain, the specimens achieved their maximum strength. At that point, the shear loading was removed and the test terminated. As before, the elastic constants Young's modulus and Poisson's ratio were determined from the initial portions of the shear loading of each test. These results are listed in Table 4. The average Young's modulus from these tests is 21.9 GPa which agrees very well with the 21.6-GPa modulus determined from the UC tests. However, the average Poisson's ratio determined from the TXC tests (0.15) was less than that obtained from the UC tests (0.19).

Peak or ultimate strengths from the TXC tests are listed in Table 3 and are plotted in Figure 20. On average, the specimens sheared at the lower confining pressure, i.e., 0.70 MPa, had a strength of 26.9 MPa and at the higher confining pressure, i.e., 3.46 MPa, a strength of 36.4 MPa.

All of the failure data for both the UC and TXC tests are plotted as open circles in Figure 21. Average strengths from the unconfined and TXC tests are plotted as filled triangles in this figure. The mean normal stress p associated with these average strengths q were calculated using

$$p = \frac{q}{3} + \sigma_c \tag{10}$$

where σ_c is the nominal confining pressure. A linear regression fit to these three data points was used to represent the material's TXC failure behavior. This line has a slope $\alpha = 1.749$ and a principal stress difference intercept $A =$ 9.32 MPa. Using these values and the following equations,

$$\phi = \sin^{-1}\left(\frac{3\alpha}{6+\alpha}\right) \tag{11}$$

$$C = A\left(\frac{3-\sin\phi}{6\cos\phi}\right) \tag{12}$$

the classical Mohr-Coulomb friction coefficients C (cohesion) and ϕ (angle of internal friction) were calculated to be

$$C = 4.90 \text{ MPa}$$

$$\phi = 42.6°$$

However, these friction coefficients do not account for the strength data obtained from the direct shear tests. The following section will use both the triaxial compression data and the direct shear data to develop a representative failure envelope for the RCC.

Direct Shear Tests

Sixteen direct shear tests were conducted to characterize the shear properties of the RCC and the RCC lift interfaces. Half of the shear specimens contained a lift interface and half did not. Results from the tests are provided in Plates 27-42 and are summarized in Table 5. Tests were performed at three nominal values of normal stress; 0.139, 0.278, and 0.553 MPa. Peak shear strengths from these tests are plotted in Figure 22. Half of the specimens were sheared in the left-right abutment direction and half in the upstream-downstream direction. No effect due to shear direction was evident in the data. Peak shear strengths are plotted versus normal stress in Figure 23. The specimens sheared along a lift interface appear to be just as strong as the specimens without an interface.

Both the triaxial compression and direct shear data were used to determine the most representative failure envelope for the RCC. This assumes that the material's true failure relation is stress path independent and that the material's strength is direction independent. Failure data from both types of tests are plotted in Figure 24. To transform the triaxial compression failure data to normal stresses, σ_n, and shear stresses, τ, the following transformation equations were used.

$$\sigma_n = \frac{\sigma_a + \sigma_r}{2} - \frac{\sigma_a - \sigma_r}{2} \cos 2\theta \tag{13}$$

$$\tau = \frac{\sigma_a - \sigma_r}{2} \sin 2\theta \tag{14}$$

where

$$\theta = \frac{\pi}{4} - \frac{\phi}{2} \tag{15}$$

A failure relation was constructed through the failure points to represent the material's strength envelope. This envelope is linear up to a normal stress of about 4 MPa with a $C = 2.82$ MPa and $\phi = 55.7$ deg. For normal stresses between 4 and 7 MPa, the envelope is nonlinear concave to the normal stress axis. For normal stresses greater than 7 MPa, the curve is again linear with a $\phi = 36.7$ deg.

Unconfined Tension Tests

Results from the suite of unconfined (direct-pull) tension tests are provided in Plates 43-55 and are summarized in Table 6. Four of the tests were performed on specimens containing a visually identified lift interface. Tests 9604A28 and 9604A31 were performed on specimens that should have an interface, but the interfaces could not be visually identified. Therefore, the results from these last two tests should be considered suspect. The remaining seven tests were performed on specimens without an interface.

Peak tensile strengths from these tests are plotted in Figure 25. The specimens without interfaces had an average tensile strength of 0.96 MPa. Therefore, the RCC has an unconfined tensile to compressive strength ratio of about 4.5 percent. The specimens with lift interfaces had tensile strengths ranging from 0.28 to 0.78 MPa. However, most of the results should be considered suspect. Specimen 9604A19 contained large air voids in the interface material. Air voids were also observed in the failure surface of Specimen 9604A31. Specimens 9604A27 and 9604A29 did not fail in the lift interface. The remaining two interface tests, 9604A28 and 9604A30, had tensile strengths of 0.78 MPa and 0.72 MPa, respectively, which fall within the data scatter for the specimens without interfaces. However, due to the limited number of valid tests performed, additional experiments should be conducted to quantify the tensile strength properties of the interface material.

The stress difference versus axial strain responses for the tests are plotted in Figure 26. This figure indicates that the specimens with interfaces are less resistant to the shear loading (lower modulus) than are the specimens without interfaces. The last column in Table 6 lists the Young's moduli obtained from the initial portion of these curves. The specimens without an interface have, on average, a Young's modulus of 21.5 GPa, which agrees very well with those determined from the unconfined compression and triaxial compression tests. The average Young's modulus for the specimens with an interface is 15.7 GPa, which is considerably lower than the modulus obtained from the specimens without an interface. Again, additional experiments need to be performed to verify this observation.

Splitting Tension Tests

Results from the seven splitting tension tests are provided in Table 7 and Figure 27. Four of these tests were performed with the loading oriented in the upstream-downstream direction and three tests with the loading in the left-right abutment direction. No statistical difference was observed in the splitting tensile strength between the two directions. On average, the splitting tensile strength of the RCC was 3.3 MPa.

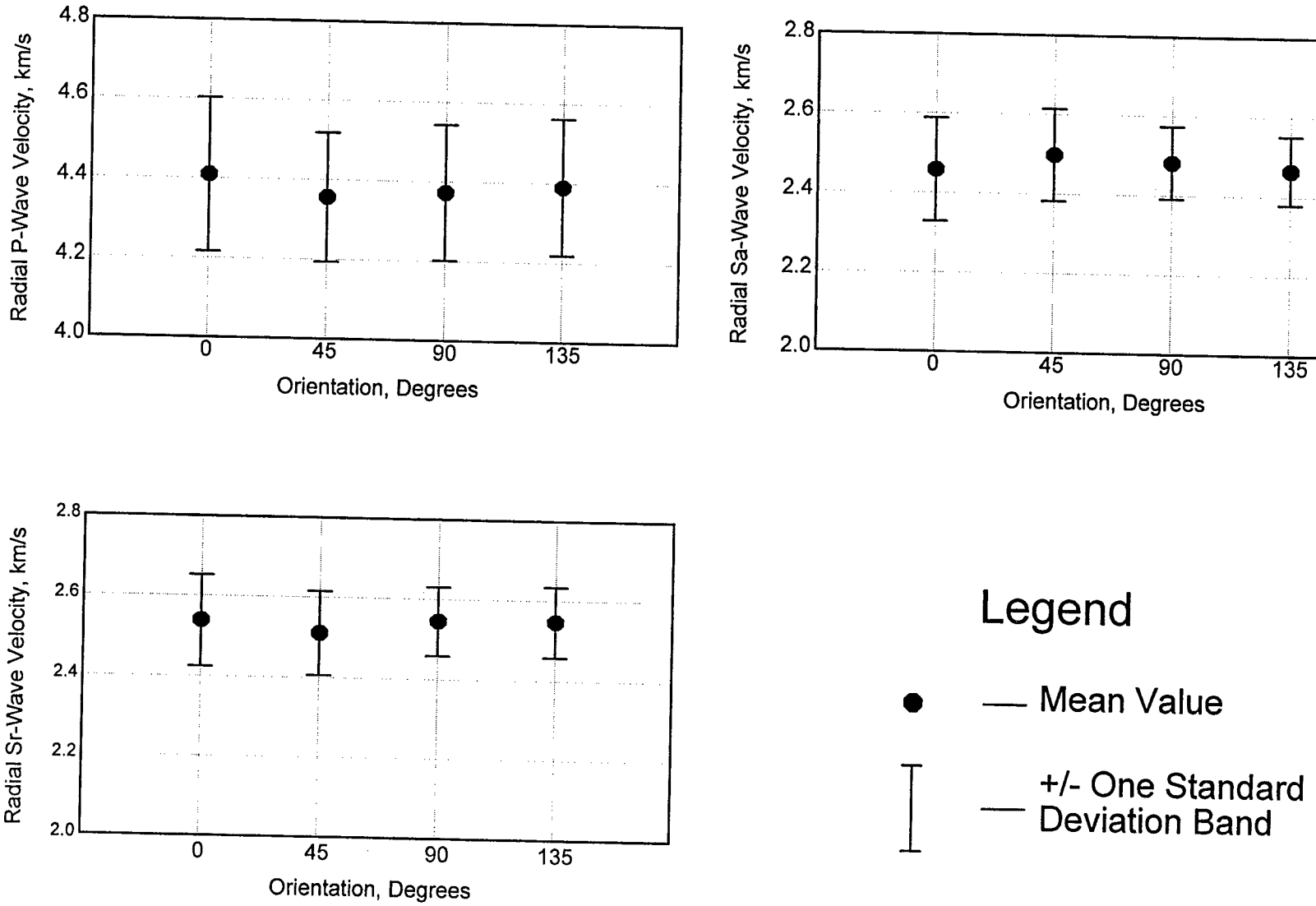

Figure 3. Mean radial P-, Sa-, and Sr-wave velocities with +/- one standard deviation bands for air-dry RCC core samples from boring WDH1

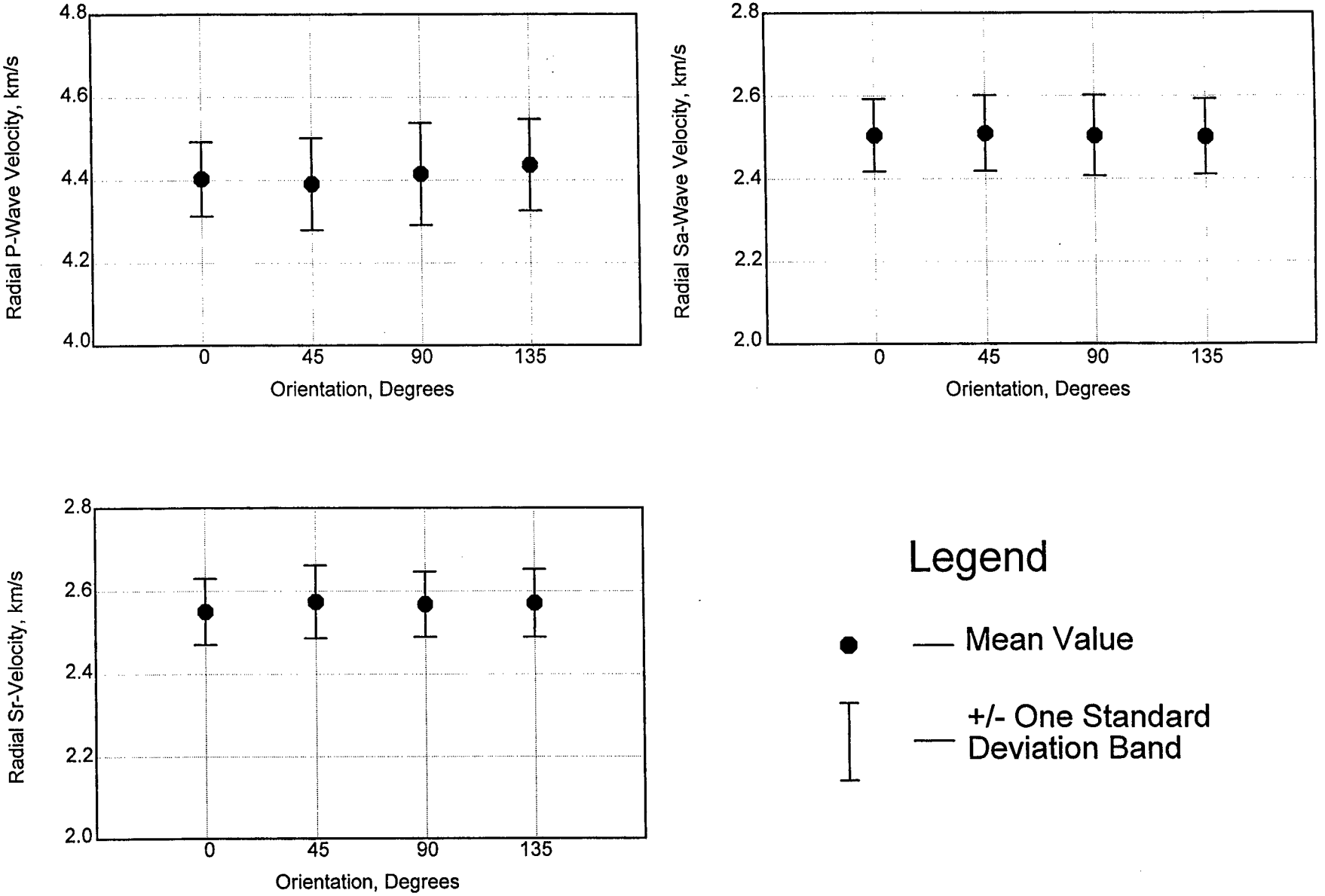

Figure 4. Mean radial P-, Sa-, and Sr-wave velocities with +/- one standard deviation bands for air-dry RCC core samples from boring WDH2

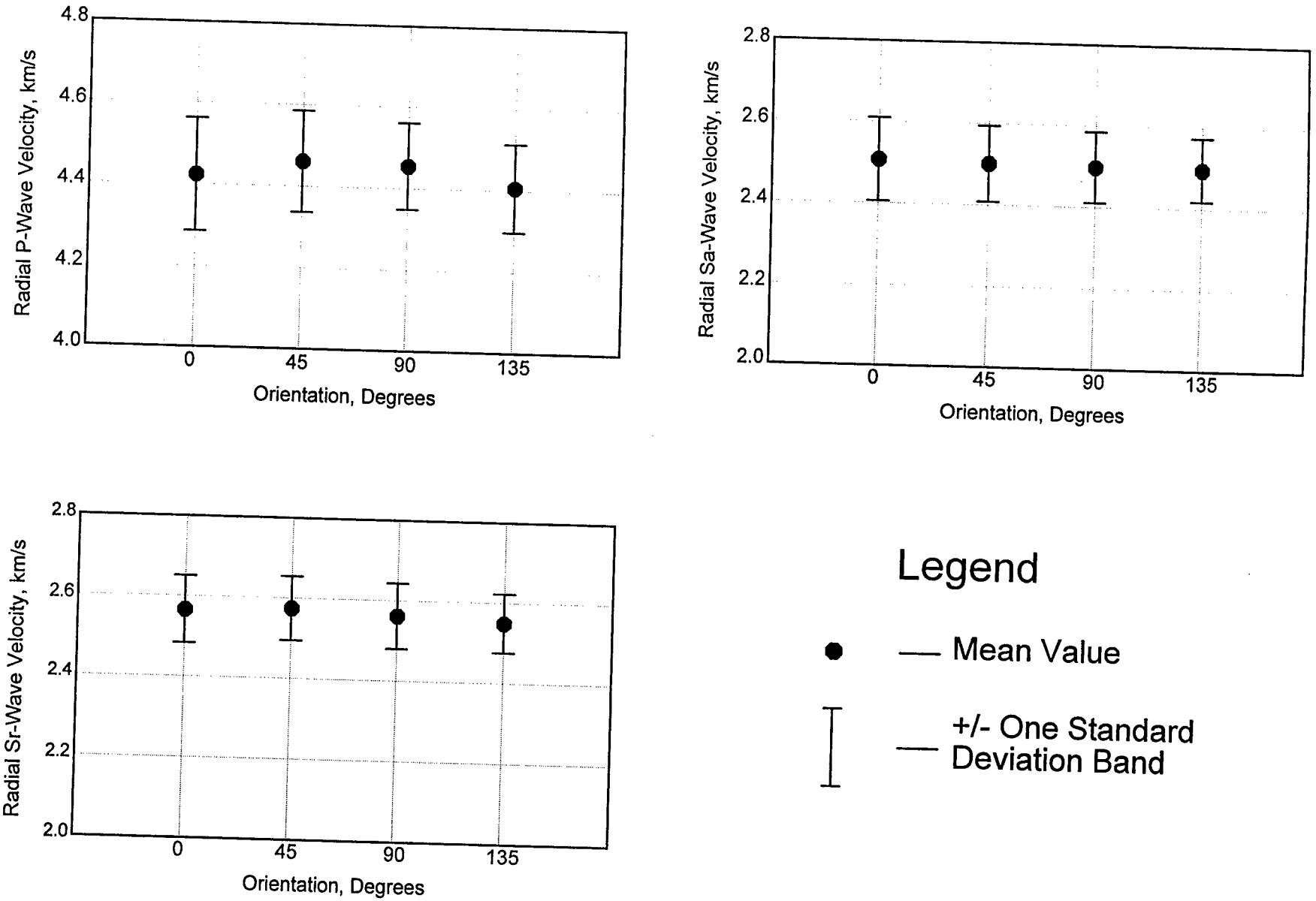

Figure 5. Mean radial P-, Sa-, and Sr-wave velocities with +/- one standard deviation bands for air-dry RCC core samples from boring WDH3

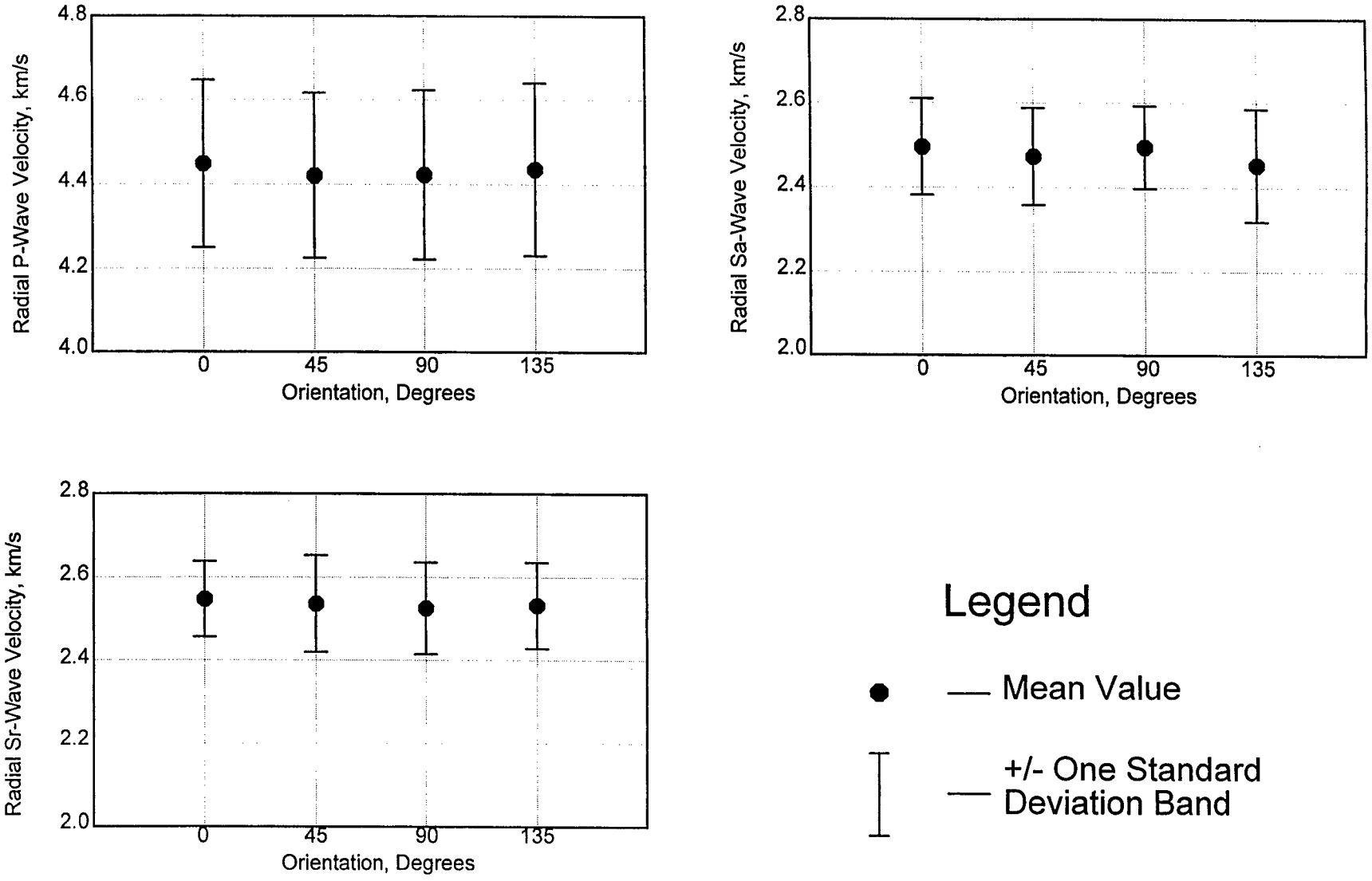

Figure 6. Mean radial P-, Sa-, and Sr-wave velocities with +/- one standard deviation bands for air-dry RCC core samples from boring WDH4

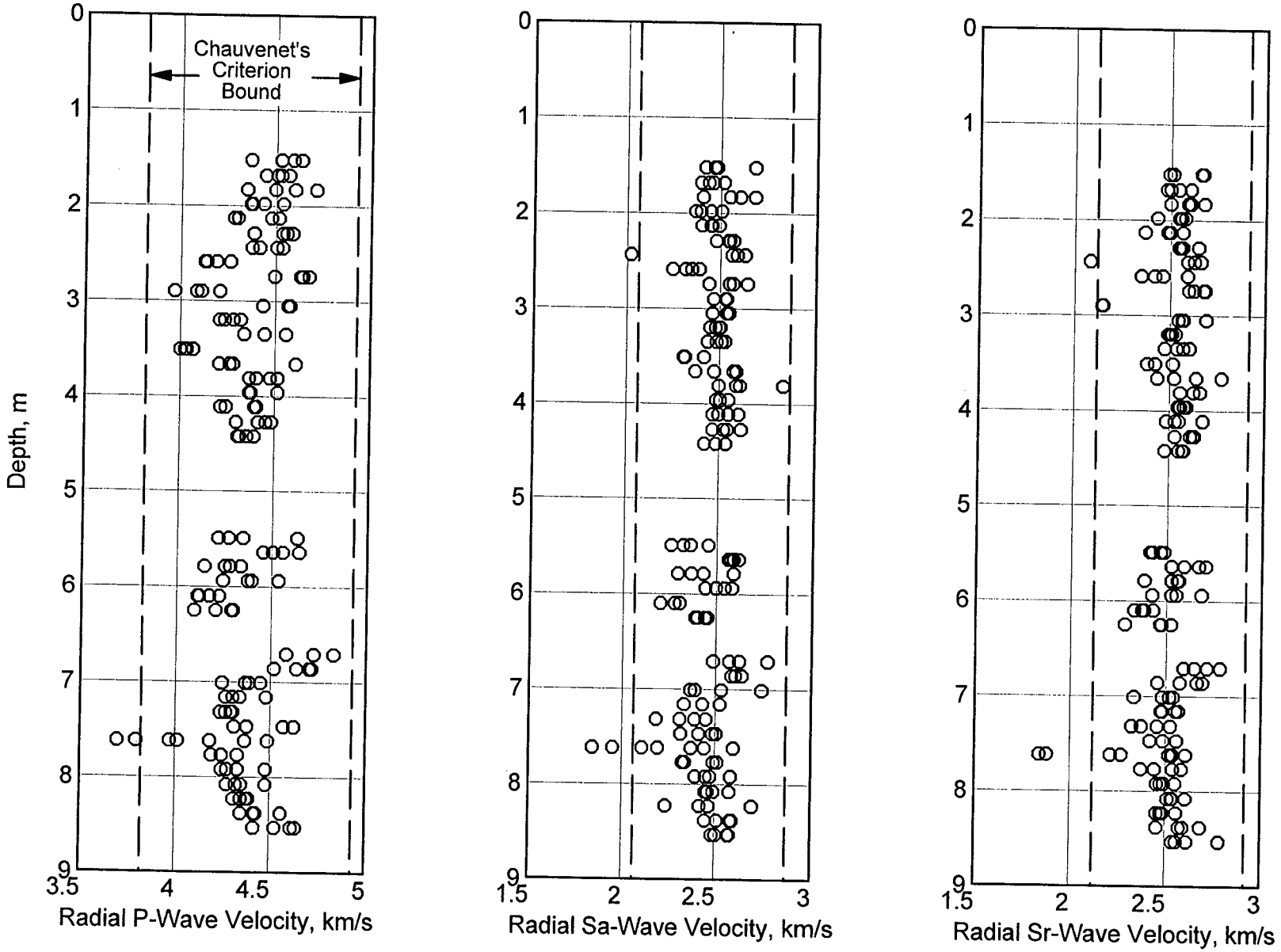

Figure 7. Radial P-, Sa-, and Sr-wave velocity logs for air-dry RCC core samples from boring WDH1

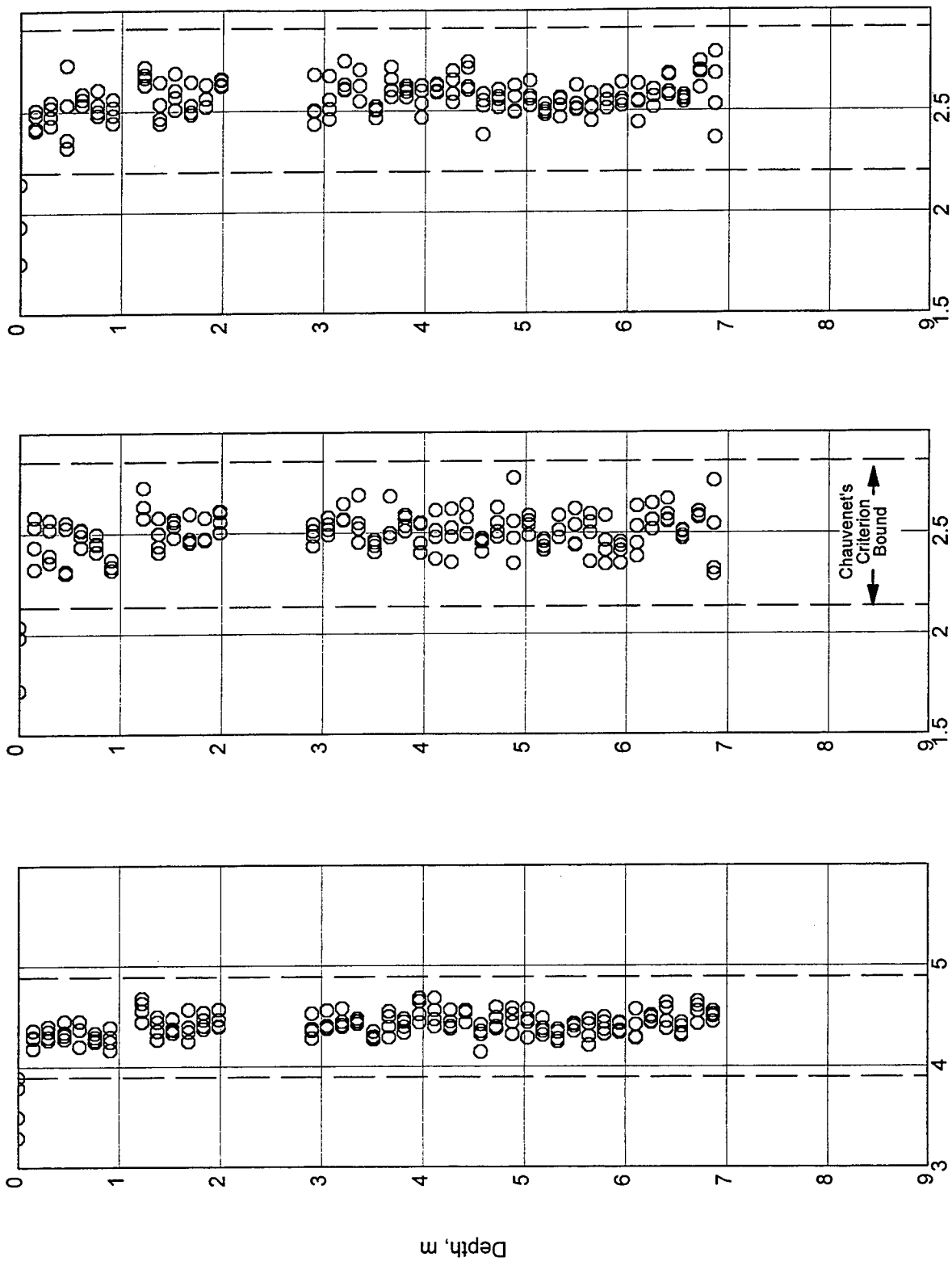

Figure 8. Radial P-, Sa-, and Sr-wave velocity logs for air-dry RCC core samples from boring WDH2

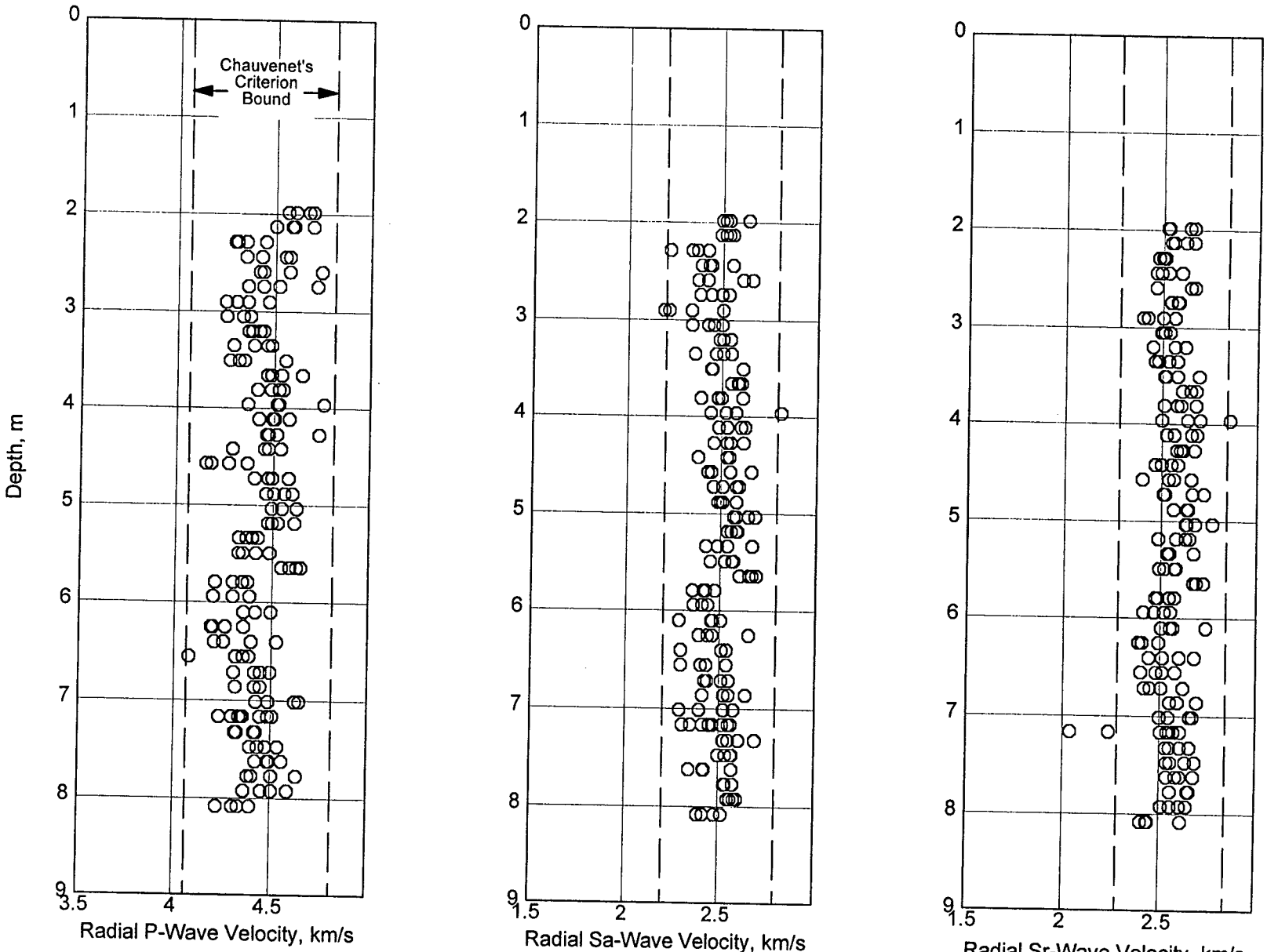

Figure 9. Radial P-, Sa-, and Sr-wave velocity logs for air-dry RCC core samples from boring WDH3

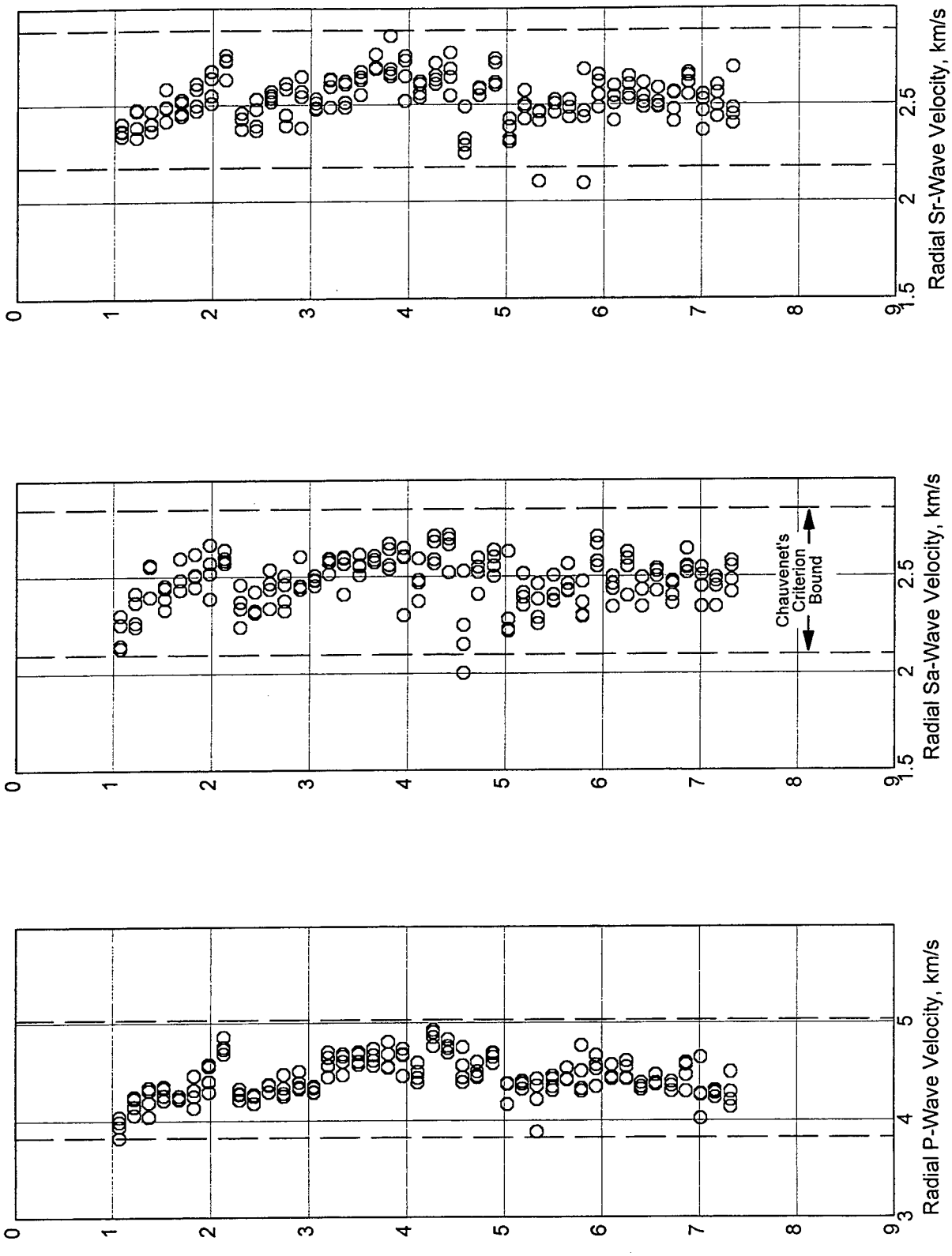

Figure 10. Radial P-, Sa-, and Sr-wave velocity logs for air-dry RCC core samples from boring WDH4

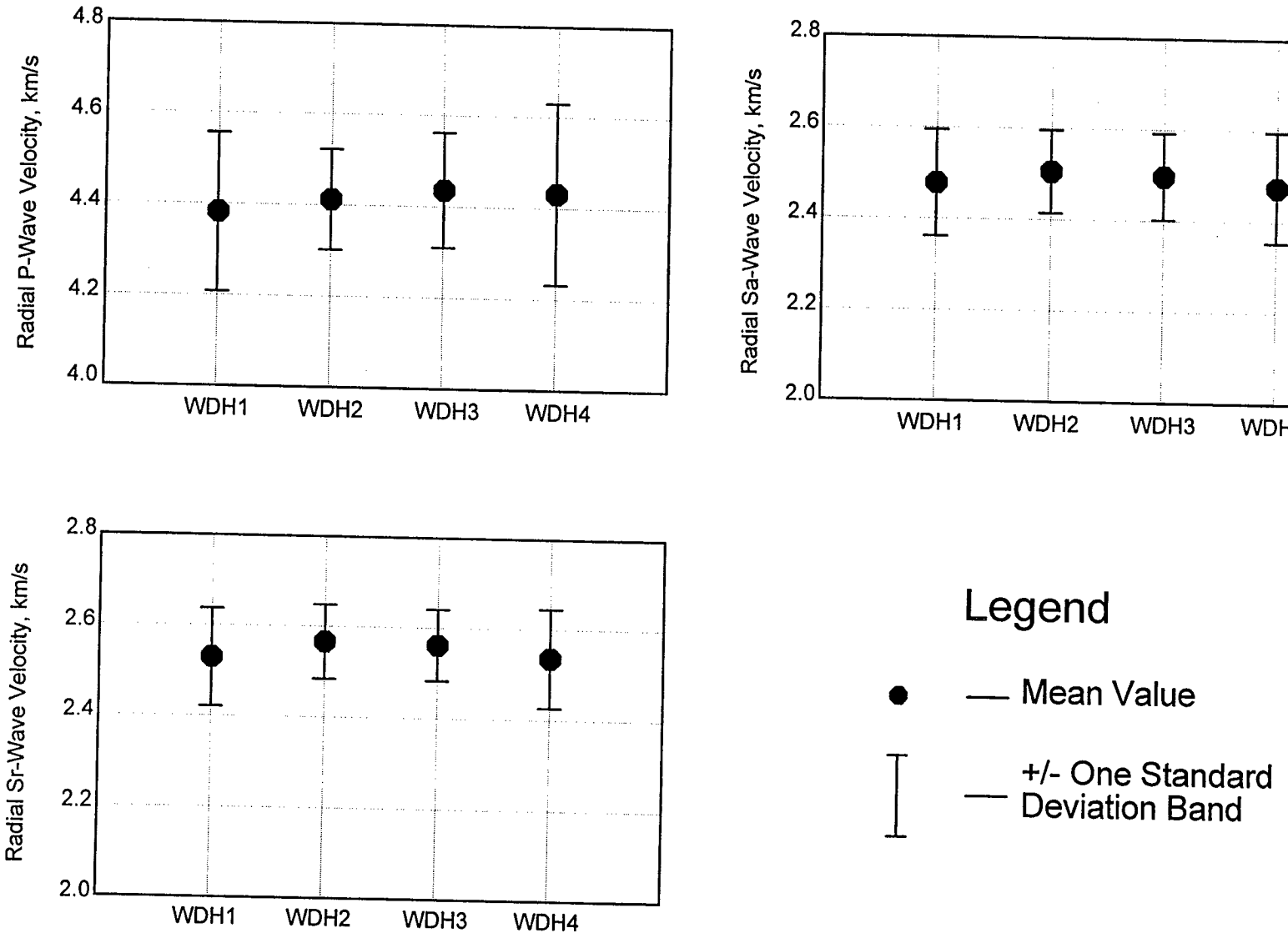

Figure 11. Mean radial P-, Sa-, and Sr-wave velocities with +/- one standard deviation bands for air-dry RCC core samples

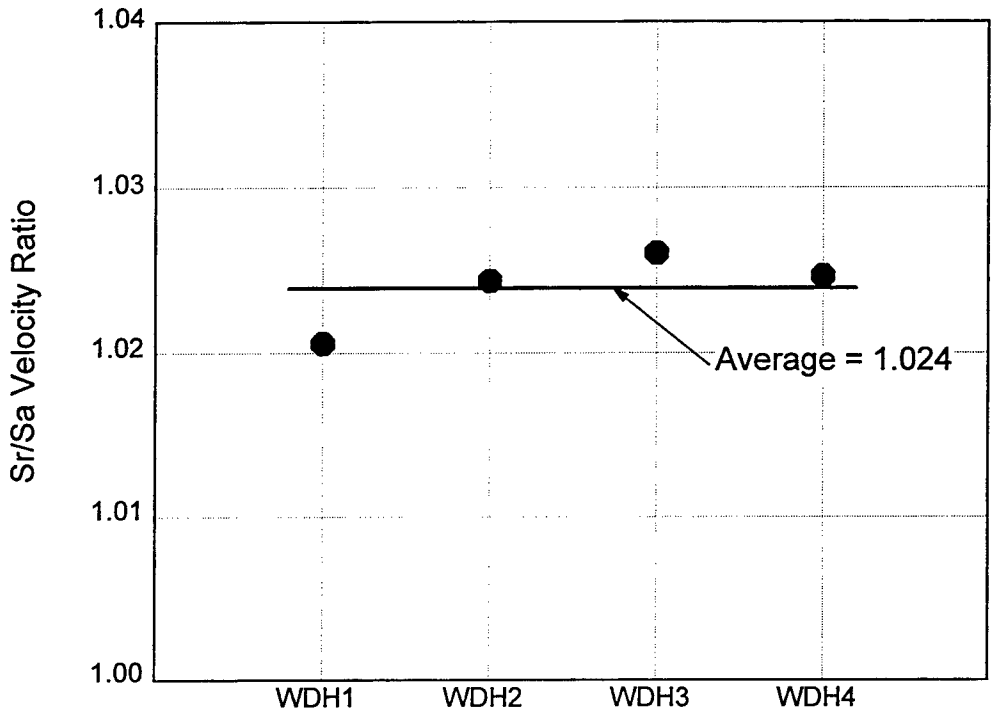

Figure 12. Radial Sr-to-Sa velocity ratios for air-dry RCC core samples

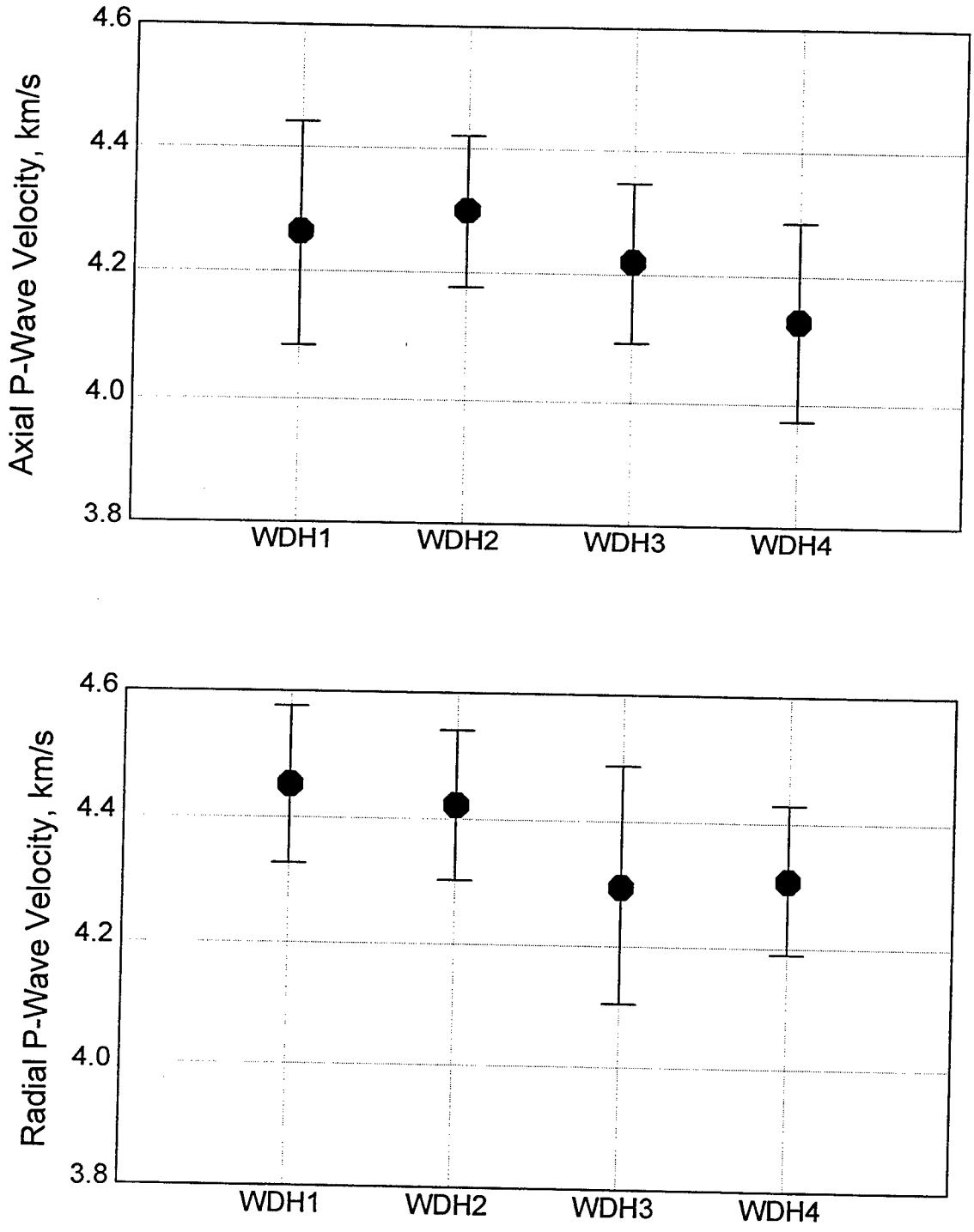

Figure 13. Average axial and radial P-wave velocities with +/- one standard deviation bands for air-dry RCC core samples

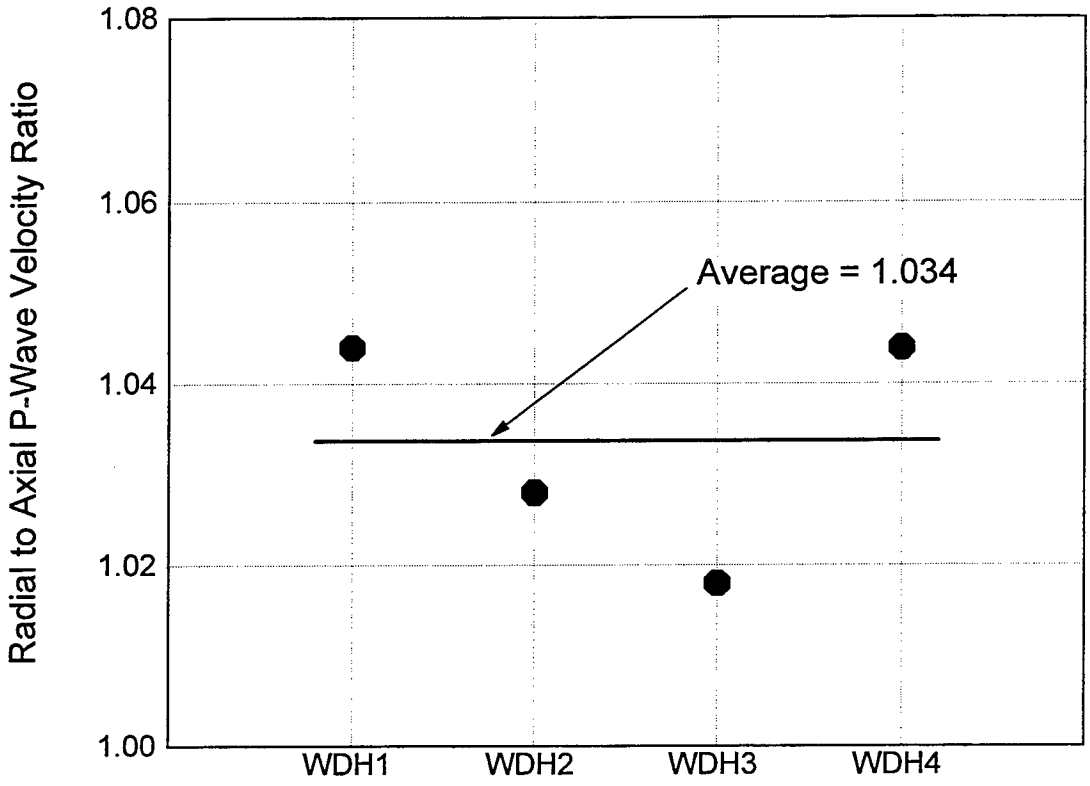

Figure 14. Radial to axial P-wave velocity ratios for air-dry RCC core samples

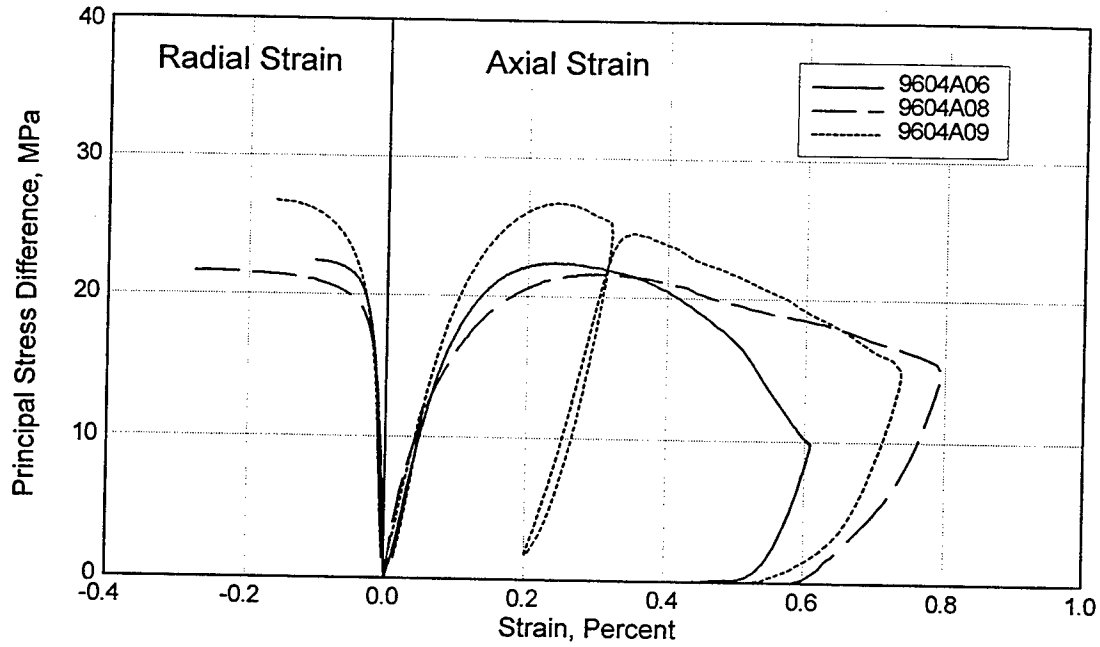

a. Boring WDH1 results

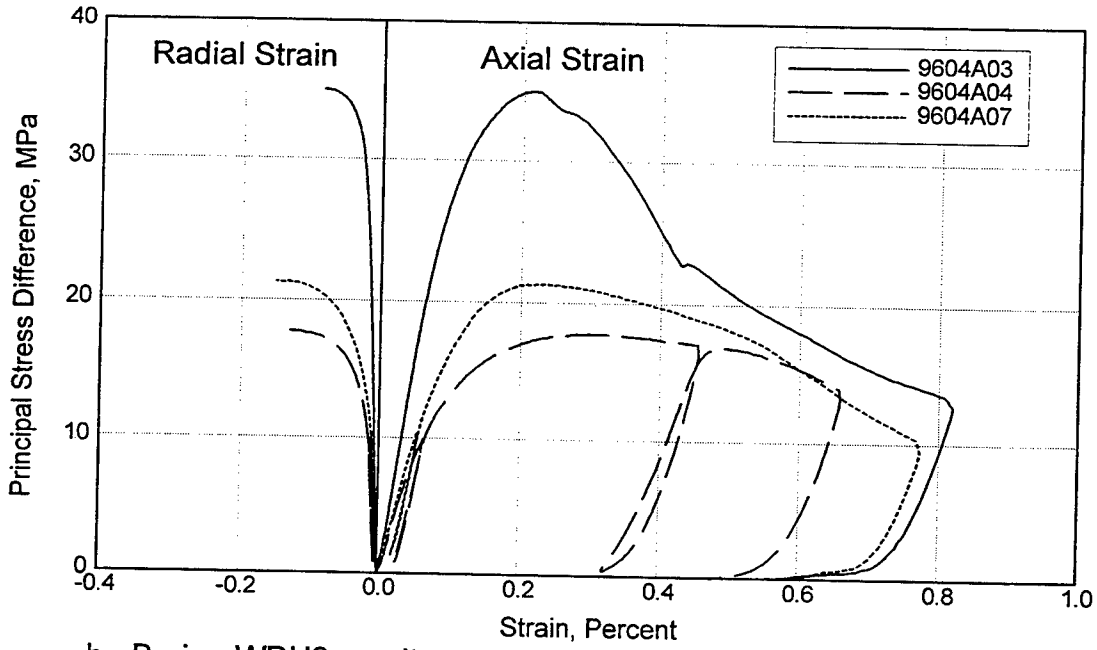

b. Boring WDH2 results

Figure 15. Unconfined compression test results for air-dry RCC specimens from borings WDH1 and WDH2. (Note: To convert stresses from MPa to psi multiply by 145)

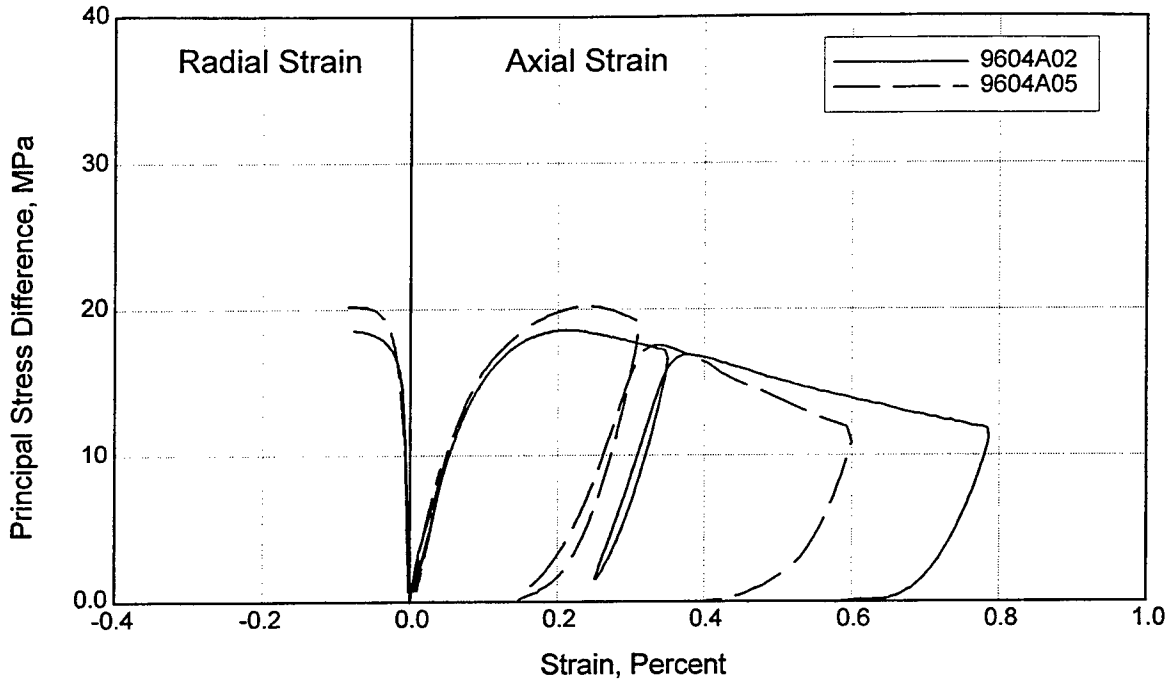

a. Boring WDH3 results

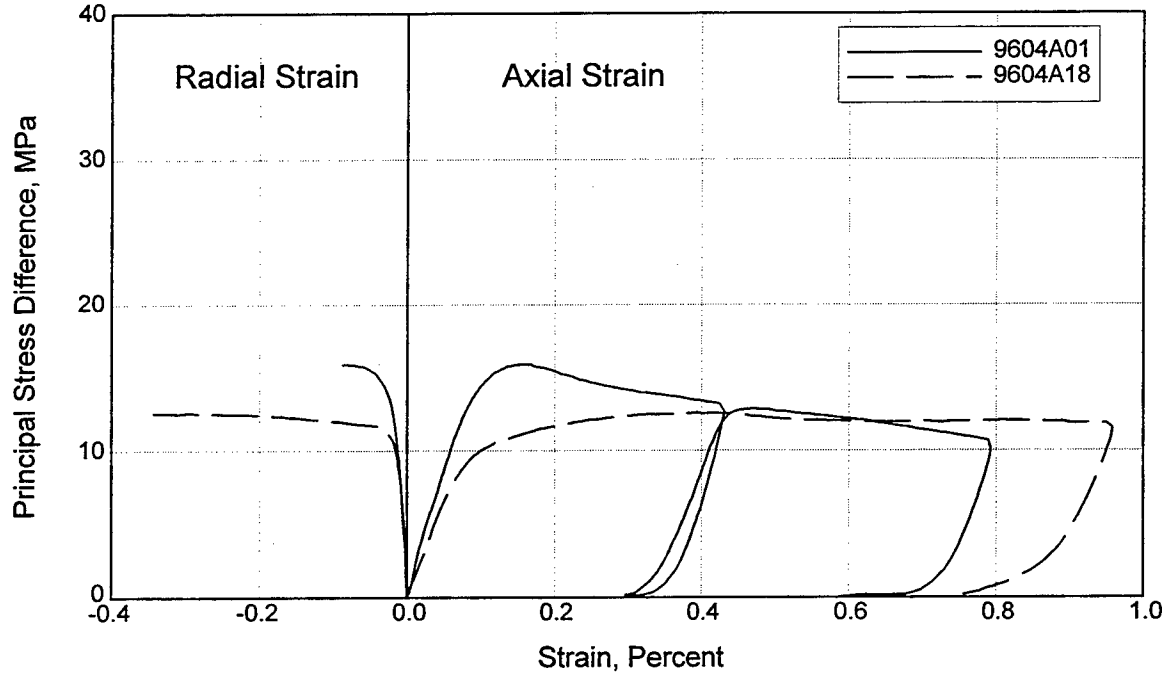

b. Boring WDH4 results

Figure 16. Unconfined compression test results for air-dry RCC specimens from borings WDH3 and WDH4. (Note: To convert stresses from MPa to psi multiply by 145)

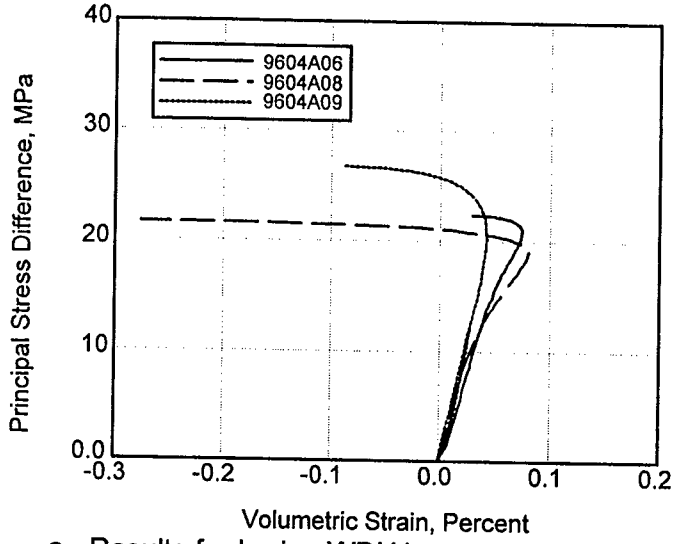

a. Results for boring WDH1

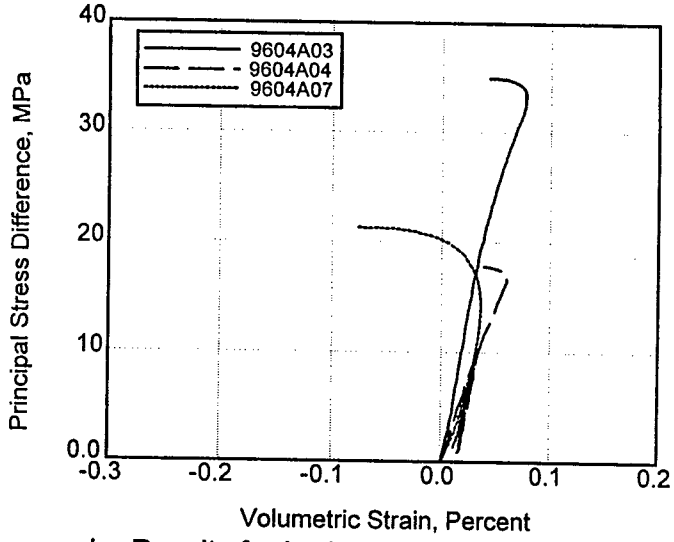

b. Results for boring WDH2

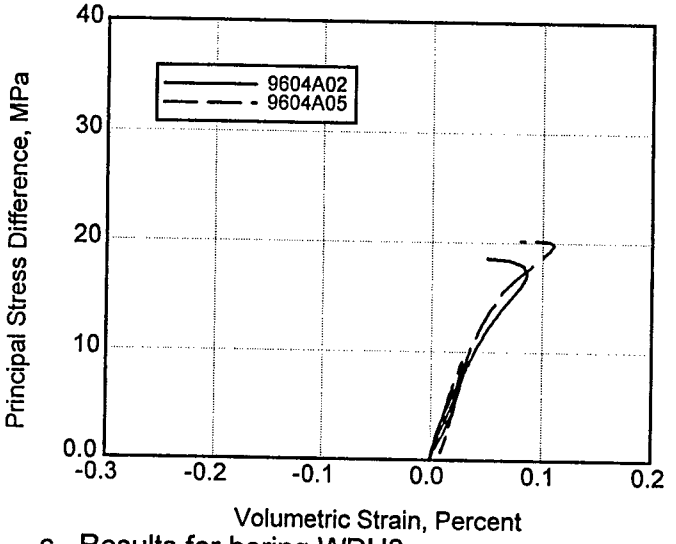

c. Results for boring WDH3

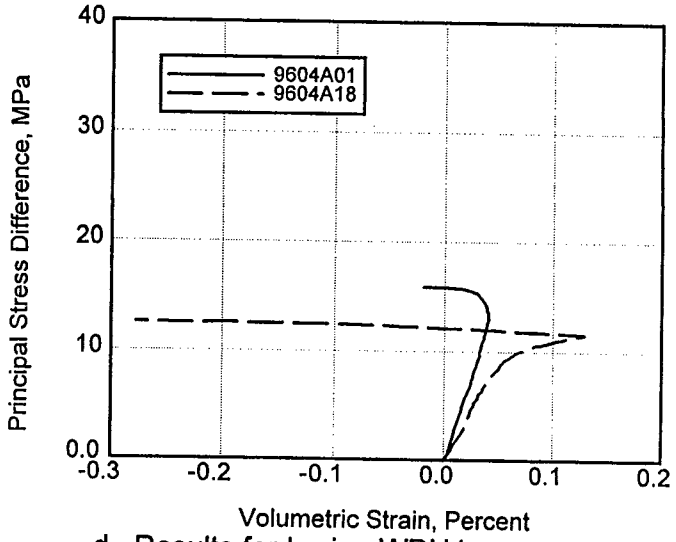

d. Results for boring WDH4

Figure 17. Volumetric responses from suite of unconfined compression tests performed on air-dry RCC specimens. (Note: To convert stresses from MPa to psi multiply by 145)

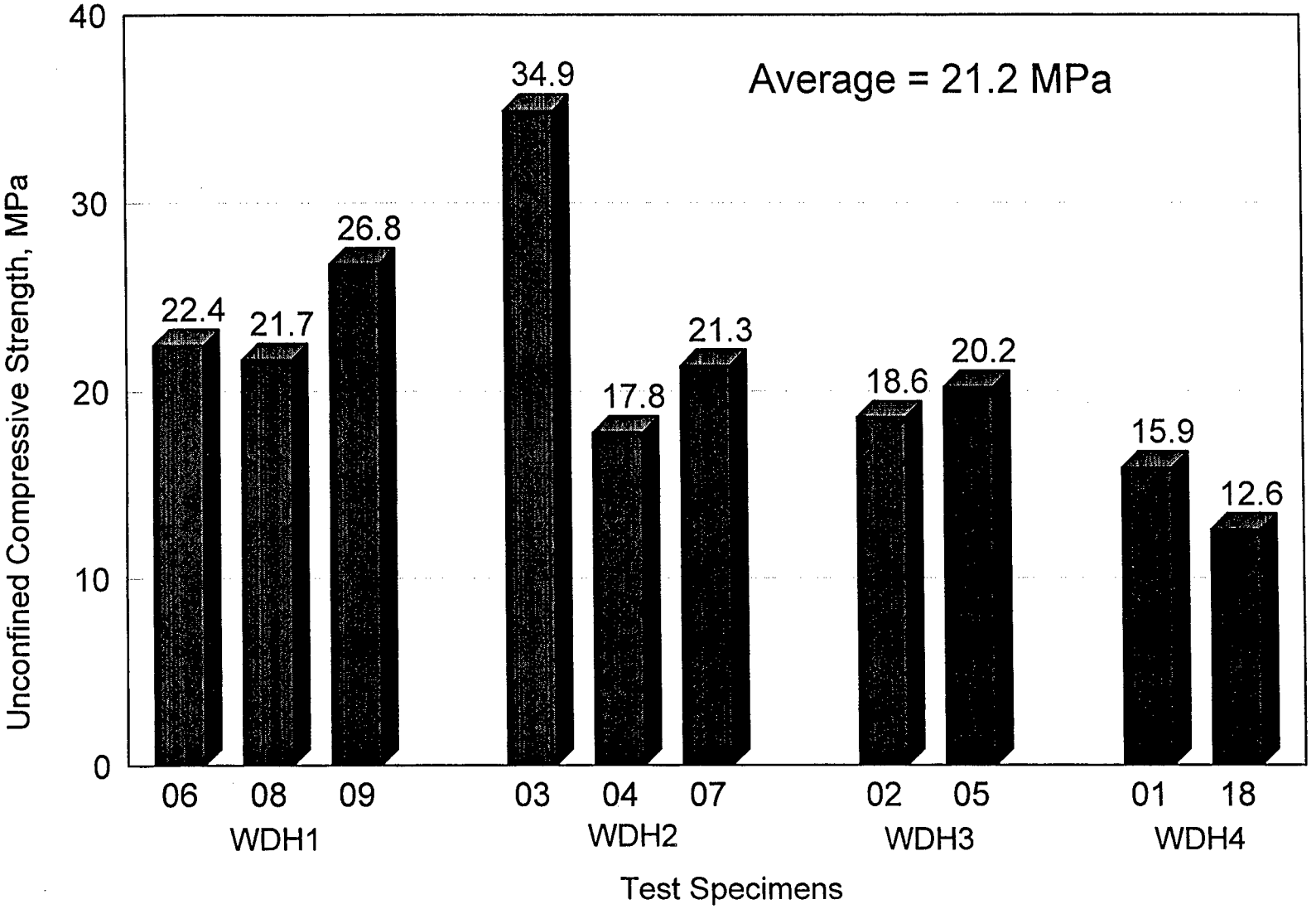

Figure 18. Unconfined compressive strengths for air-dry RCC specimens. (Note: To convert stresses from MPa to psi multiply by 145)

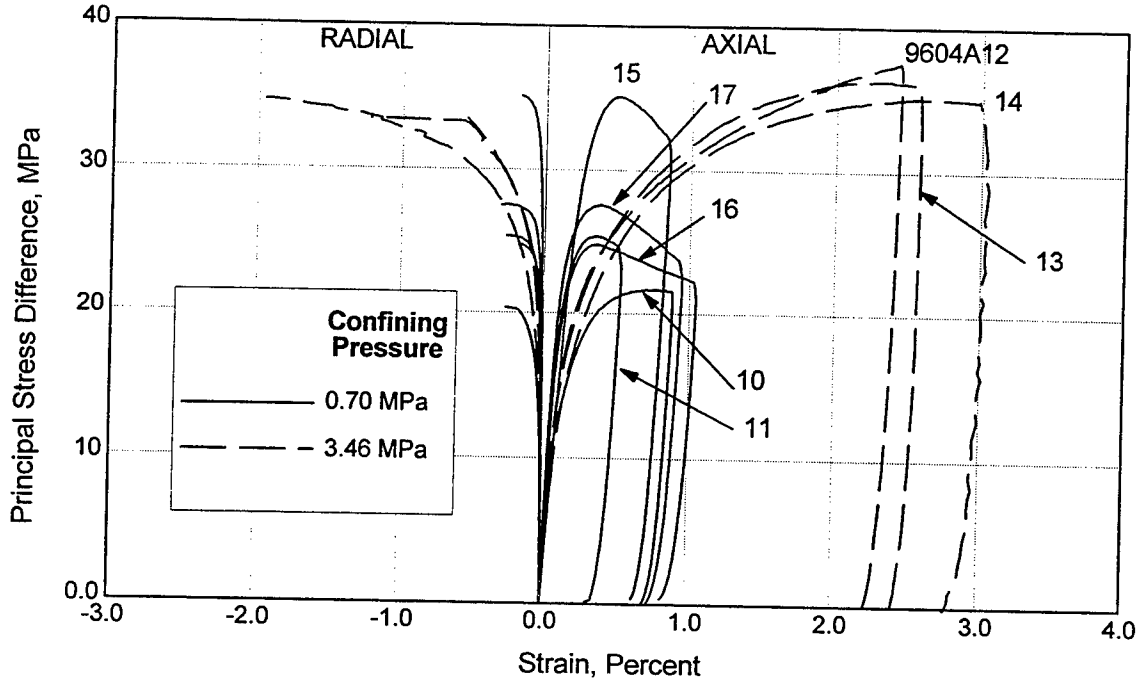

a. Shear responses

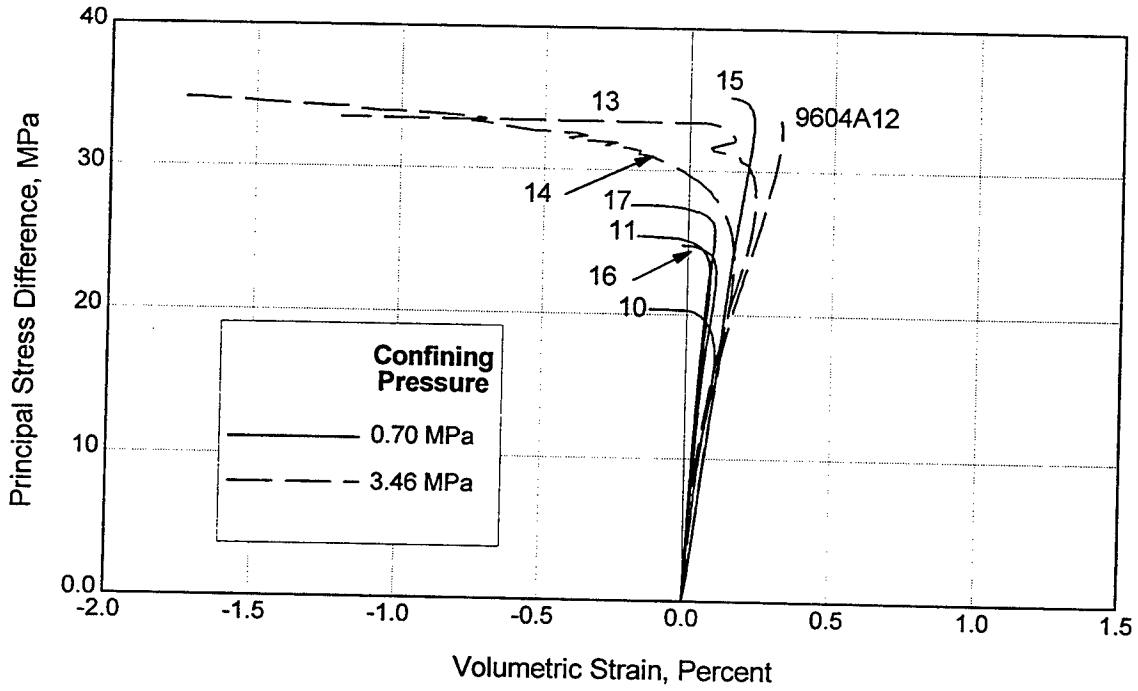

b. Volumetric responses

Figure 19. Triaxial compression test results for air-dry RCC specimens. (Note: To convert stresses from MPa to psi multiply by 145)

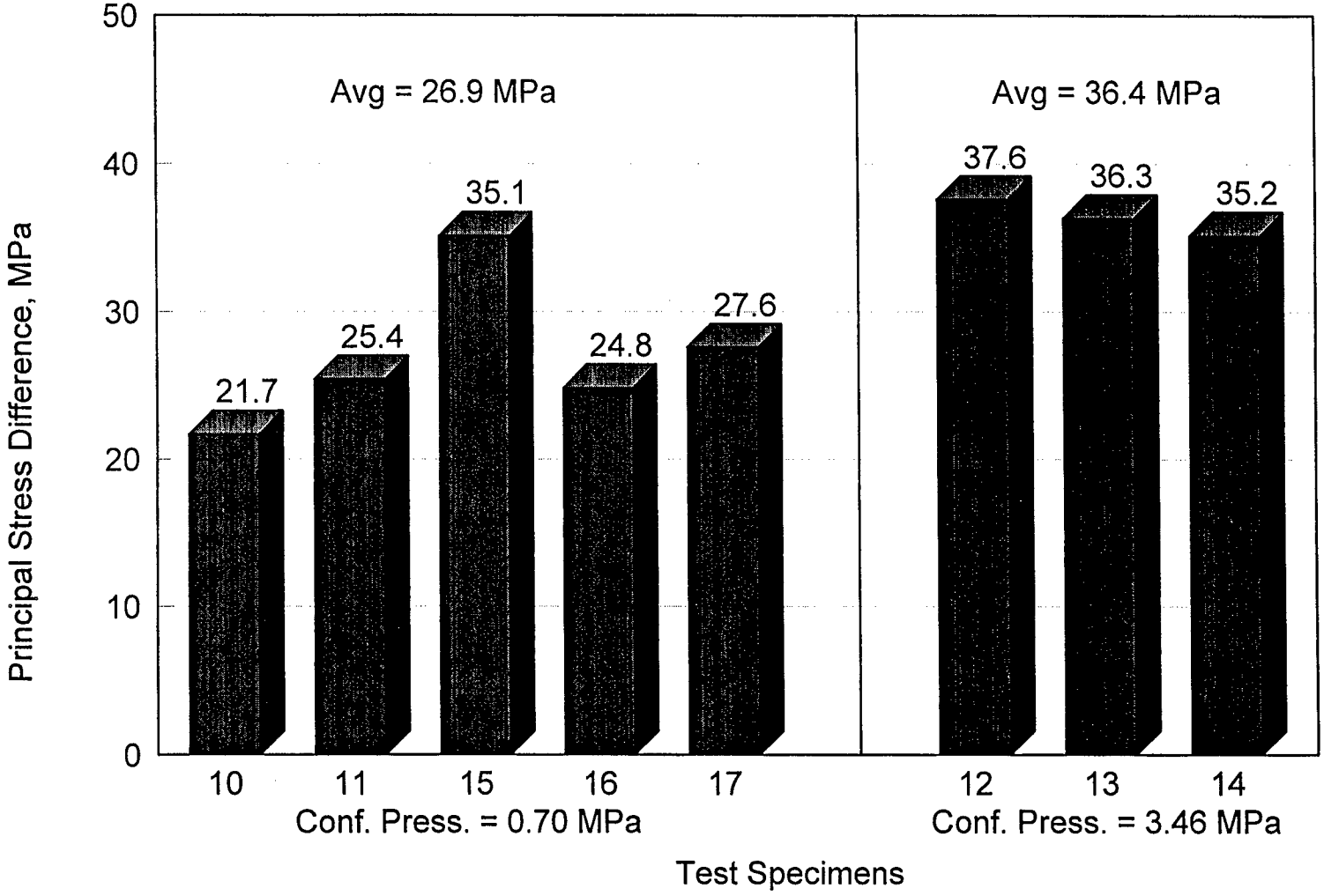

Figure 20. Peak strengths obtained from a suite of triaxial compression tests performed on air-dry RCC test specimens. (Note: To convert stresses from MPa to psi multiply by 145)

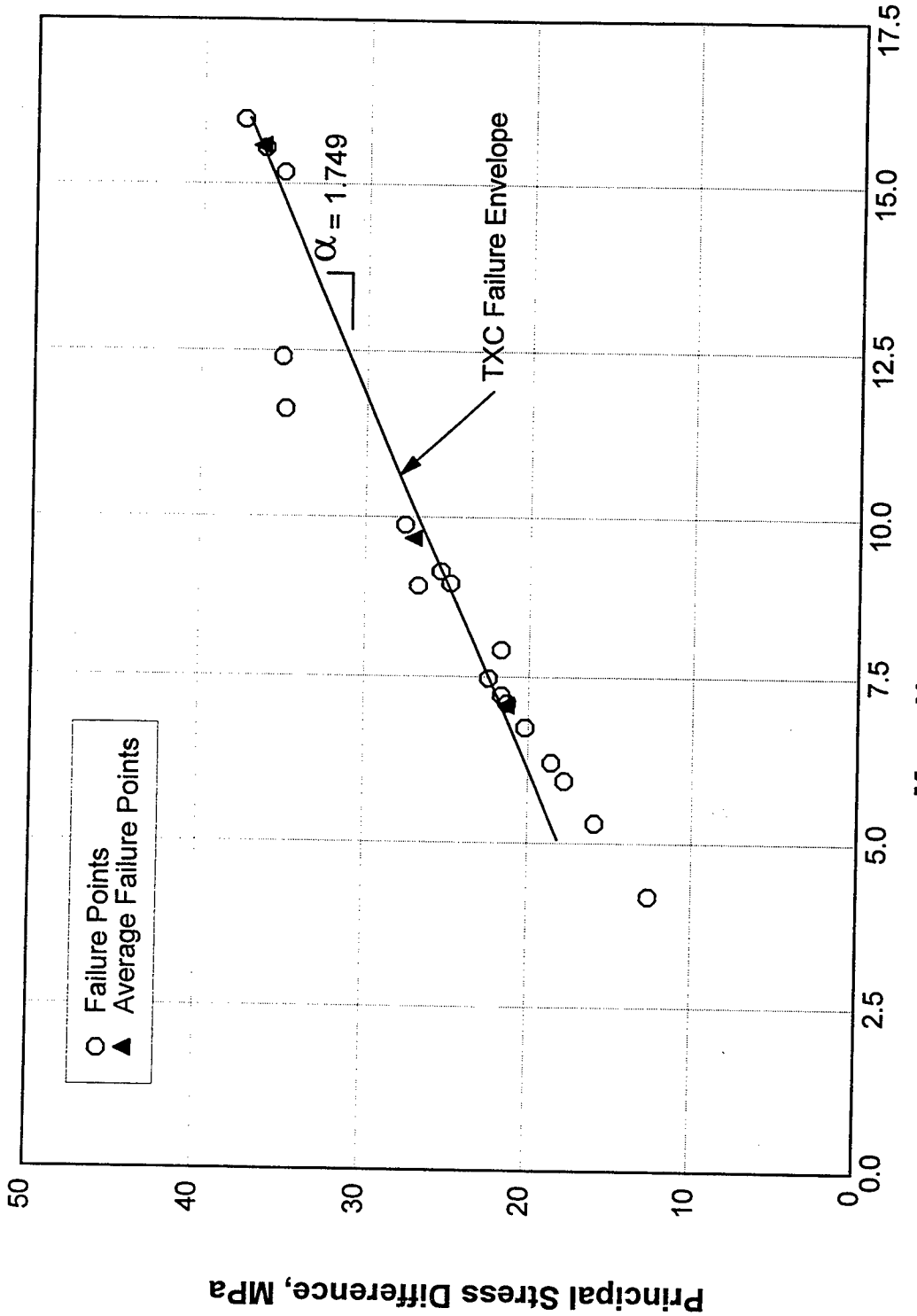

Figure 21. Triaxial compression failure data and envelope for air-dry RCC test specimens. (Note: To convert stresses from MPa to psi multiply by 145)

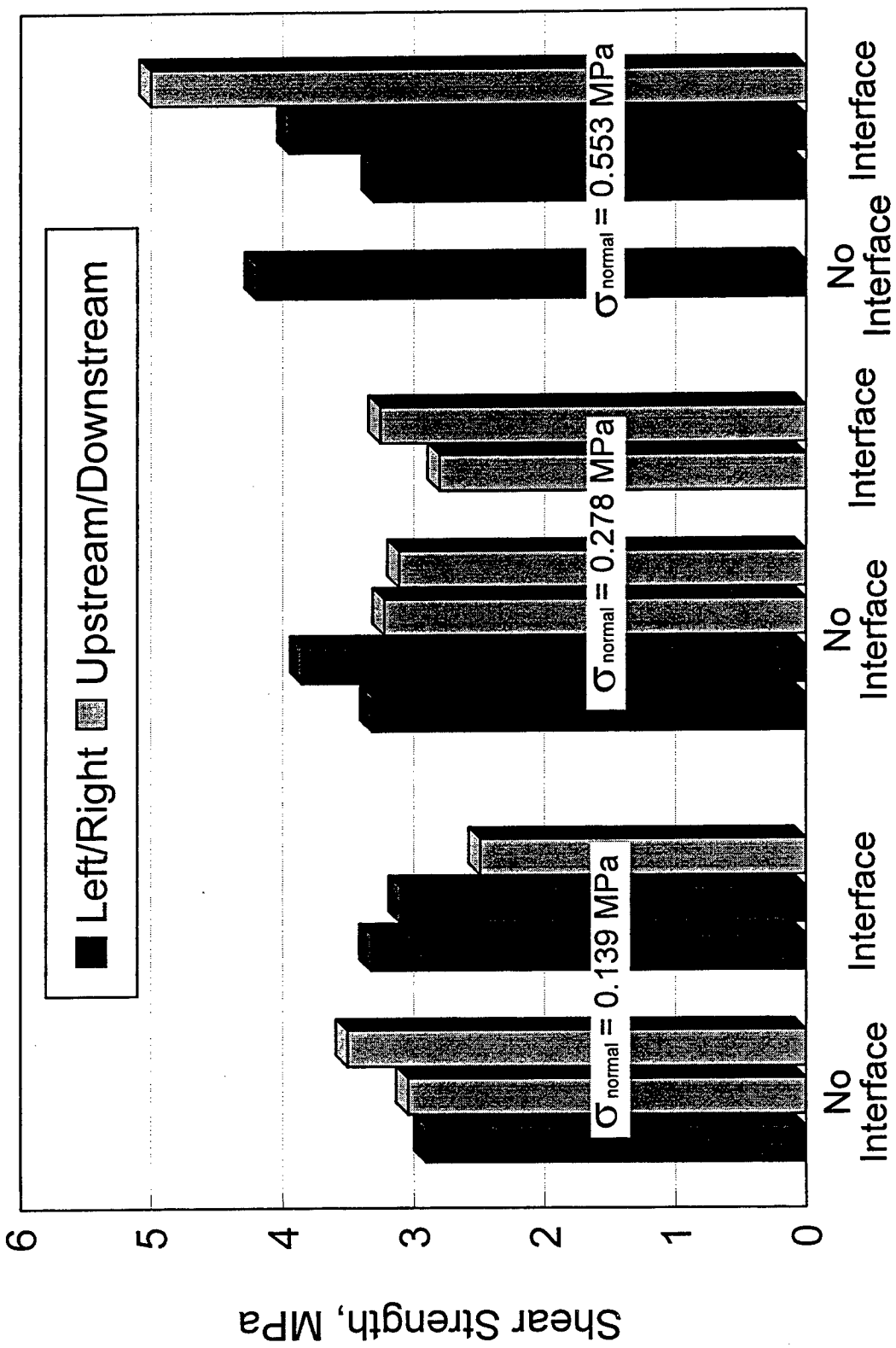

Figure 22. Peak shear strengths from a suite of direct shear tests performed on air-dry RCC test specimens. (Note: To convert stresses from MPa to psi multiply by 145)

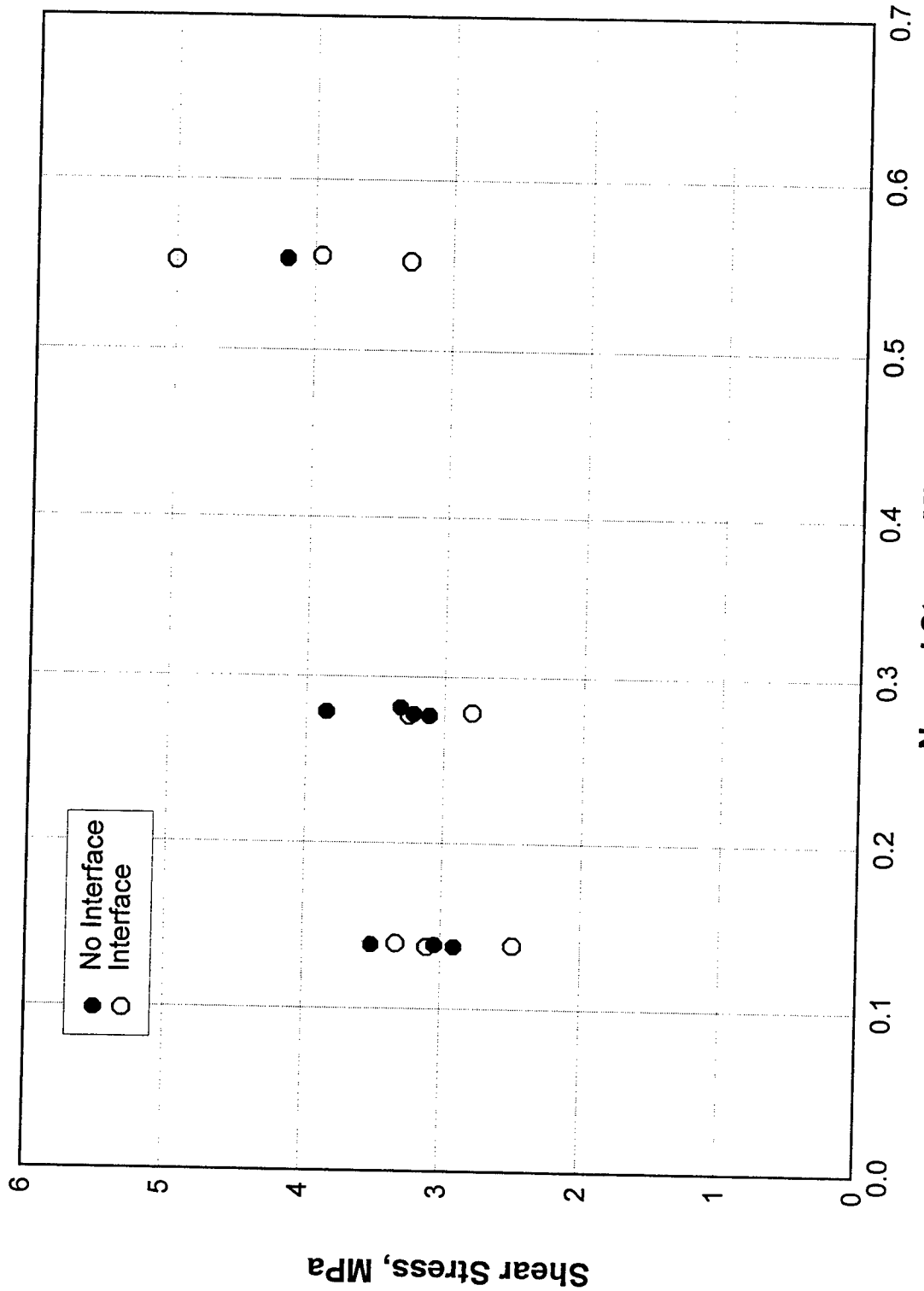

Figure 23. Failure points from a suite of direct shear tests performed on air-dry RCC test specimens. (Note: To convert stresses from MPa to psi multiply by 145)

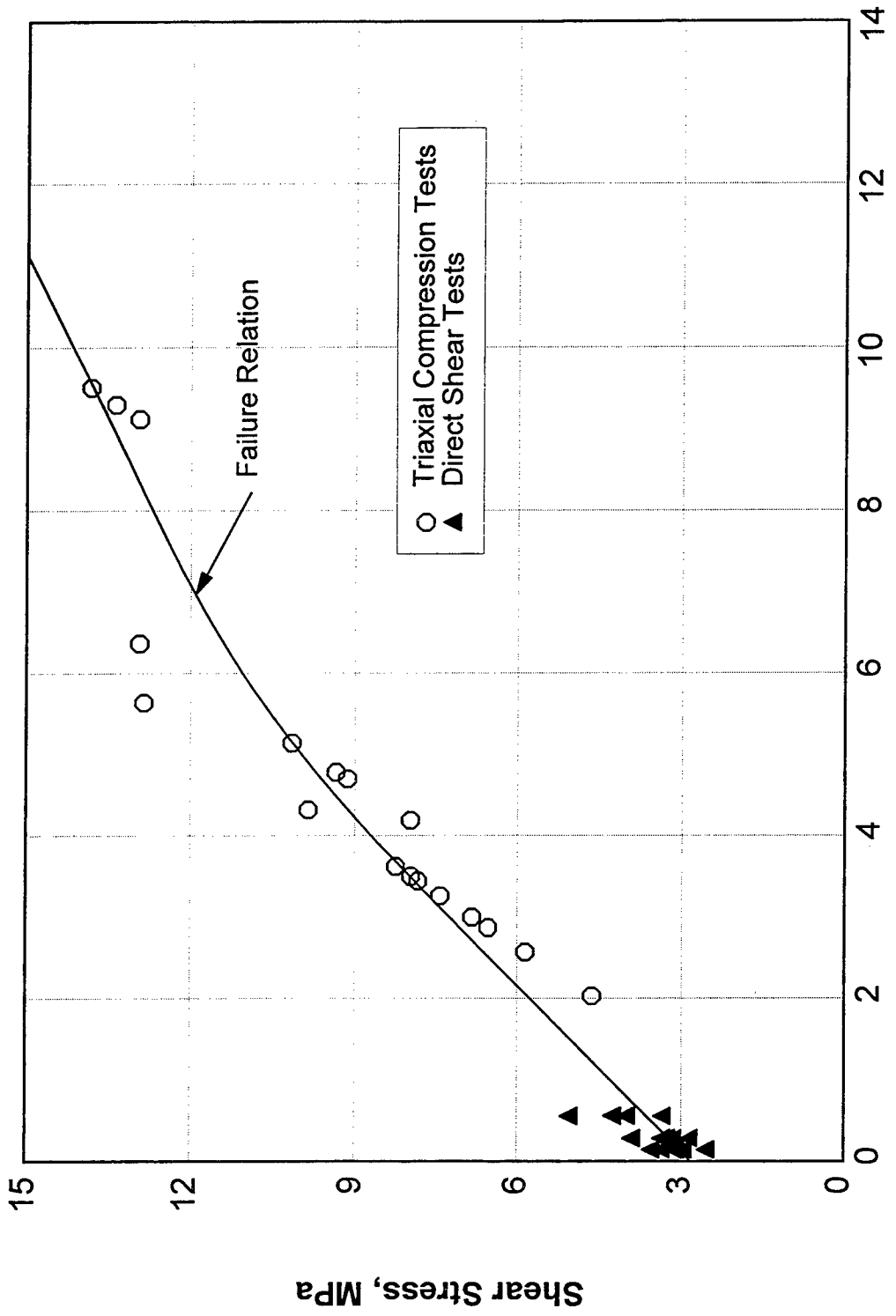

Figure 24. Failure data from triaxial compression and direct shear tests performed on air-dry RCC specimens. (Note: To convert stresses from MPa to psi multiply by 145)

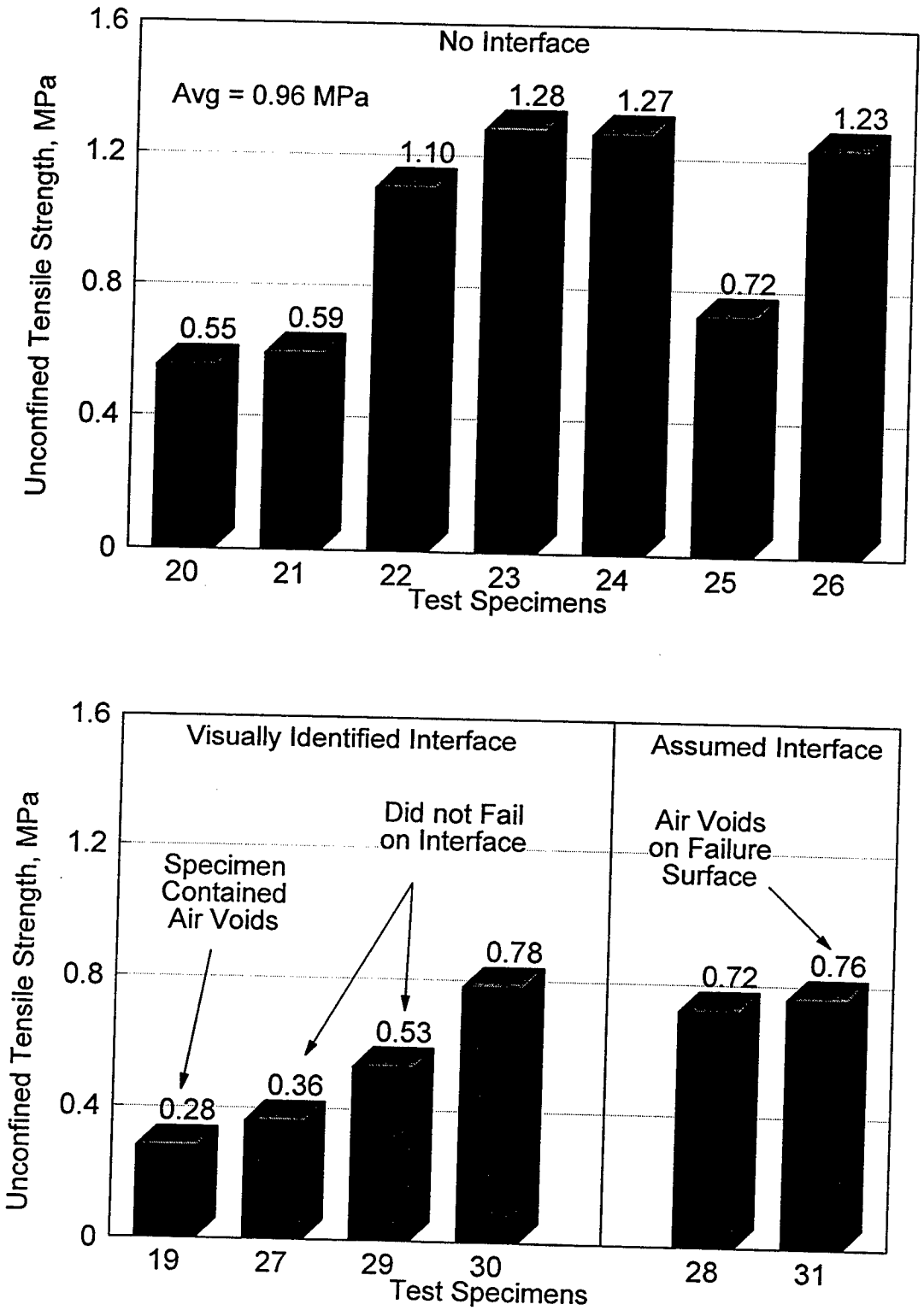

Figure 25. Unconfined (direct-pull) tensile strengths for air-dry RCC specimens. (Note: To convert stresses from MPa to psi multiply by 145)

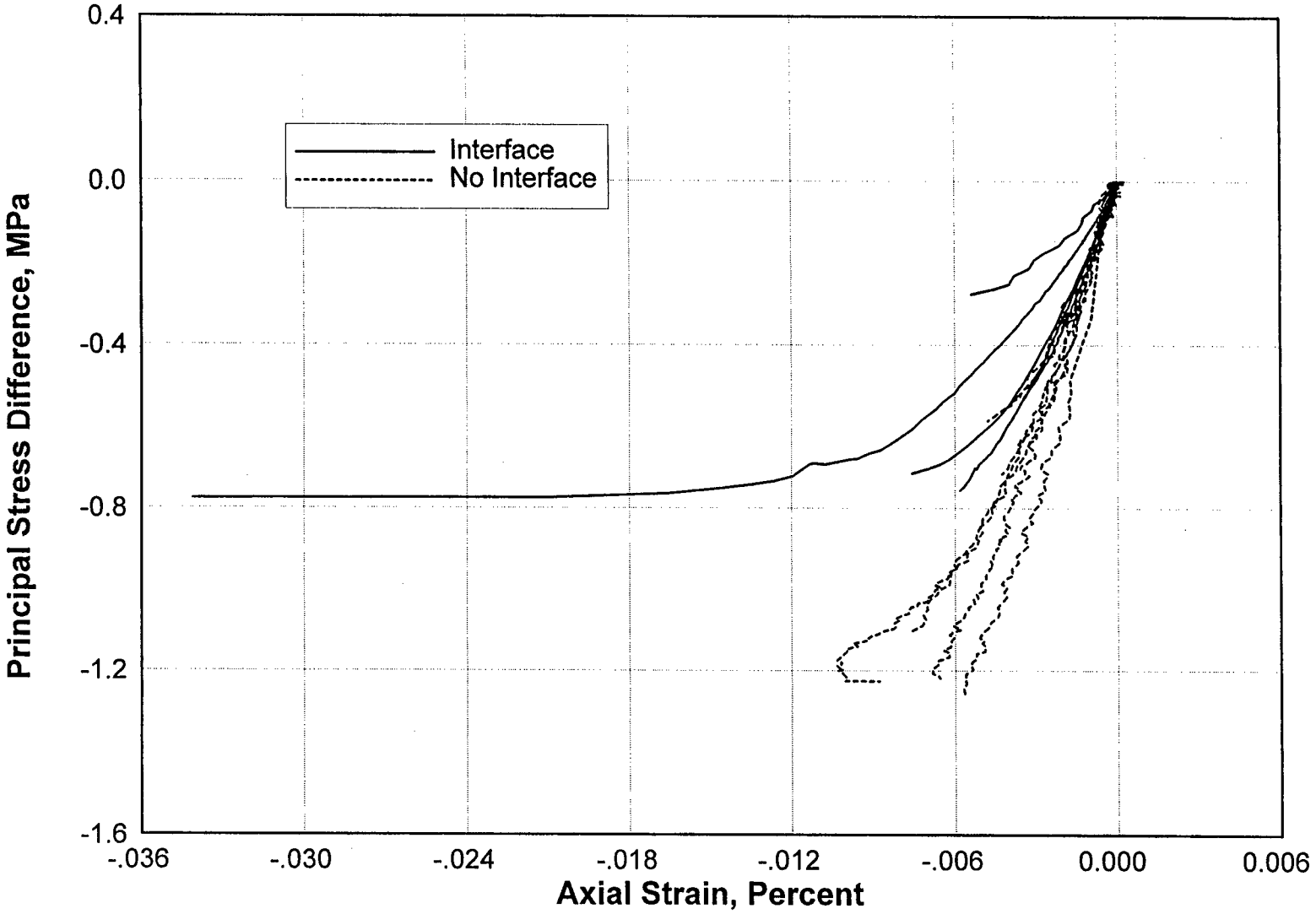

Figure 26. Unconfined (direct-pull) tension test results for air-dry RCC test specimens. (Note: To convert stresses from MPa to psi multiply by 145)

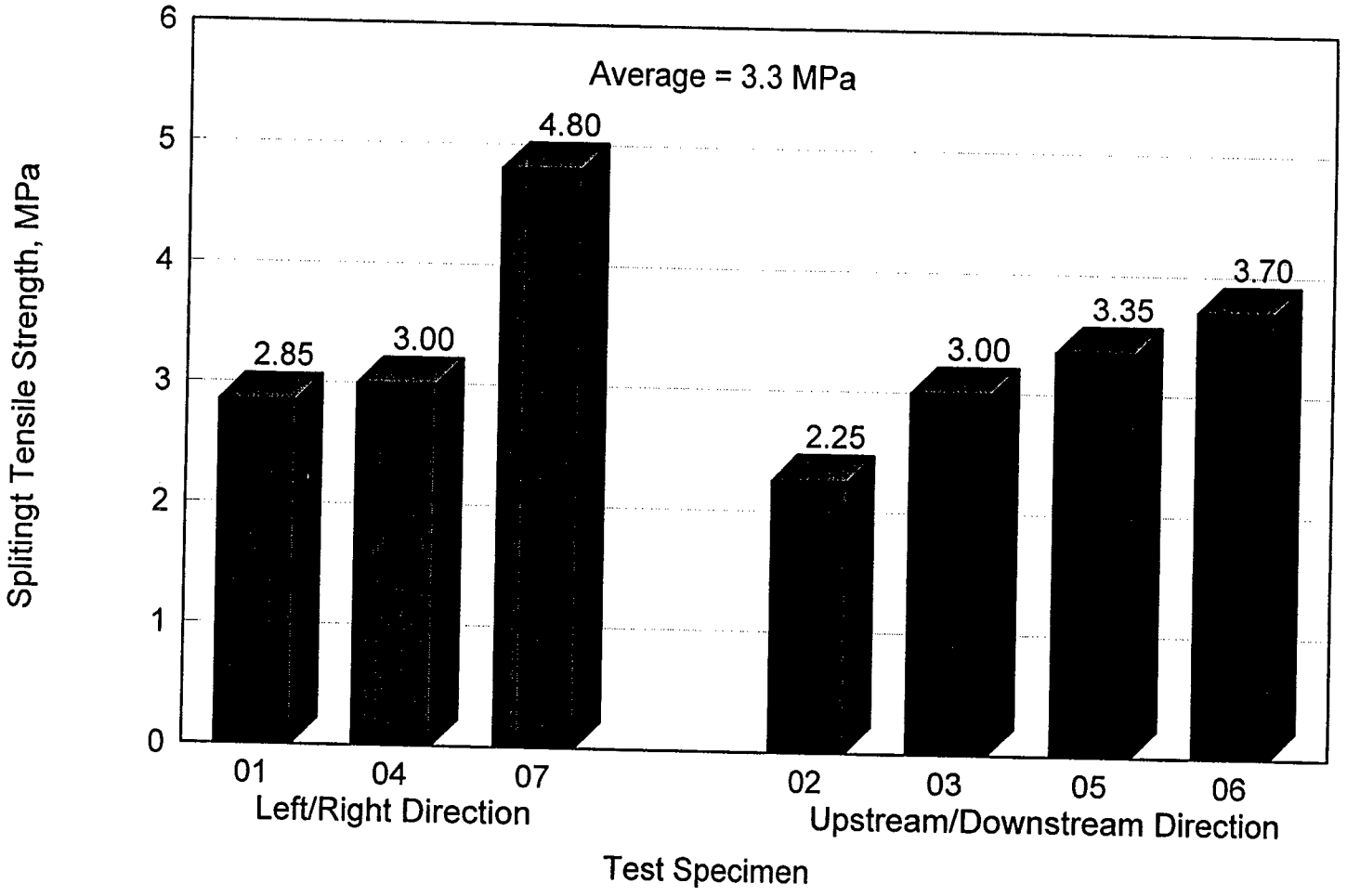

Figure 27. Splitting tensile strengths for air-dry RCC test specimens. (Note: To convert stresses from MPa to psi multiply by 145)

4 Summary

Fifty-four mechanical property tests were performed on air-dry specimens of roller-compacted concrete (RCC) obtained from the main Elk Creek Dam at Trail, Oregon, to characterize the strength and constitutive properties of the concrete. The test matrix included 10 unconfined compression, 13 unconfined tension (direct-pull), 8 triaxial compression, 16 direct shear, and 7 splitting tensile strength tests. Approximately one-half of the direct shear and unconfined tension tests were performed for the purpose of characterizing the strength properties of the interfaces between the RCC lifts. All of the tests were performed quasi-statically.

Prior to performing the mechanical property tests, an extensive suite of nondestructive pulse velocity tests were performed on the cores to assess the degree of anisotropy in the RCC. Numerous P- (compressional), Sa- (shear waves vibrating in the axial plane), and Sr- (shear waves vibrating in a radial or cross-axis plane) wave speeds were measured radially through the core with propagation directions oriented 0, 45, 90, and 135 deg from the right-abutment side of the dam core. Furthermore, axial P- and Sa-wave velocities were determined for each mechanical property test specimen prior to being mechanically deformed. Statistical analysis of the wave-speed data revealed that the velocity data were independent of propagation direction, i.e., isotropic behavior in the radial plane. However, radial Sr waves propagated through the RCC, on average, 2.4 percent faster than did the radial Sa waves. Radial P waves propagated 3.4 percent faster than did the axial P waves.

Results from the unconfined compression tests are summarized in Table 3 and Figures 15-18. On average, the concrete had an unconfined compressive strength of 21.2 MPa, a Poisson's ratio of 0.19, and Young's modulus of 21.6 GPa.

The triaxial compression and the direct shear test results are summarized in Tables 4 and 5 and Figures 19-24. The strength data derived from these tests and the unconfined compression tests were used to construct the most representative failure envelope for the RCC. As shown in Figure 24, this envelope is linear up to a normal stress of about 4 MPa with a C (cohesion) of 2.82 MPa and ϕ (angle of internal friction) of 55.7 deg. For normal stresses between 4 and 7 MPa, the envelope is nonlinear and concave to the normal stress

axis. For normal stresses greater than 7 MPa, the curve is again linear with a ϕ of 36.7 deg. The stress-strain data from the triaxial compression tests yielded a Young's modulus of 21.9 GPa and a Poisson's ratio of 0.15. One-half of the direct shear specimens contained a lift interface and one-half did not. The specimens sheared along a lift interface were as strong as the specimens without an interface.

Results from the unconfined (direct-pull) tension tests are summarized in Table 6 and Figures 25 and 26. On average, the RCC test specimens had a tensile strength of 0.96 MPa, which yielded an unconfined tensile to compressive strength ratio of about 4.5 percent. Results from four of the six tests performed on specimens with lift interfaces were suspect. Two of the four specimens contained air voids in the interface material. The other two specimens failed in the RCC material and not in the lift interface. The two valid tests yielded tensile strengths of 0.78 and 0.72 MPa which fall within the data scatter for the specimens without interfaces. The specimens without an interface have, on average, a Young's modulus of 21.5 GPa, which agrees very well with those determined fom the unconfined compression and triaxial compression tests. The specimens with interfaces had a lower Young's modulus (on average) of 15.7 GPa. However, due to the limited number of valid tests performed, additional experiments should be performed to better quantify the tensile strength properties of the interface material.

The splitting tension test results are provided in Table 7 and Figure 27. On average, the splitting tensile strength of the RCC was 3.3 MPa.

References

Al-Hussaini, M. M., and Townsend, F. C. (1973). "Tensile testing of soils: A literature review," Miscellaneous Paper S-73-24, U.S. Army Engineer Waterways Experiment Station, Vicksburg, MS.

American Society for Testing and Materials. (1991). Designation E 380-91a. "Standard practice for use of the international system of units (the modernized metric system)." Philadelphia, PA

American Society for Testing and Materials. (1996). *1996 Annual Book of ASTM Standards*, Philadelphia, PA.

a. Designation C 39-86. "Standard test method for compressive strength of concrete specimens."

b. Designation C 42-90. "Standard test method for obtaining and testing drilled cores and sawed beams of concrete."

c. Designation C 496-90. "Standard test method for splitting tensile strength of cylindrical concrete specimens."

d. Designation C 597-83. "Standard test method for pulse velocity through concrete."

e. Designation C 801-91. "Standard test method for determining the mechanical properties of hardened concrete under triaxial loads."

Coleman, H. W., and Steele, W. G. (1989). "Statistical considerations in measurement uncertainties." *Experimentation and uncertainty analysis for engineers.* Wiley, New York, 30-34.

U.S. Army Engineer Waterways Experiment Station. (1949). Designation C 164-92. "Standard test method for direct tensile strength of cylindrical concrete or mortar specimens," *Handbook for concrete and cement* (with quarterly supplements). Vicksburg, MS.

ELK CREEK DAM
TEST NO. 9604A01

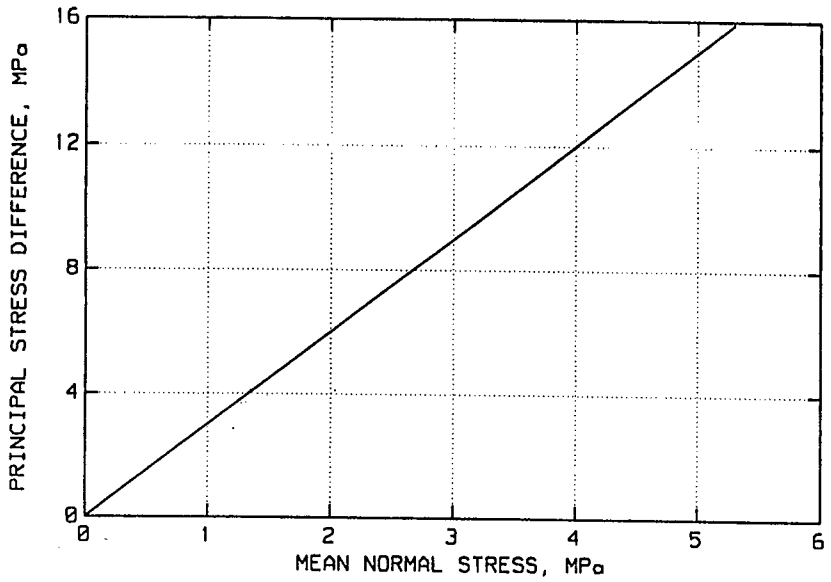

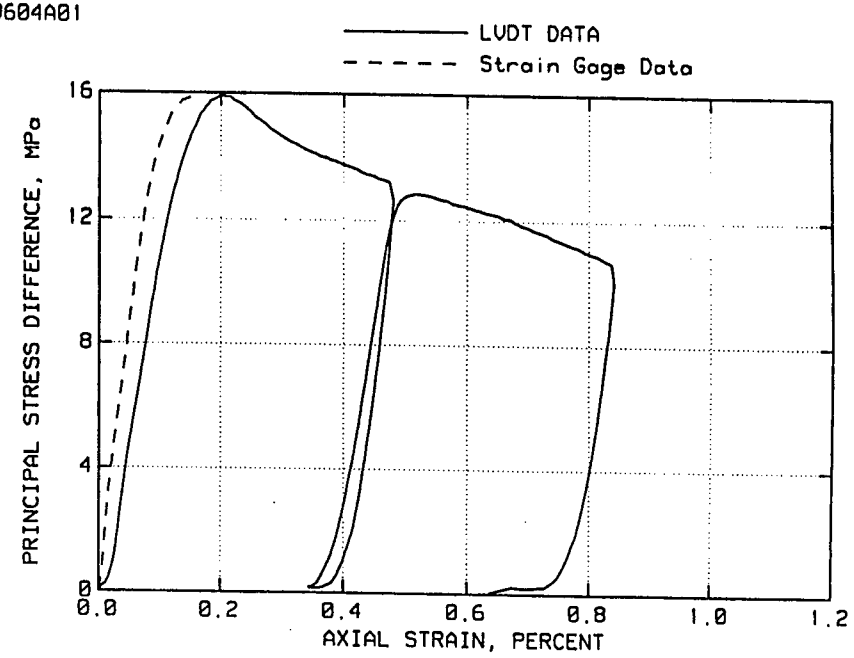

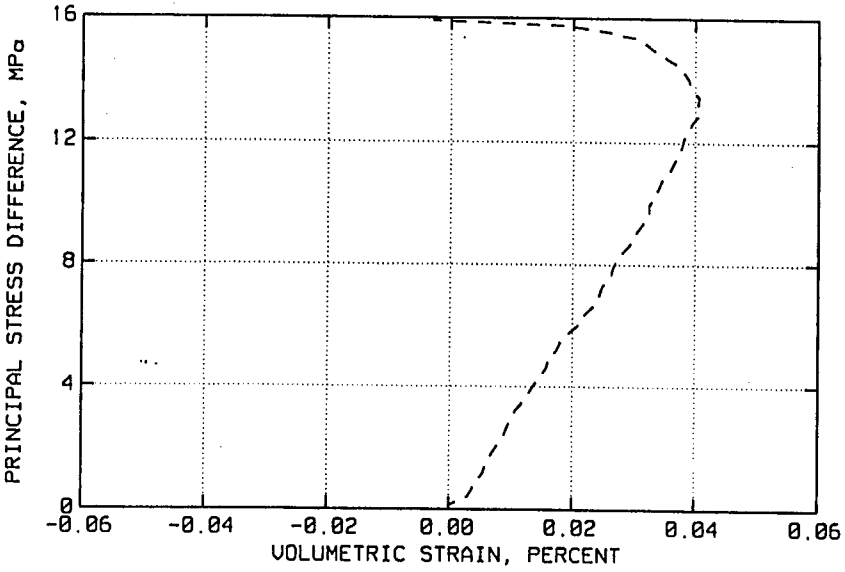

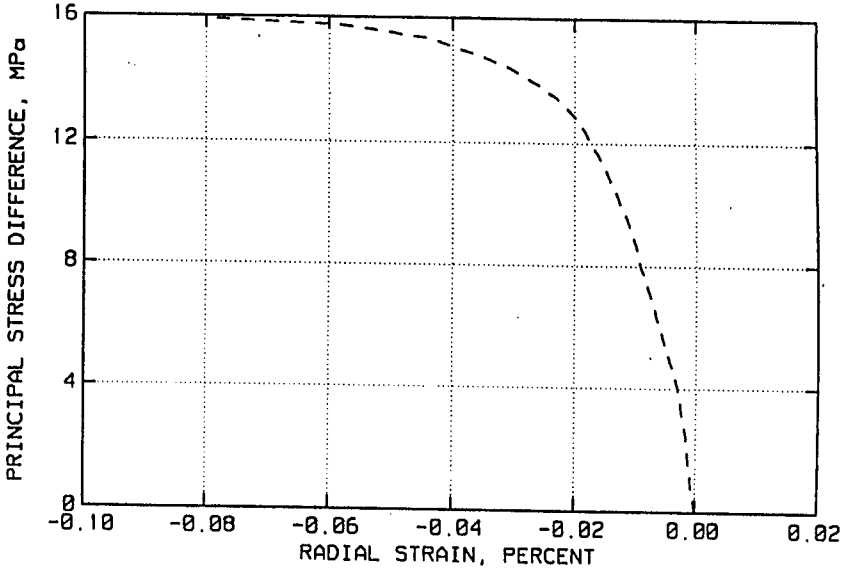

Plate 1

Plate 2

ELK CREEK DAM
TEST NO. 9604A02

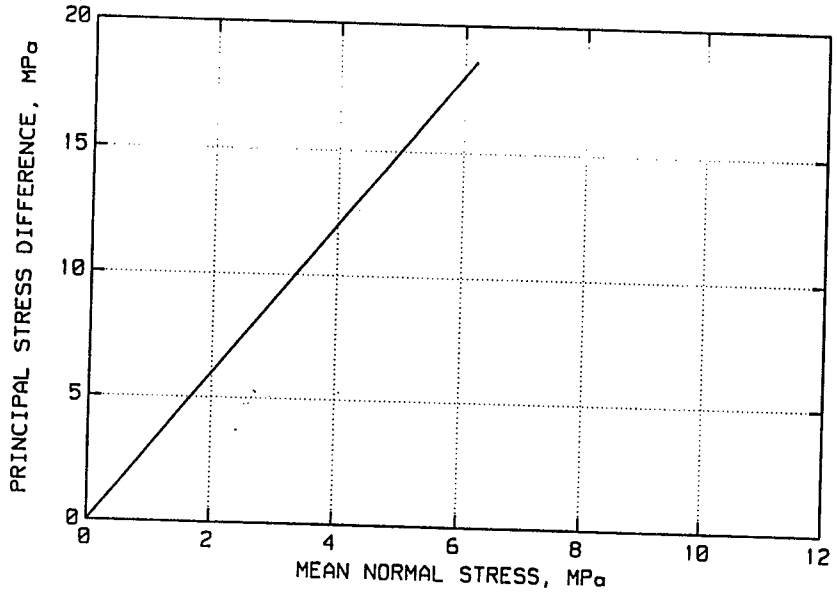

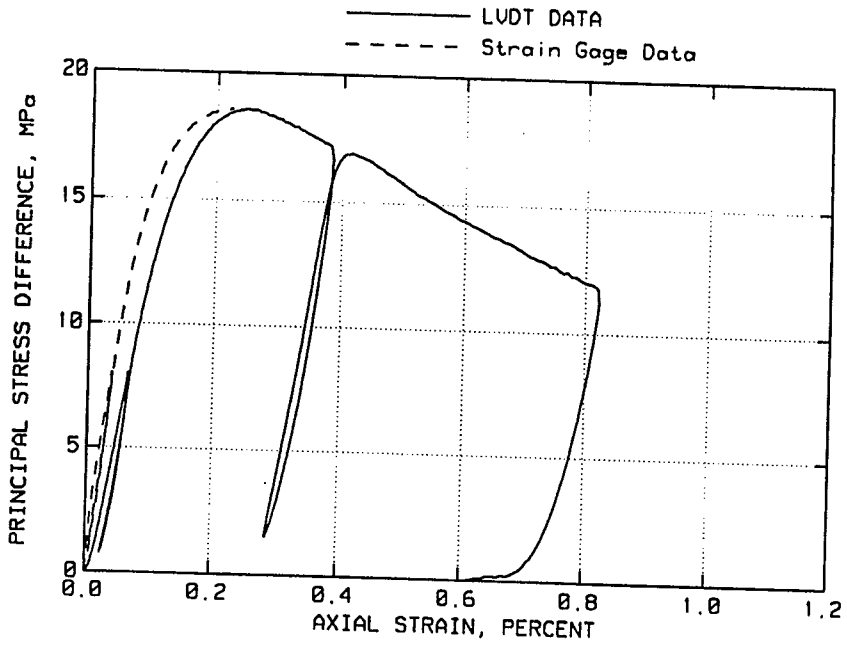

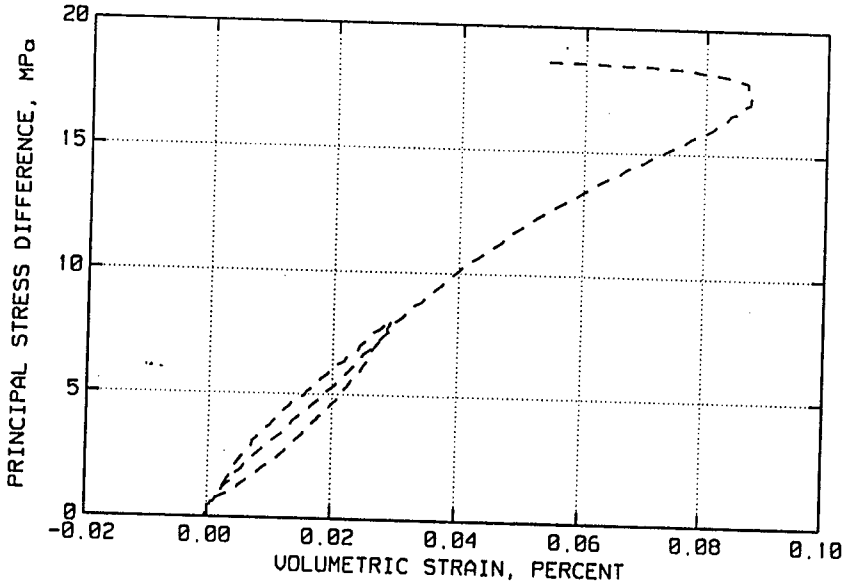

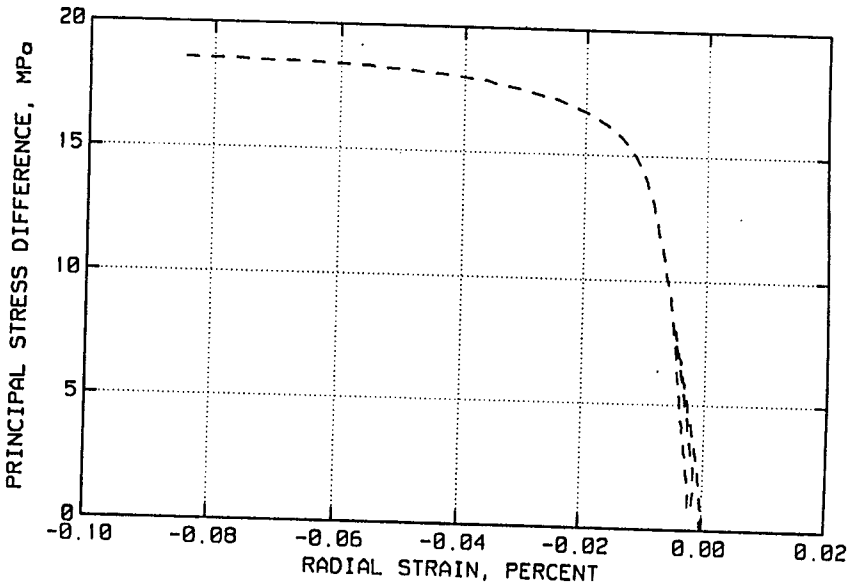

ELK CREEK DAM
TEST NO. 9604A03

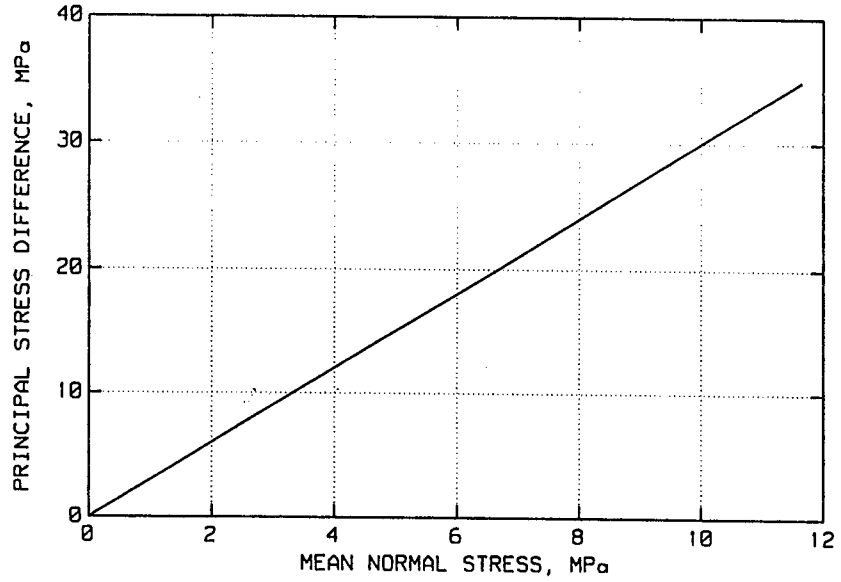

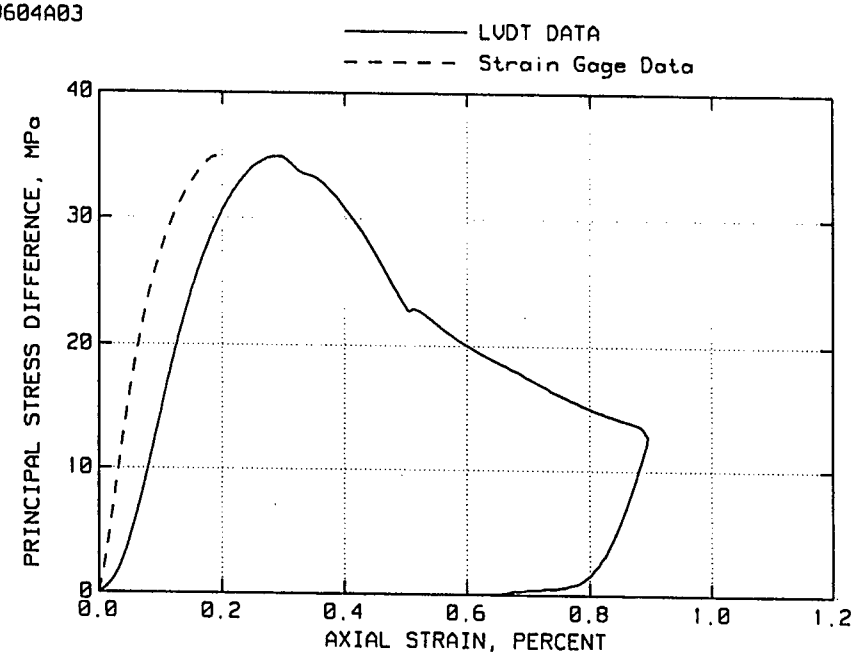

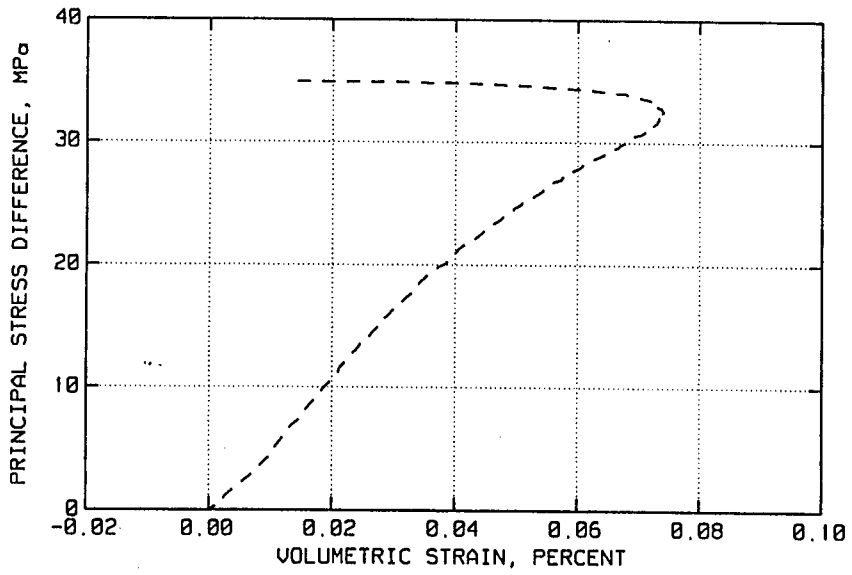

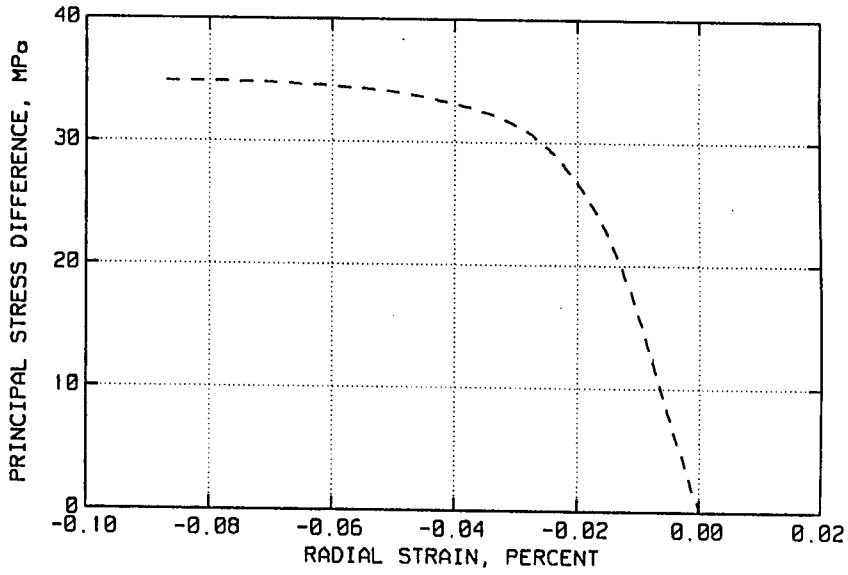

Plate 3

Plate 4

ELK CREEK DAM
TEST NO. 9604A04

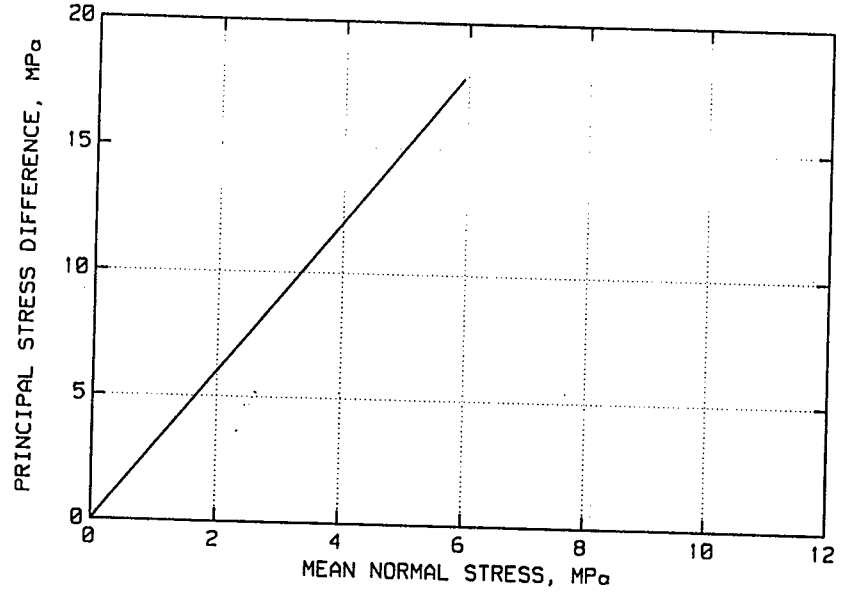

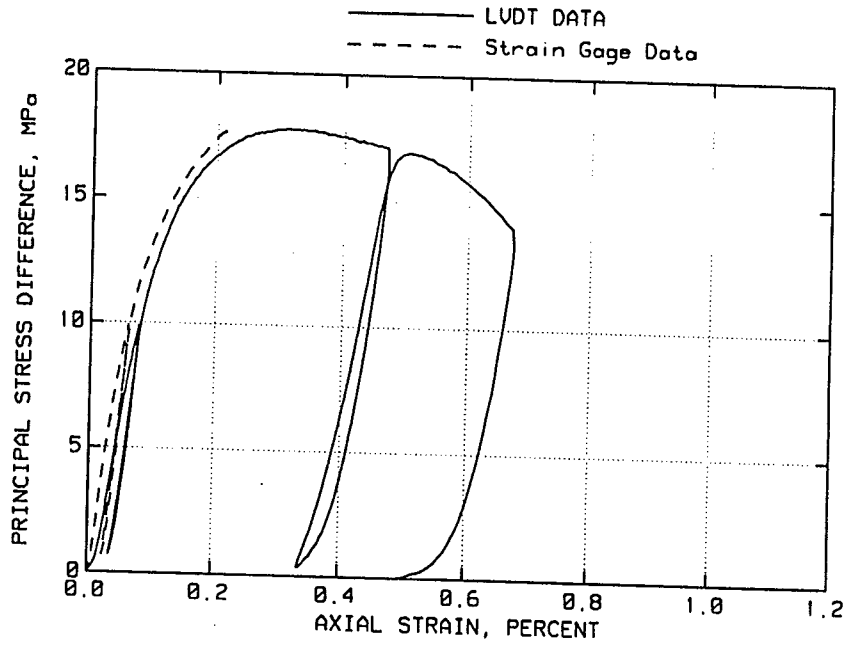

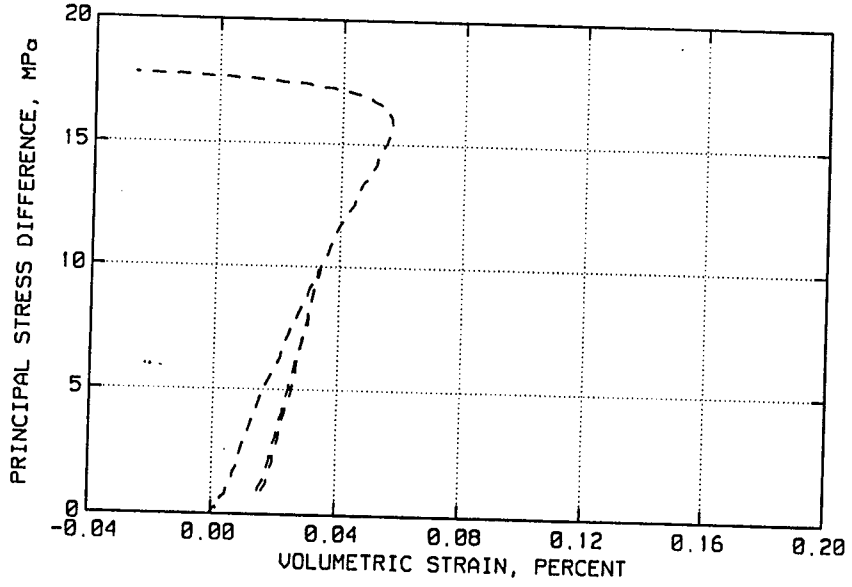

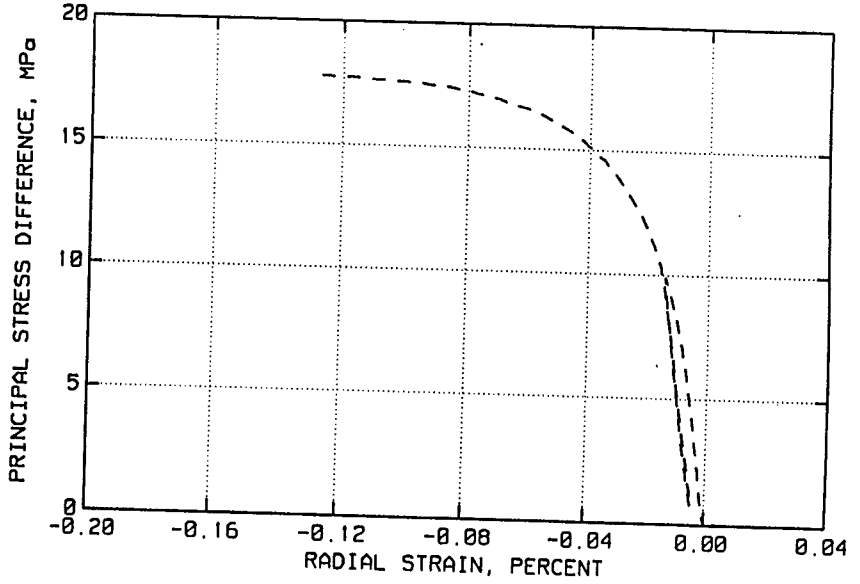

ELK CREEK DAM
TEST NO. 9604A05

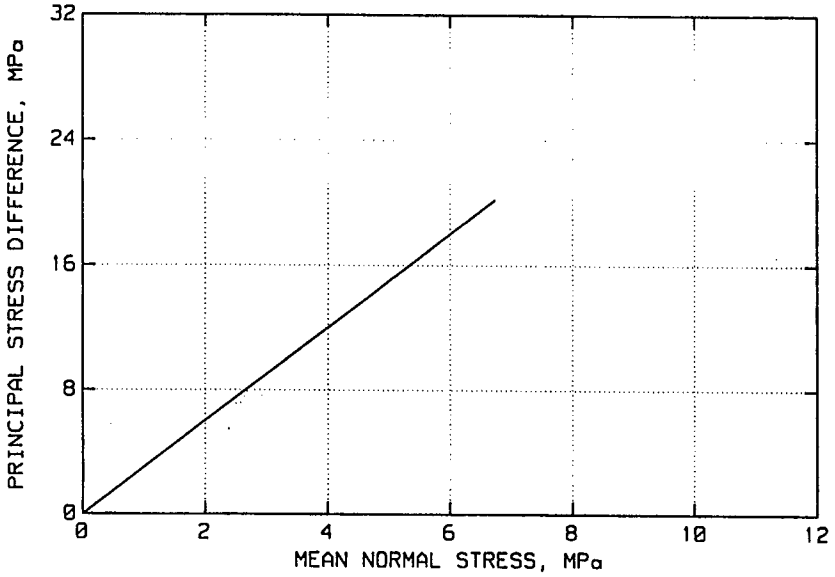

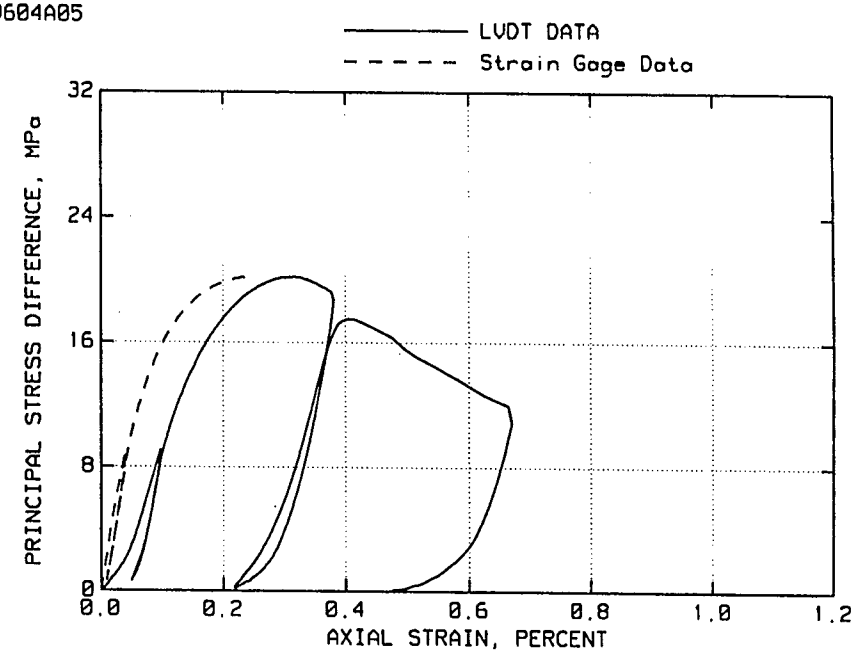

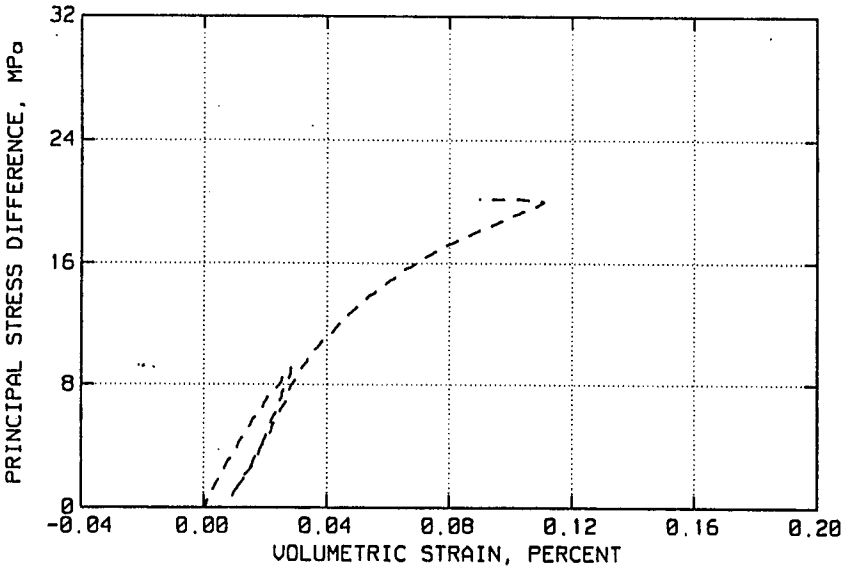

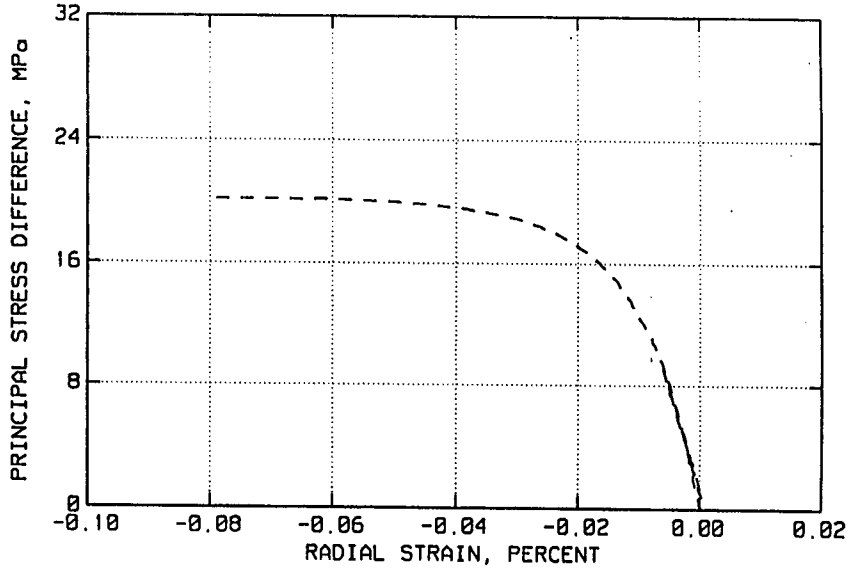

Plate 5

Plate 6

ELK CREEK DAM
TEST NO. 9604A06

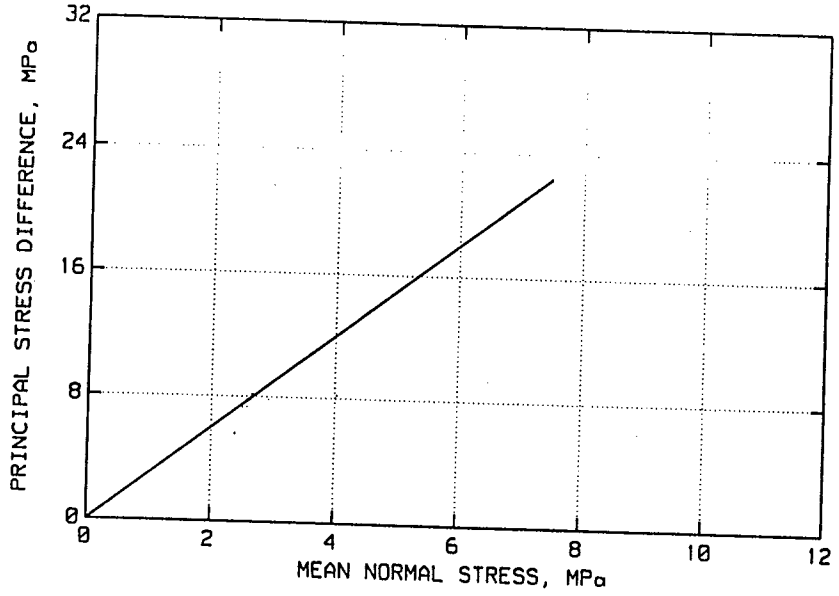

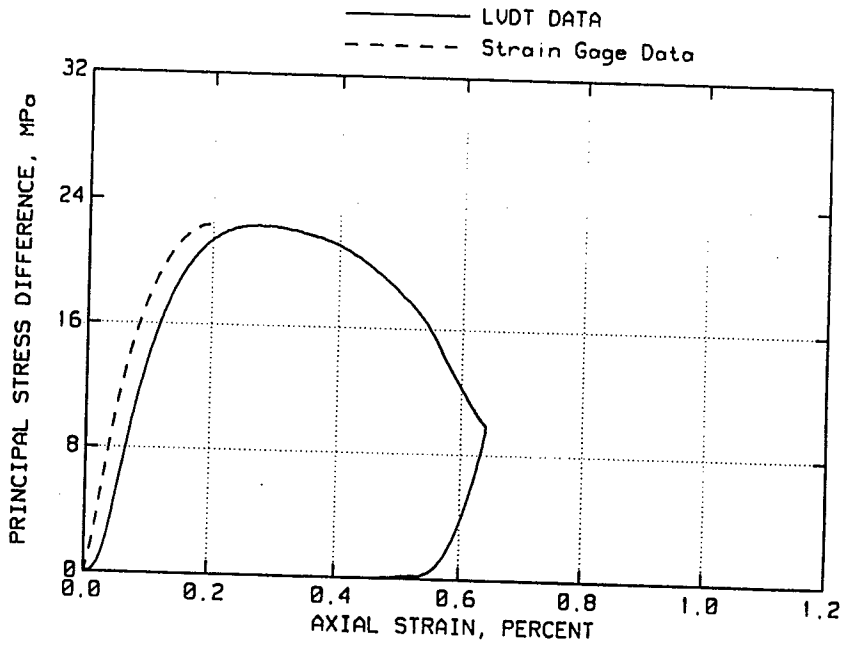

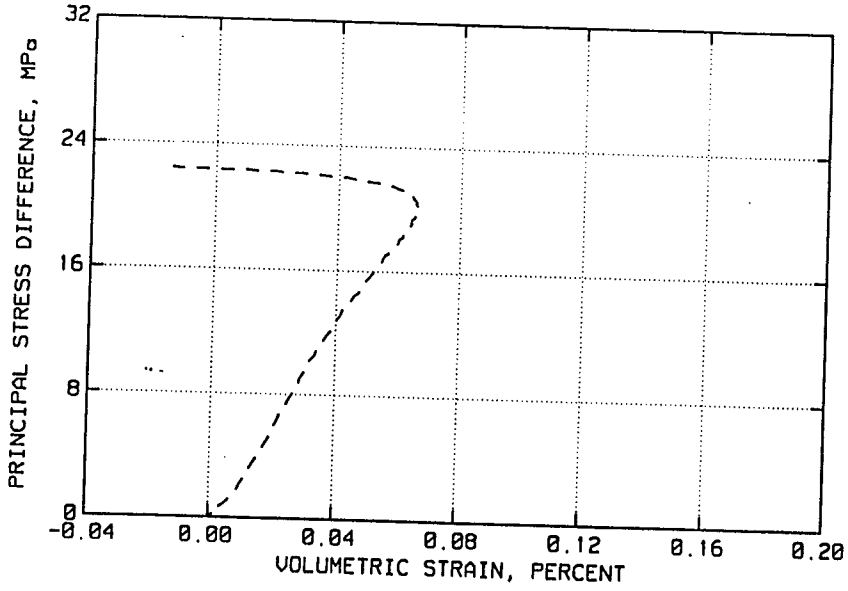

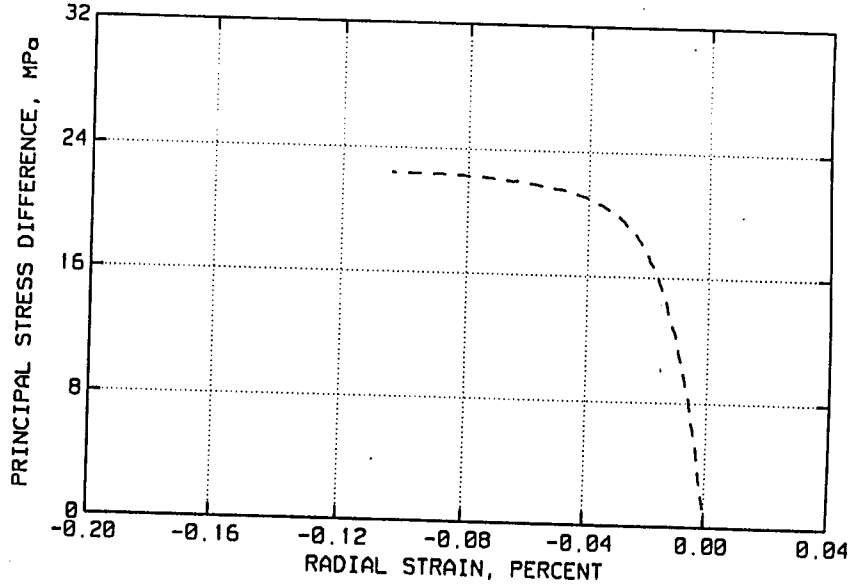

ELK CREEK DAM
TEST NO. 9604A07

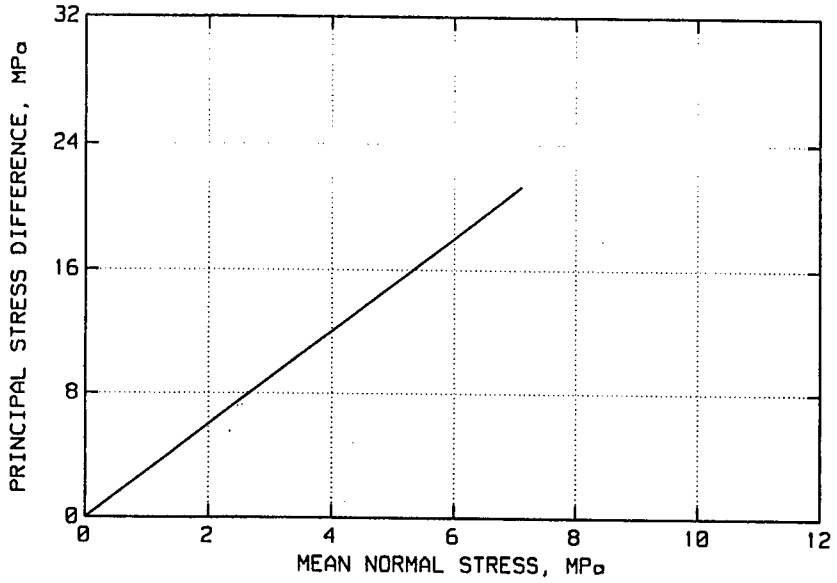

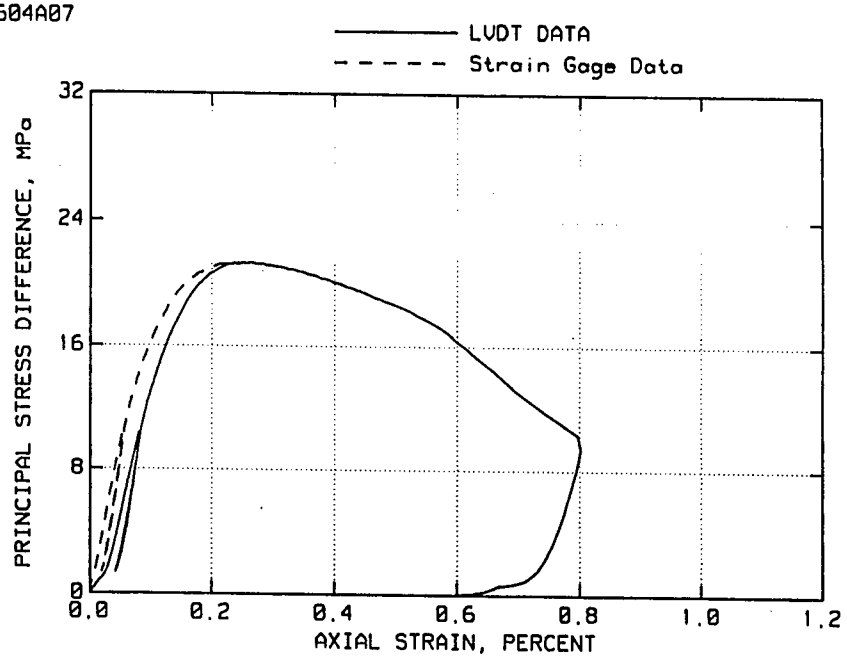

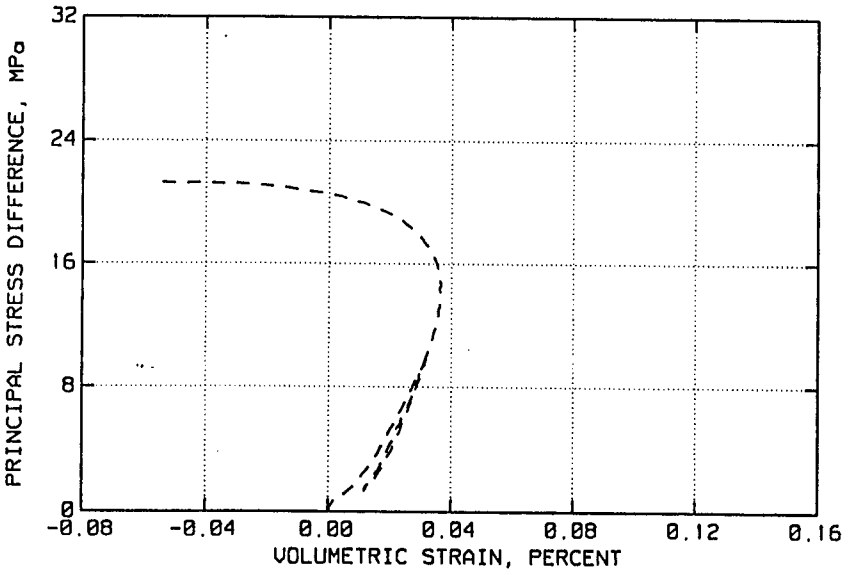

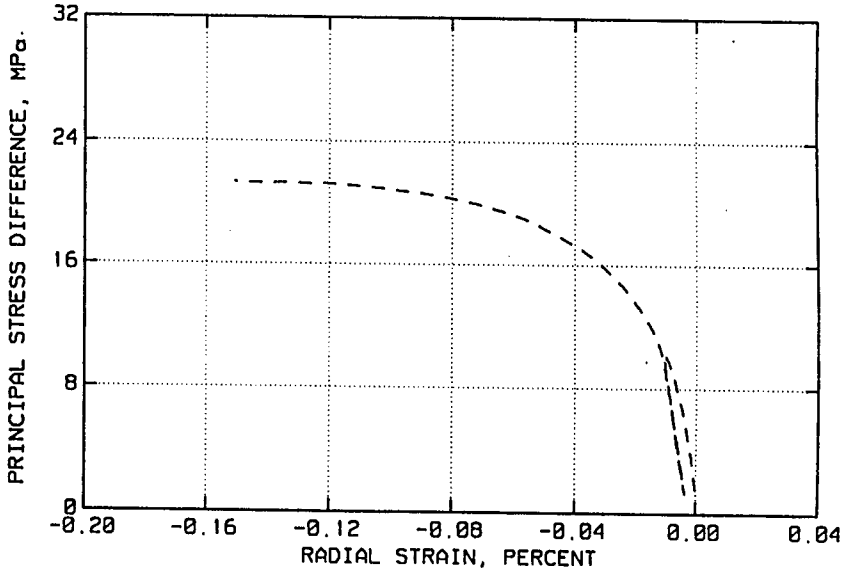

Plate 7

Plate 8

ELK CREEK DAM
TEST NO. 9604A08

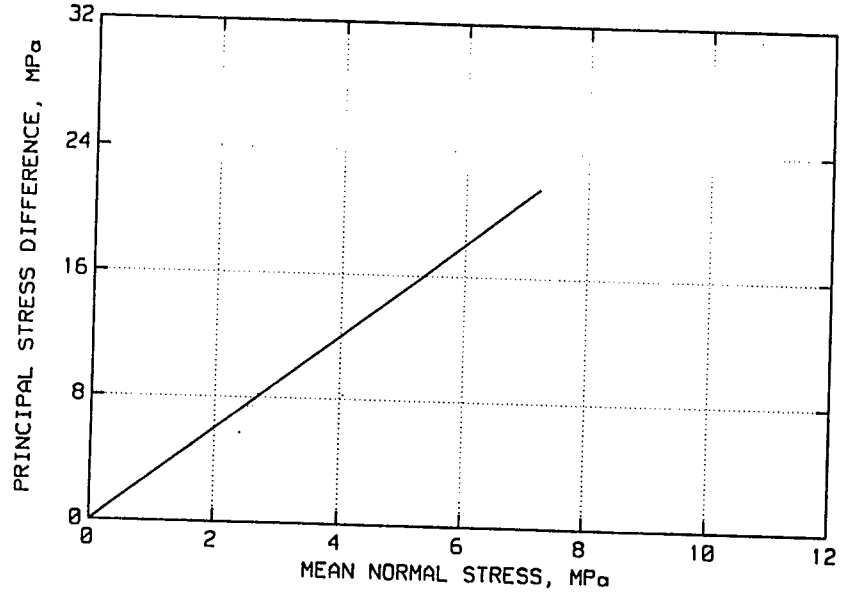

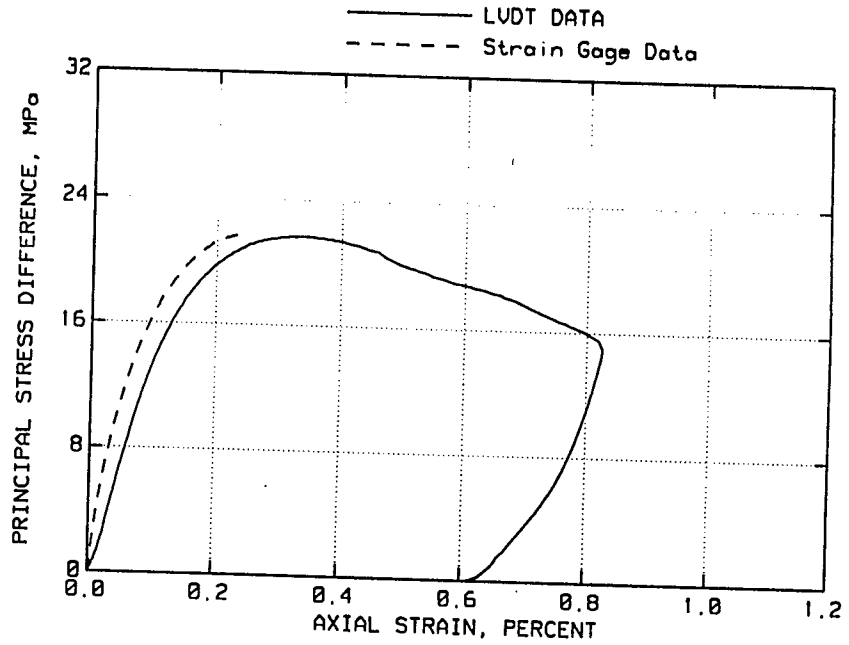

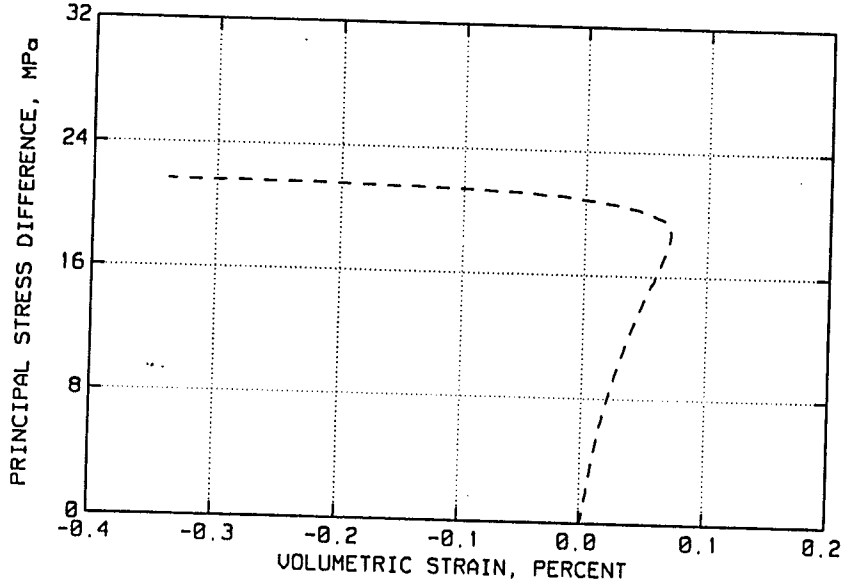

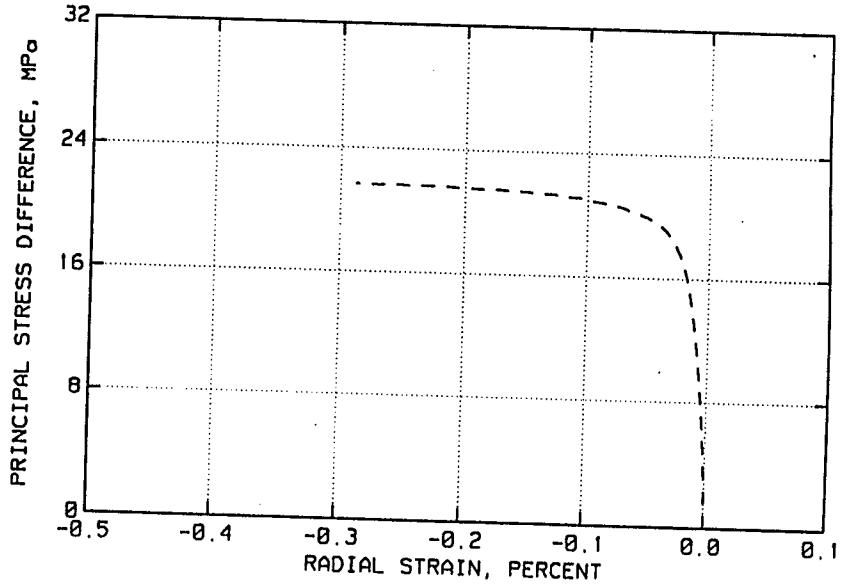

ELK CREEK DAM
TEST NO. 9604A09

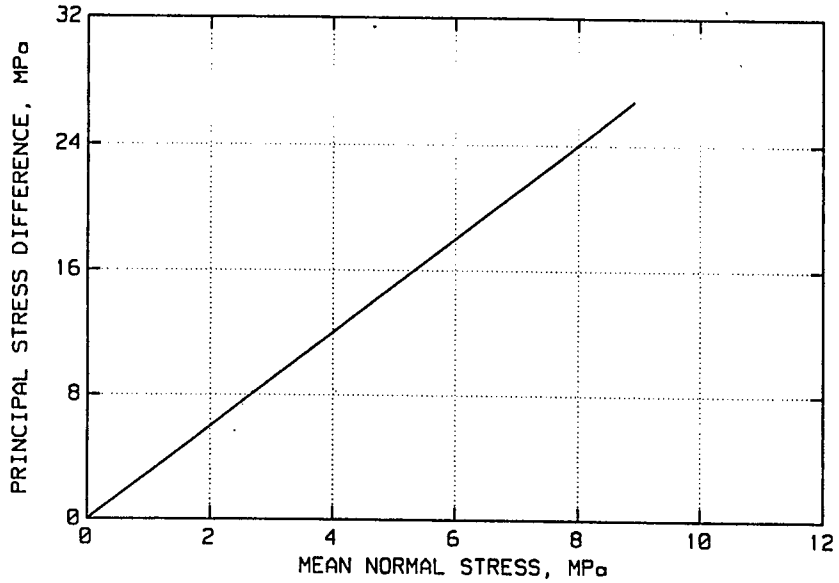

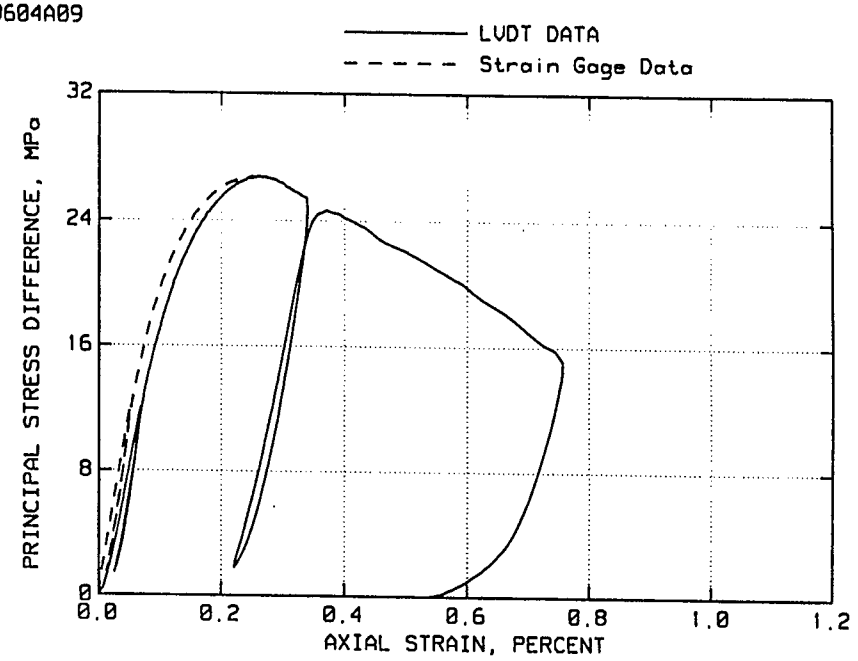

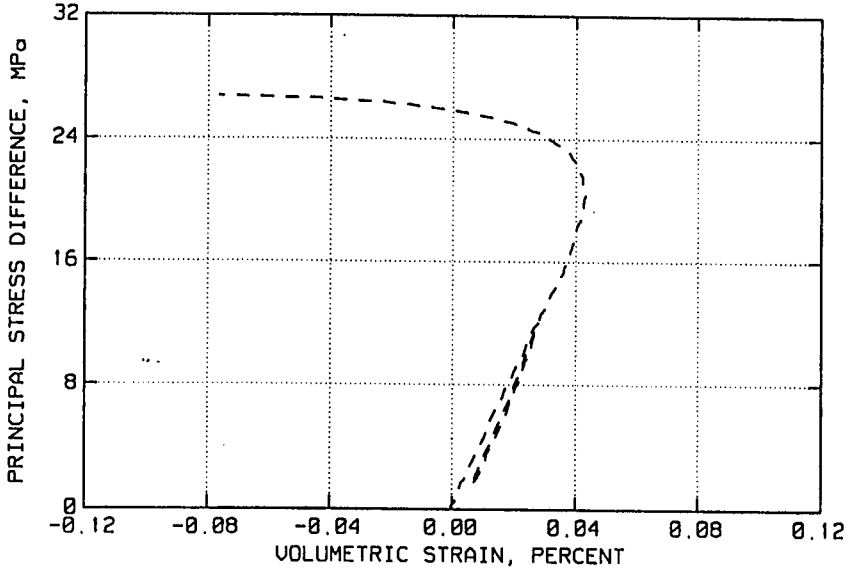

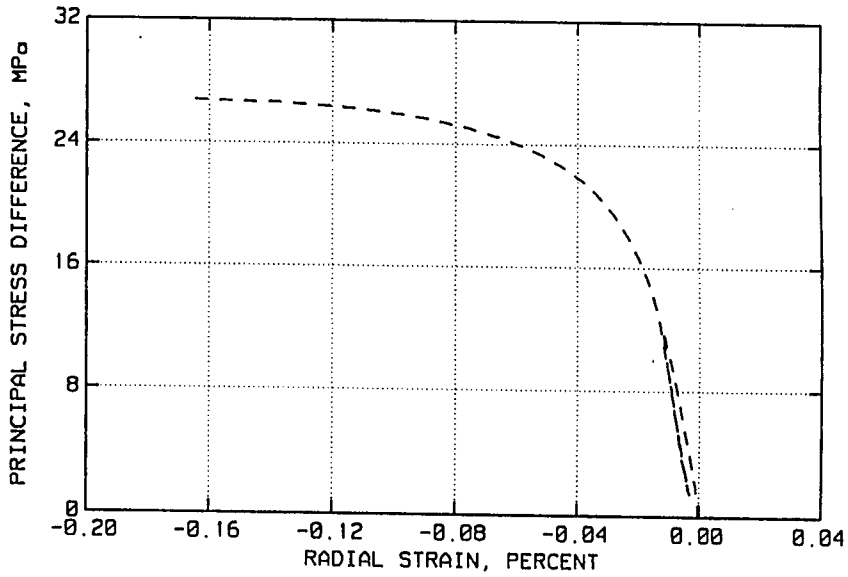

Plate 9

Plate 10

ELK CREEK DAM
TEST NO. 9604A18

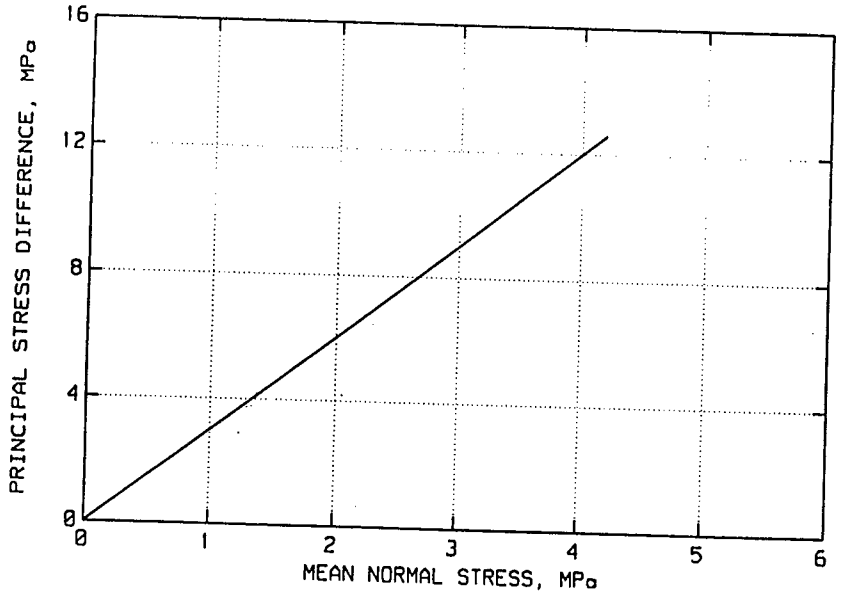

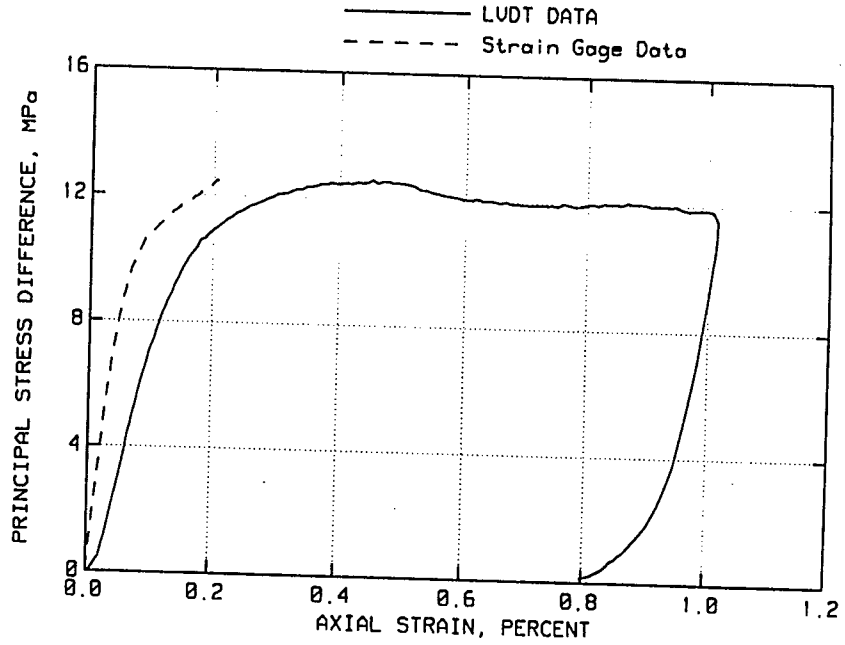

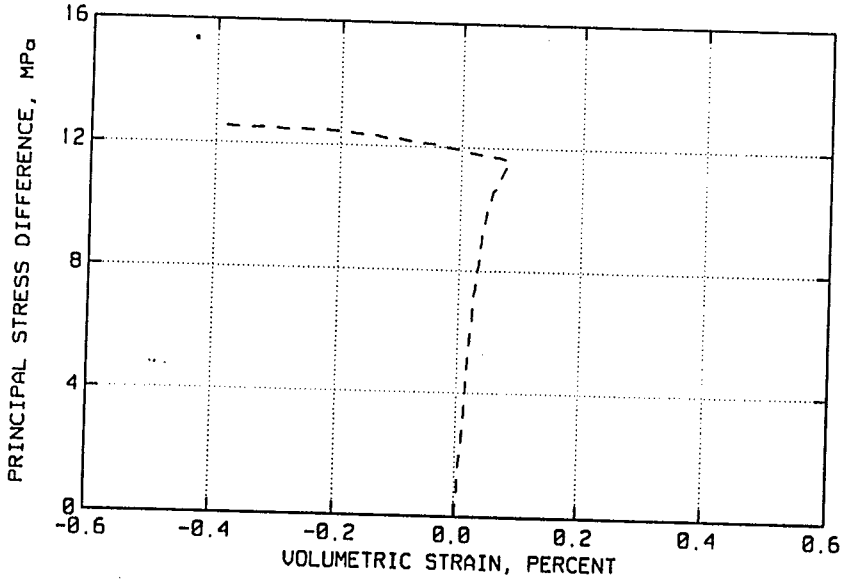

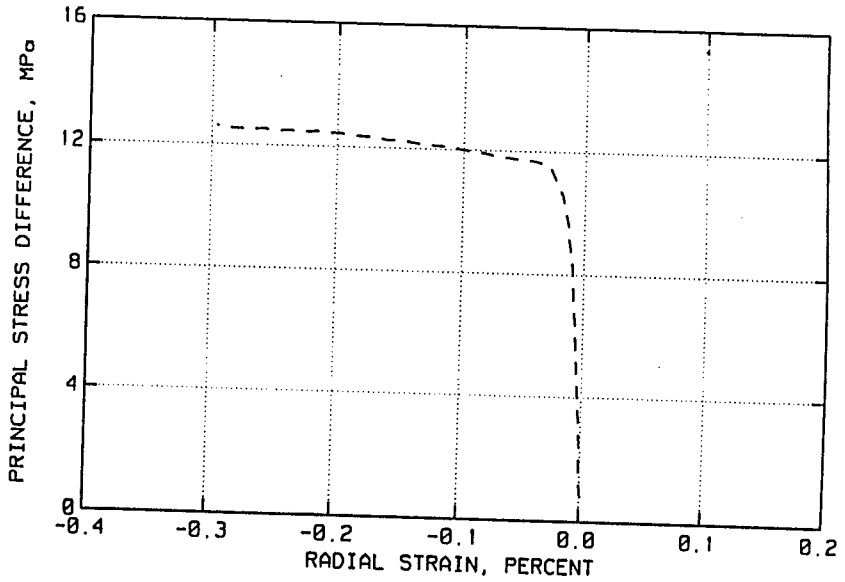

ELK CREEK DAM
TEST NO. 9604A10

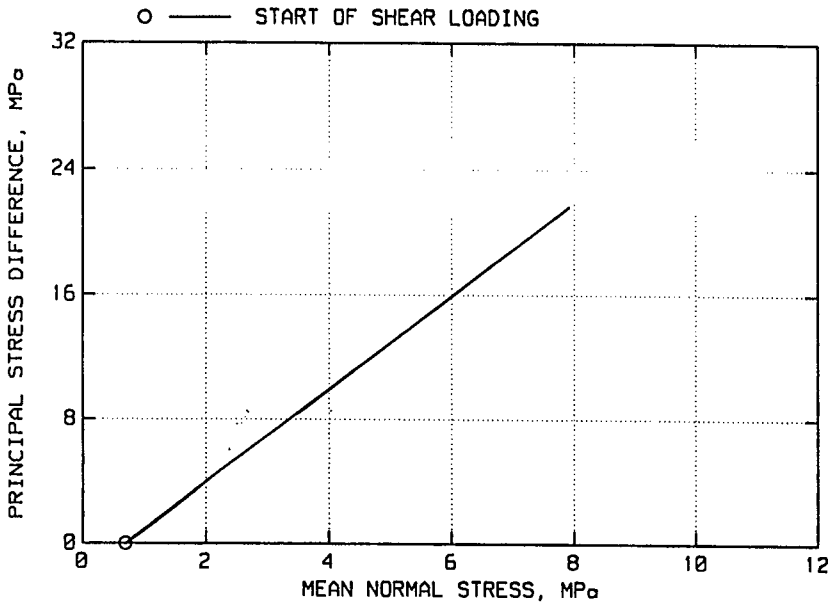

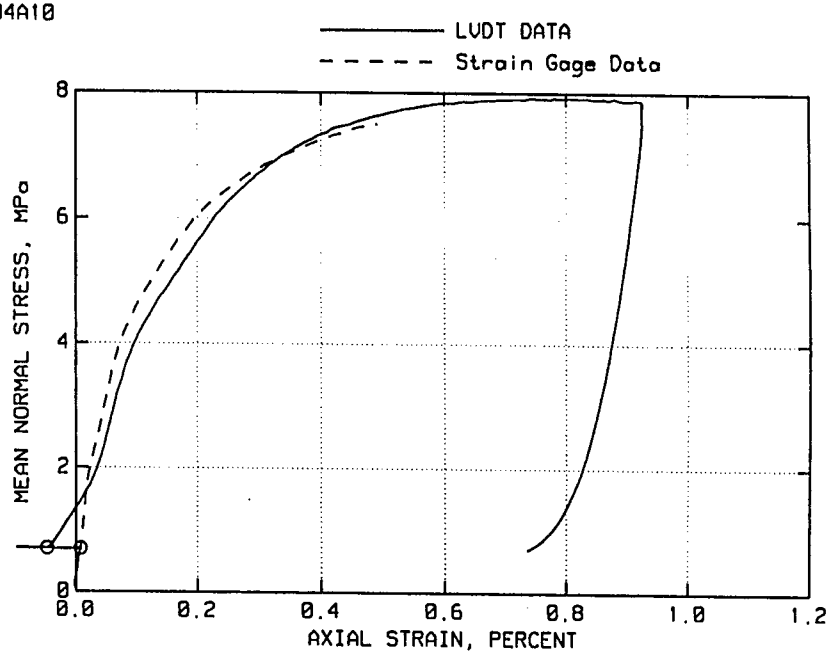

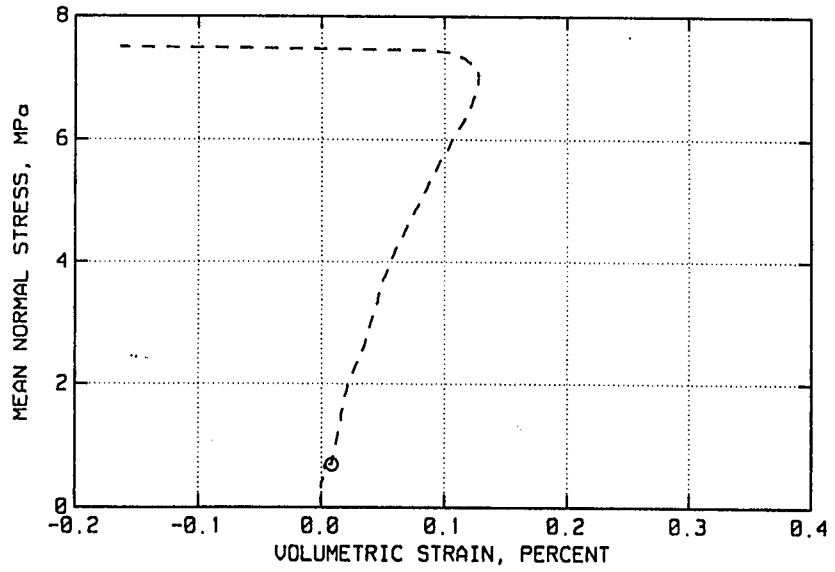

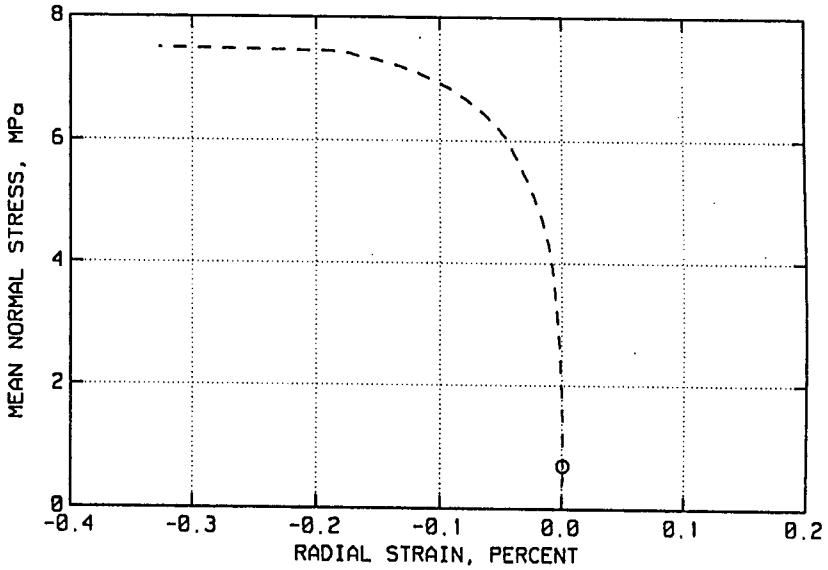

Plate 11

Plate 12

ELK CREEK DAM
TEST NO. 9604A10

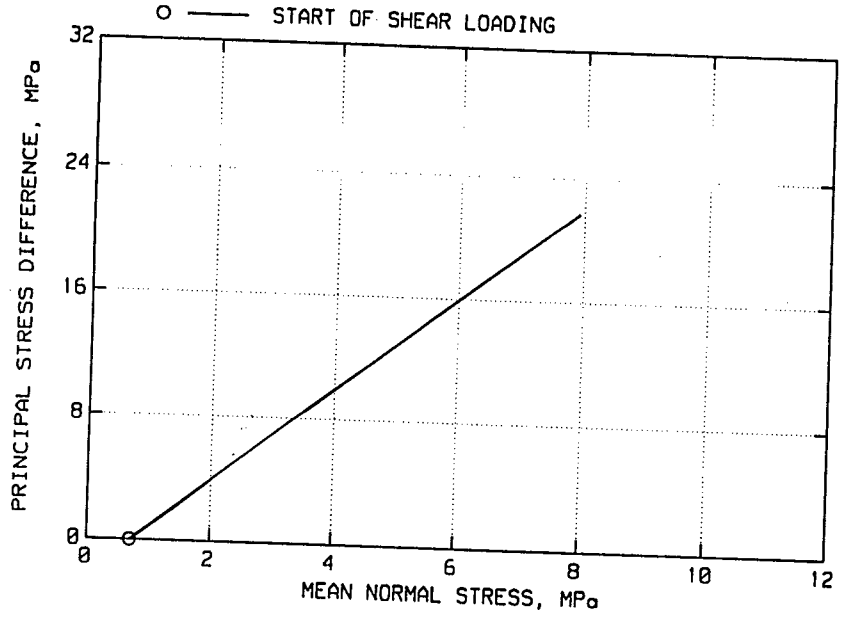

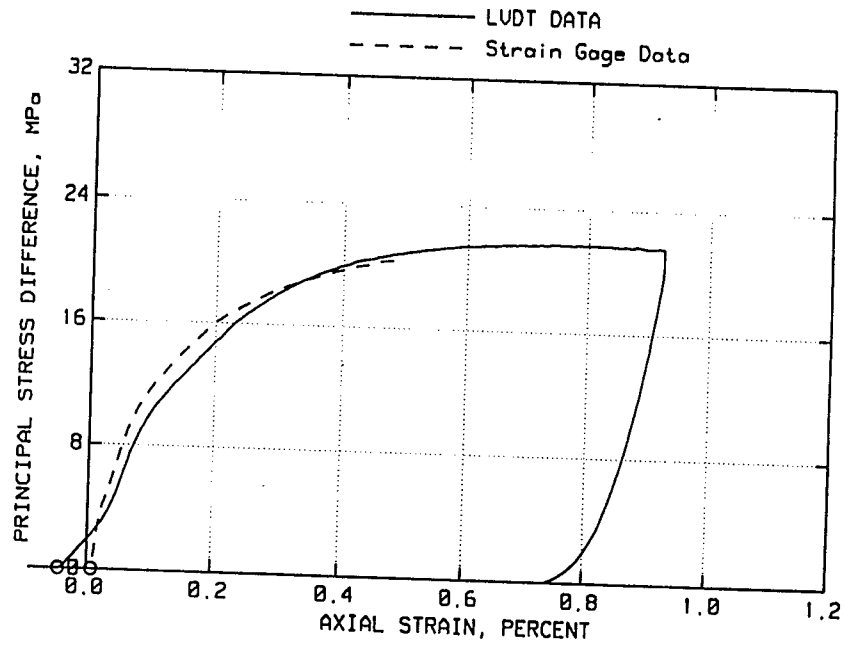

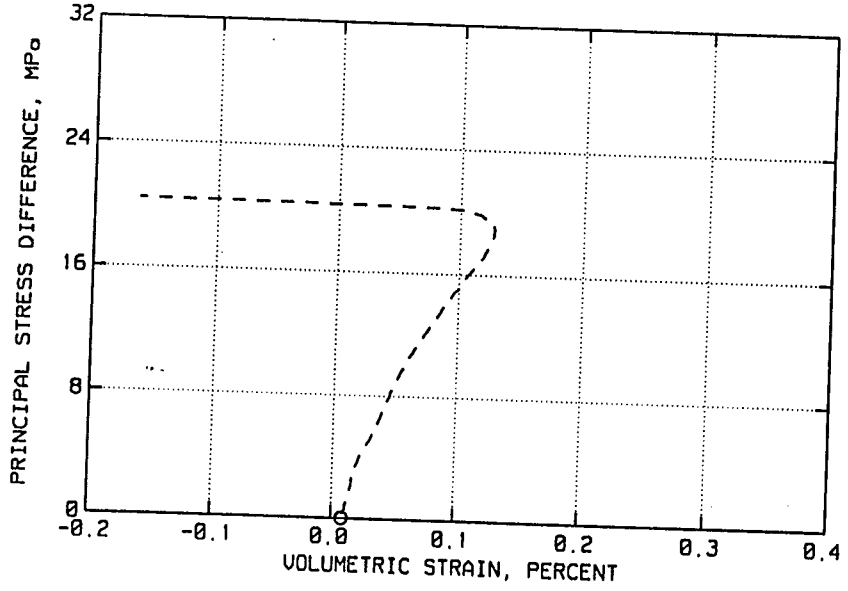

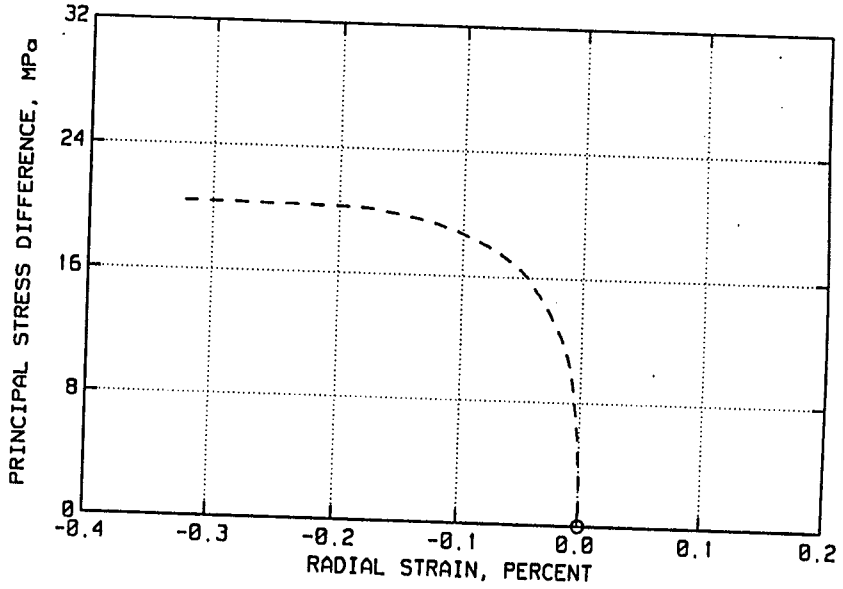

ELK CREEK DAM
TEST NO. 9604A11

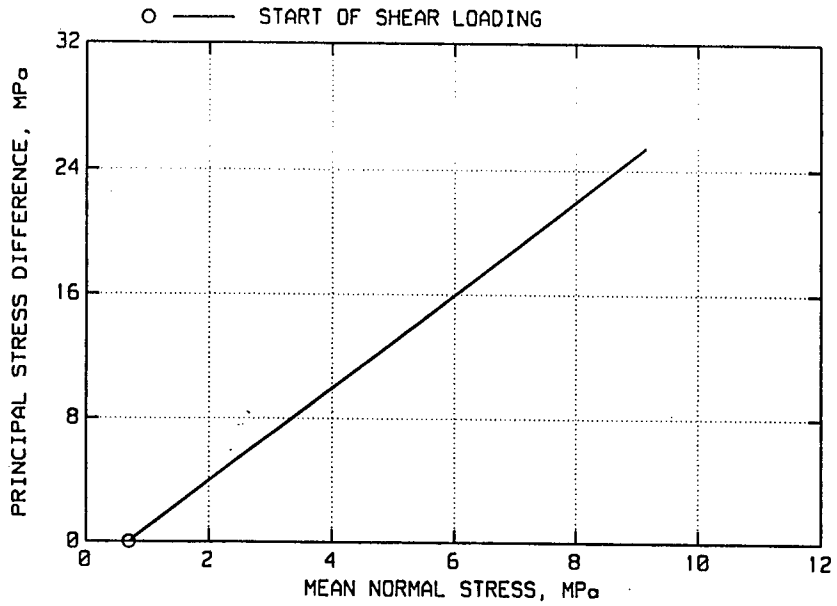

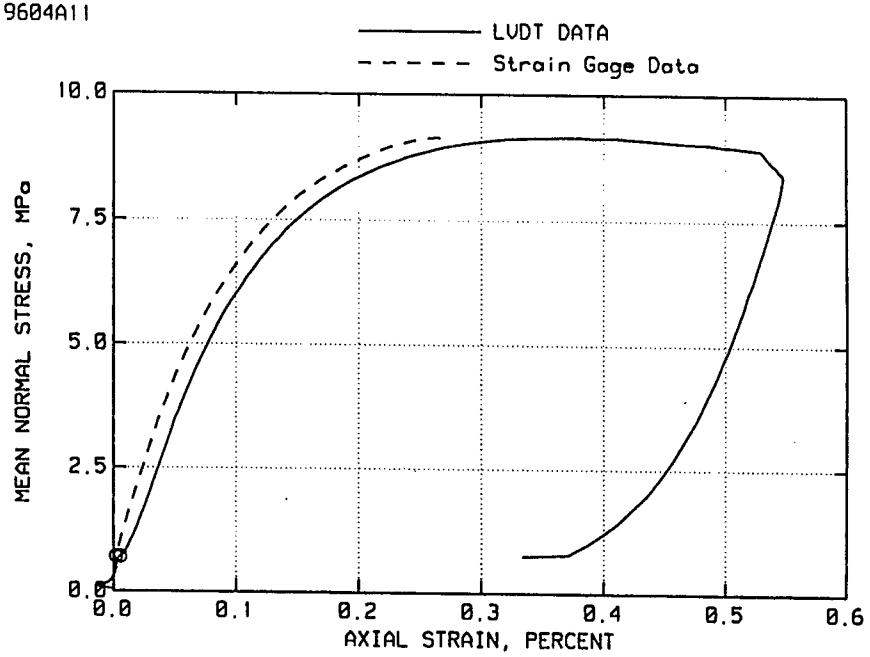

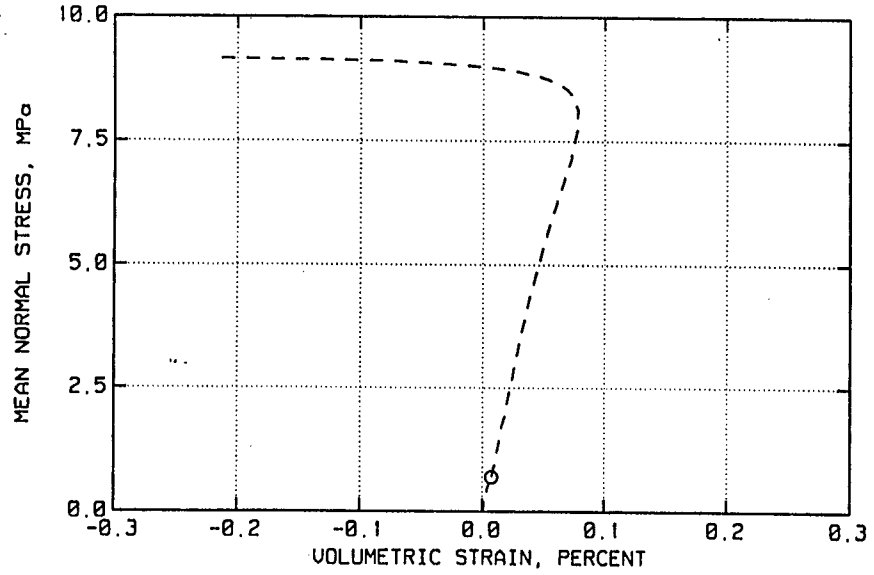

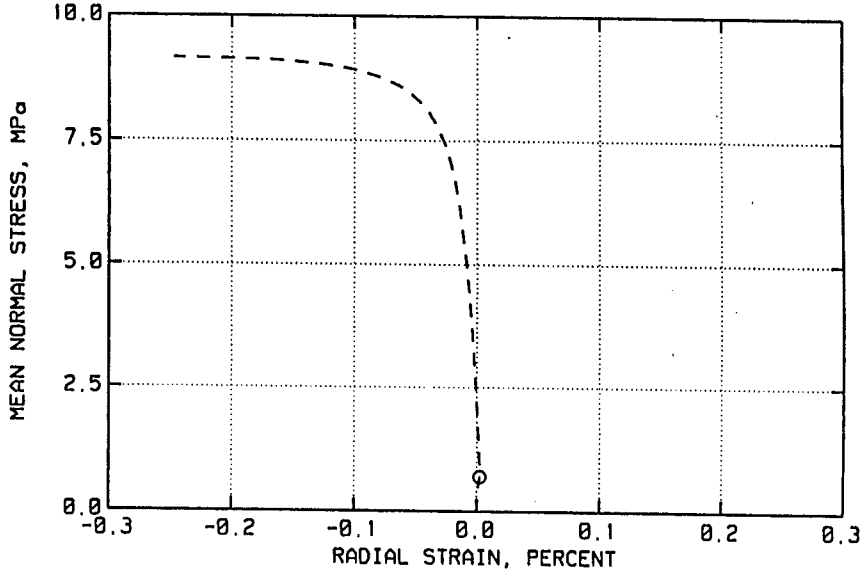

Plate 13

Plate 14

ELK CREEK DAM
TEST NO. 9604A11

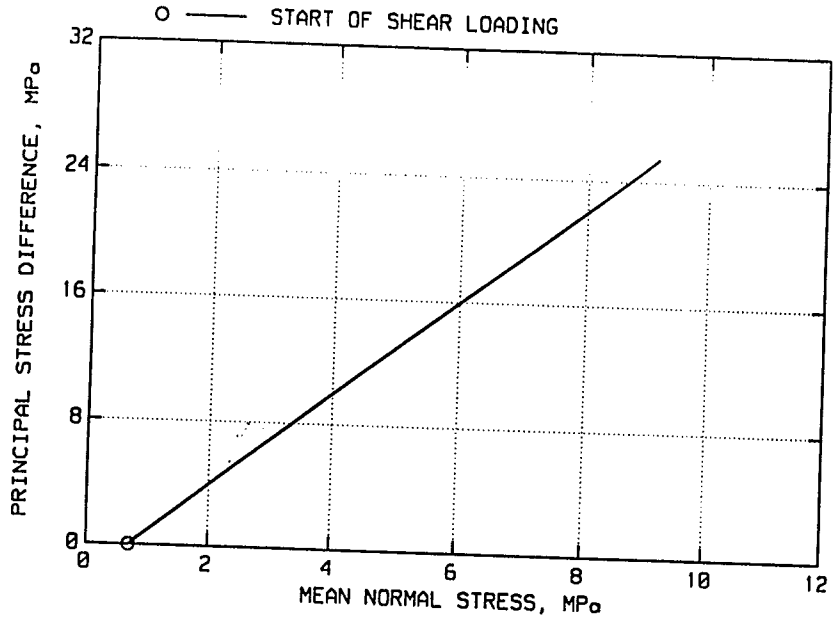

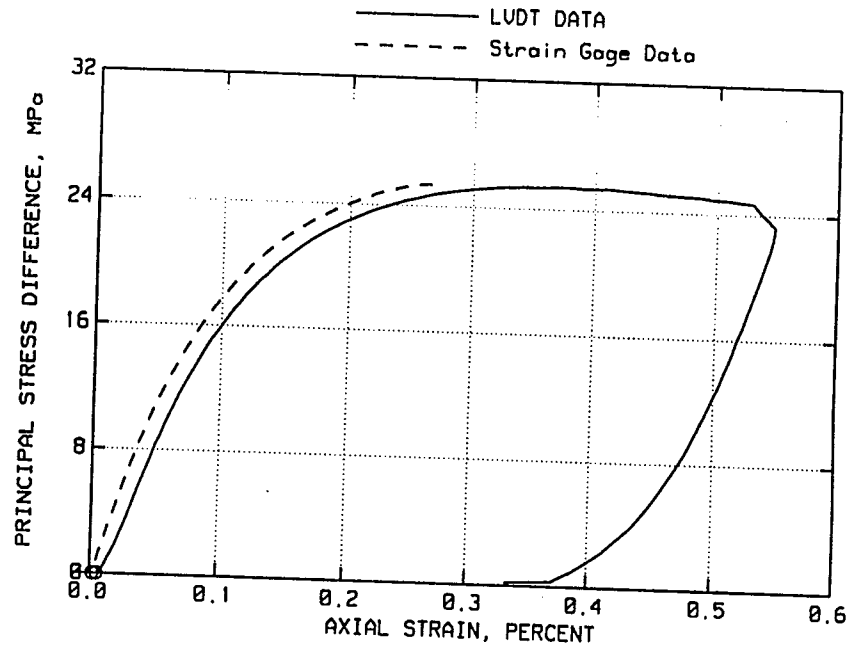

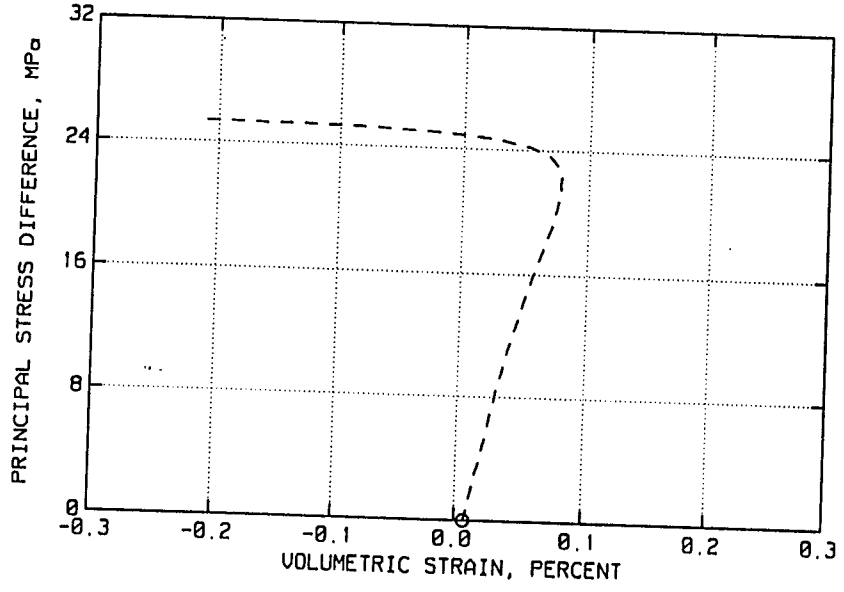

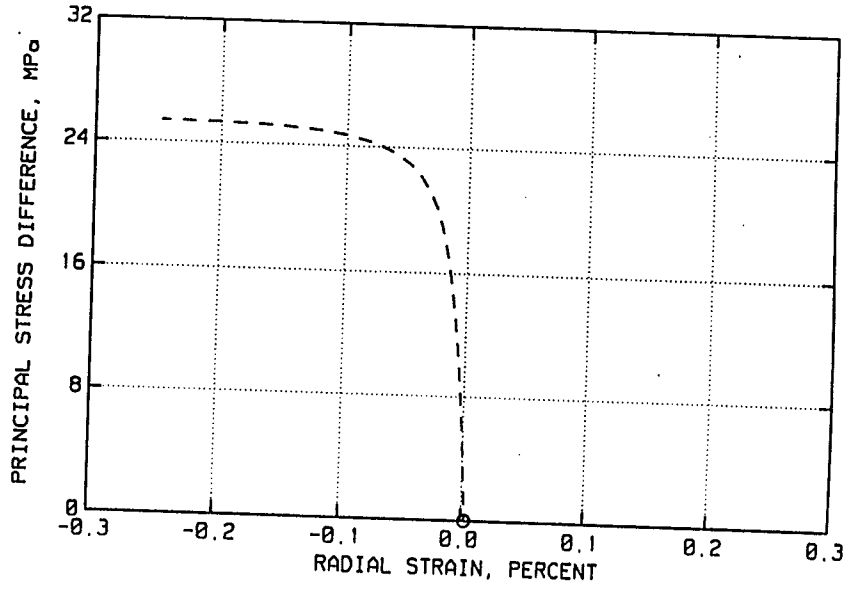

ELK CREEK DAM
TEST NO. 9604A12

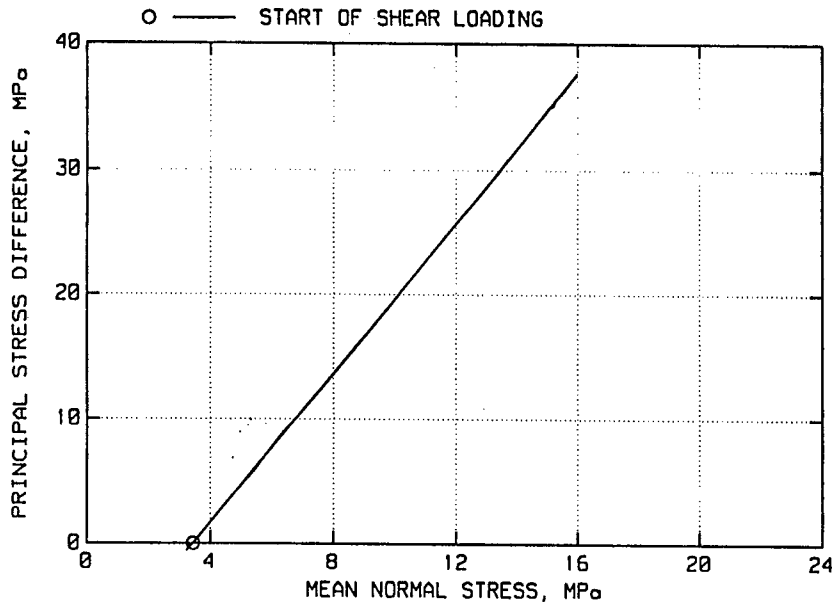

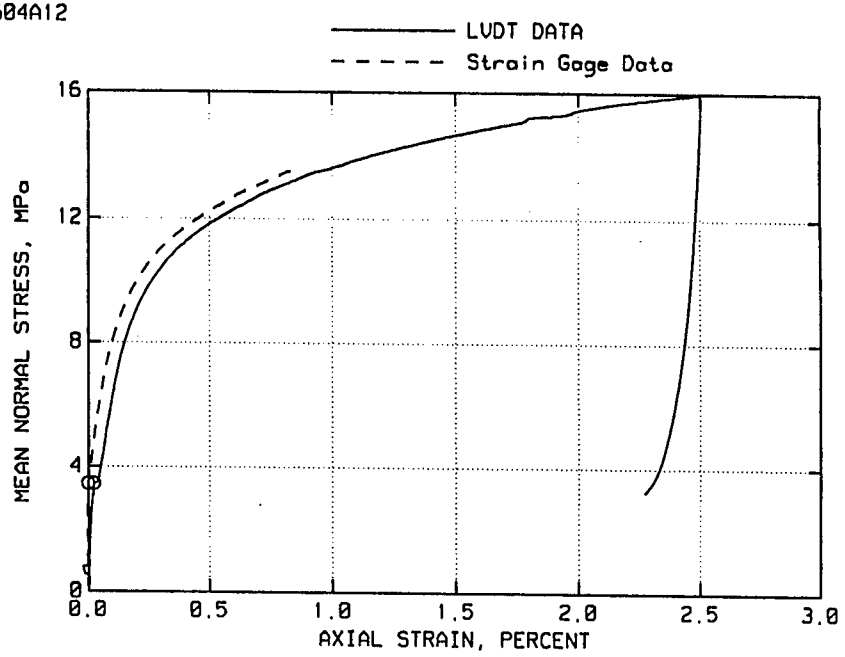

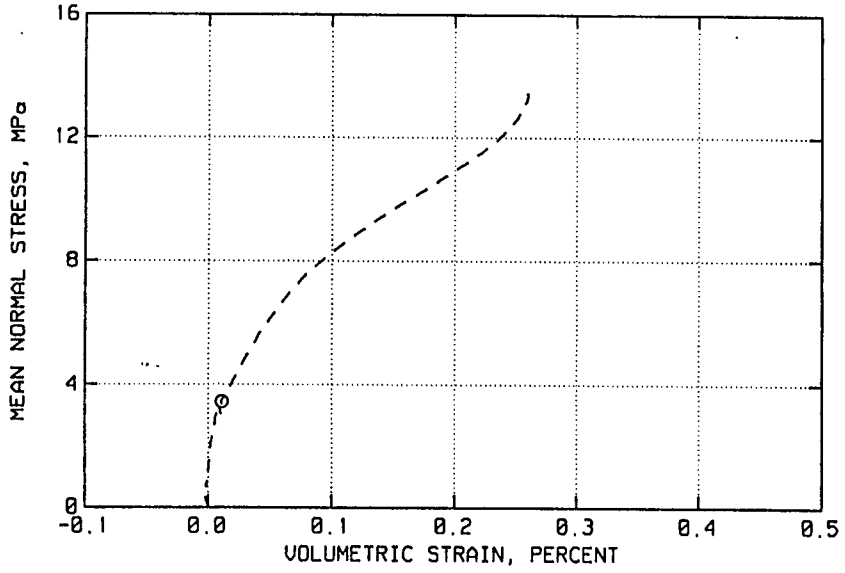

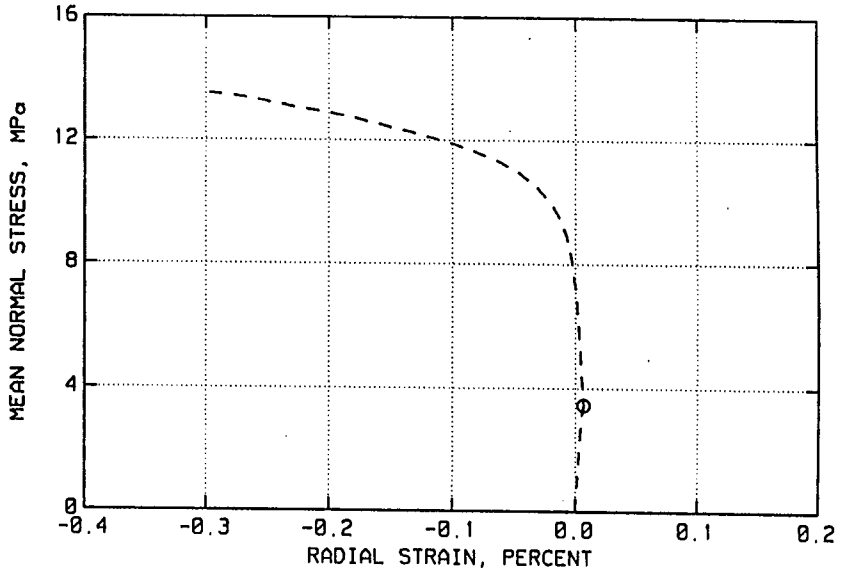

Plate 15

Plate 16

ELK CREEK DAM
TEST NO. 9604A12

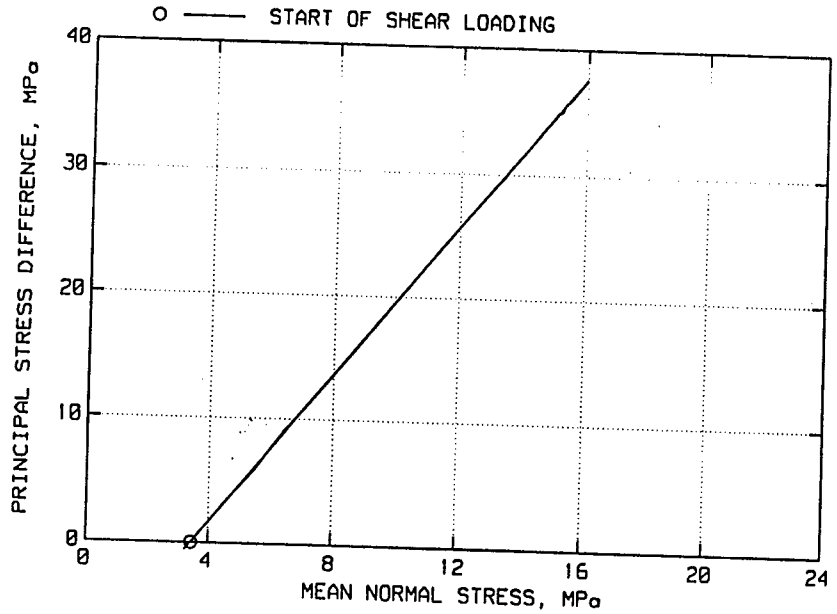

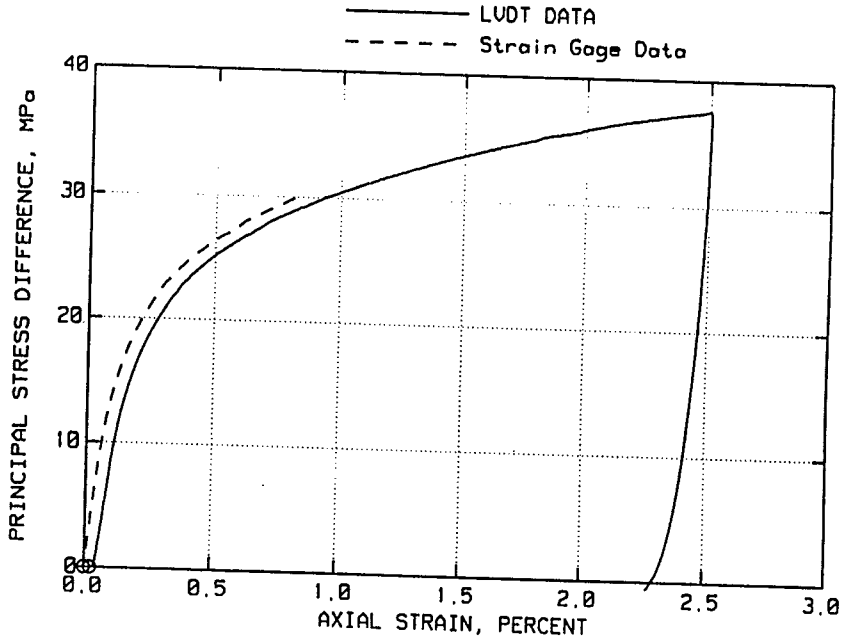

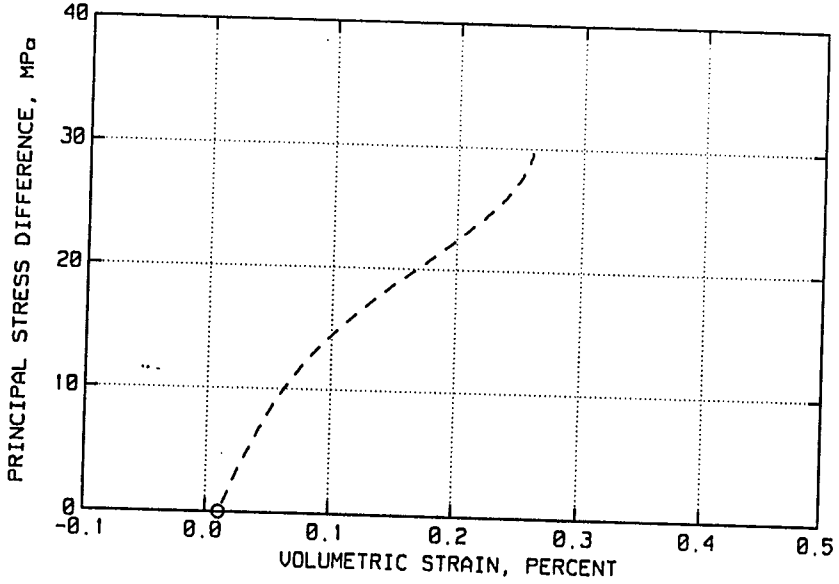

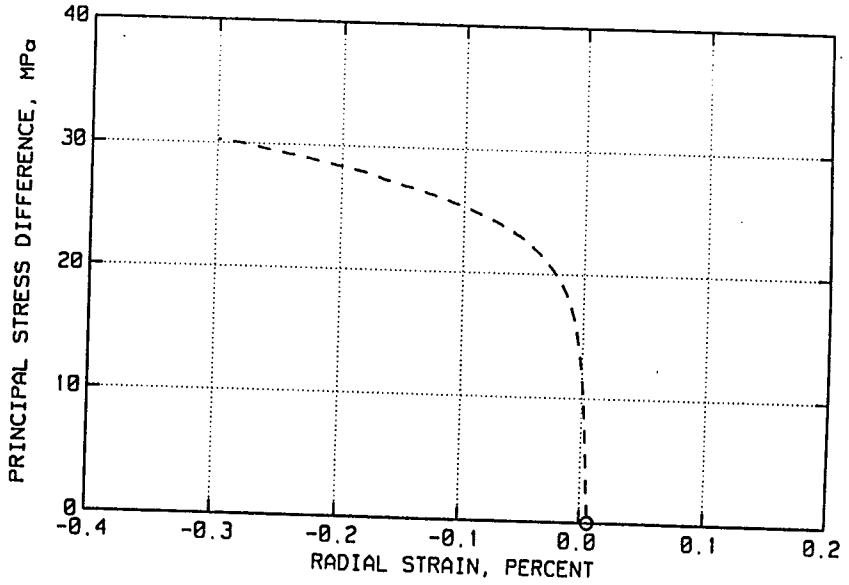

ELK CREEK DAM

TEST NO. 9604A13

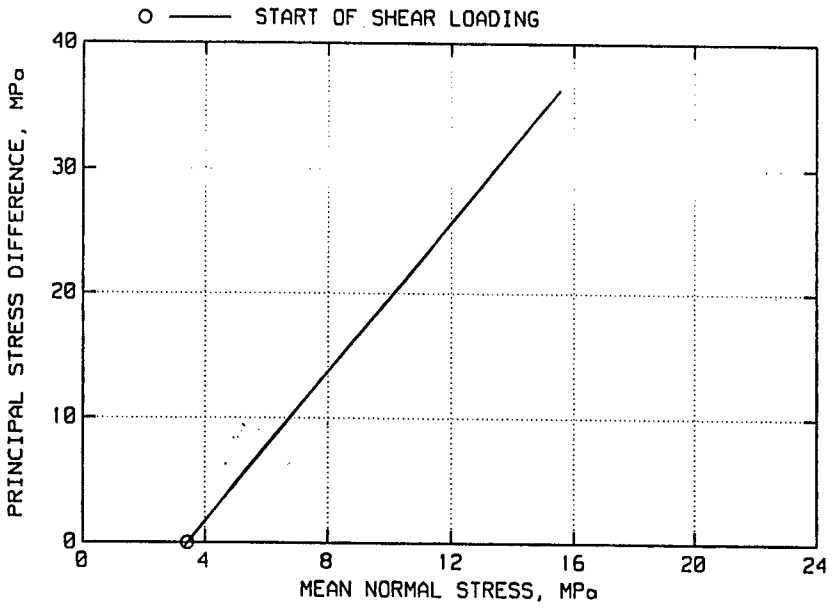

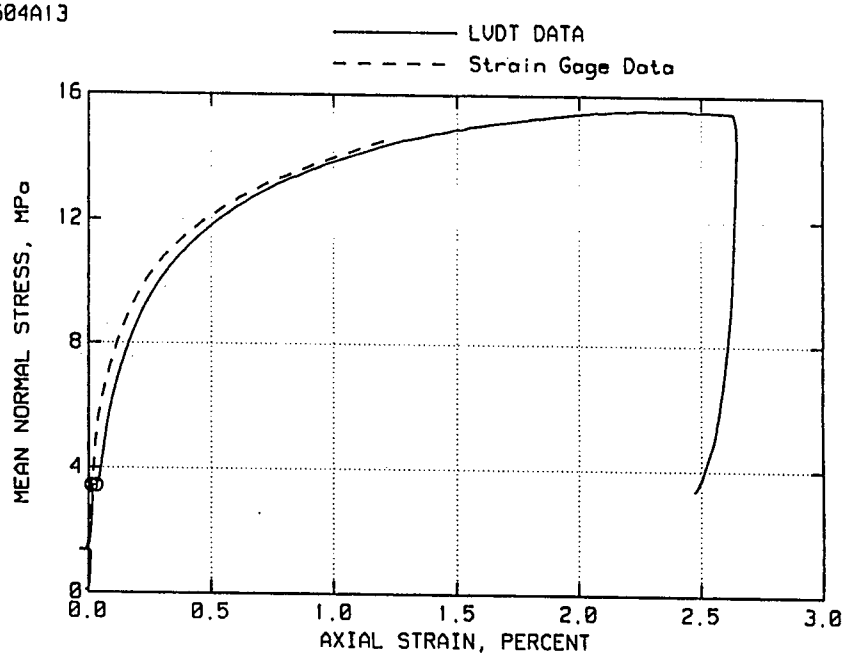

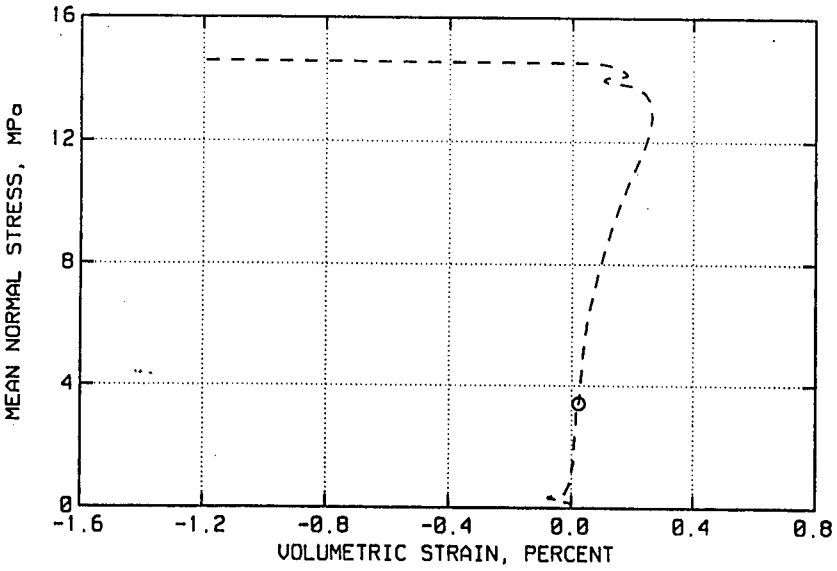

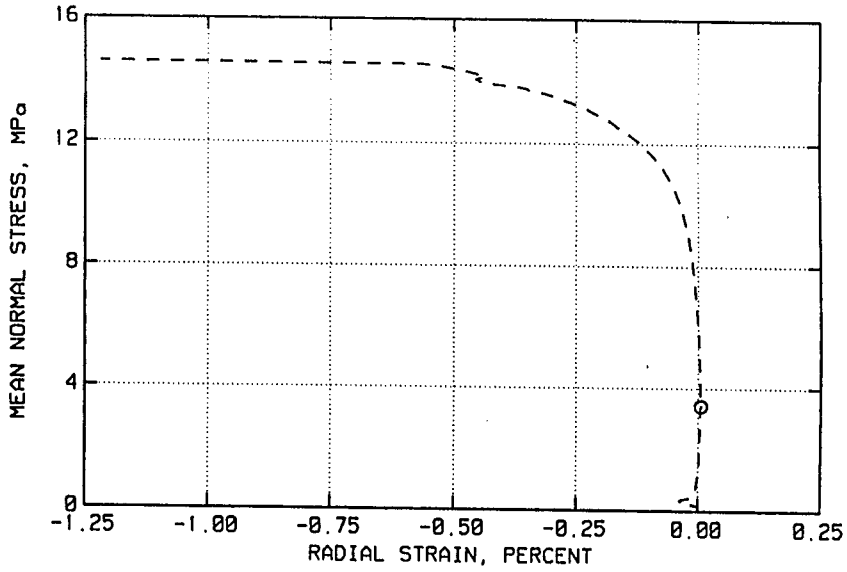

Plate 17

Plate 18

ELK CREEK DAM
TEST NO. 9604A13

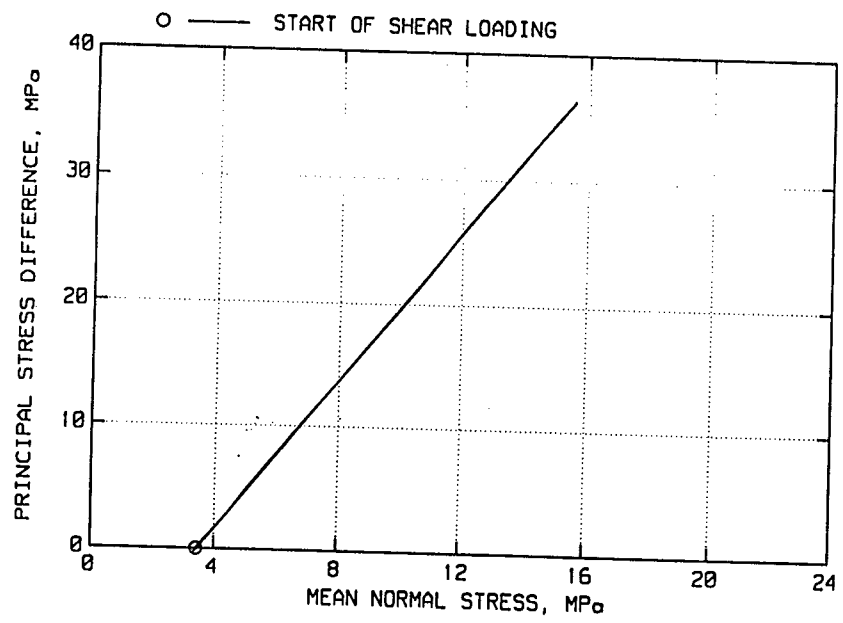

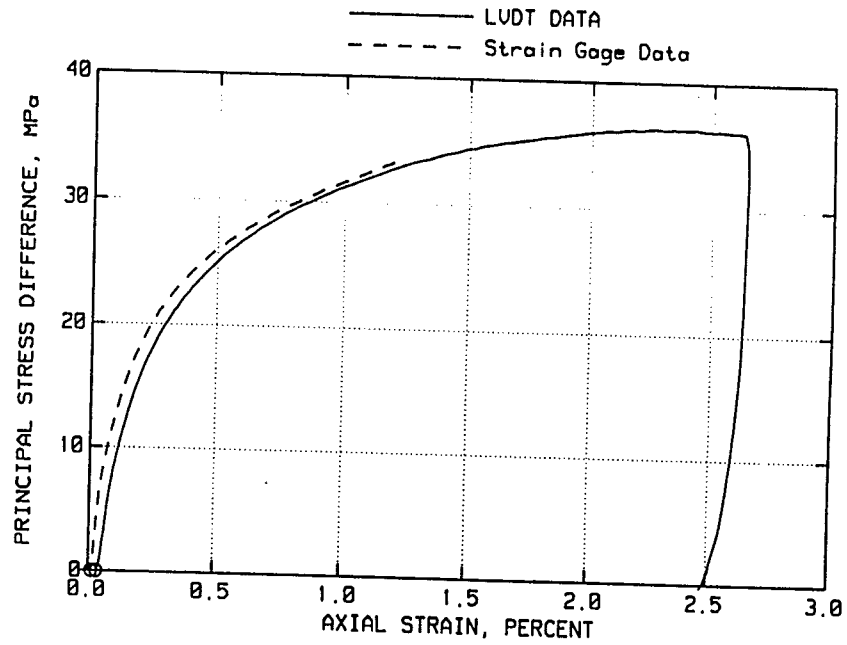

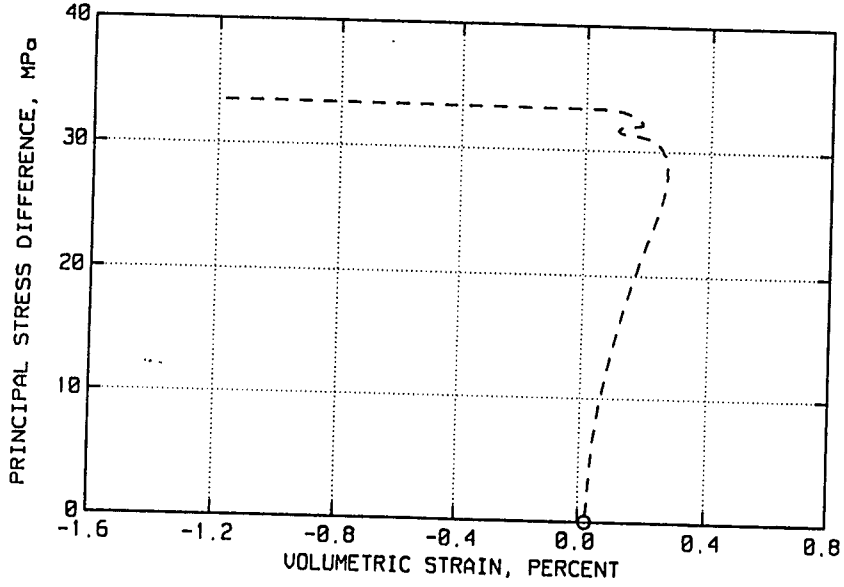

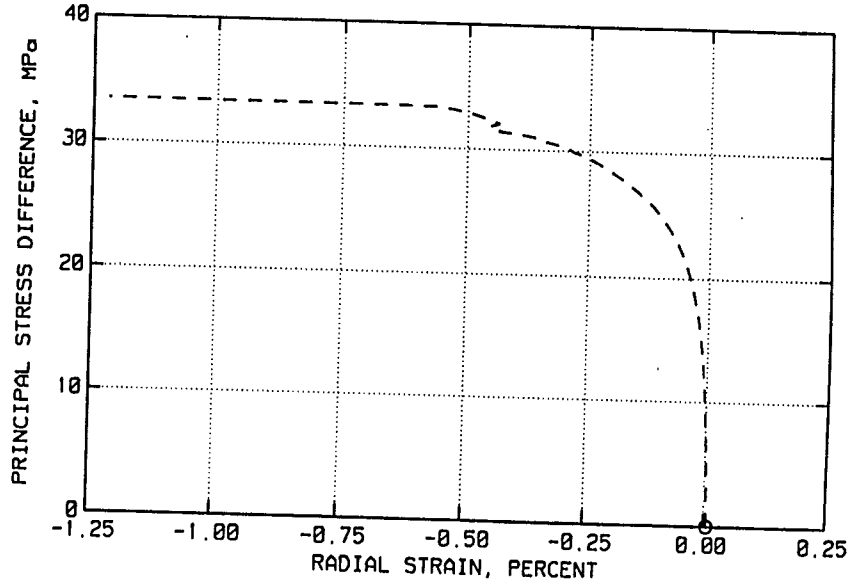

ELK CREEK DAM
TEST NO. 9604A14

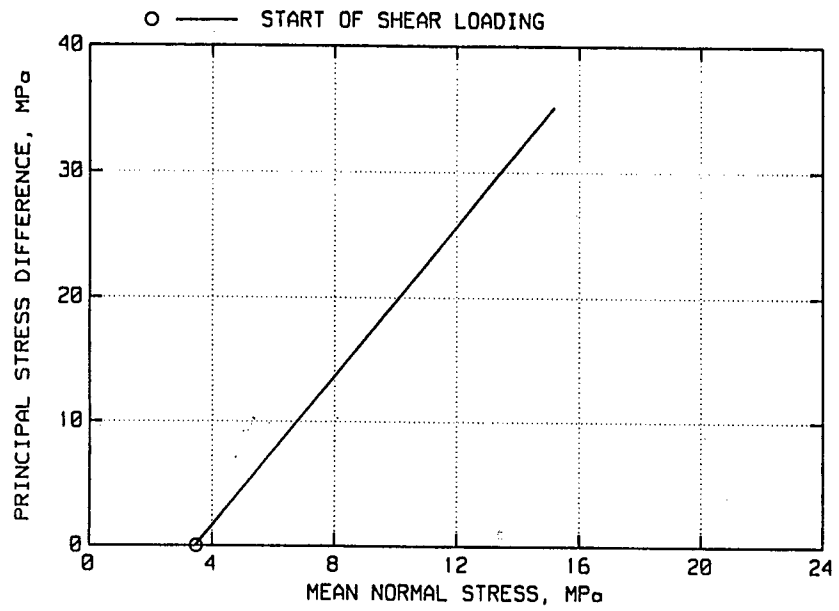

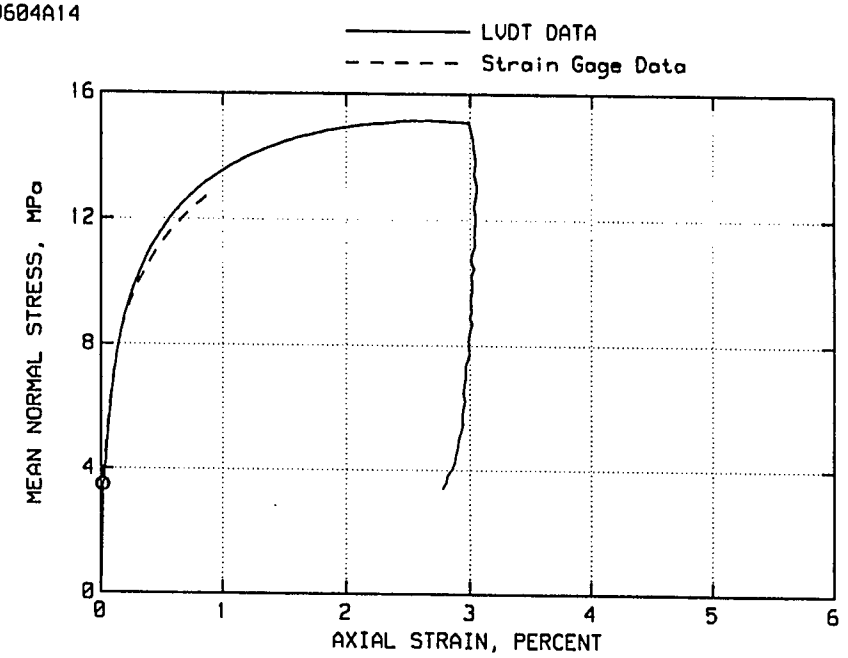

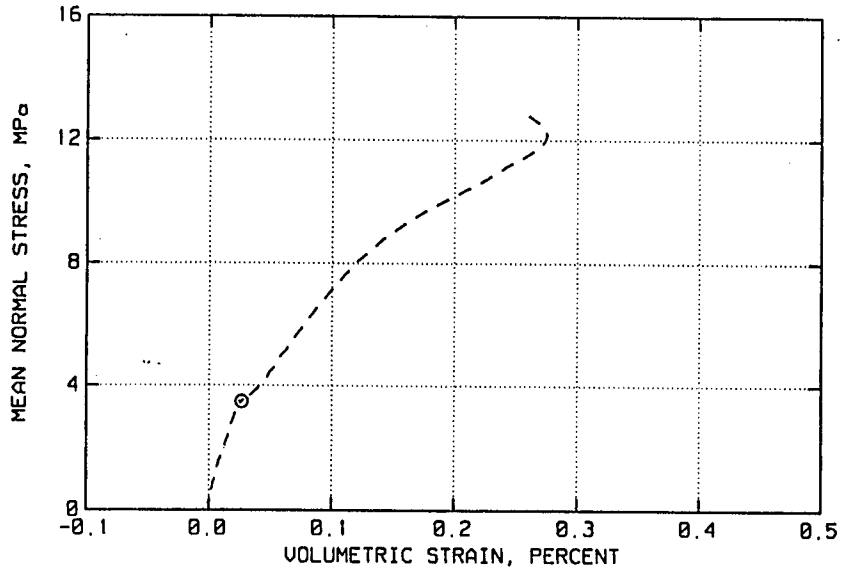

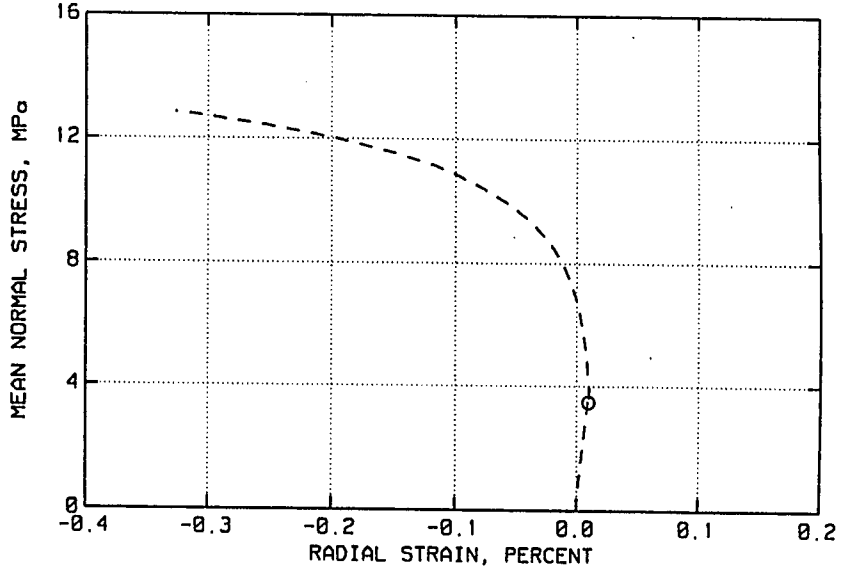

Plate 19

Plate 20

ELK CREEK DAM
TEST NO. 9604A14

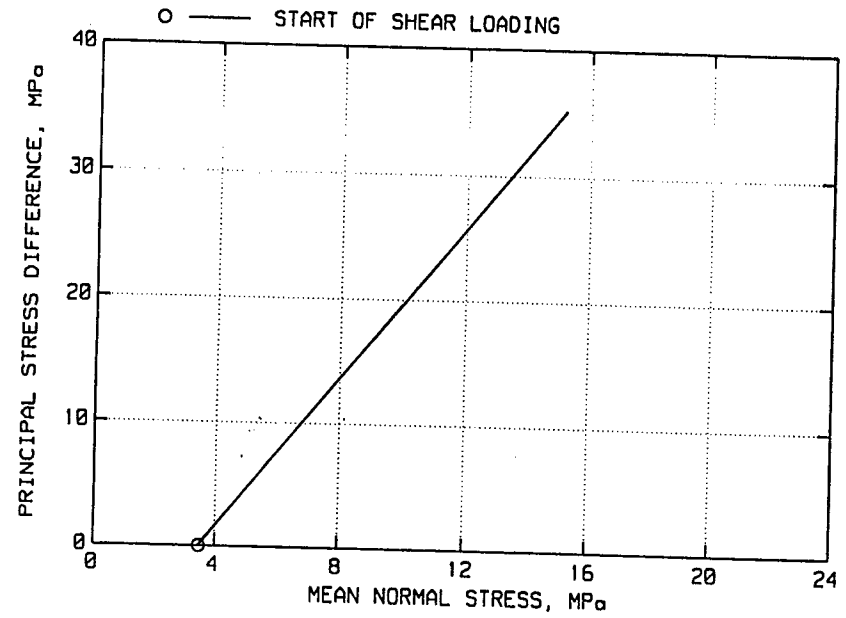

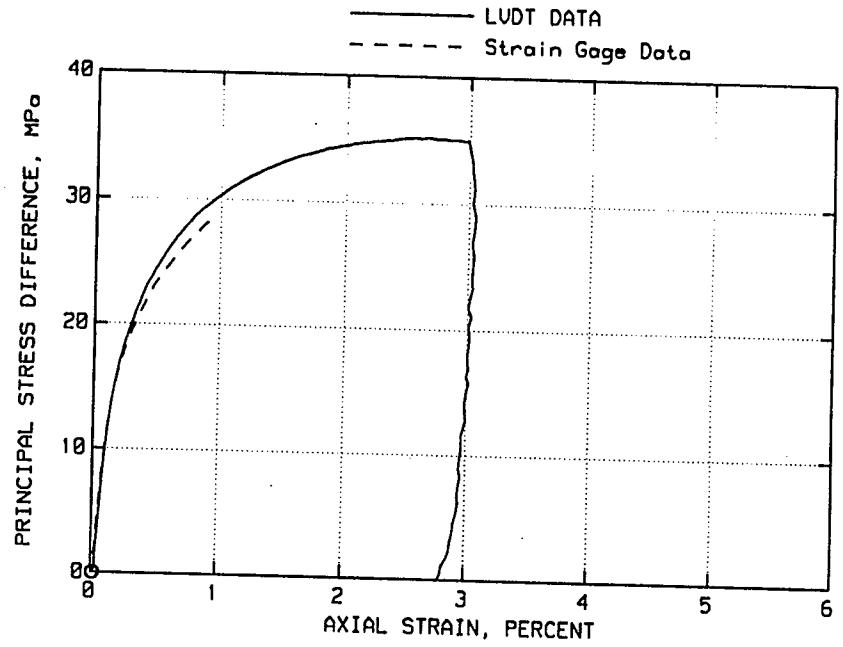

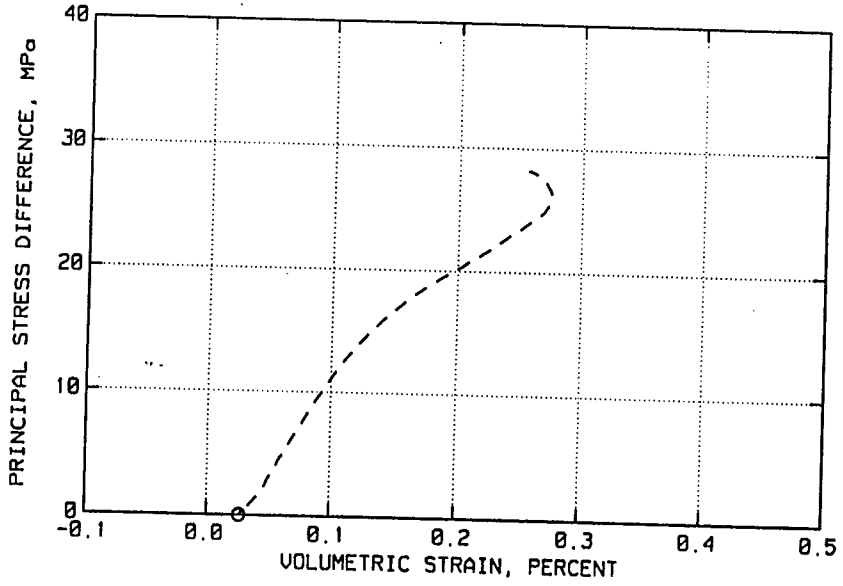

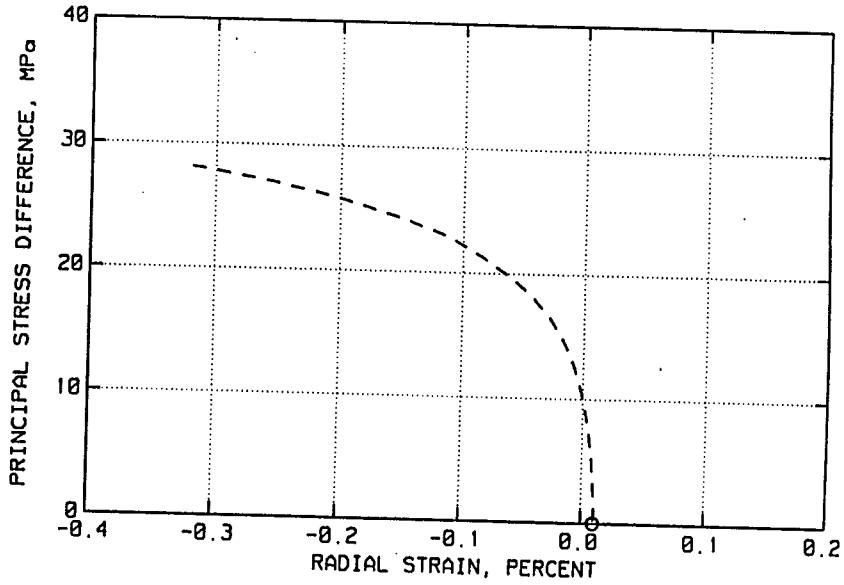

ELK CREEK DAM
TEST NO. 9604A15

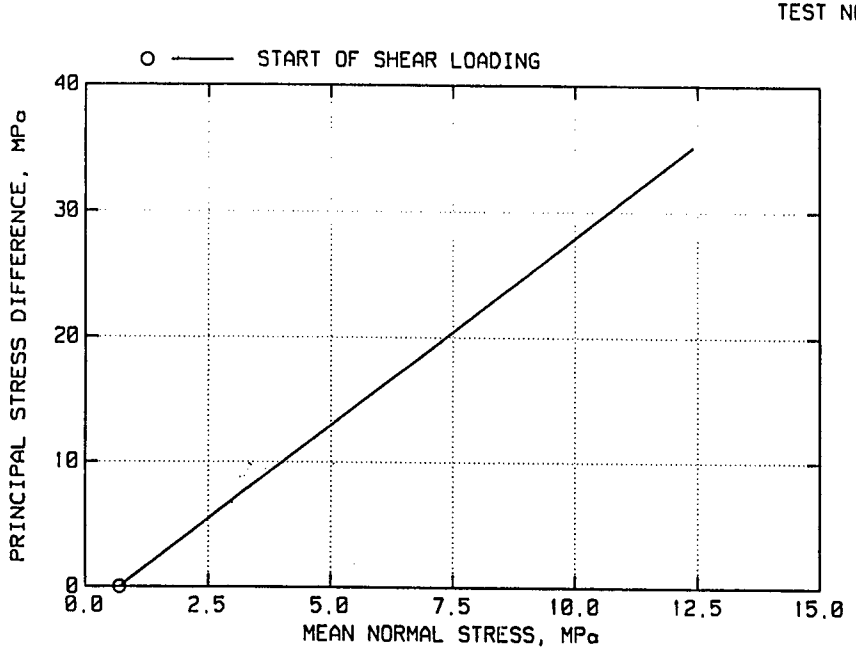

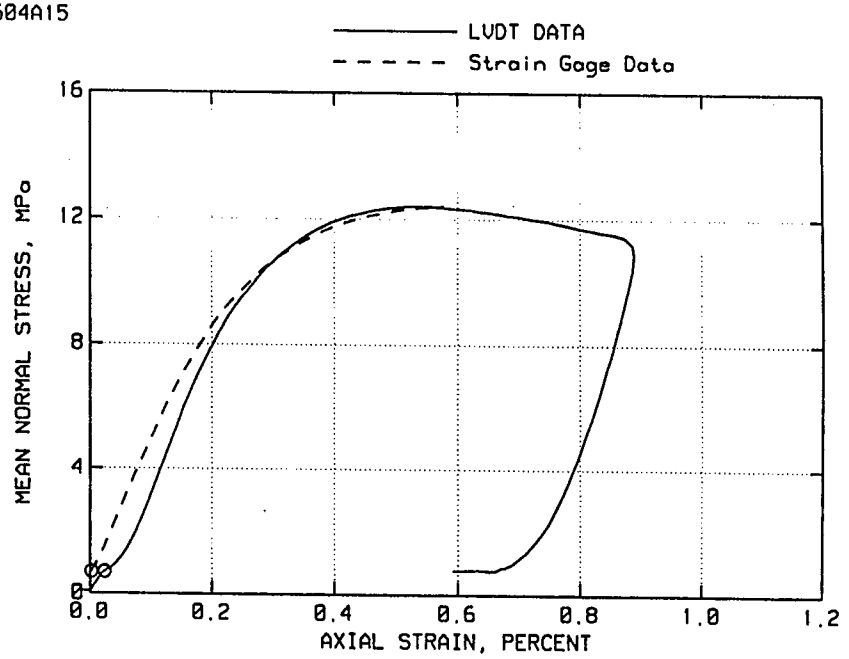

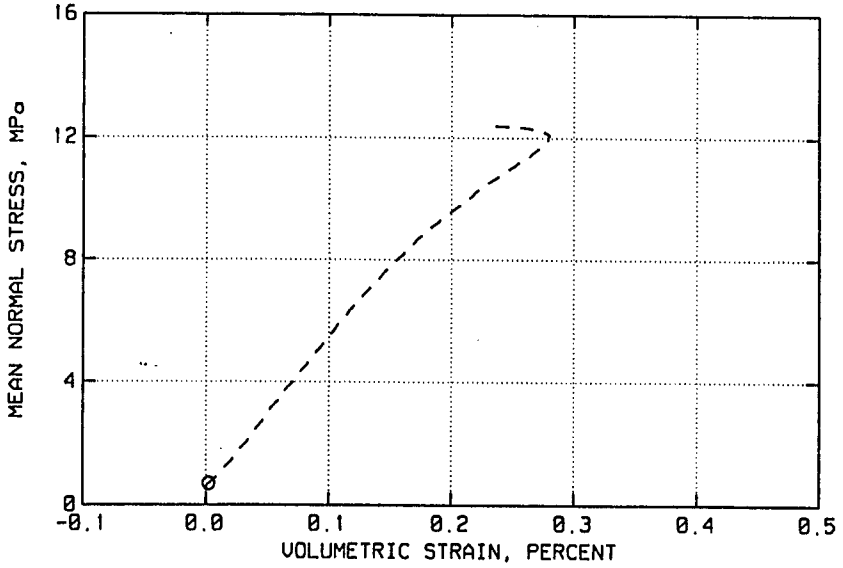

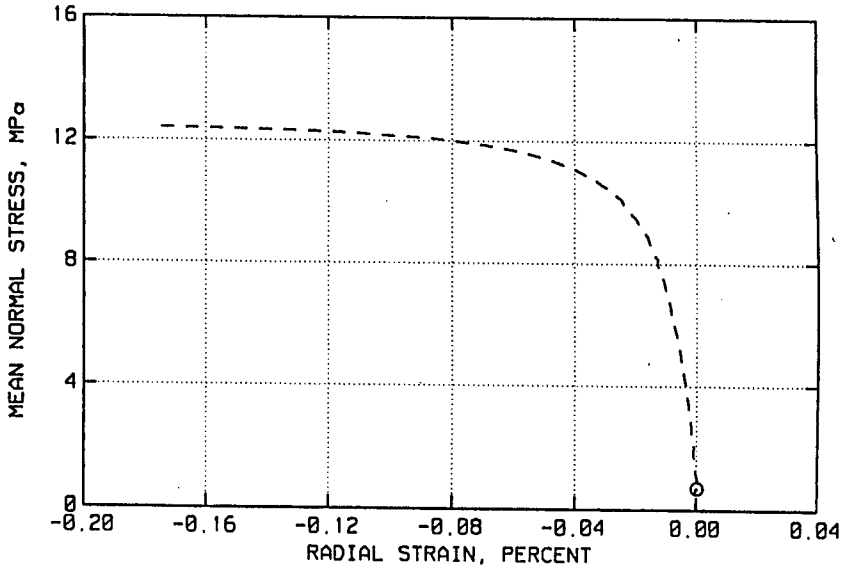

Plate 21

Plate 22

ELK CREEK DAM
TEST NO. 9604A15

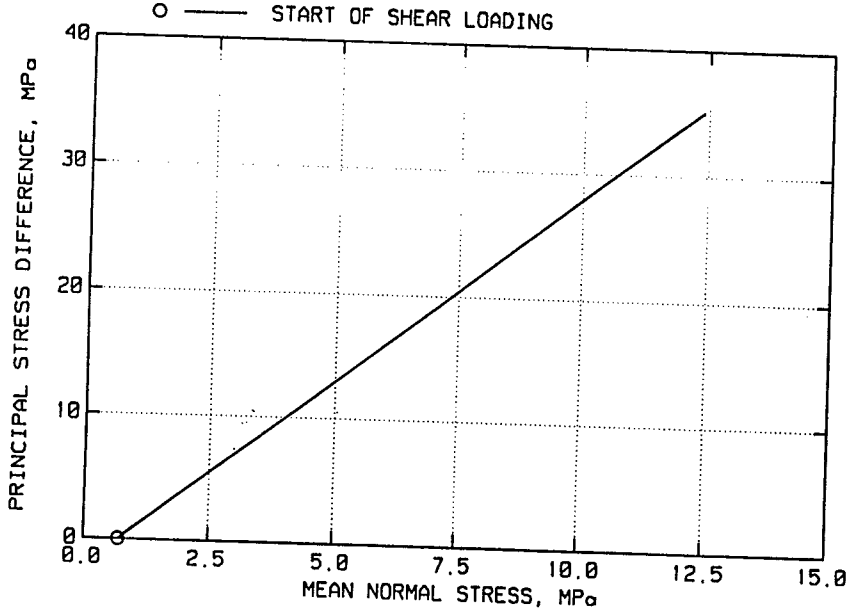

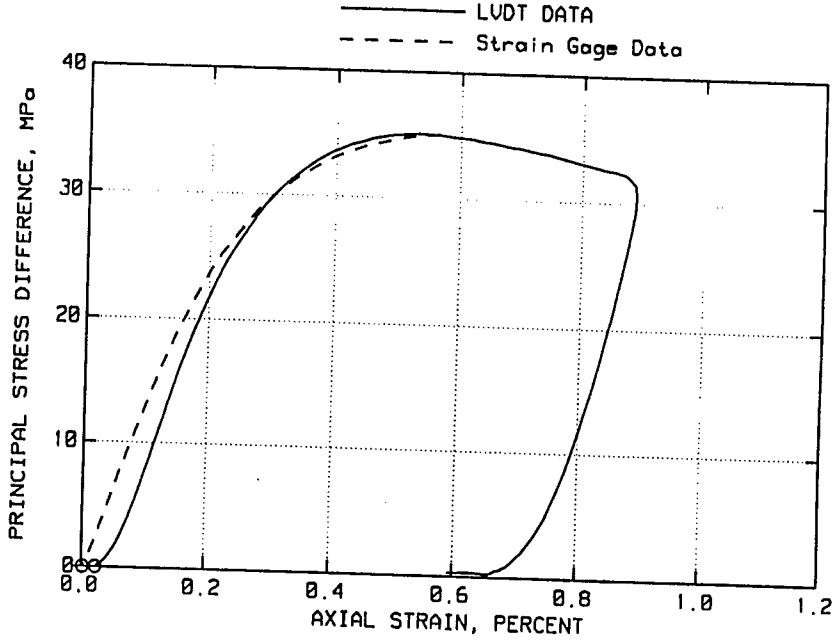

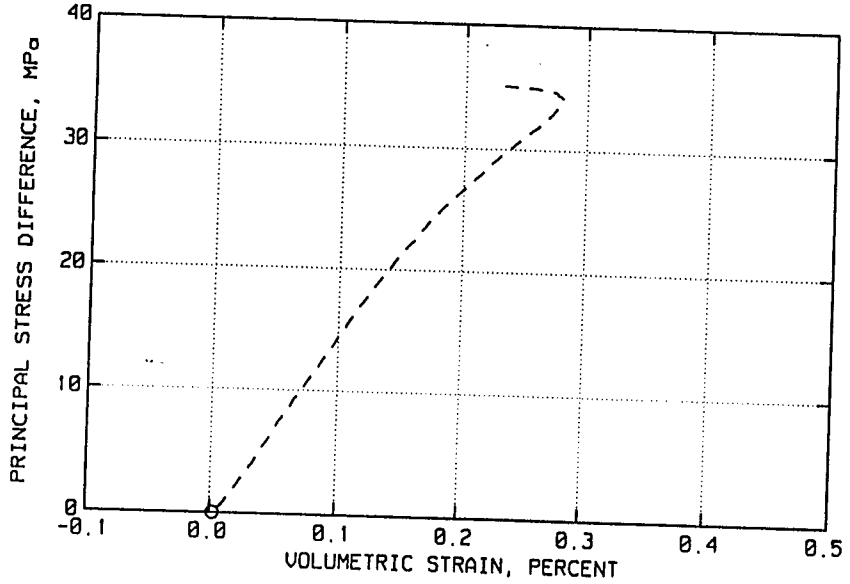

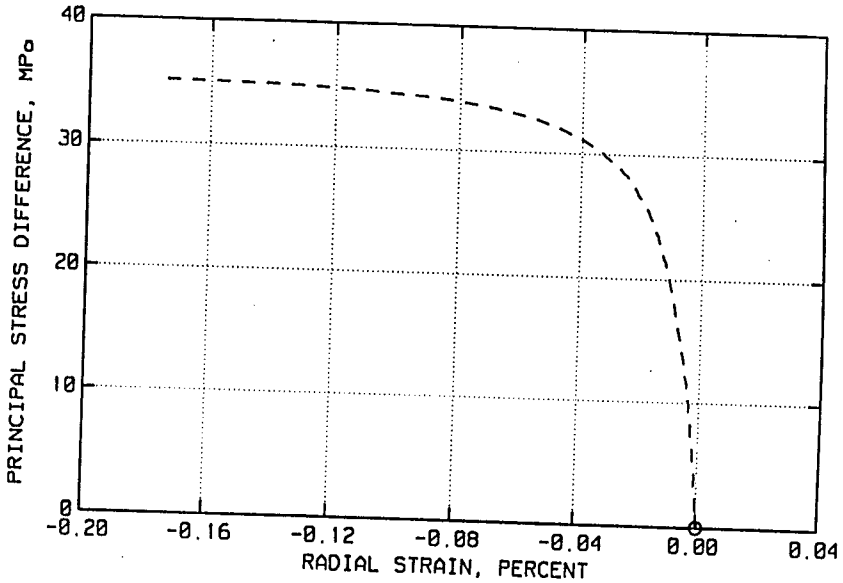

ELK CREEK DAM
TEST NO. 9604A16

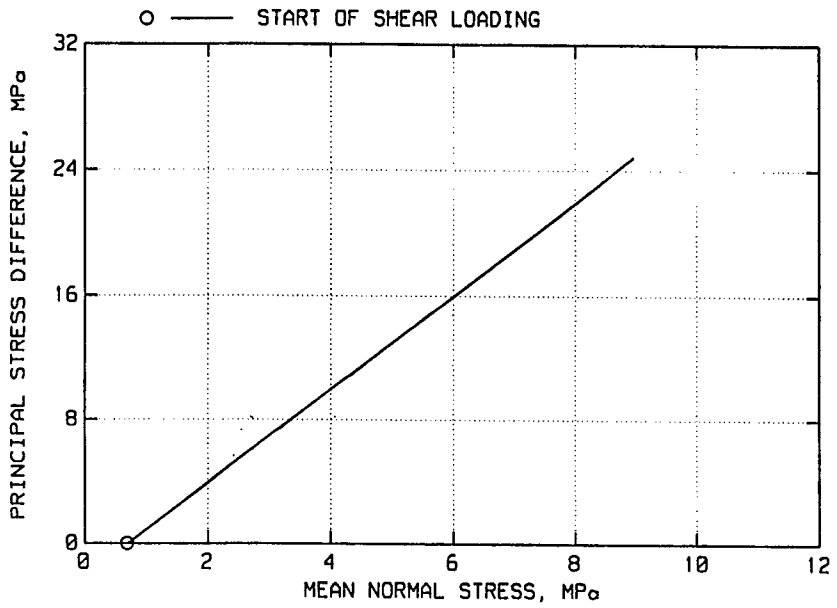

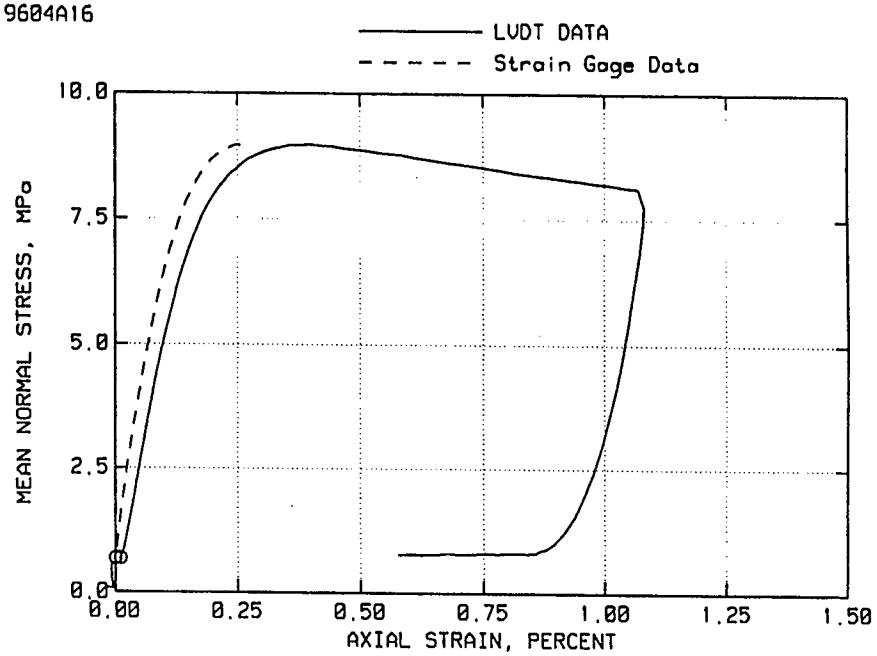

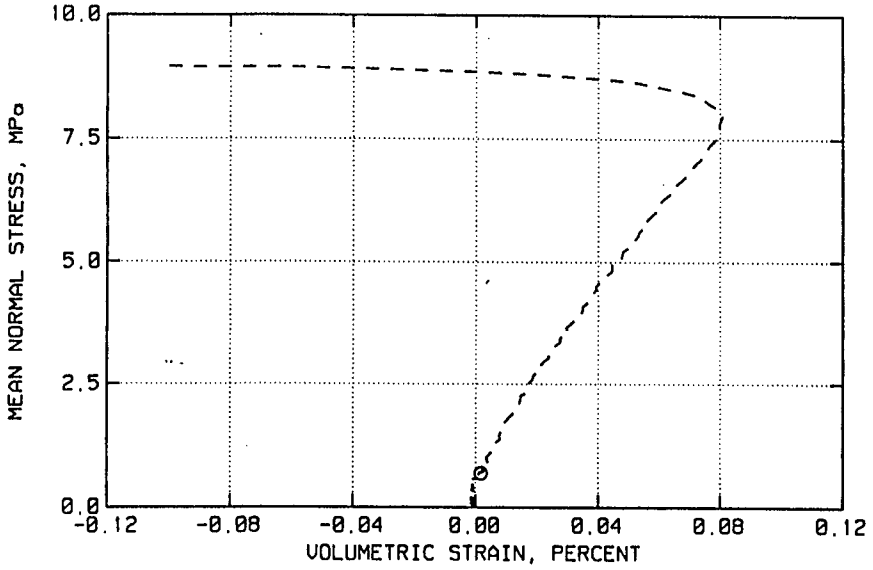

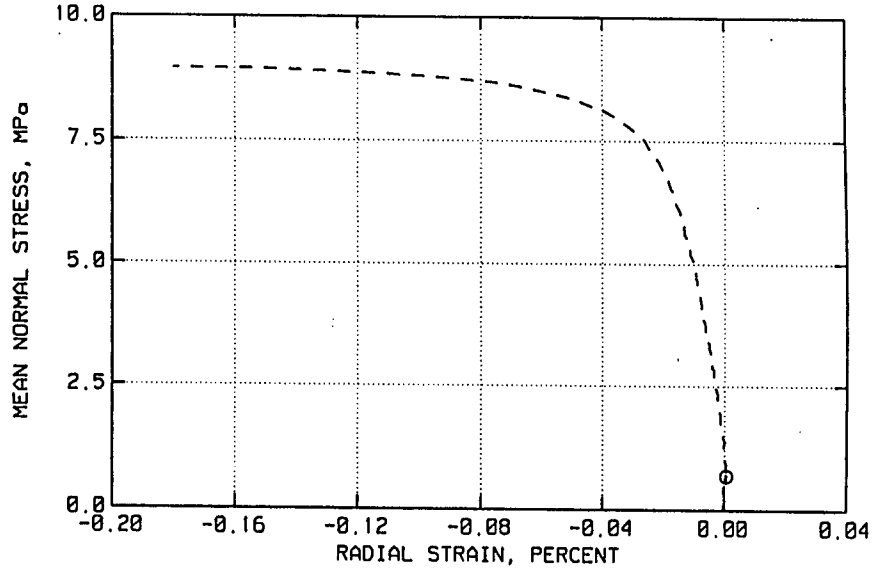

Plate 23

Plate 24

ELK CREEK DAM
TEST NO. 9604A16

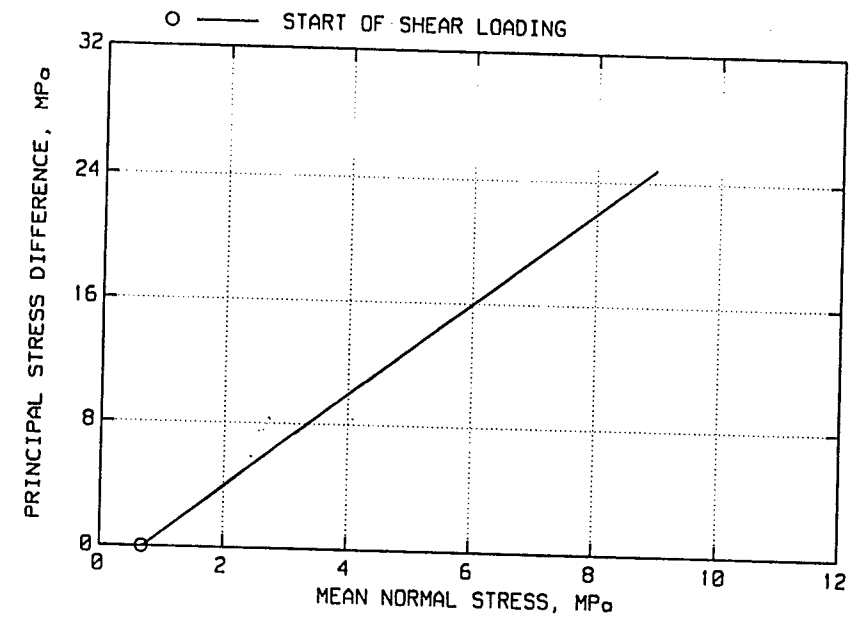

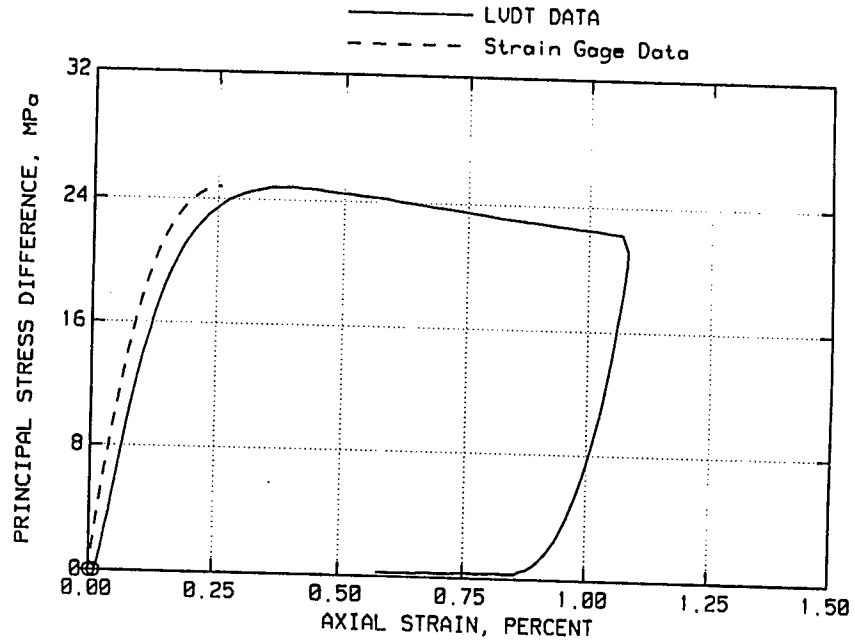

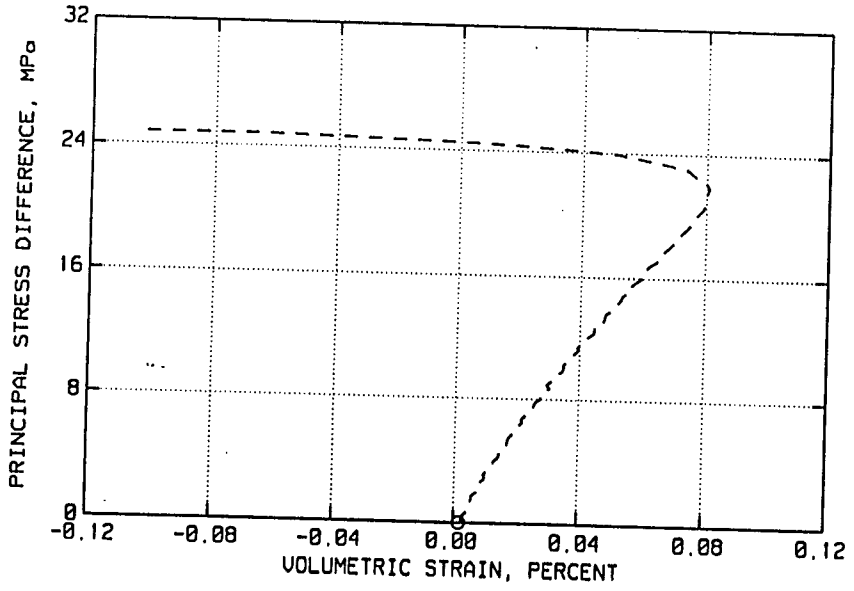

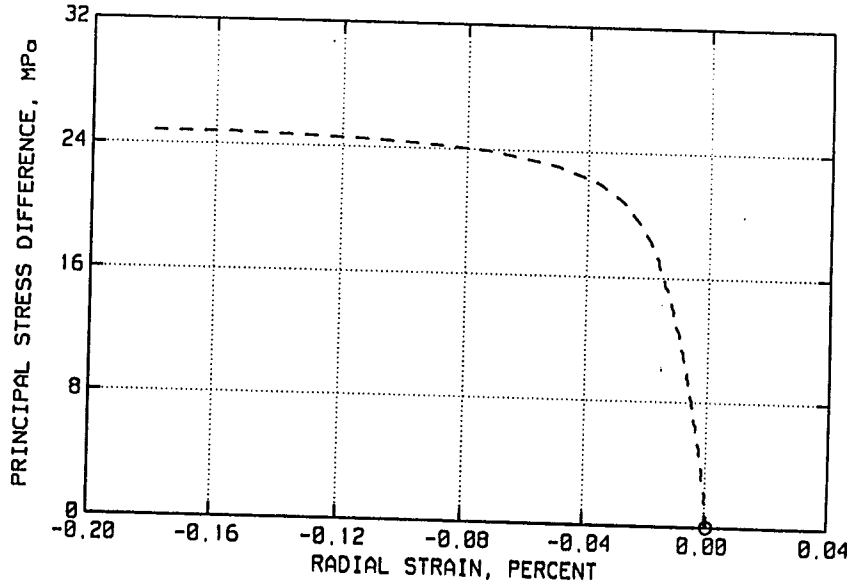

ELK CREEK DAM
TEST NO. 9604A17

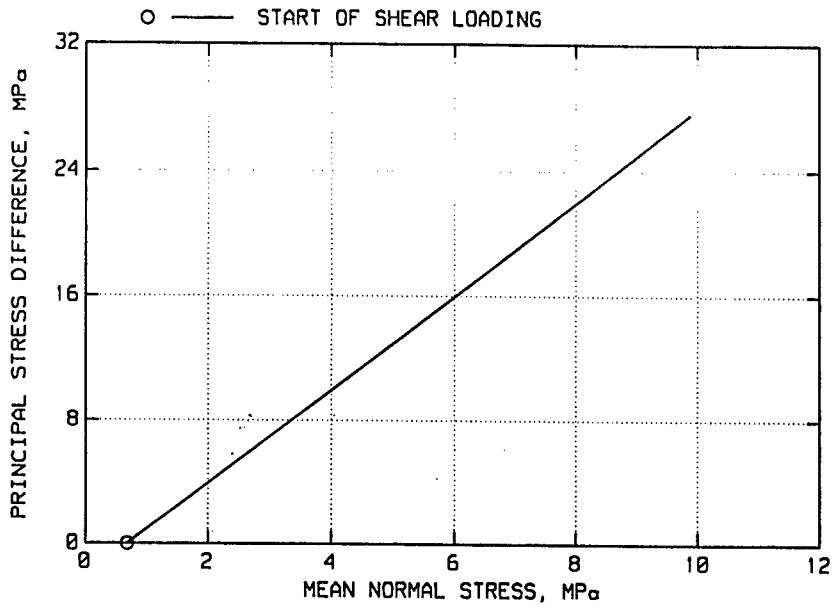

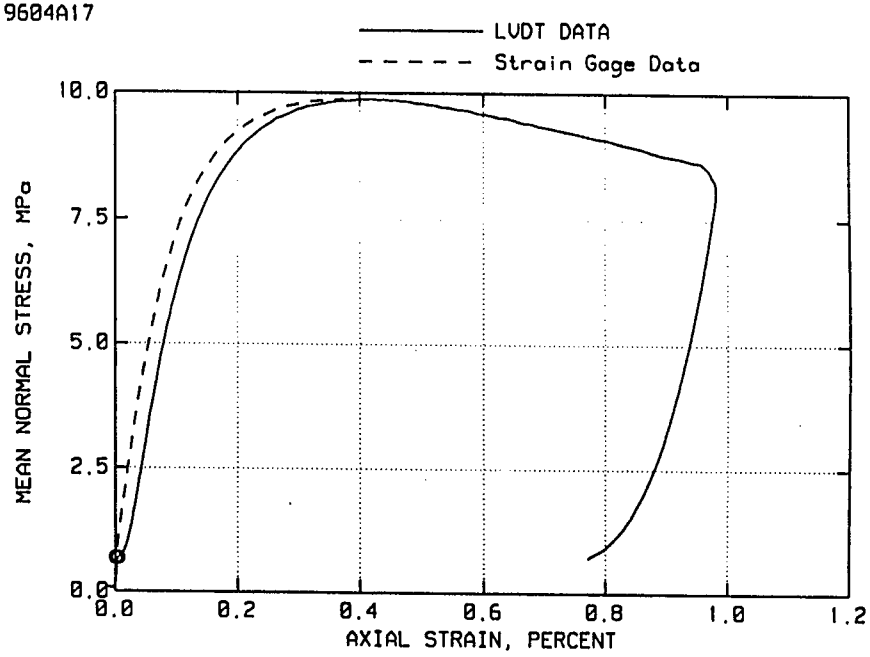

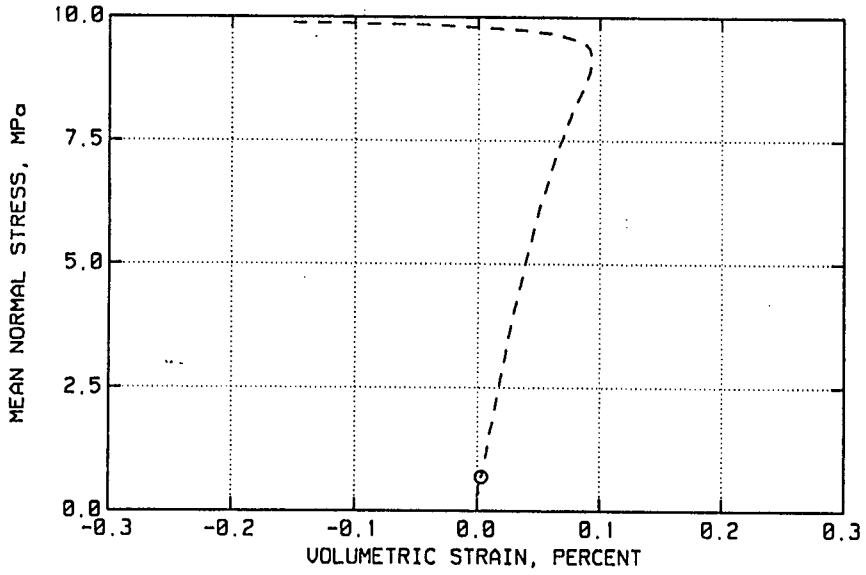

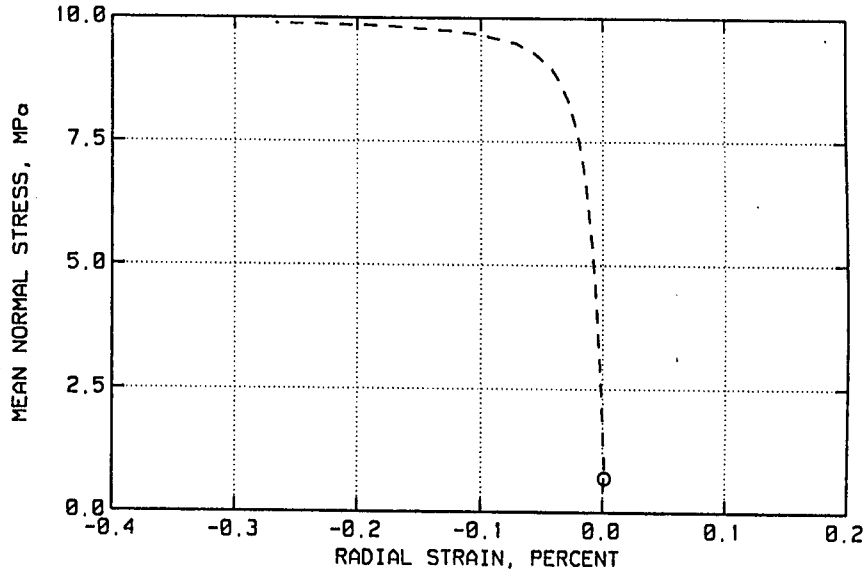

Plate 25

Plate 26

ELK CREEK DAM
TEST NO. 9604A17

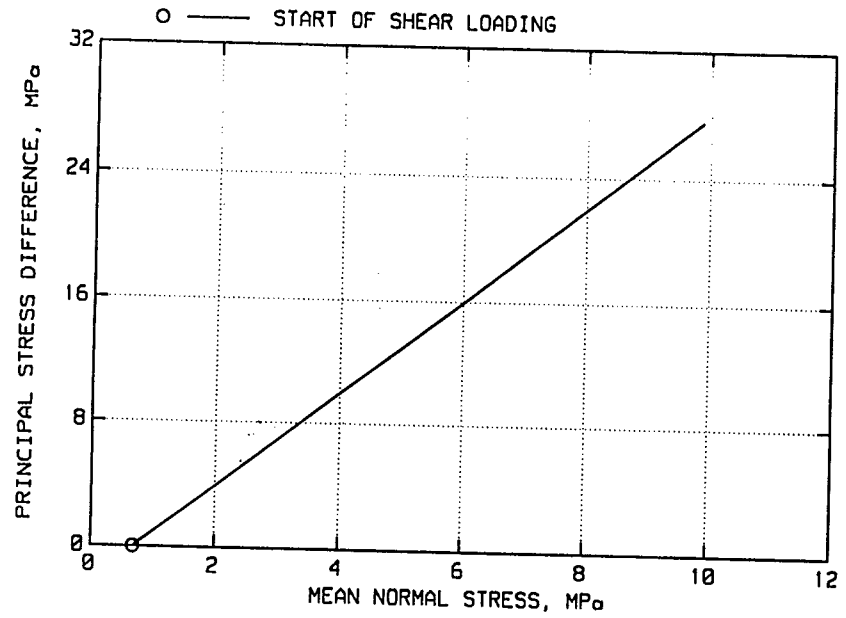

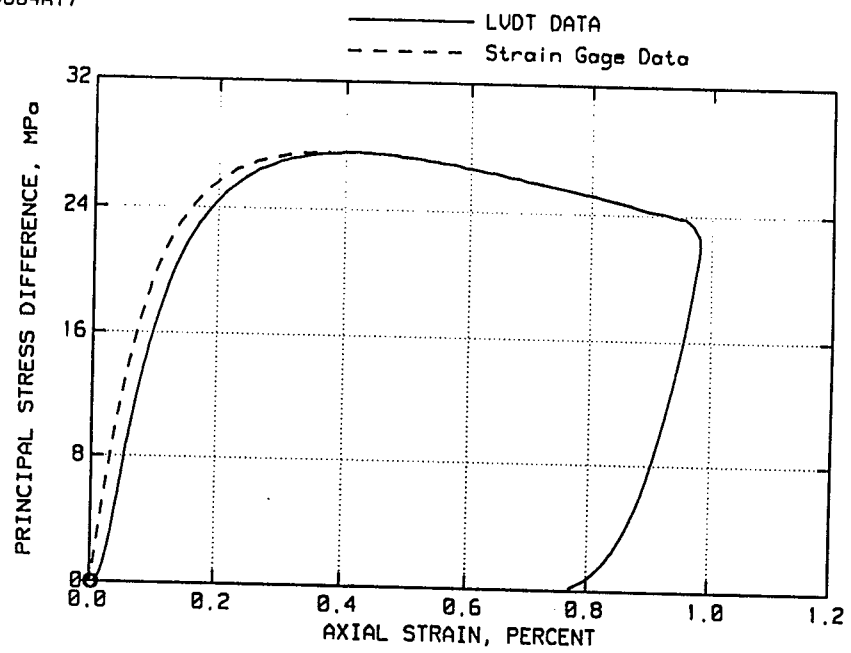

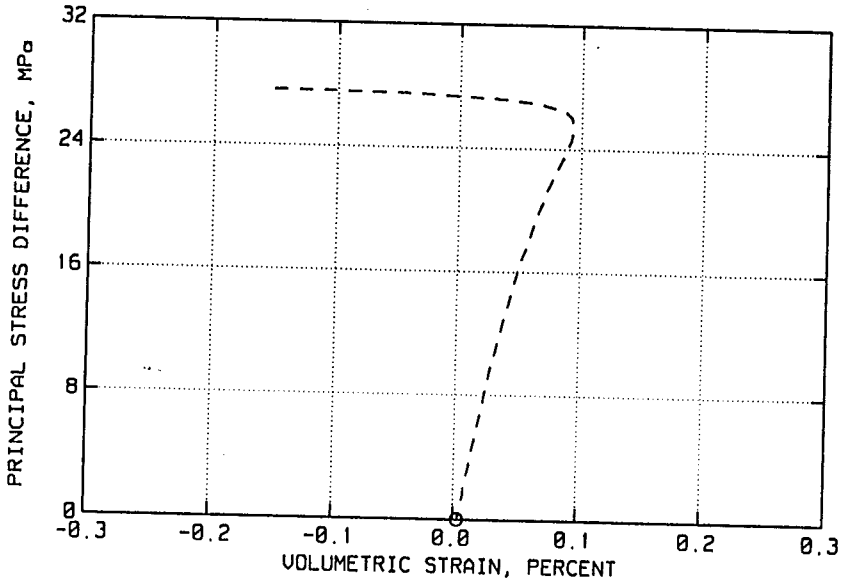

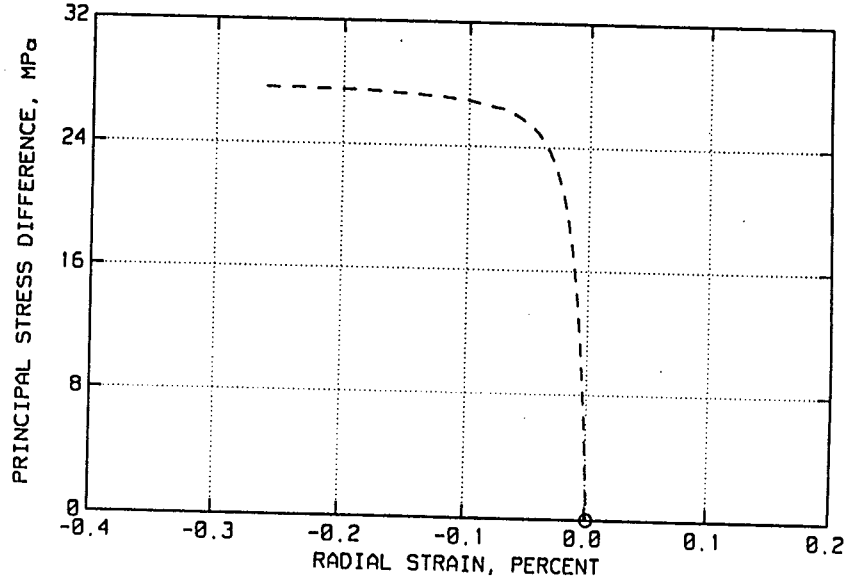

ELK CREEK DAM

TEST NO. 9604Y01

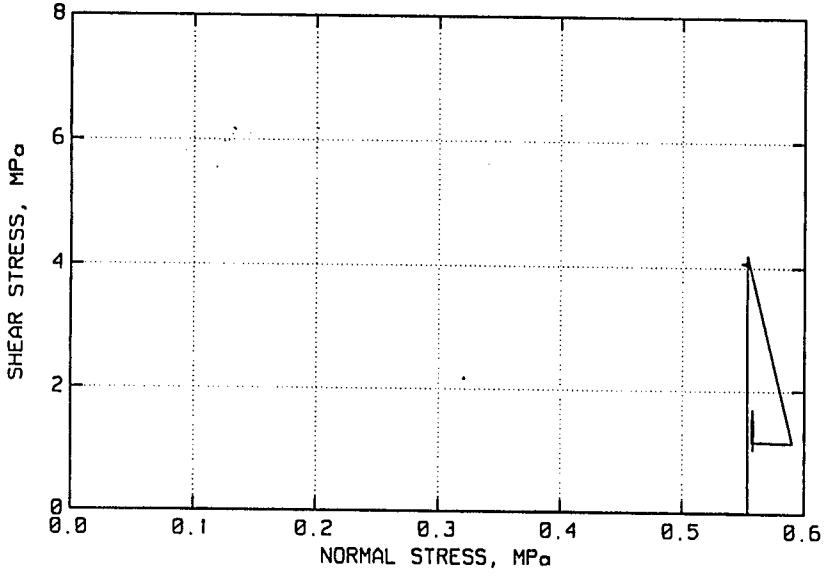

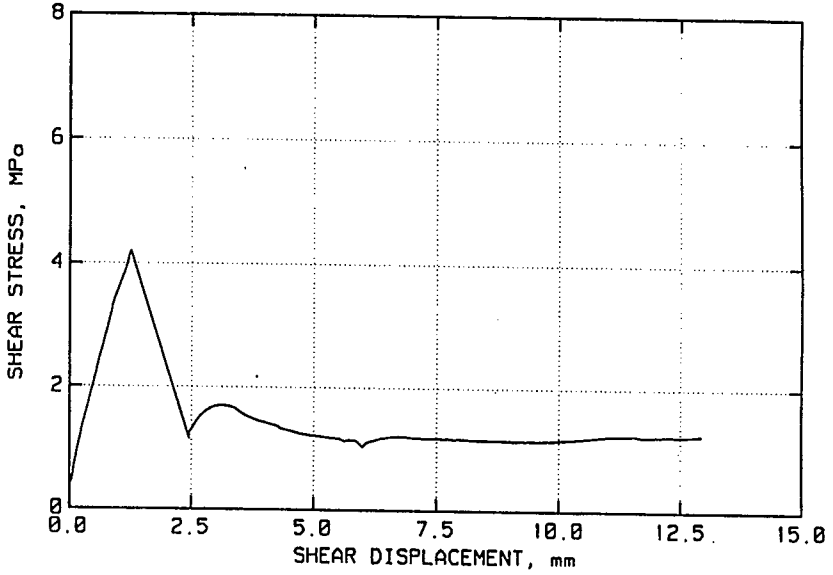

Plate 27

Plate 28

ELK CREEK DAM
TEST NO. 9604Y02

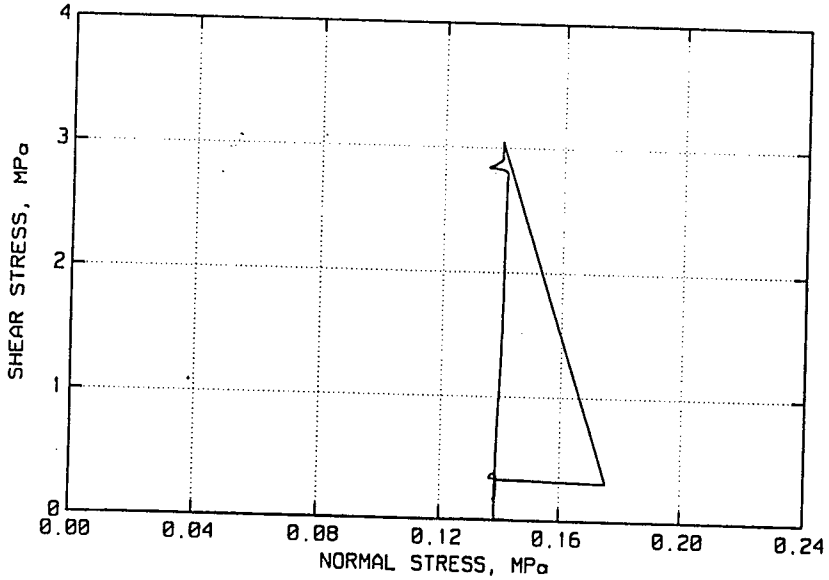

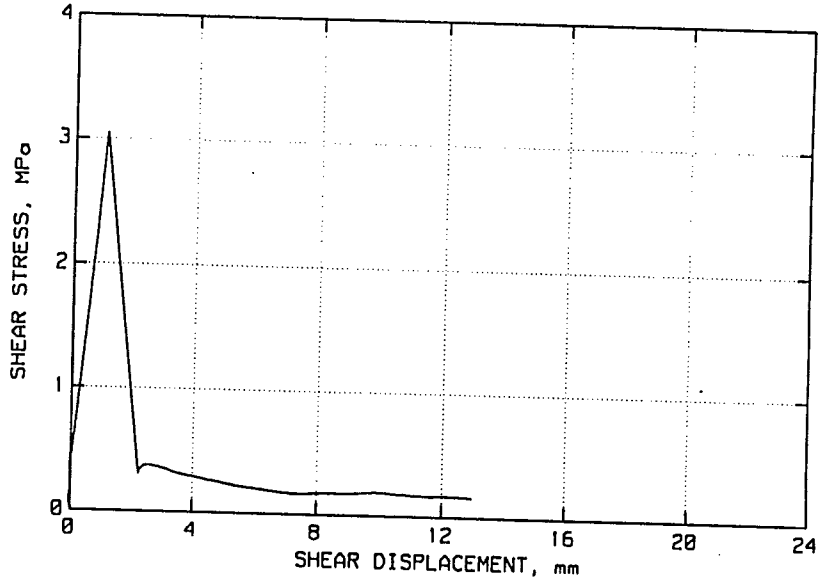

ELK CREEK DAM

TEST NO. 9604Y03

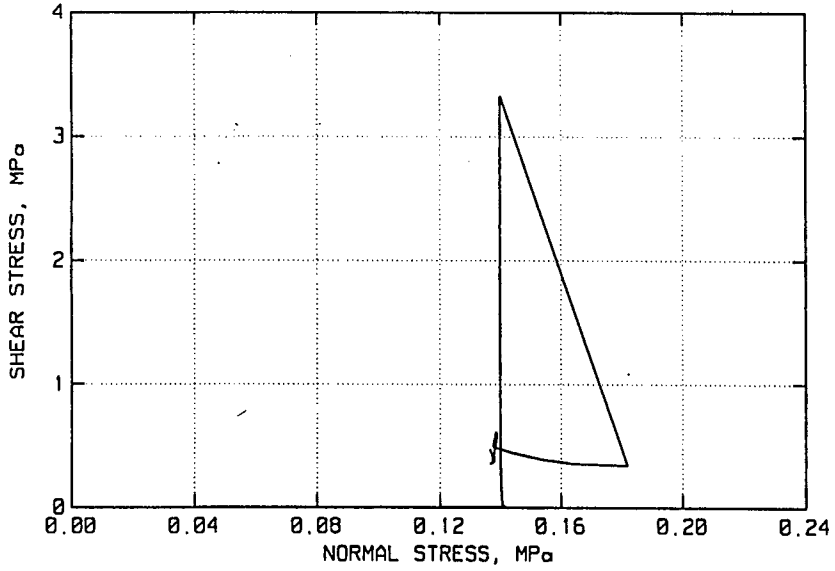

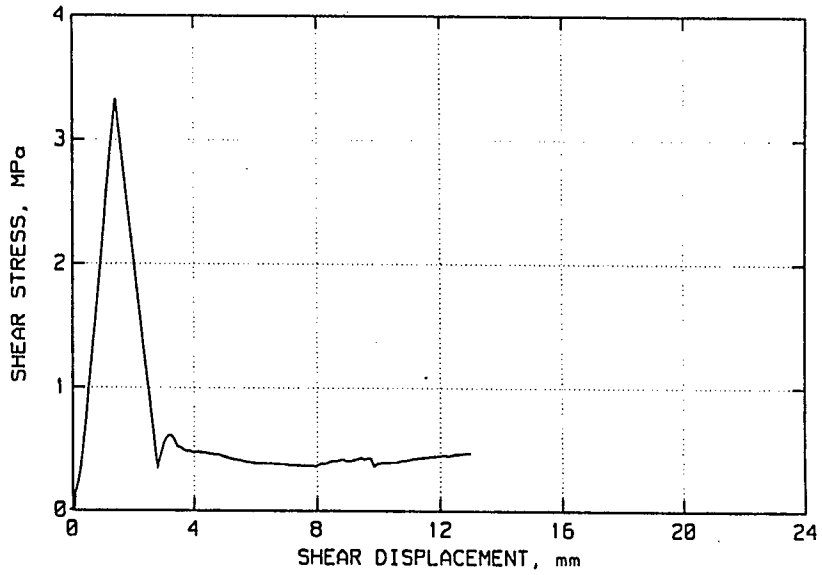

Plate 29

Plate 30

ELK CREEK DAM
TEST NO. 9604Y04

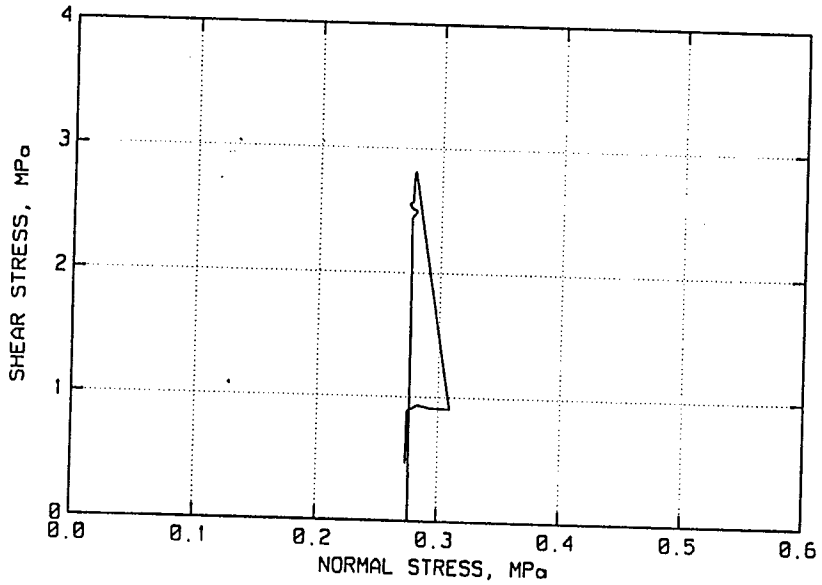

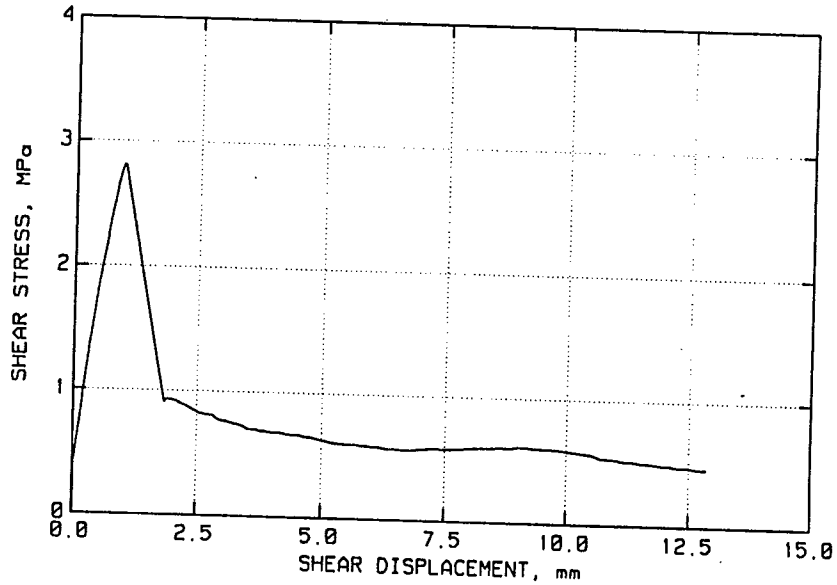

ELK CREEK DAM

TEST NO. 9604Y05

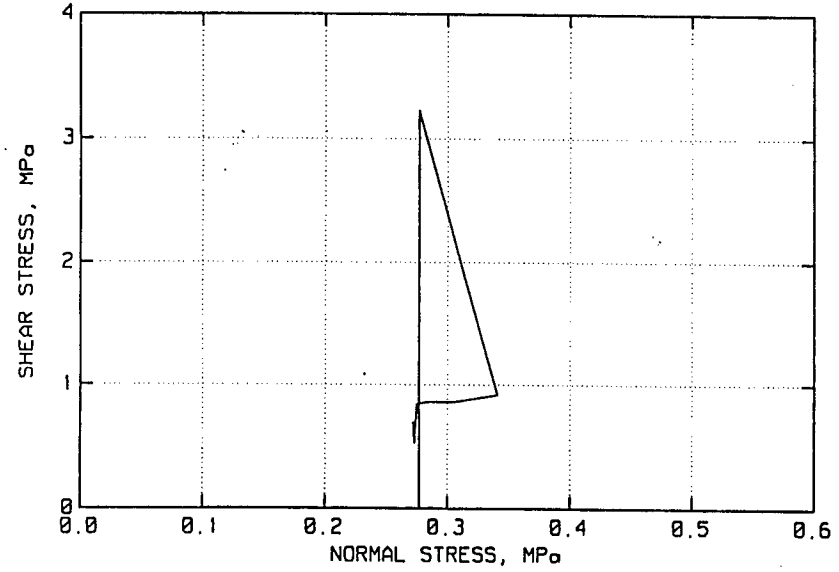

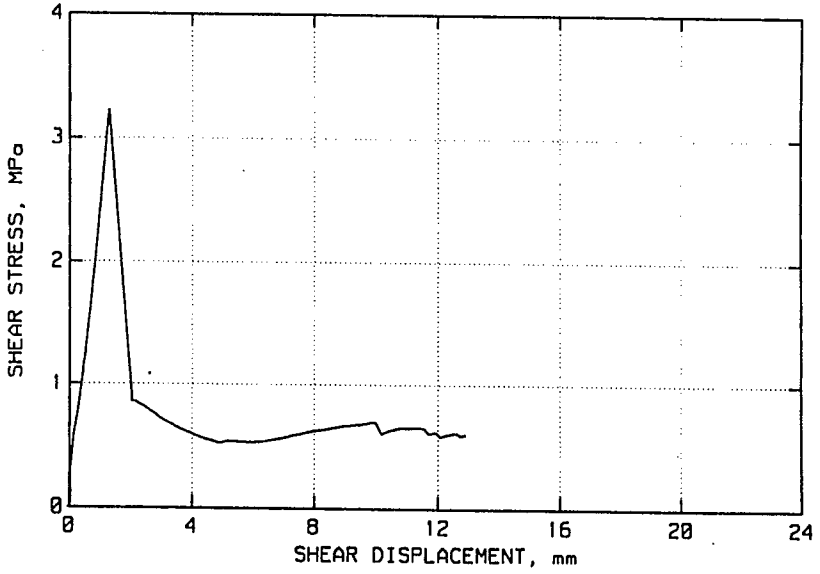

Plate 32

ELK CREEK DAM
TEST NO. 9604Y06

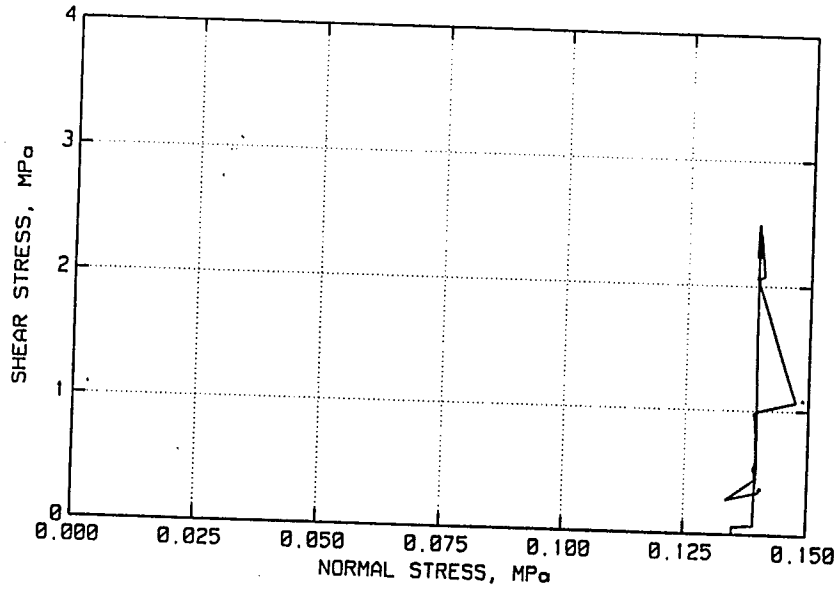

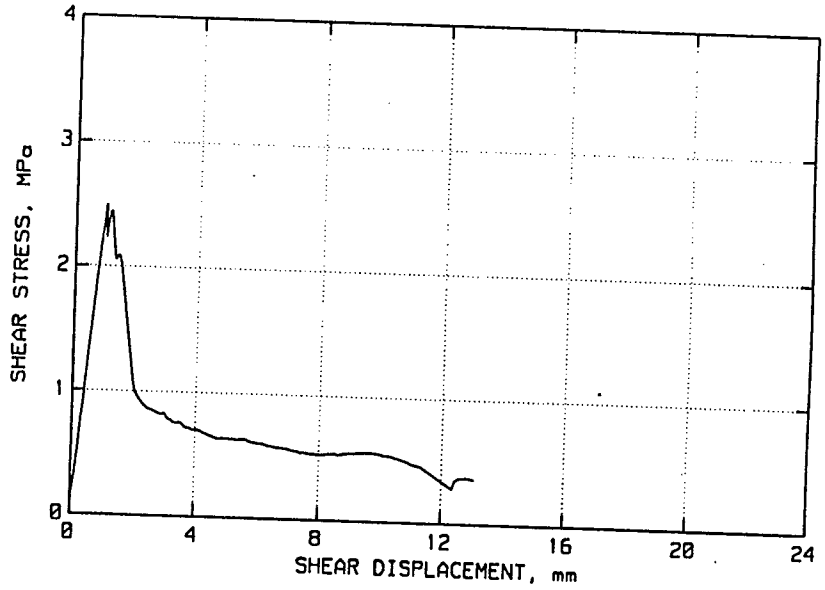

ELK CREEK DAM

TEST NO. 9604Y07

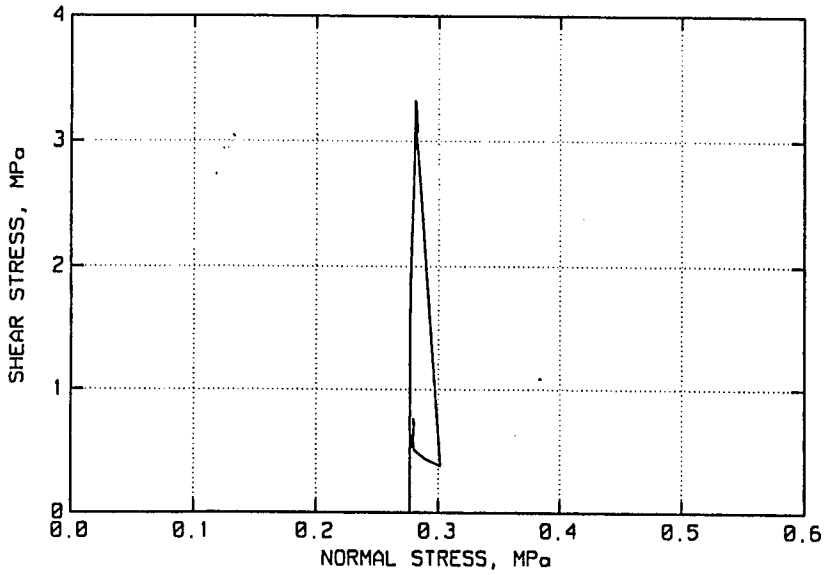

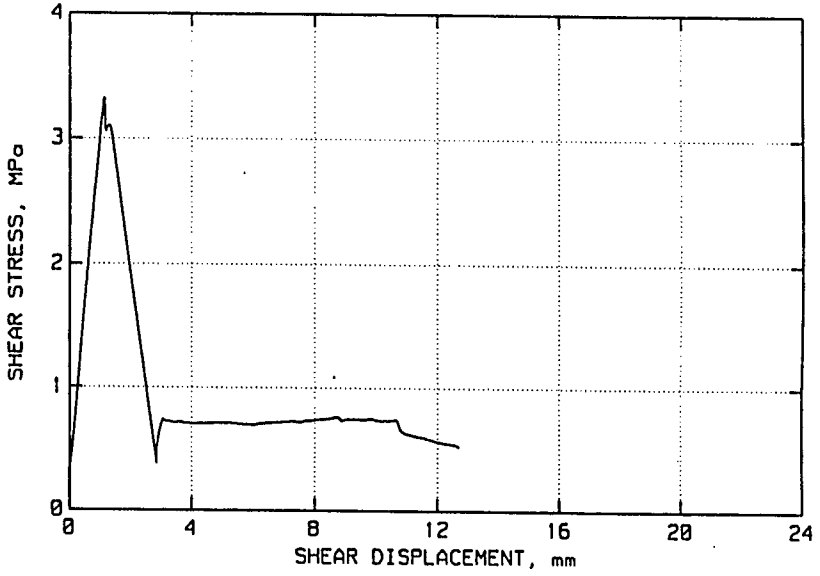

Plate 33

Plate 34

ELK CREEK DAM
TEST NO. 9604Y08

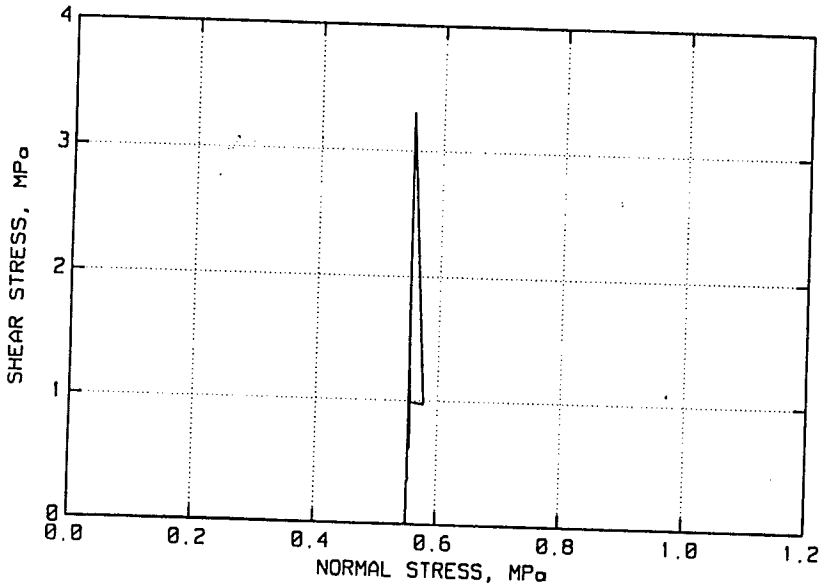

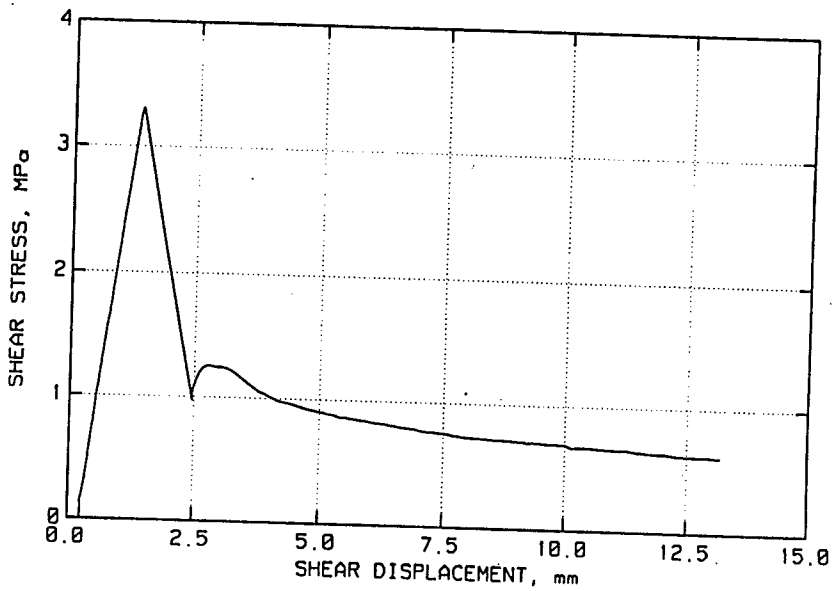

ELK CREEK DAM
TEST NO. 9604Y09

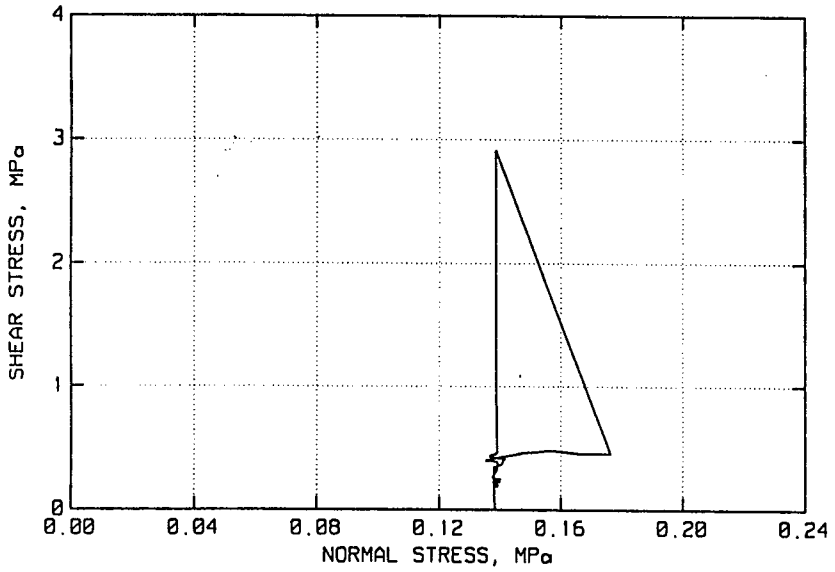

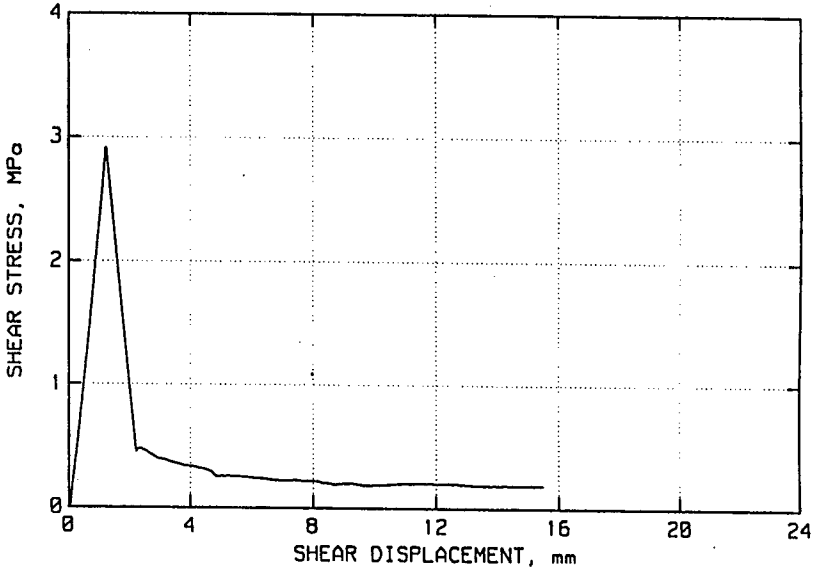

Plate 35

Plate 36

ELK CREEK DAM
TEST NO. 9604Y10

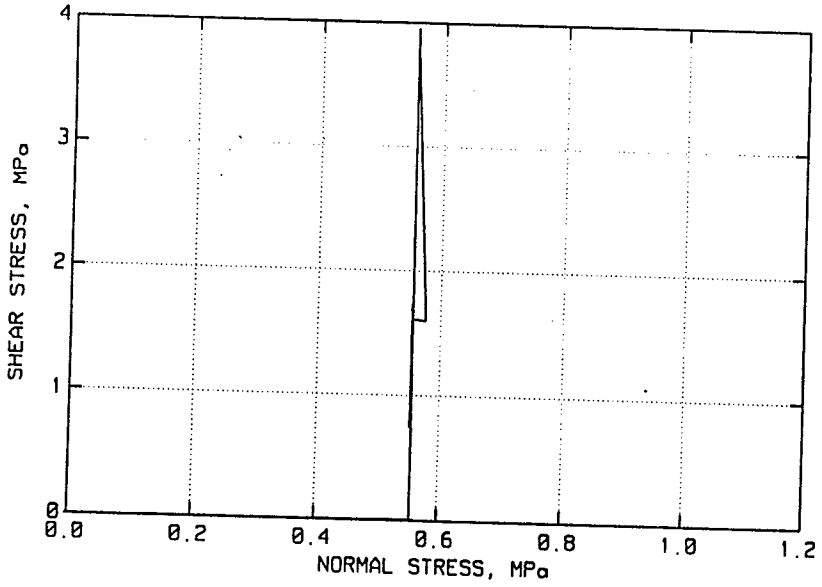

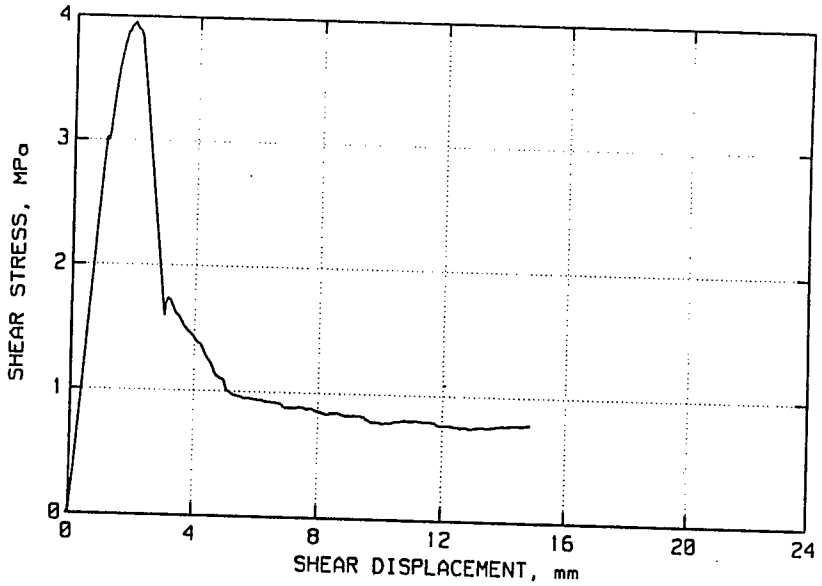

ELK CREEK DAM

TEST NO. 9604Y11

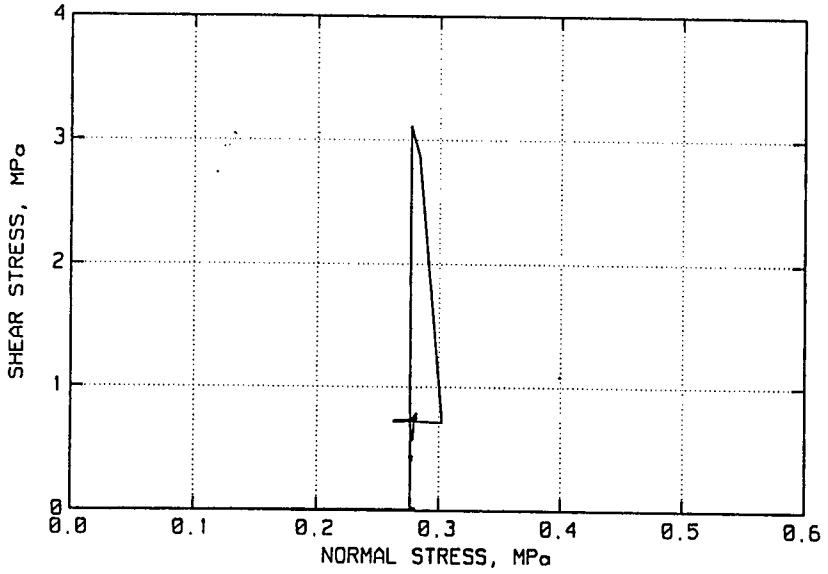

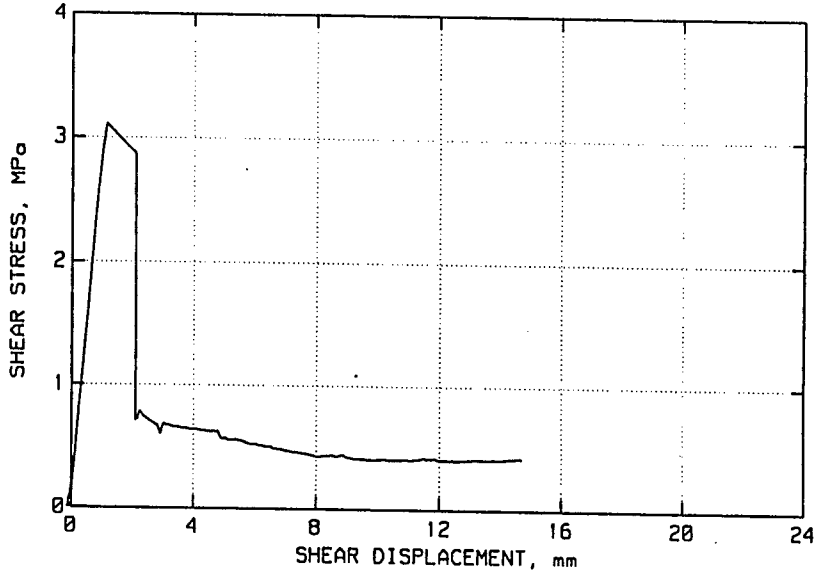

Plate 37

Plate 38

ELK CREEK DAM
TEST NO. 9604Y12

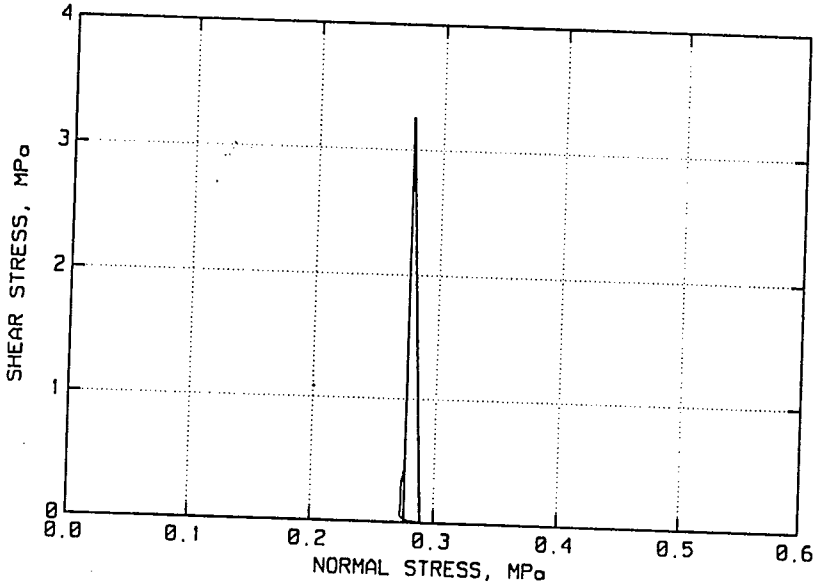

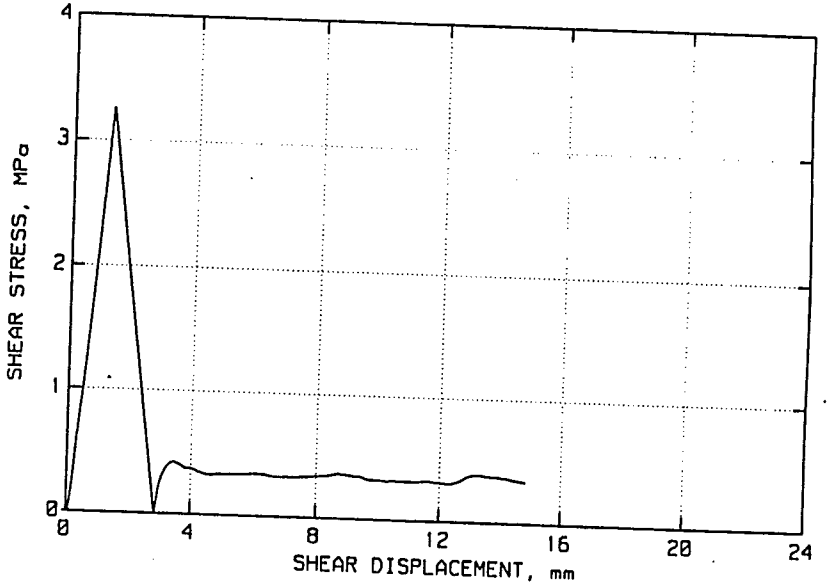

ELK CREEK DAM
TEST NO. 9604Y13

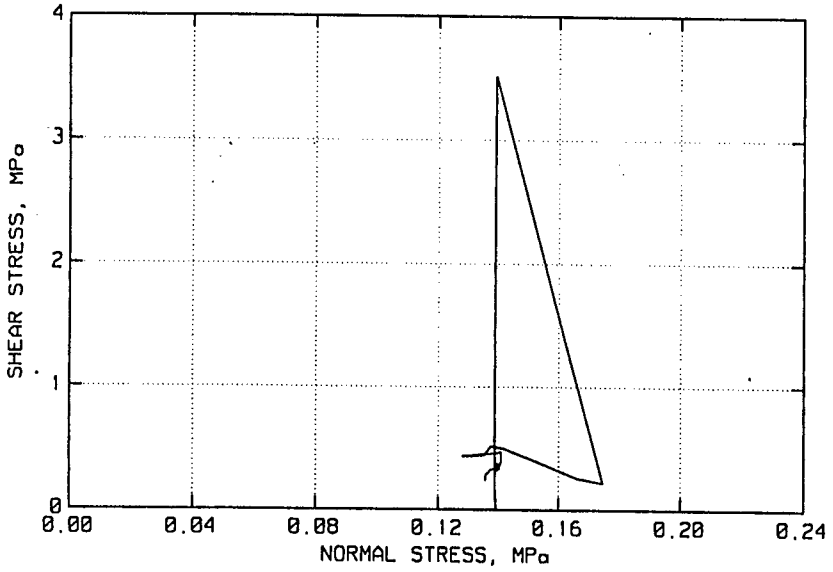

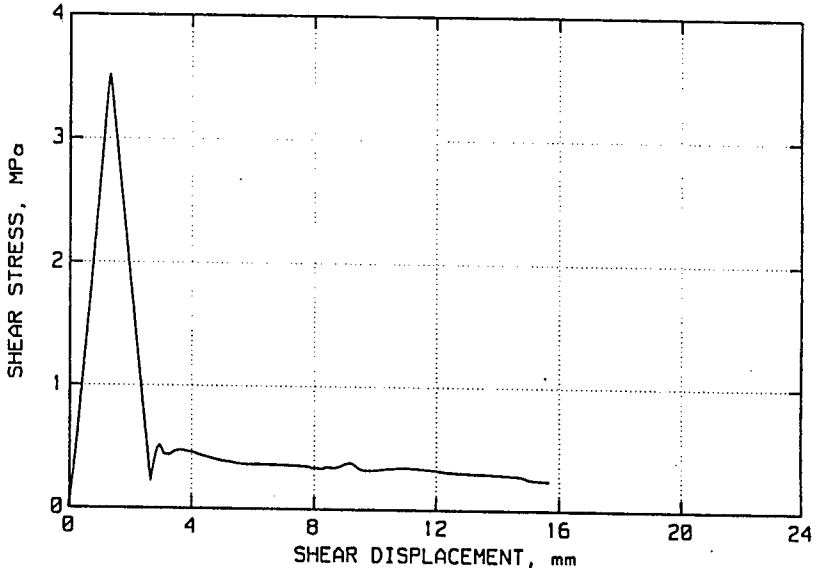

Plate 39

Plate 40

ELK CREEK DAM
TEST NO. 9604Y14

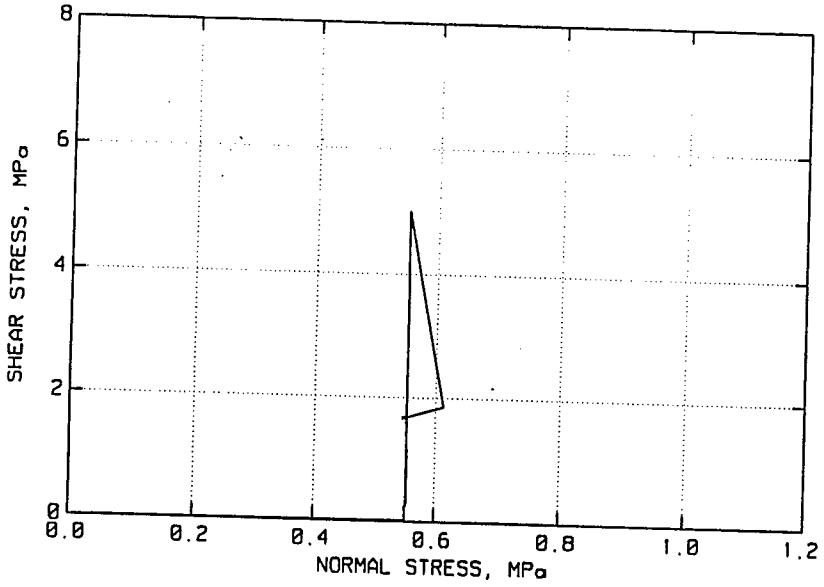

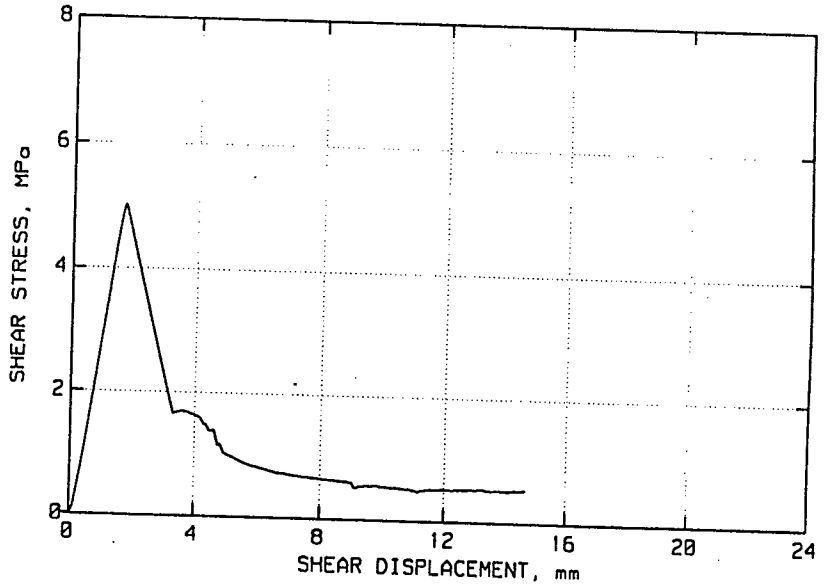

ELK CREEK DAM

TEST NO. 9604Y15

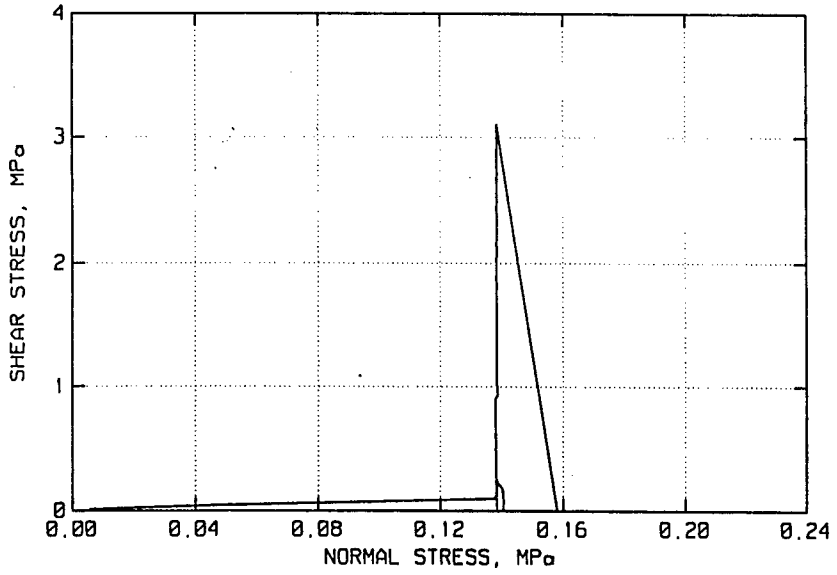

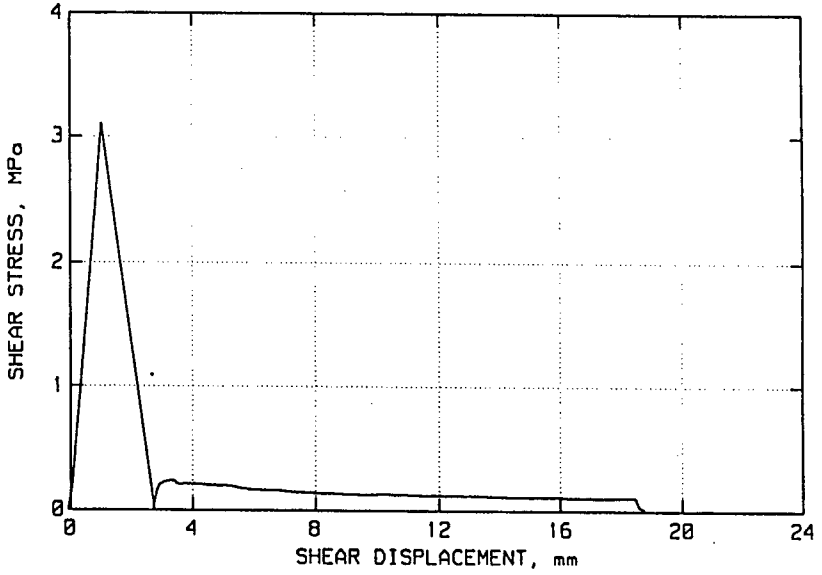

Plate 41

Plate 42

ELK CREEK DAM
TEST NO. 9604Y16

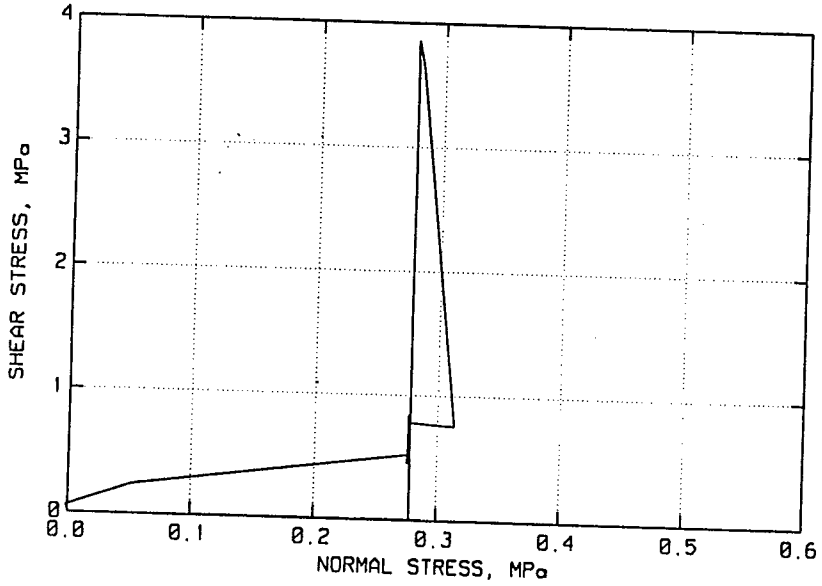

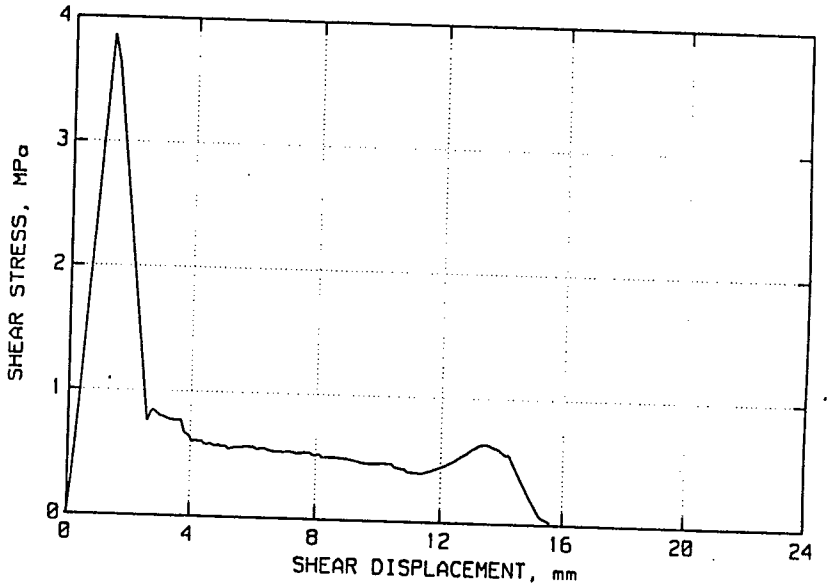

ELK CREEK DAM

TEST NO. 9604A19

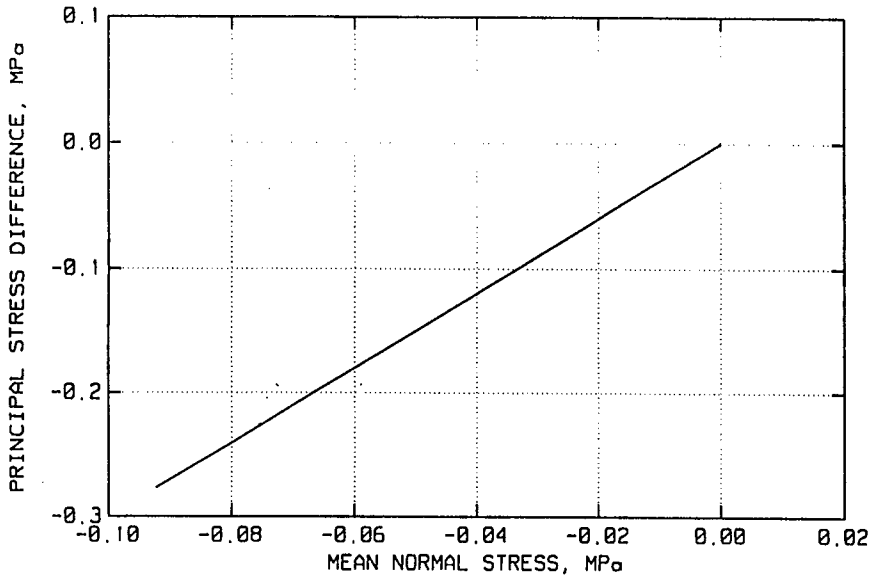

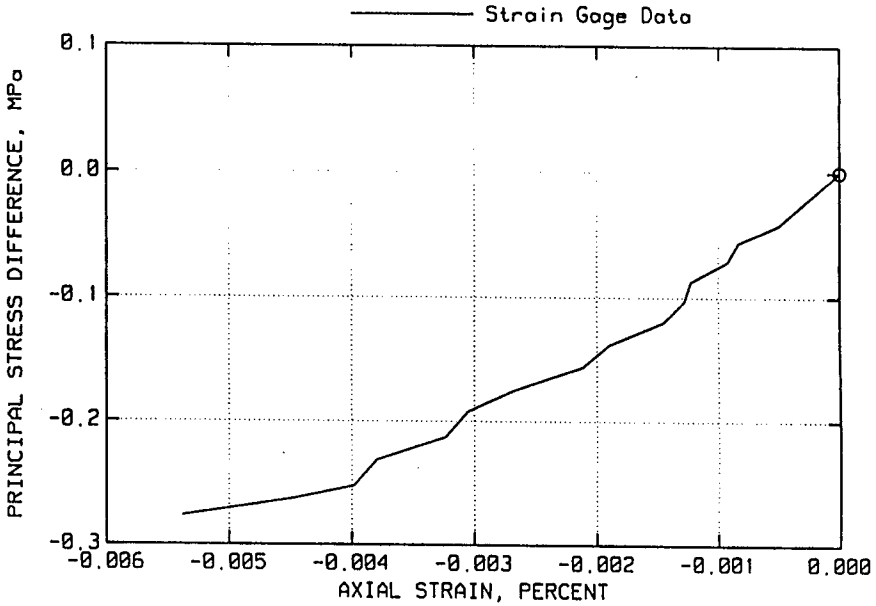

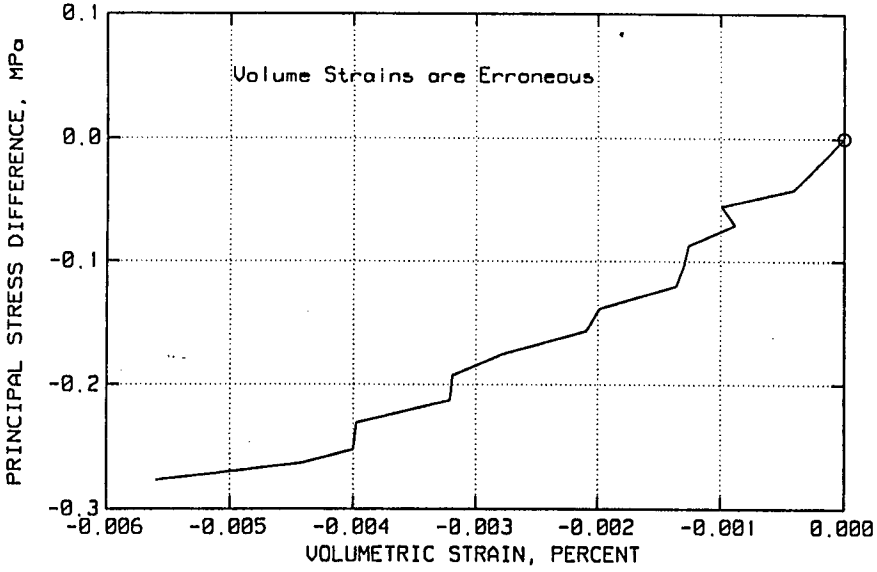

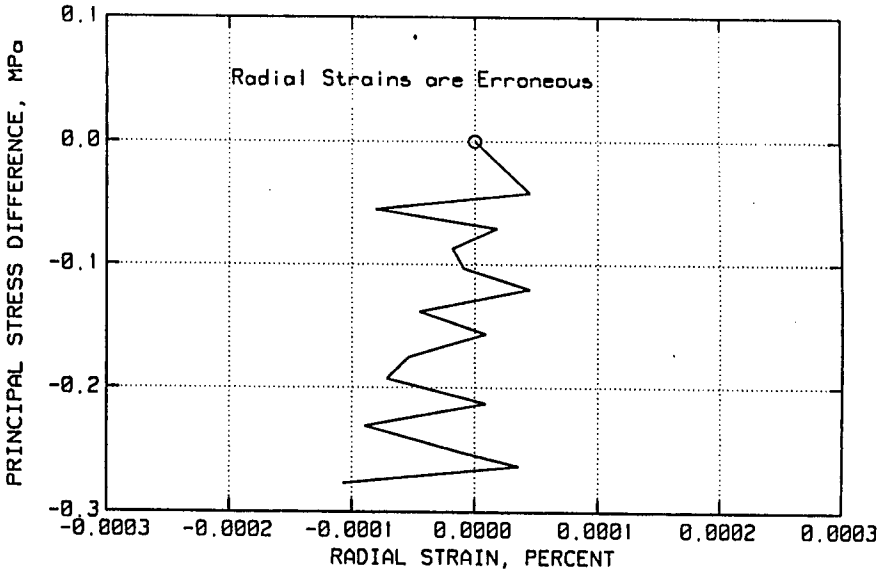

Plate 43

Plate 44

ELK CREEK DAM
TEST NO. 9604A20

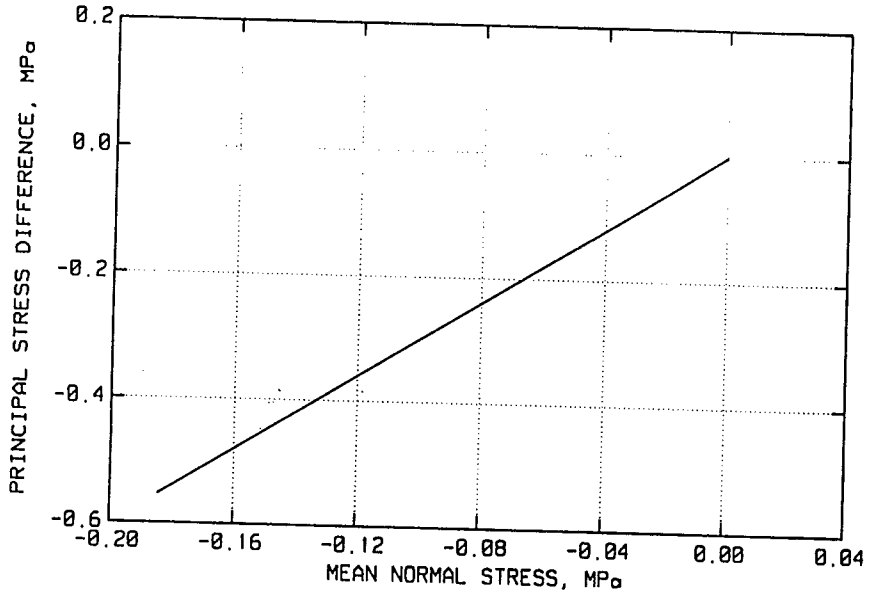

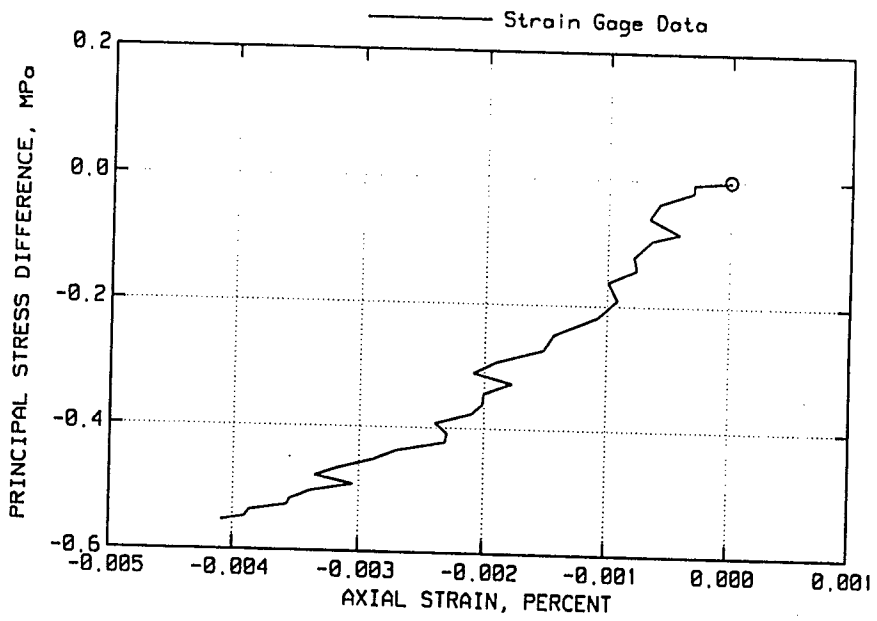

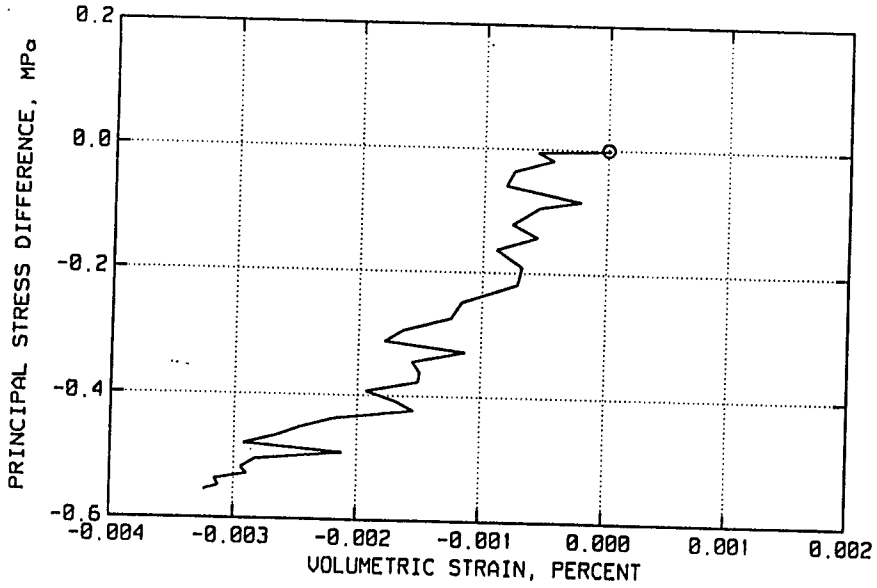

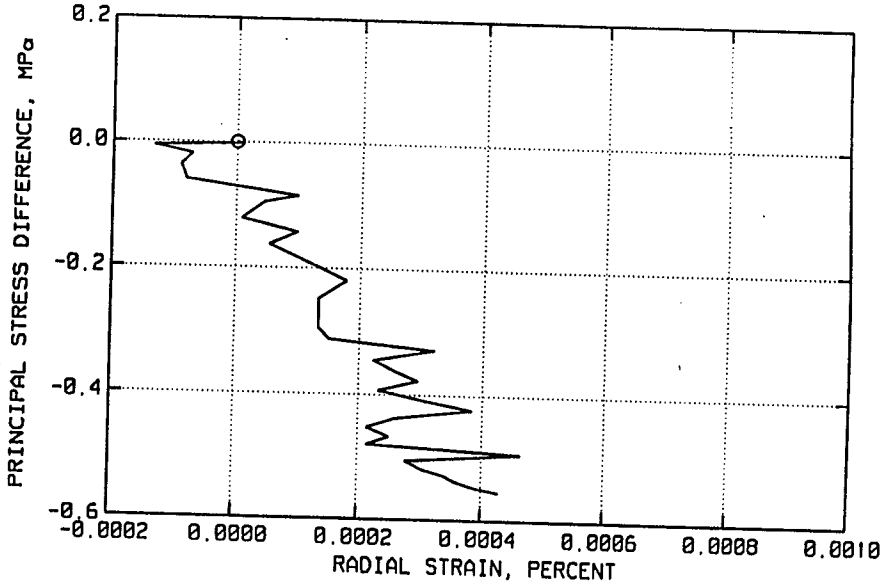

ELK CREEK DAM
TEST NO. 9604A21

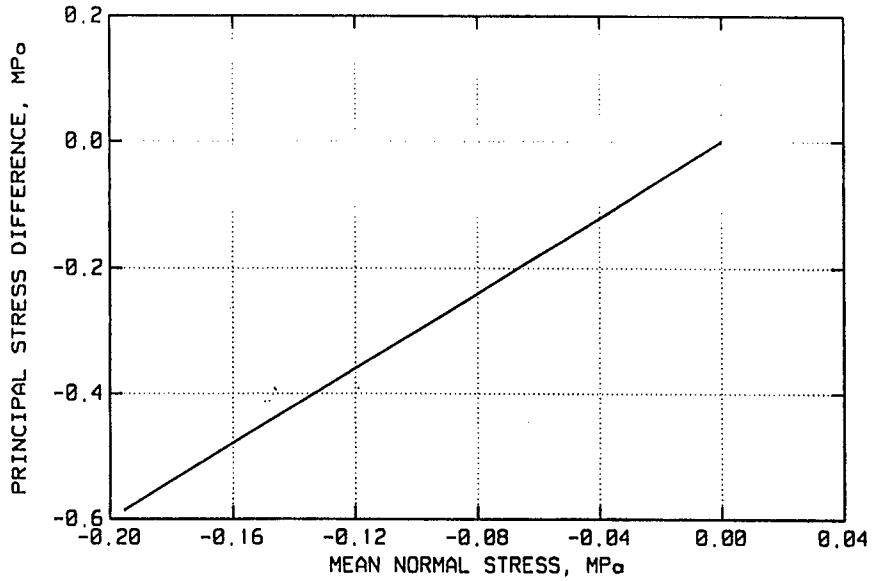

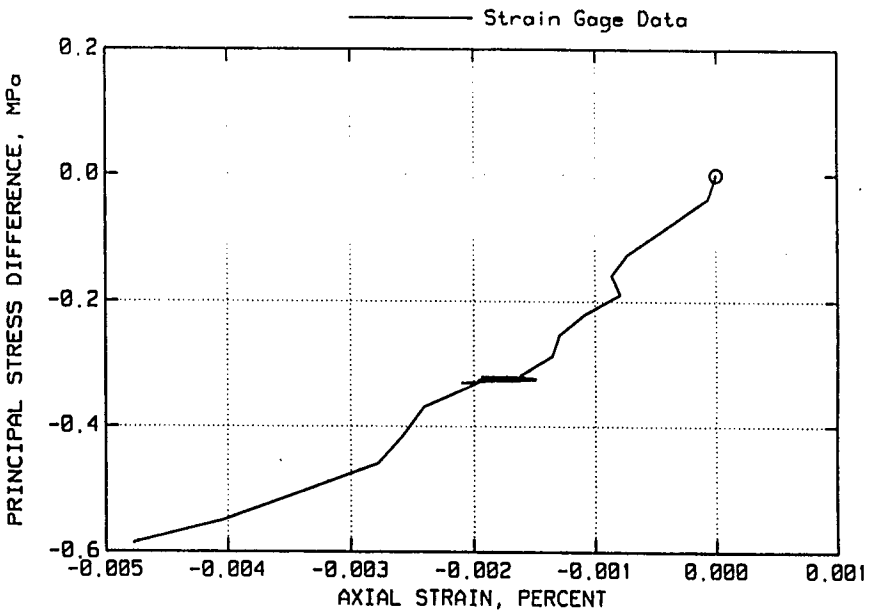

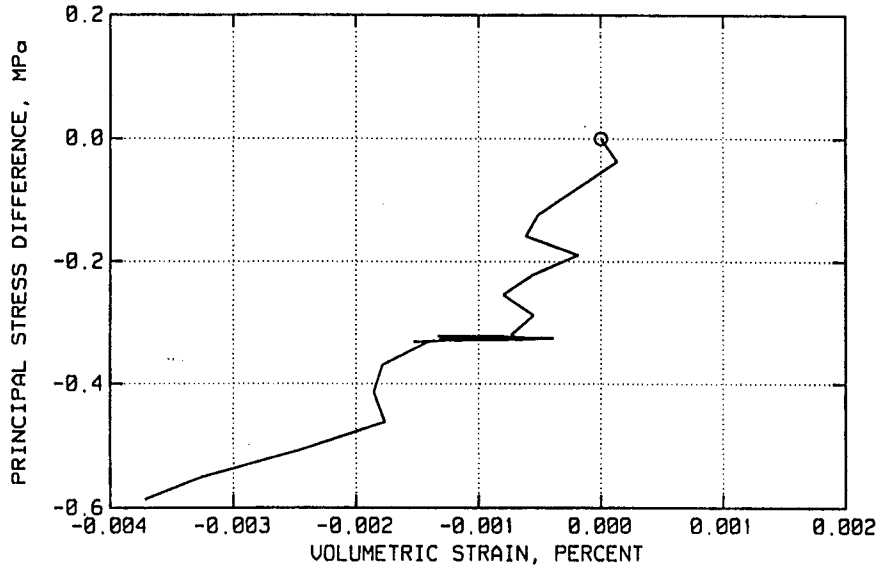

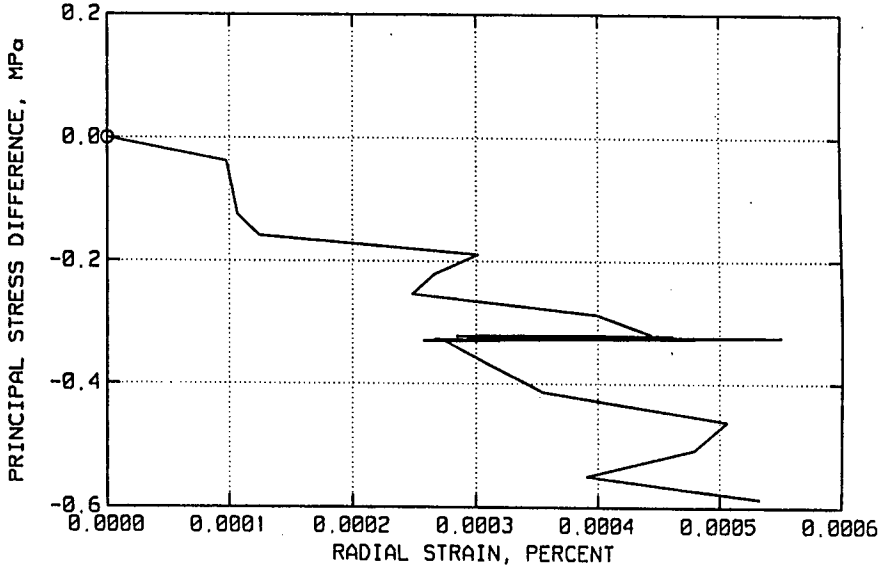

Plate 45

ELK CREEK DAM
TEST NO. 9604A22

Plate 46

ELK CREEK DAM
TEST NO. 9604A23

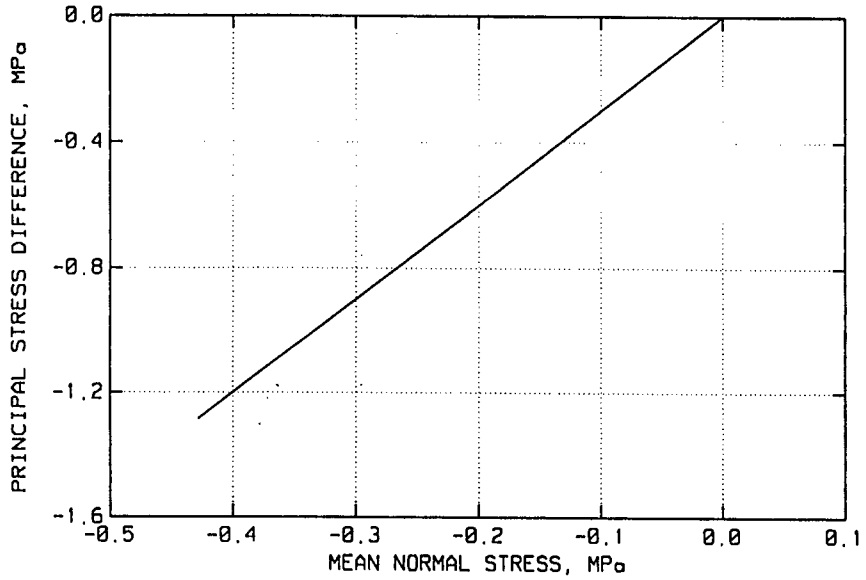

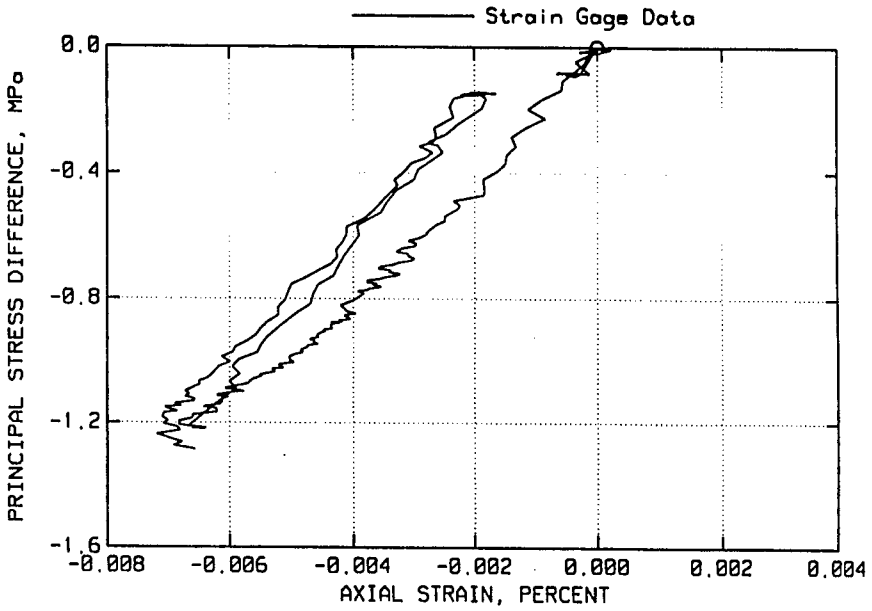

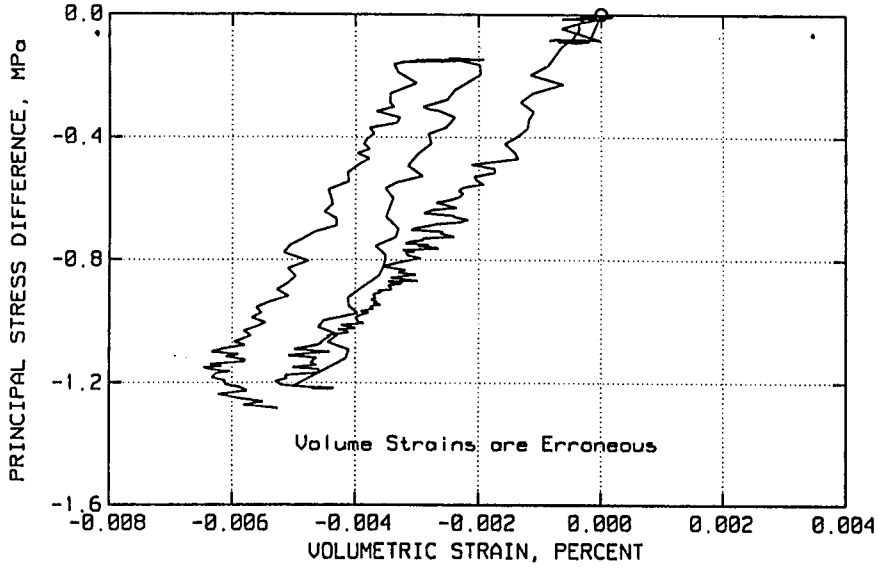

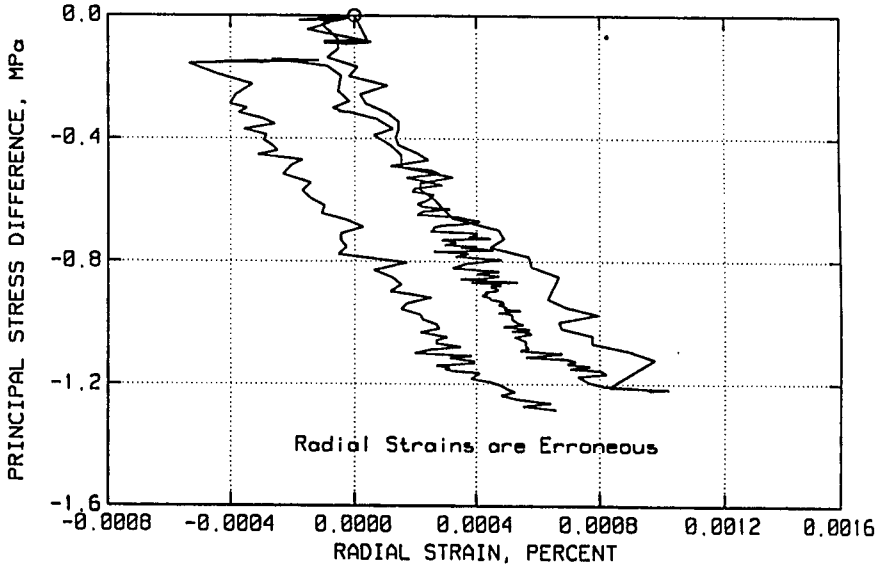

Plate 47

Plate 48

ELK CREEK DAM
TEST NO. 9604A24

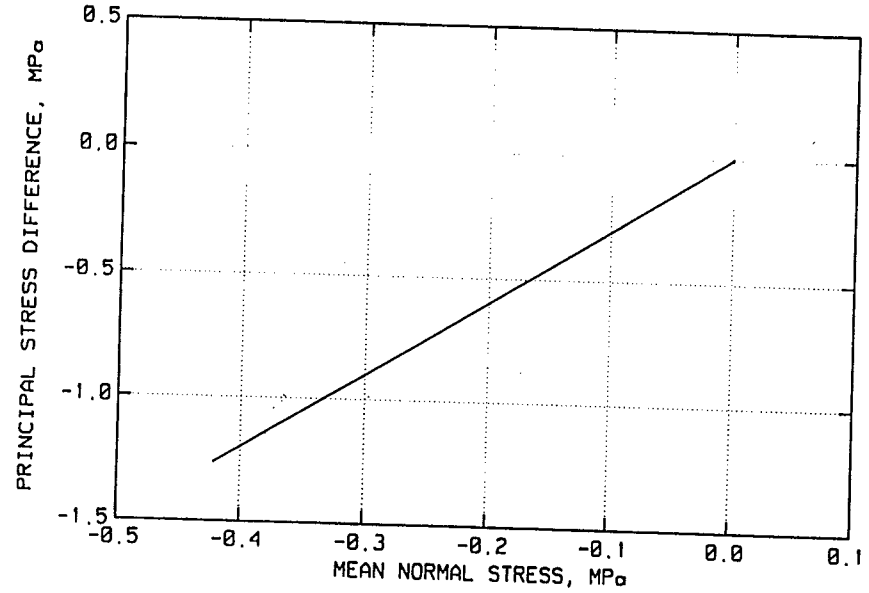

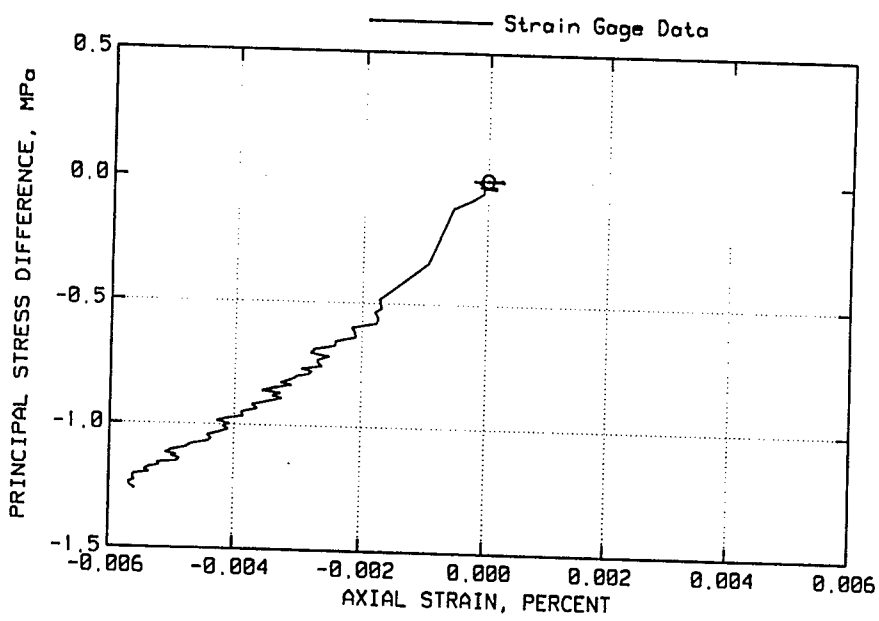

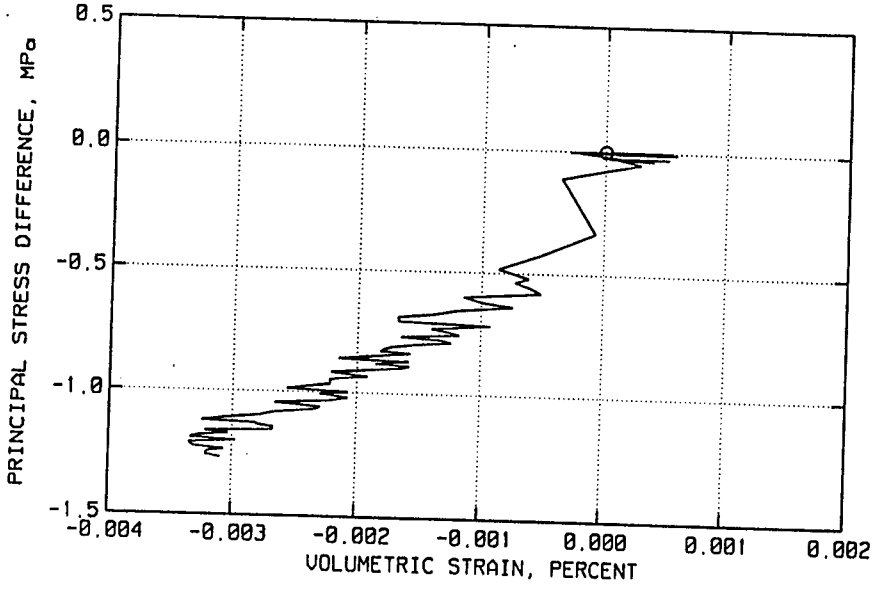

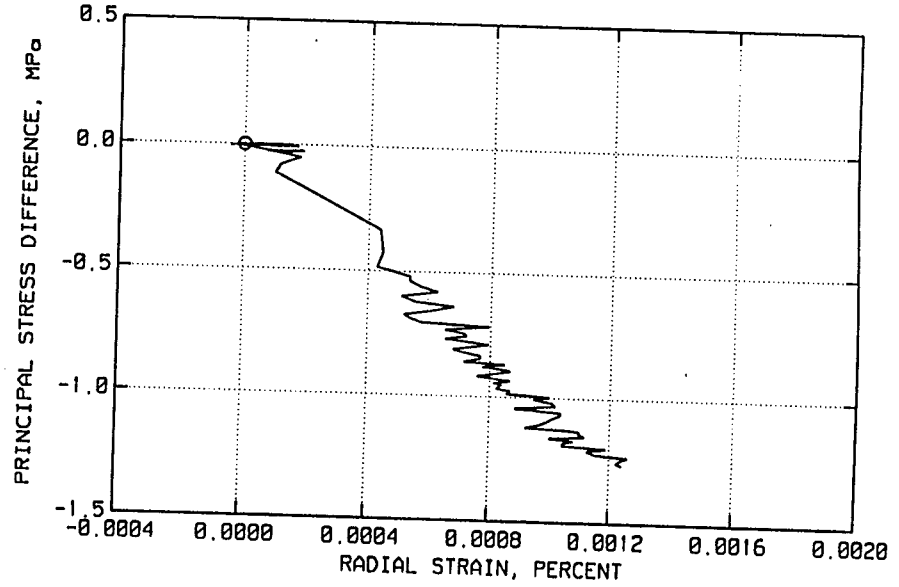

ELK CREEK DAM
TEST NO. 9604A25

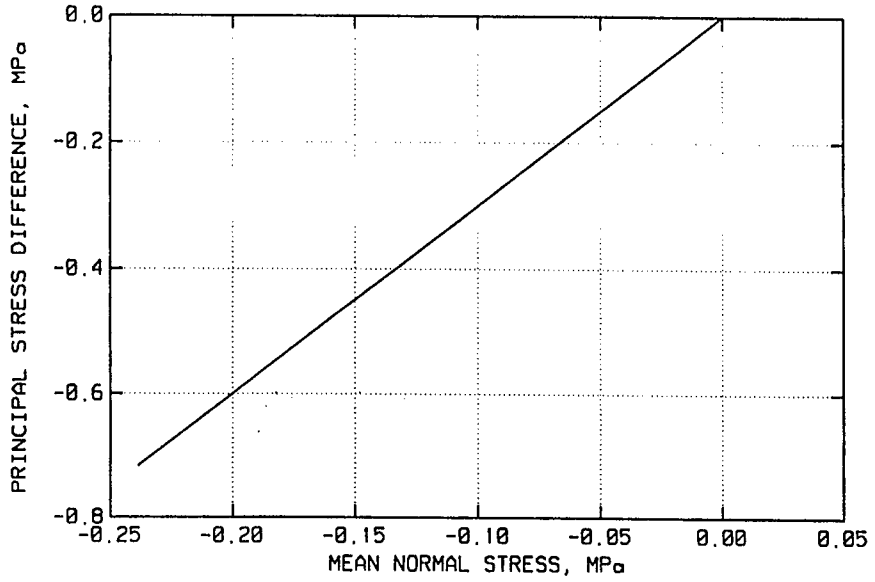

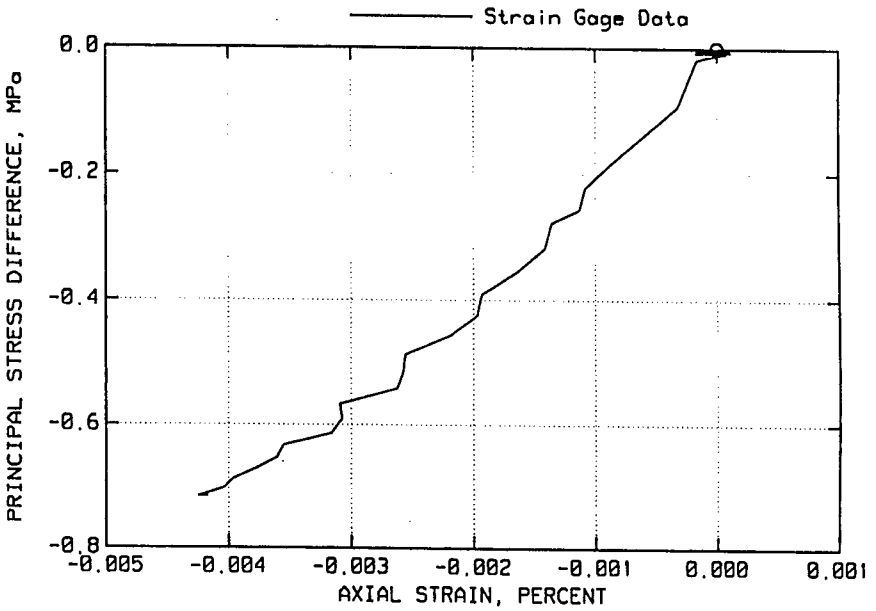

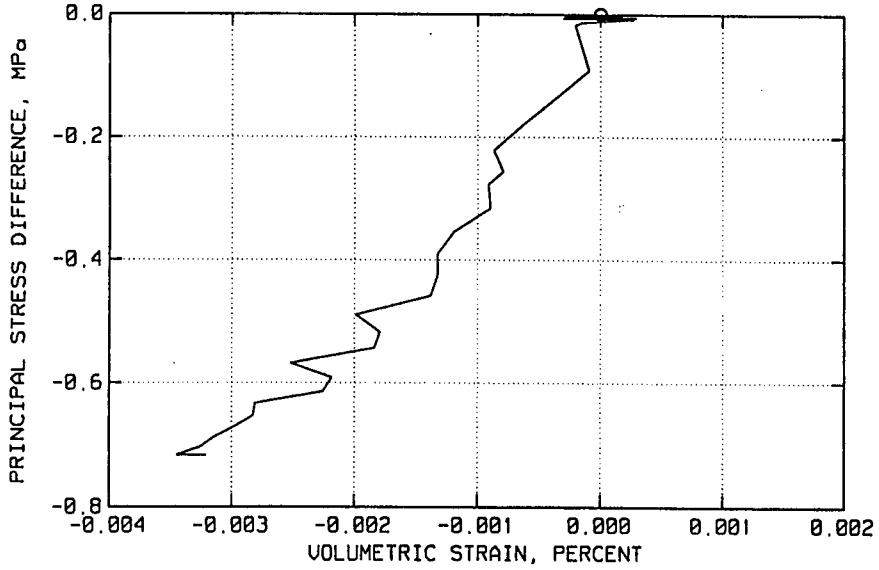

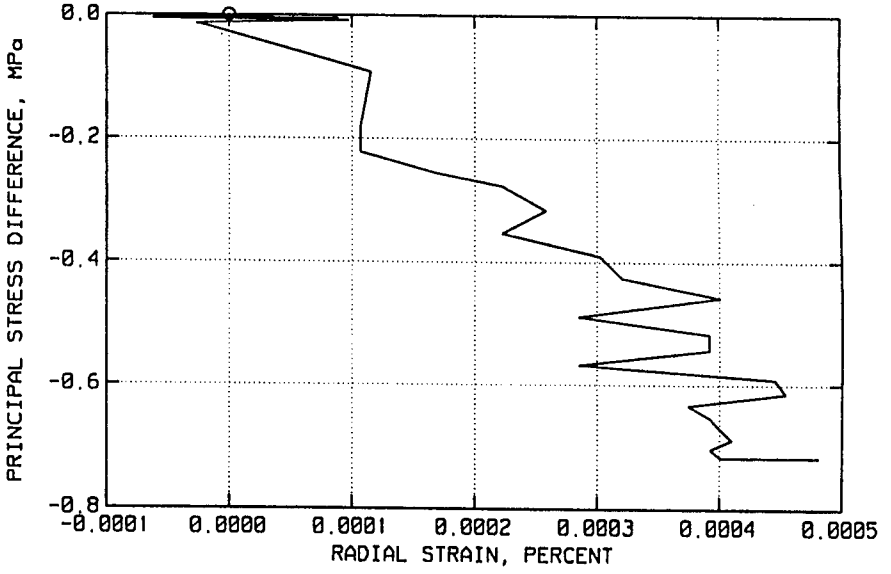

Plate 49

Plate 50

ELK CREEK DAM
TEST NO. 9604A26

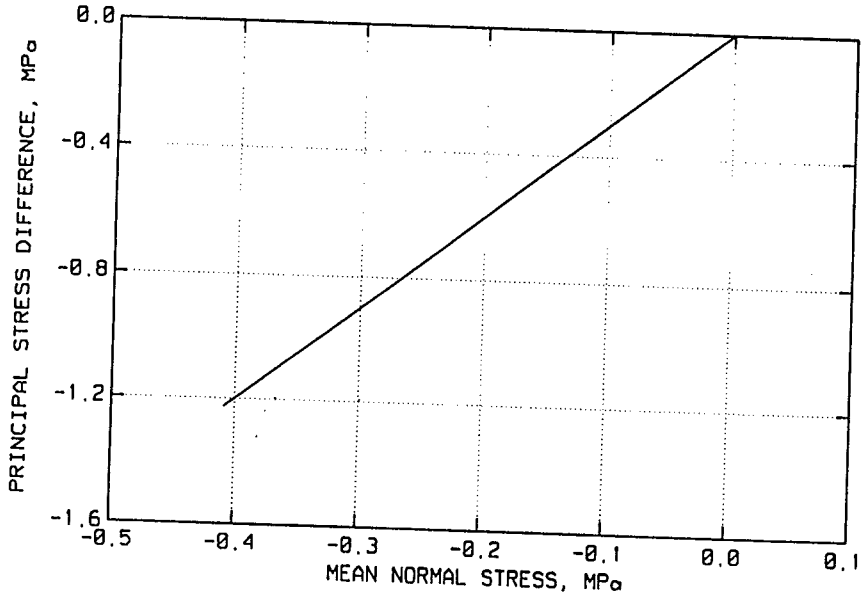

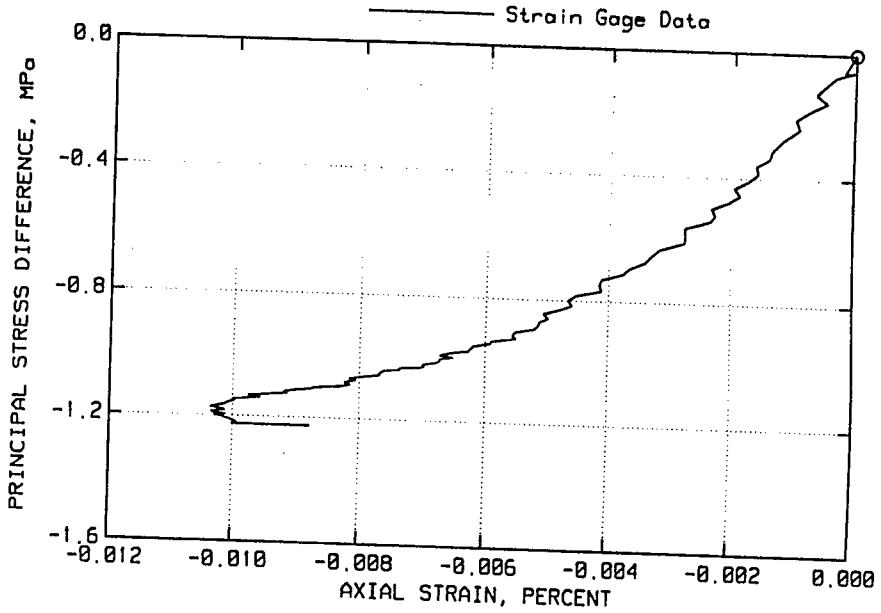

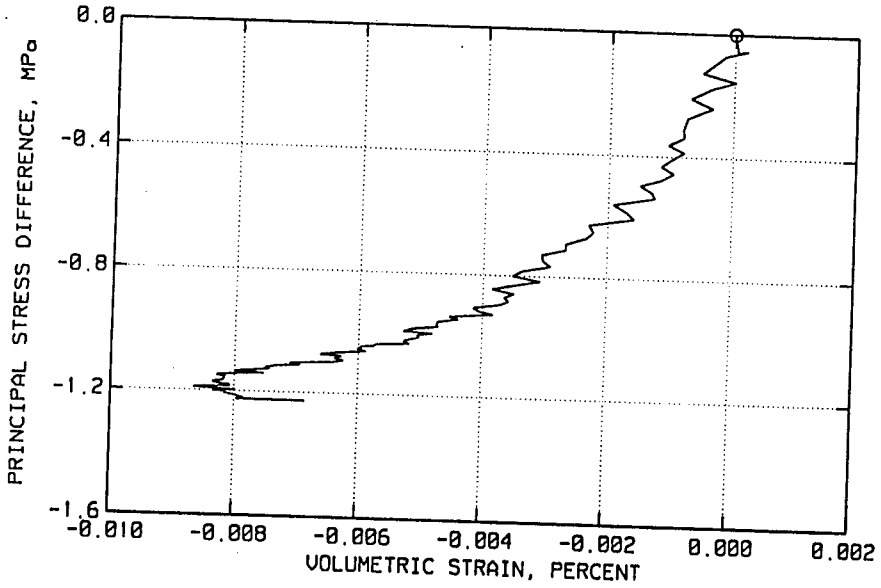

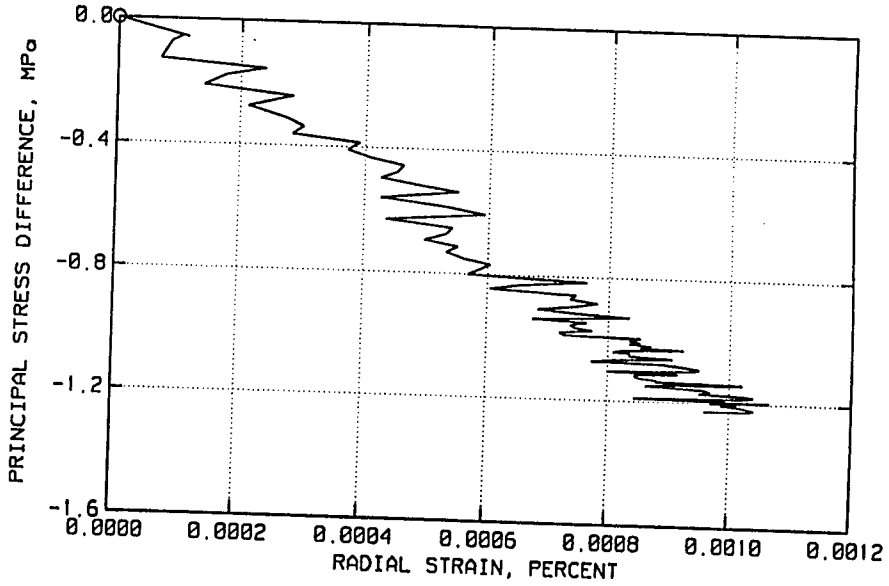

ELK CREEK DAM
TEST NO. 9604A27

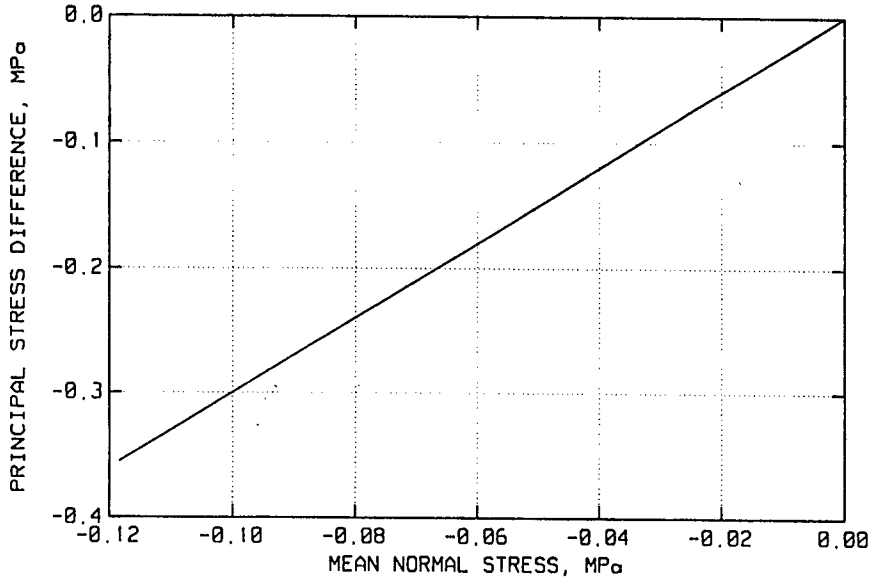

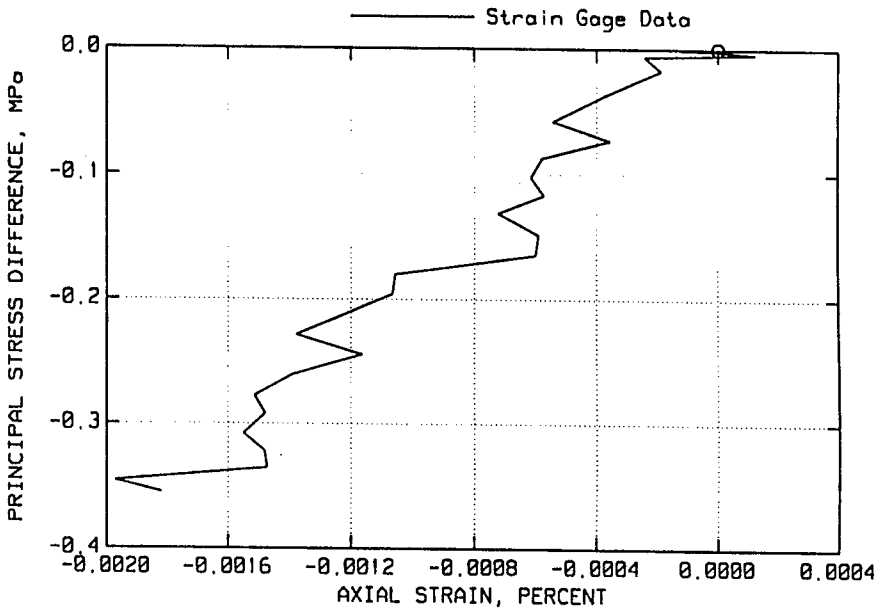

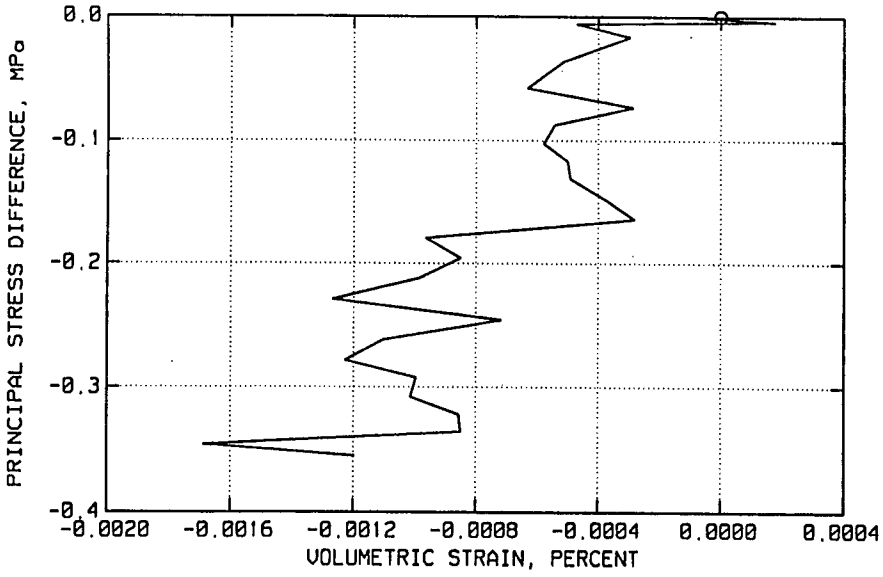

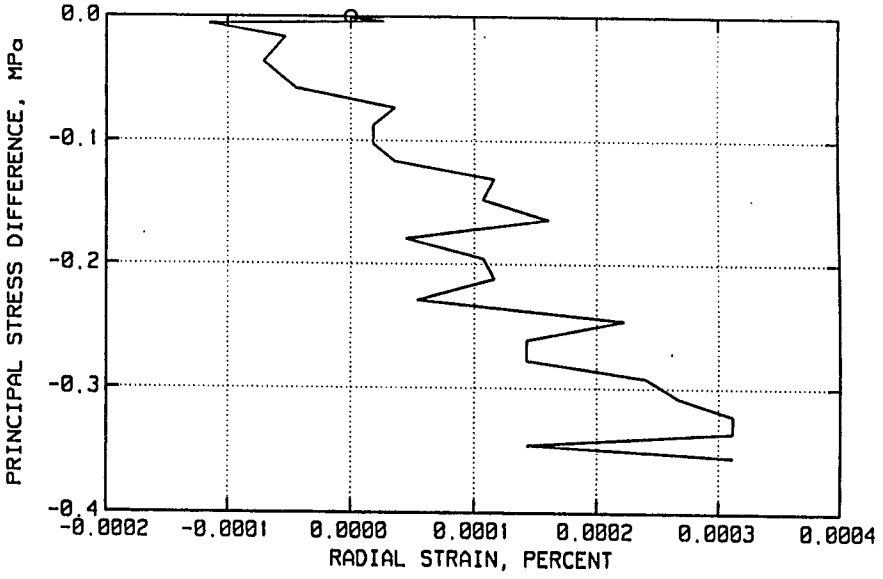

Plate 51

Plate 52

ELK CREEK DAM
TEST NO. 9604A28

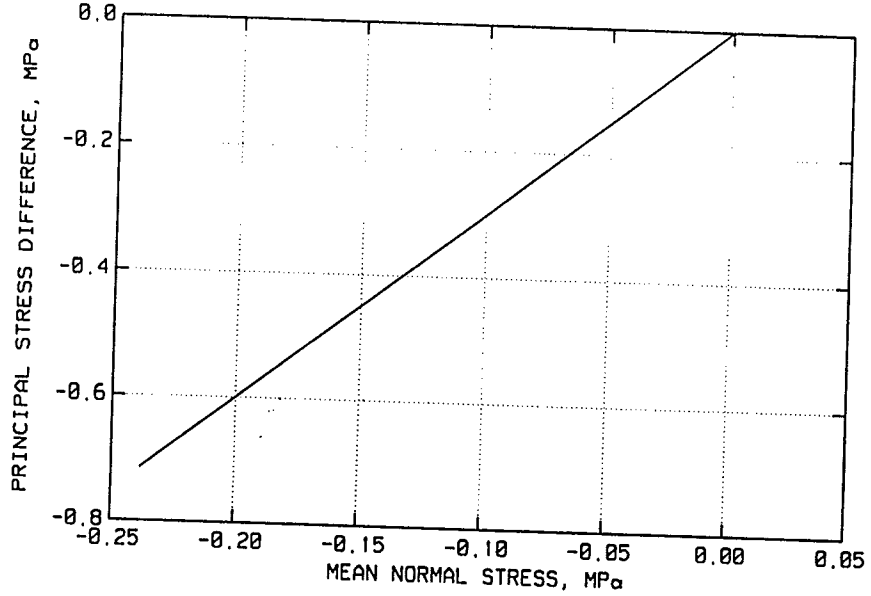

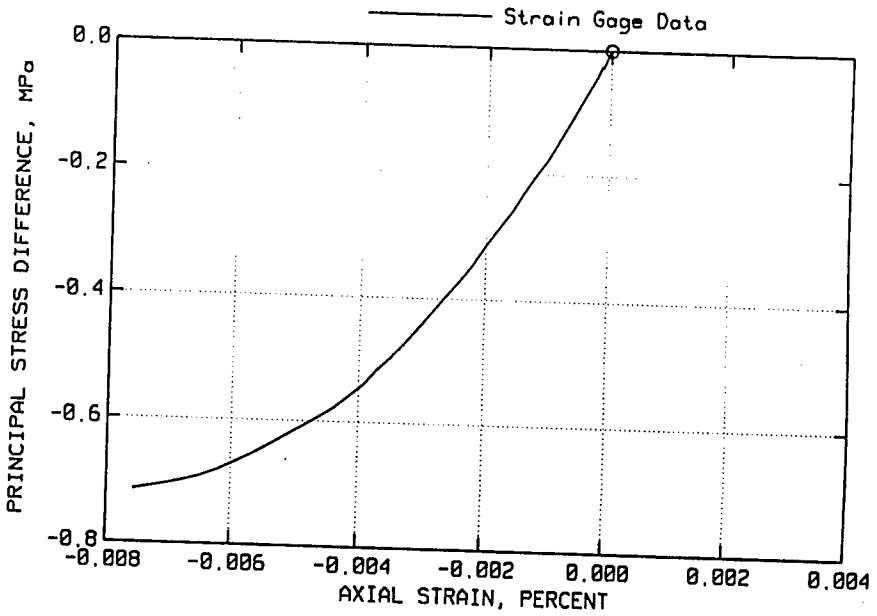

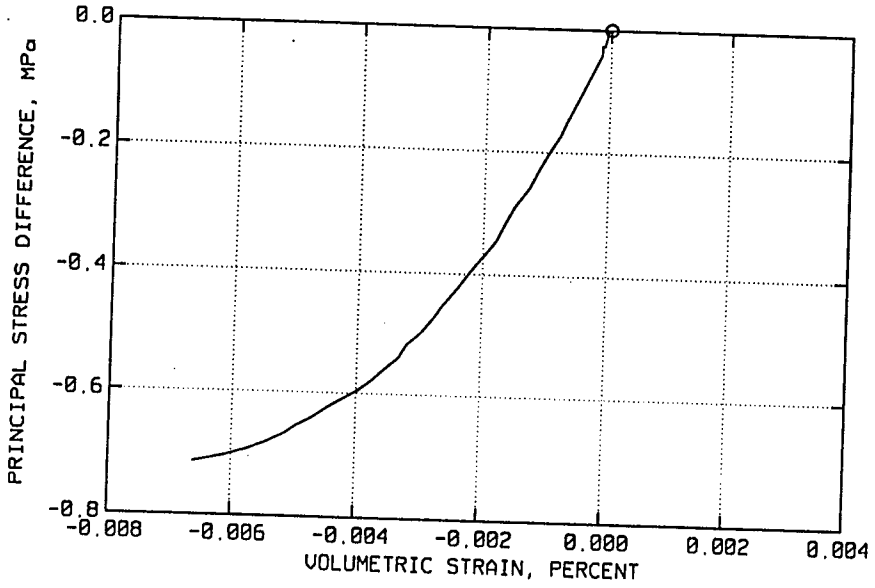

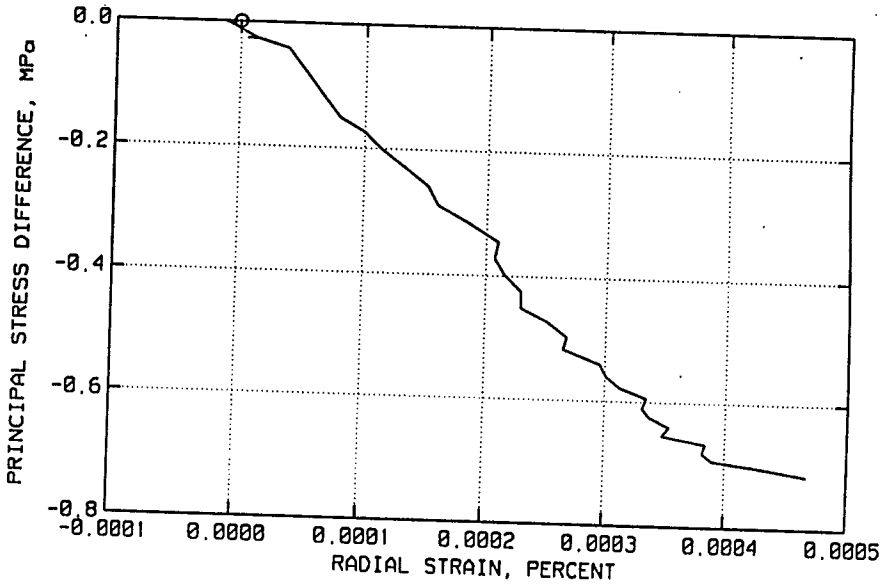

ELK CREEK DAM
TEST NO. 9604A29

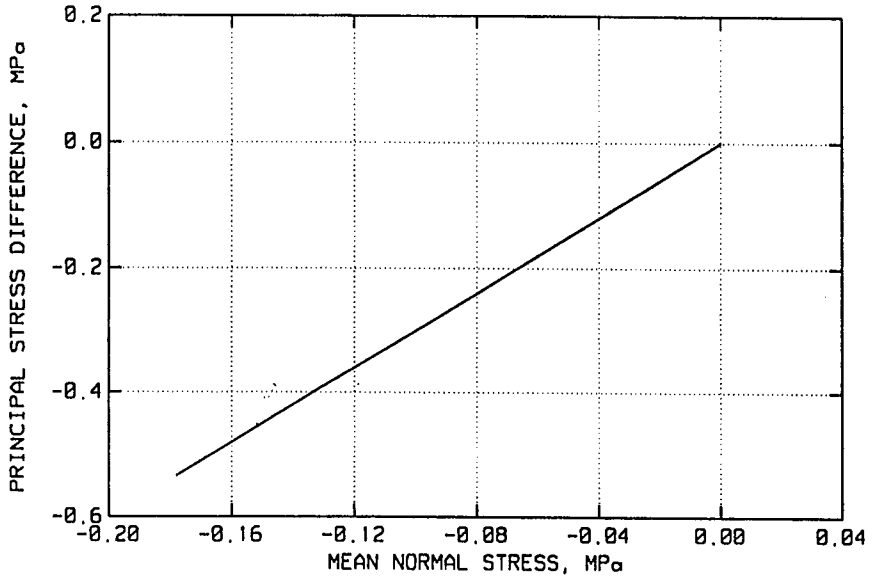

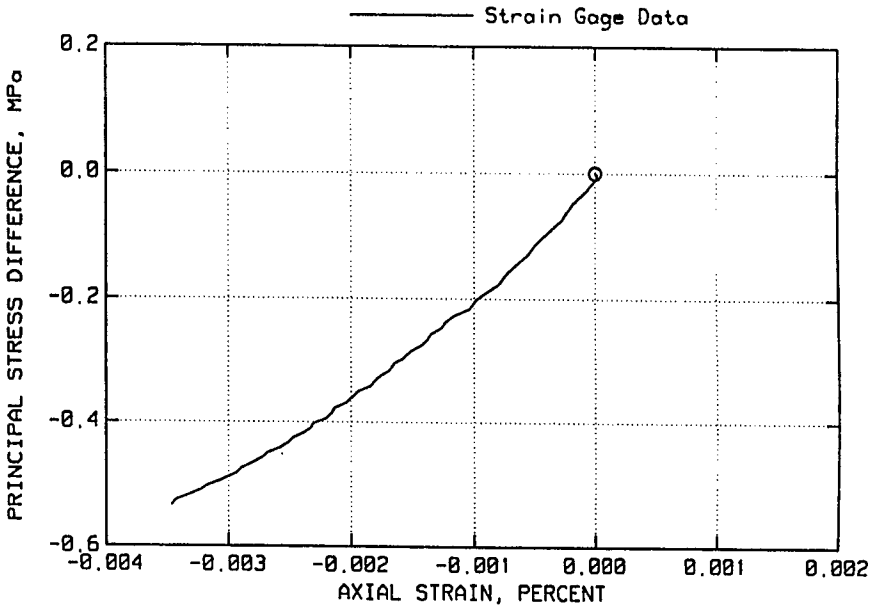

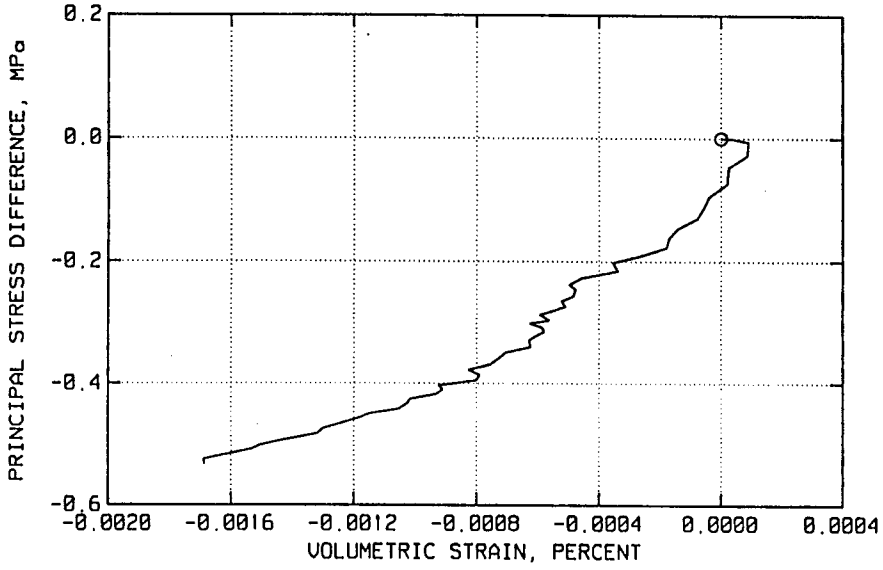

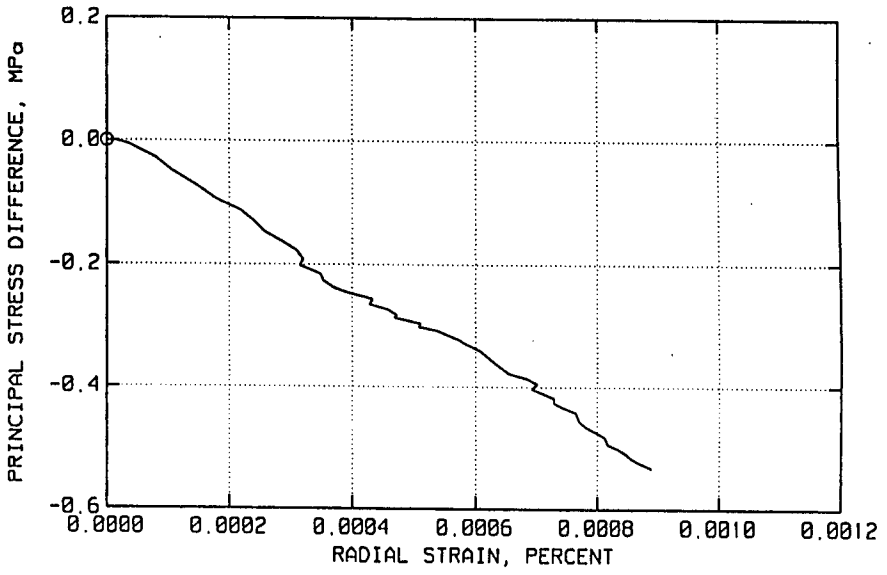

Plate 53

Plate 54

ELK CREEK DAM
TEST NO. 9604A30

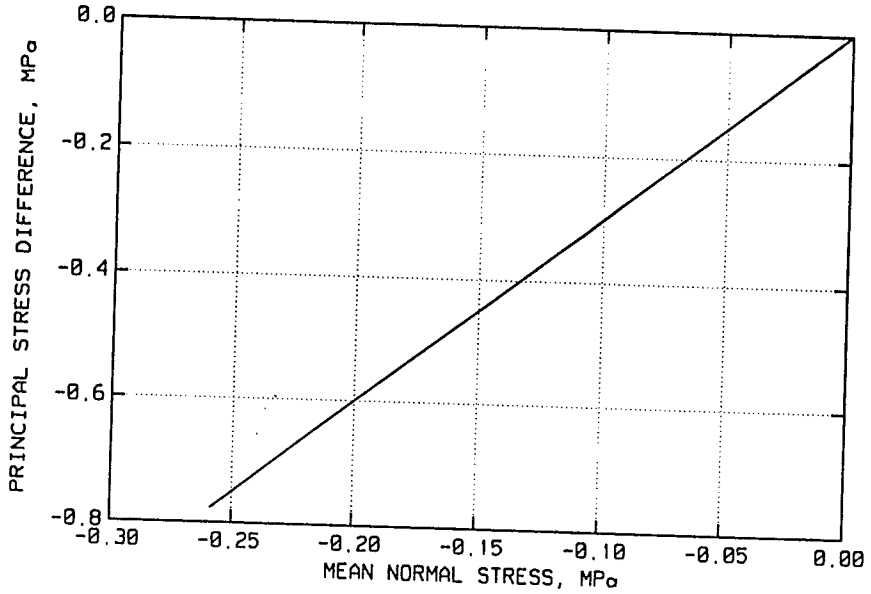

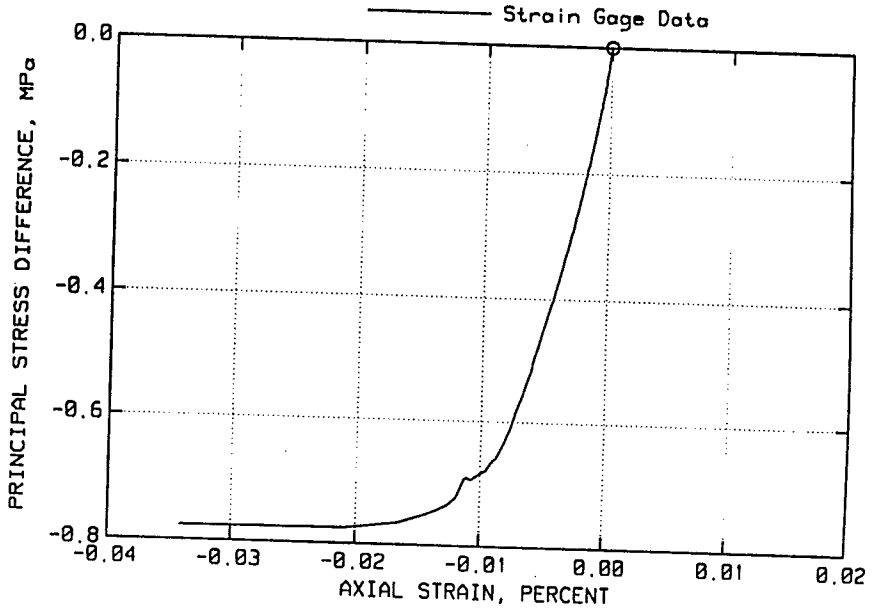

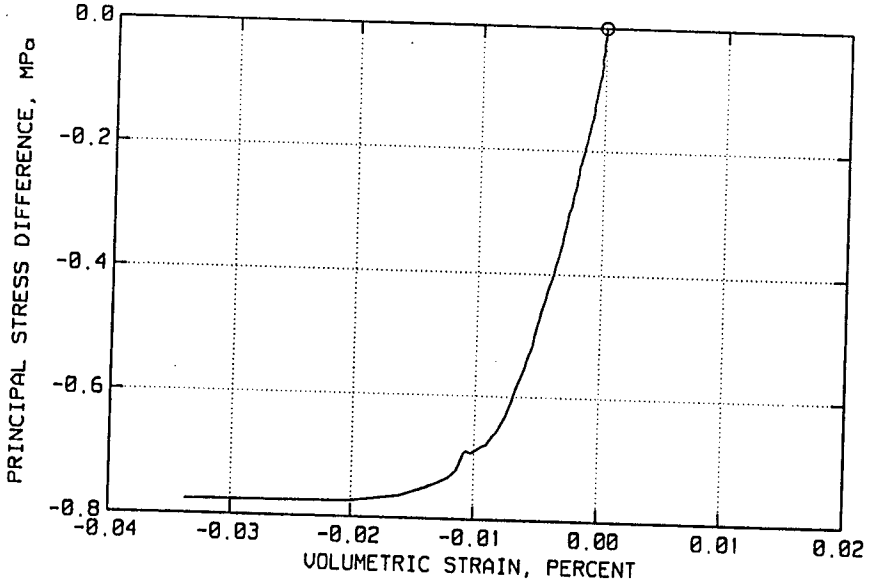

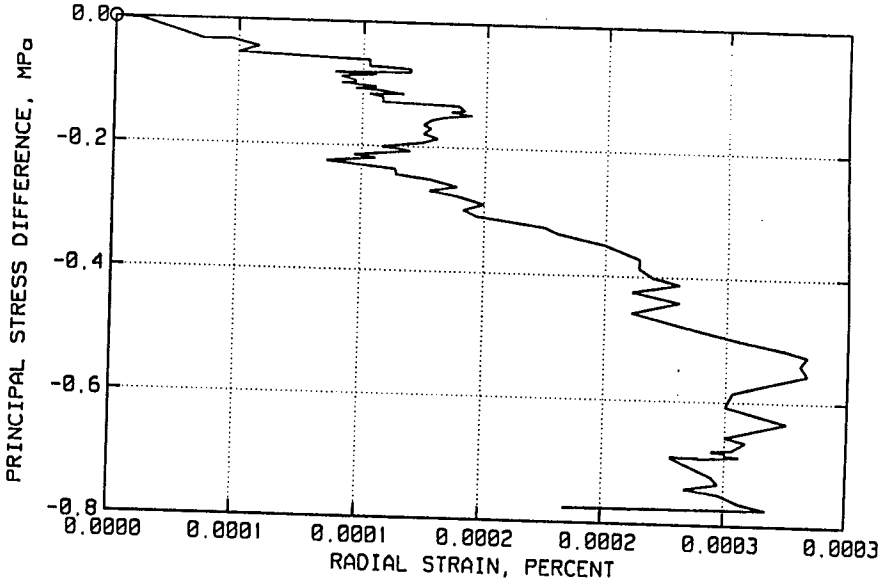

ELK CREEK DAM
TEST NO. 9604A31

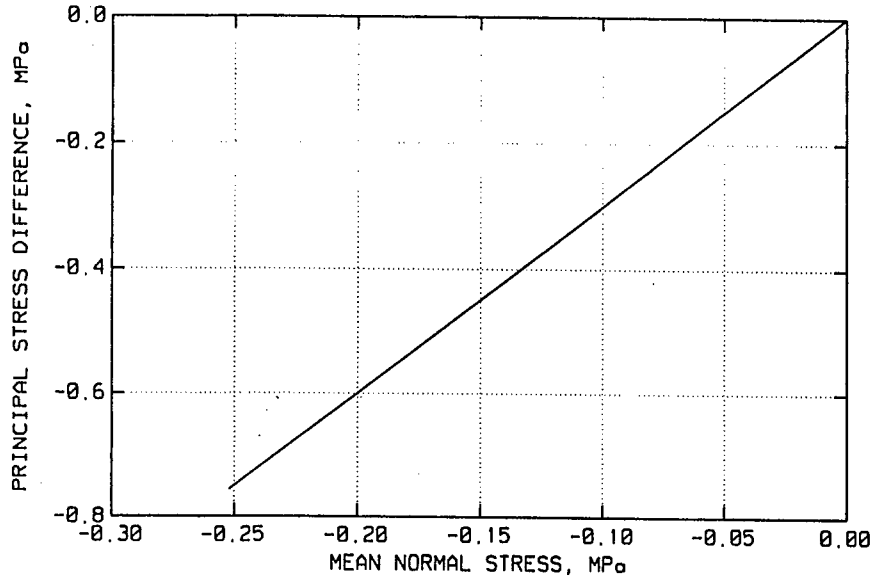

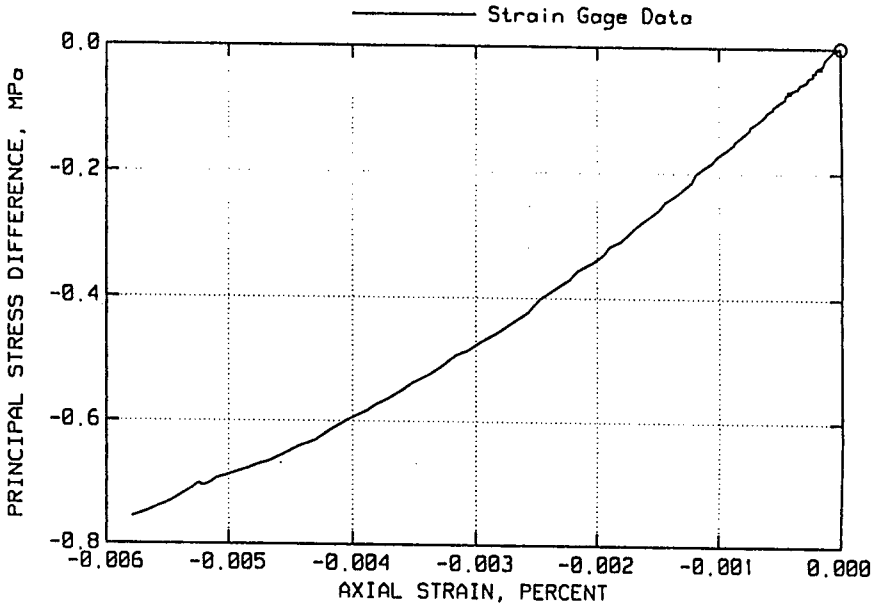

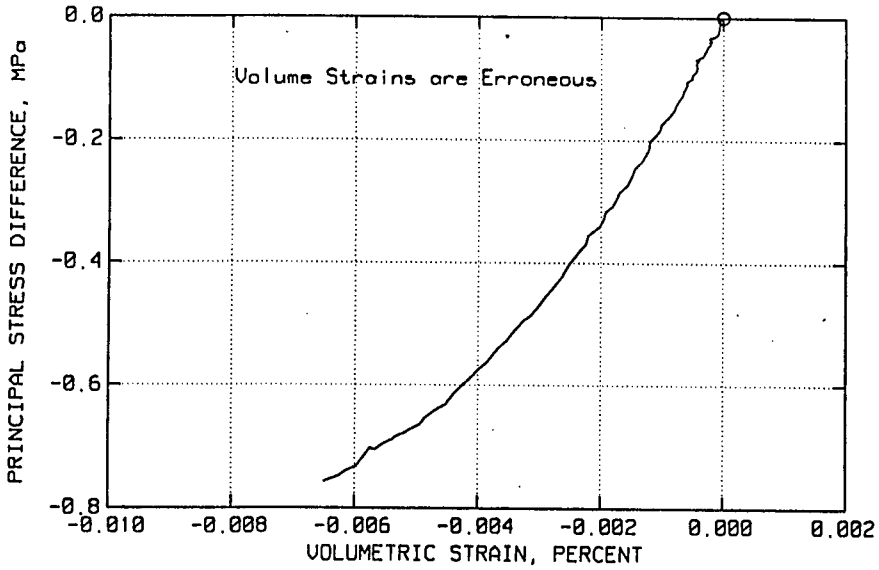

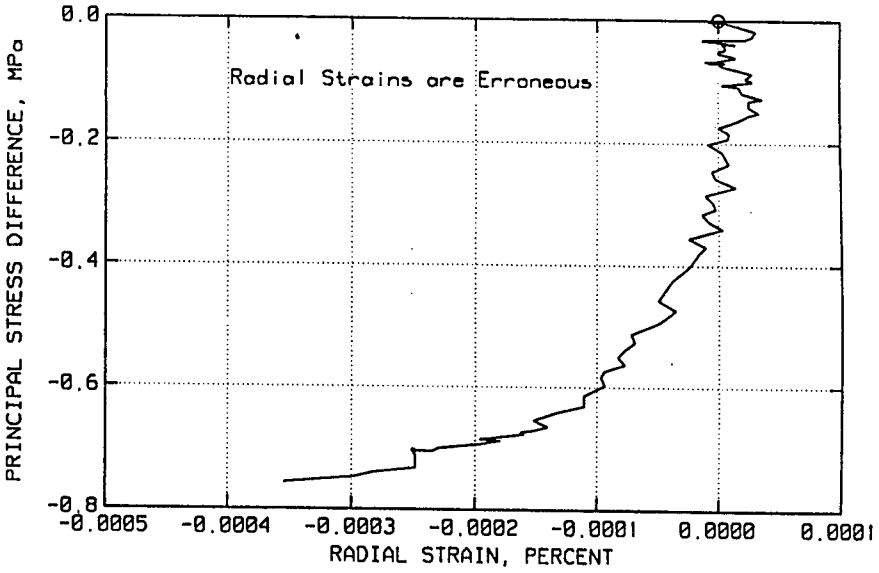

Plate 55

Appendix A
Equipment, Methods, and Procedures Used to Obtain the Large-Diameter RCC Cores

CENPP-PE-G

27 Nov. 1995

MEMORANDUM FOR Luis de Bejar
Waterways Experiment Station
Structural Material Laboratory
3909 Halls Ferry Road
Vicksburg, MS 39180-6199

ATTN: CEWES-RM-B

SUBJECT: Large Diameter Core Drilling of the Main Dam Roller Compacted Concrete (RCC) at Elk Creek Dam, Trail, Oregon.

1. Reference your MIPR No. W81EWF52063831

2. The following is a discussion of the equipment, methods, and procedures used to obtain the required large diameter core samples.

a. With the drill rig (truck mounted Mobil Drill, B-80) set up on the drill hole site and the casing shim collar in place, the top of the hole was painted with two colors of spray paints or one color of paint-stick to orient the core parallel to the dams' construction base line (CBL). Marking the top of the core in this fashion wasn't very successful as the surface was usually too wet or contained too many latent fines, which caused the paint not to adhere to the concrete surface. Core orientation was difficult to maintain on a run by run basis, but could be tracked from one piece of core to the next up and down the hole with few problems. The biggest problem encountered was that a 42 inch long core sample weighs about 166 pounds and is a little much to be handled by one person alone.

b. Several methods of core orientation were tried before one was settled on as workable.

1) The first method tried used a device constructed out of ½ inch electrical conduit and included a sponge block with red and black dye applied to it. This seemed to work well enough until drill cuttings built up in the hole. The cuttings build-up were caused by not being able to drill as intended. The drilling system that was to be used was a wireline system. It had so many mechanical problems that the driller switched over and used thewireline barrel as a conventional core drilling barrel. With a wireline system, the drill rods virtually fill the entire drill hole, the water needed to flush the drill cuttings out of the hole is relatively small and the pumps on site were adequate to handle it. The conventional system utilized HQ rods and the water pumps couldn't produce enough water to flush out the drill hole, thus the buildup of drill cuttings in the bottom of the

hole. All the dye was lost from the sponge when the sponge block was pushed through the cuttings.

2) The next method tried was the same apparatus as the first, but replaced the ink with paint. This didn't work at all and was dropped immediately.

3) The third method tried is the method we stayed with and was first used on the second run in WDH-2. This consisted of utilizing one 30 foot side of the original apparatus and taping a red paint stick to it. This was then lowered into the hole on the side aligned with the right abutment. Once the paint stick was on the bottom, it was repeatedly jabbed onto the top of the next run of core. Even this did not mark the top of the run 100% of the time. It was at this point that rapid work progress halted. The two ends of adjacent cores had to be matched and fitted, and the orientation mark carried up or down and this meant manhandling around at least two pieces of core, weighing about 165 pounds each. This had to be done carefully for safety reasons and to protect the core from breaking. In all the drilling, no core sample was lost due to breakage from mishandling of the sample. The orientation of the core is noted on the drill logs.

4) The core orientation explanation is as follows:

a) WDH-1, the orientation is marked with white paint stick and is marked left or red left. This means the red mark or line on the side of the core is oriented towards the left abutment. Standing with the core on end with the mark up and to your left, you are looking downstream, the CBL is behind you, and the left and right abutments are on your left and right.

b) WDH-2, WDH-3, and WDH-4 are all oriented on the right abutment and the red paint stick mark is labeled red right or just right. Holding the core the same as WDH-1 with exception that the mark is on the right, you are now facing the same direction as WDH-1, downstream with the CBL behind you and the correct abutments on your left and right respectively.

c. The drilling procedure was fairly straight forward:

1) The drill rig is located over the site and rigged up.

2) The core barrel was suspended over the hole location, the top core orientation marks are set, and the core barrel is checked for plumbness.

3) the starting rotation was about 50 rpm, the advance was maintained by hank control, and the water pump was run at it's lowest throttle setting and in low gear (none of the gages operated, so a lot was guess work). If a wobble started, the rotation was slowed even more and we would hold the barrel steady with pry bars. If a growling noise started, we would pull back

the barrel and clean the loose rubble out of the way and proceed ahead. Once we had gotten below the matrix of the bit by a couple of tenths of a foot, we proceeded ahead with normal drilling rates and speeds (i.e. rotation approx. 150 to 180 rpm, high gear, approx. 30 to 32 gpm) (4th gear/throttled back), and attempted to maintain 80 to 100 psi down pressure. But with most of the gages and the hydraulic pumps not working or only partially working, the driller had to work with his knowledge of the drill and of drilling than with the actual data).

4) Drilling times were varying from 40 to 55 minutes per 42 inch (3.50foot) run, averaging about 50 minutes, which is about 4.2 feet per hour. At the end of the run we pulled back and broke the core loose, and then flushed to hole for 5 to 10 minutes to reduce some of the drill cuttings in the hole.

5) Pulling the rods was a slow process as the hydraulic pump to run the tuggers was only putting out 5 to 7 gpm instead of the normal 45 gpm it was supposed to be putting out. After getting the rods and barrel up out of the hole, we lifted the barrel with the sand line and pulled it into position with a fork lift. The barrel was broken down, the core tipped out and put into the bottom half of a core box (which was on the fork lift) and everyone looked for the core orientation mark and measured for length between the two shortest points to verify that we indeed have a minimum of 36 inches of undisturbed core. If it was found all was well and good and if not it was the effort of matching the ends of the two runs up.

6) Before doing anything else the core orientation mark was applied, then the core barrel was assembled and put back into the hole. The entire process was taking about 1 hour and 30 minutes, start to start, which lowered the production rate from about 4.2 feet to about 2.3 feet per hour when everything operated at a minimum.

d. The core handling procedures were as follows:

1) The orientation line was scribed with a point stick along the axis of the core and labeled (left or right).

2) Then the core was washed down an measured, the box labeled with the core footage, and photographed as best as possible.

3) The core was logged with particular attention being given to the lift lines, then to the condition of the core, and finally to the RCC itself.

4) Finally the core was prepared for shipment.

a) If it was to long, the core was trimmed to a usable length with a gas-powered hand-held concrete trim saw, care was taken not to shorten up on the left lines if at all

possible.

b) Next the core was rewetted to keep the spay form from adhering to it. The lower half of the core box, containing the core, was tipped to assure that the core was solidly seated. Minimally expanding spray foam was injected into gaps, on the ends, and around the core. Where applicable styrofoam peanuts or broken styrofoam sheeting was used as filler. The upper half was filled with spray styrofoam and the two halves were secured together with 2 inch and 2 ½ inch drywall screws.

5) For shipment the filled core boxes were transported to Lost Creek Dam Project Office, placed on pallets, and banded for shipment.

e. Lift line recognition was accomplished in the following fashion.

1) The core was wetted to make the component elements more visible and recognizably.

2) From the previous runs lowest identified lift line (or from the top of the hole) measure down the core (down hole) 2 feet.

[Note 1: By the contract specifications each lift was to be nominally 24 inches thick after compaction. Reality is that the lifts ranged from about 20 inches to 26 inches at the location being drilled and the measurement was not meant to definitively identify a lift line location, but was utilized to identify the area that needed to be more closely scrutinized.]

[Note 2: the main dam RCC consisted of aggregate (sand sized to a maximum aggregate size of 3 inches), type II Portland Cement, and Class F fly ash. The aggregate was recently quarried, crushed to the specified sizes, and stockpiled on site, which reduced the number of times the material was handled and thus it retained an angular to extremely angular shape and rough exterior surface. The bedding mortar was a sand/cement mortar with a designed ultimate strength to match that of the main dam RCC and was spread between lifts in a designed thickness of 1/4 to ½ inch and was meant to reduce seepage along the lift lines and enhance the bondage between lifts. The bedding mortar observed averaged about 1/4 inch, with a few instances of it not being recognizably present. There also were a few untypical instances that the bedding mortar was found to be 2 inches or greater in thickness. The variations can be attributed to the local irregularities in the previous lifts surface, the method of spreading the mortar, the method of spreading the lift aggregate, and the particular circumstances involved with the compaction of the lift at that point. The variations can not be construed as being poor quality control, poor placement methodology, or poor design criteria, but as a vagary of the construction.]

3) In the vicinity of the measured 2 feet interval, the following characteristics are scrutinized for:

a) A thin zone containing nothing but bedding mortar.

b) A zone of an inch or so that contains aggregate no greater than 3/4 inch and any elongated clasts are horizontal.

c) A zone where all the elongated clasts (3 inch on down) are horizontal.

d) A zone that aggregate greater than 3/4 inch do not intrude across.

e) A zone that all larger sizes of the aggregate are seemingly excluded.

The lift line may be defined by one or more of the above or may not be recognizable under any circumstance.

f. Characteristics that can be mistaken as a lift line or lift line indication are:

1) During the placement process the RCC mix is batched, conveyed to the placement area, loaded onto end-dump Euclids, dumped on the advancing placement, and spread and compacted with a bulldozer to build the lift. At any point in this process, aggregate segregation in a small short extent can and does occur. While segregation of the aggregate in the placement is actively sought to be eliminated or minimized, it does get by the CQC/QA team and unfortunately the drill hole penetrates it.

a) With large diameter core, these zones do not generally cross the full diameter of the core.

b) If the zones do cross the diameter of the core, the thickness of the zone normally varies to a contrasting degree.

c) Due to the method of placement, spreading, and compaction, this zone generally appears to be angled or inclined across the diameter of the core.

d) Usually elongated aggregate clasts can be found crossing or parallel to the cores axis in these zones.

Appendix B
Laboratory Ultrasonic Pulse Velocity Data

Table B1
Radial P-Wave Velocity Log for Boring WDH1 Core Samples

Depth (m)	P-Wave Velocity, km/s				
	0 deg	45 deg	90 deg	135 deg	All Orientations
1.52	4.588	4.632	4.365	4.525	
1.68	4.505	4.567	4.444	4.525	
1.83	4.709	4.494	4.346	4.599	
1.98	4.374	4.365	4.434	4.536	
2.13	4.515	4.279	4.298	4.474	
2.29	4.588	4.384	4.536	4.557	
2.44	4.505	4.414	4.374	4.536	
2.59	4.127	4.136	4.261	4.188	
2.74	4.676	4.632	4.494	4.643	
2.90	4.206	4.110	3.969	4.084	
3.05	4.567	4.434	4.434	4.578	
3.20	4.206	4.233	4.317	4.279	
3.35	4.557	4.557	4.336	4.444	
3.51	4.034	4.001	4.025	4.067	
3.66	4.610	4.261	4.206	4.279	
3.81	4.365	4.474	4.515	4.404	
3.96	4.365	4.365	4.515	4.374	
4.11	4.404	4.243	4.394	4.215	
4.27	4.454	4.298	4.414	4.484	
4.42	4.317	4.394	4.355	4.307	
5.49	4.632	4.215	4.270	4.346	
5.64	4.643	4.505	4.454	4.557	
5.79	4.279	4.252	4.144	4.336	
5.94	4.536	4.374	4.243	4.394	
6.10	4.171	4.110	4.118	4.224	
6.25	4.298	4.093	4.289	4.206	
6.71	4.828	4.581	4.828	4.724	
6.86	4.635	4.518	4.701	4.713	
7.01	4.245	4.387	4.367	4.446	
7.16	4.339	4.264	4.477	4.301	
7.32	4.236	4.264	4.292	4.301	
7.47	4.377	4.570	4.624	4.310	
7.62	4.367	4.182	4.182	4.487	
7.62	3.971	3.696	3.795	4.012	
7.77	4.245	4.191	4.329	4.191	
7.92	4.273	4.329	4.477	4.245	
8.08	4.273	4.477	4.320	4.348	
8.23	4.387	4.348	4.310	4.377	
8.38	4.348	4.426	4.417	4.560	
8.53	4.613	4.528	4.635	4.417	
All Points					
Mean	4.409	4.340	4.358	4.390	4.374
St Dev	0.193	0.191	0.192	0.172	0.187
No. Pts	40	40	40	40	160
Chauvenet's Criterion					
Tau	2.498	2.498	2.498	2.498	2.955
Lower Bound	3.927	3.863	3.878	3.960	3.821
Upper Bound	4.891	4.817	4.838	4.820	4.927
All Points within Lower and Upper Chauvenet's Criterion Bound					
Mean	4.409	4.356	4.372	4.390	4.382
St Dev	0.193	0.162	0.171	0.172	0.174
No. Pts	40	39	39	40	158

Table B2
Radial Sa-Wave Velocity Log for Boring WDH1 Core Samples

Depth (m)	Sa-Wave Velocity, km/s				All Orientations
	0 deg	45 deg	90 deg	135 deg	
1.52	2.418	2.682	2.479	2.467	
1.68	2.436	2.517	2.461	2.395	
1.83	2.550	2.682	2.406	2.604	
1.98	2.448	2.366	2.505	2.395	
2.13	2.492	2.401	2.455	2.448	
2.29	2.570	2.479	2.550	2.543	
2.44	2.632	2.021	2.563	2.590	
2.59	2.247	2.389	2.316	2.349	
2.74	2.646	2.550	2.570	2.442	
2.90	2.467	2.537	2.530	—	
3.05	2.550	2.461	2.543	2.537	
3.20	2.479	2.498	2.505	2.448	
3.35	2.436	2.511	2.485	2.530	
3.51	2.316	2.310	2.418	2.310	
3.66	2.590	2.576	2.372	2.473	
3.81	2.836	2.590	2.611	2.498	
3.96	2.505	2.550	2.505	2.485	
4.11	2.498	2.550	2.604	2.467	
4.27	2.467	2.524	2.543	2.618	
4.42	2.537	2.537	2.485	2.424	
5.49	2.257	2.321	2.360	2.455	
5.64	2.590	2.618	2.576	2.563	
5.79	2.294	2.366	2.590	2.430	
5.94	2.583	2.543	2.442	2.498	
6.10	2.202	2.278	2.305	2.305	
6.25	2.442	2.389	2.401	2.455	
6.71	2.774	2.572	2.626	2.487	
6.86	2.640	2.605	2.585	2.605	
7.01	2.532	2.367	2.391	2.744	
7.16	2.334	2.525	2.432	2.334	
7.32	2.312	2.184	2.391	2.450	
7.47	2.414	2.487	2.506	2.317	
7.62	2.373	2.444	2.599	—	
7.62	2.194	1.841	1.950	2.109	
7.77	2.339	2.512	2.493	2.328	
7.92	2.396	2.585	2.450	2.475	
8.08	2.462	2.578	2.493	2.450	
8.23	2.420	2.698	2.238	2.468	
8.38	2.450	2.585	2.512	2.592	
8.53	2.578	2.572	2.506	2.487	
All Points					
Mean	2.468	2.470	2.469	2.463	2.467
St Dev	0.142	0.170	0.123	0.112	0.137
No. Pts	40	40	40	38	158
Chauvenet's Criterion					
Tau	2.498	2.498	2.498	2.479	2.951
Lower Bound	2.113	2.045	2.162	2.185	2.063
Upper Bound	2.823	2.895	2.776	2.741	2.871
All Points within Lower and Upper Chauvenet's Criterion Bound					
Mean	2.458	2.498	2.482	2.465	2.478
St Dev	0.130	0.116	0.091	0.086	0.117
No. Pts	39	38	39	36	155

Table B3
Radial Sr-Wave Velocity Log for Boring WDH1 Core Samples

Depth (m)	Sr-Wave Velocity, km/s				All Orientations
	0 deg	45 deg	90 deg	135 deg	
1.52	2.492	2.660	2.667	2.511	
1.68	2.479	2.498	2.543	2.604	
1.83	2.675	2.590	2.498	2.604	
1.98	2.576	2.430	2.543	2.556	
2.13	2.366	2.498	2.563	2.485	
2.29	2.646	2.550	2.563	2.543	
2.44	2.590	2.081	2.625	2.660	
2.59	2.349	2.590	2.418	2.461	
2.74	2.682	2.625	2.597	2.675	
2.90	--	2.144	2.149	--	
3.05	2.563	2.570	2.543	2.689	
3.20	2.492	2.498	2.530	2.511	
3.35	2.604	2.473	2.570	2.537	
3.51	2.383	2.424	2.383	2.517	
3.66	2.772	2.639	2.436	2.524	
3.81	2.660	2.660	2.625	2.556	
3.96	2.543	2.576	2.590	2.556	
4.11	2.530	2.485	2.675	2.550	
4.27	2.530	2.611	2.632	2.625	
4.42	2.570	2.550	2.576	2.479	
5.49	2.412	2.467	2.424	2.485	
5.64	2.524	2.590	2.667	2.704	
5.79	2.524	2.556	2.383	2.563	
5.94	2.682	2.524	2.550	2.424	
6.10	2.383	2.372	2.430	2.332	
6.25	2.467	2.284	2.524	2.473	
6.71	2.782	2.592	2.713	2.647	
6.86	2.572	2.456	2.662	2.691	
7.01	2.334	2.481	2.538	2.519	
7.16	2.551	2.475	2.481	2.565	
7.32	2.456	2.323	2.373	2.525	
7.47	2.558	2.487	2.558	2.420	
7.62	2.532	2.519	2.605	2.538	
7.62	2.213	1.841	1.880	2.269	
7.77	2.444	2.538	2.585	2.373	
7.92	2.493	2.456	2.551	2.475	
8.08	2.532	2.605	2.512	2.538	
8.23	2.487	2.456	2.475	2.558	
8.38	2.456	2.592	2.572	2.683	
8.53	2.782	2.558	2.538	2.612	
All Points					
Mean	2.530	2.483	2.519	2.539	2.518
St Dev	0.124	0.161	0.147	0.097	0.135
No. Pts	39	40	40	39	158
Chauvenet's Criterion					
Tau	2.489	2.498	2.498	2.489	2.951
Lower Bound	2.221	2.081	2.152	2.298	2.120
Upper Bound	2.839	2.885	2.886	2.780	2.916
All Points within Lower and Upper Chauvenet's Criterion Bound					
Mean	2.539	2.511	2.545	2.547	2.529
St Dev	0.114	0.105	0.086	0.088	0.108
No. Pts	38	38	38	38	155

Table B4
Radial P-Wave Velocity Log for Boring WDH2 Core Samples

Depth (m)	P-Wave Velocity, km/s				All Orientations
	0 deg	45 deg	90 deg	135 deg	
0.00	3.893	3.795	3.299	3.504	
0.15	4.283	4.183	4.359	4.292	
0.30	4.349	4.264	4.292	4.398	
0.46	4.311	4.448	4.340	4.274	
0.61	4.448	4.369	4.201	4.448	
0.76	4.264	4.330	4.292	4.246	
0.91	4.292	4.165	4.246	4.388	
1.22	4.441	4.554	4.629	4.673	
1.37	4.492	4.267	4.441	4.352	
1.52	4.362	4.333	4.471	4.372	
1.68	4.564	4.249	4.391	4.343	
1.83	4.401	4.372	4.461	4.533	
1.98	4.461	4.401	4.564	4.391	
2.90	4.277	4.372	4.352	4.522	
3.05	4.382	4.372	4.401	4.554	
3.20	4.391	4.575	4.441	4.411	
3.35	4.421	4.441	4.471	4.451	
3.51	4.267	4.343	4.277	4.295	
3.66	4.391	4.492	4.286	4.543	
3.81	4.441	4.333	4.391	4.471	
3.96	4.515	4.434	4.676	4.643	
4.11	4.557	4.394	4.676	4.464	
4.27	4.374	4.394	4.557	4.444	
4.42	4.434	4.536	4.536	4.557	
4.57	4.317	4.144	4.414	4.346	
4.72	4.394	4.484	4.374	4.588	
4.88	4.317	4.515	4.434	4.578	
5.03	4.570	4.436	4.282	4.467	
5.18	4.348	4.310	4.377	4.477	
5.33	4.273	4.339	4.245	4.367	
5.49	4.348	4.426	4.397	4.417	
5.64	4.417	4.467	4.301	4.209	
5.79	4.436	4.487	4.320	4.367	
5.94	4.434	4.336	4.355	4.424	
6.10	4.289	4.279	4.567	4.414	
6.25	4.444	4.484	4.505	4.434	
6.40	4.578	4.374	4.632	4.444	
6.55	4.434	4.394	4.307	4.326	
6.71	4.546	4.599	4.424	4.643	
6.86	4.444	4.546	4.515	4.494	
All Points					
Mean	4.390	4.376	4.387	4.414	4.392
St Dev	0.120	0.144	0.214	0.183	0.168
No. Pts	40	40	40	40	160
Chauvenet's Criterion					
Tau	2.498	2.498	2.498	2.498	2.955
Lower Bound	4.090	4.016	3.852	3.957	3.896
Upper Bound	4.690	4.736	4.922	4.871	4.888
All Points within Lower and Upper Chauvenet's Criterion Bound					
Mean	4.403	4.391	4.415	4.437	4.412
St Dev	0.090	0.111	0.123	0.110	0.110
No. Pts	39	39	39	39	156

Table B5
Radial Sa-Wave Velocity Log for Boring WDH2 Core Samples

Depth (m)	Sa-Wave Velocity, km/s				All Orientations
	0 deg	45 deg	90 deg	135 deg	
0.00	2.039	1.722	--	1.986	
0.15	2.433	2.533	2.580	2.324	
0.30	2.566	2.520	2.357	2.392	
0.46	2.302	2.553	2.313	2.527	
0.61	2.520	2.489	2.514	2.433	
0.76	2.451	2.445	2.495	2.409	
0.91	2.369	2.369	2.318	2.335	
1.22	2.575	2.630	2.725	2.630	
1.37	2.575	2.497	2.405	2.435	
1.52	2.555	2.478	2.568	2.535	
1.68	2.595	2.453	2.471	2.459	
1.83	2.465	2.471	2.575	2.575	
1.98	2.602	2.503	2.555	2.609	
2.90	2.509	2.484	2.435	2.542	
3.05	2.490	2.542	2.516	2.575	
3.20	2.568	2.644	2.568	2.562	
3.35	2.522	2.548	2.687	2.453	
3.51	2.465	2.405	2.453	2.435	
3.66	2.497	2.478	2.497	2.680	
3.81	2.535	2.509	2.588	2.575	
3.96	2.401	2.448	2.543	2.550	
4.11	2.479	2.372	2.611	2.511	
4.27	2.479	2.618	2.524	2.355	
4.42	2.576	2.498	2.492	2.639	
4.57	2.473	2.461	2.406	2.455	
4.72	2.479	2.550	2.505	2.625	
4.88	2.473	2.772	2.556	2.349	
5.03	2.538	2.558	2.487	2.585	
5.18	2.468	2.432	2.414	2.456	
5.33	2.475	2.585	2.512	2.475	
5.49	2.444	2.619	2.438	2.538	
5.64	2.592	2.356	2.551	2.500	
5.79	2.345	2.585	2.414	2.462	
5.94	2.455	2.412	2.436	2.349	
6.10	2.383	2.448	2.632	2.530	
6.25	2.517	2.646	2.563	2.517	
6.40	2.667	2.563	2.590	2.556	
6.55	2.511	2.505	2.473	2.485	
6.71	2.604	2.576	2.583	2.604	
6.86	2.757	2.321	2.294	2.543	
All Points					
Mean	2.494	2.490	2.504	2.489	2.494
St Dev	0.113	0.154	0.097	0.122	0.122
No. Pts	40	40	39	40	159
Chauvenet's Criterion					
Tau	2.498	2.498	2.489	2.498	2.953
Lower Bound	2.212	2.105	2.263	2.184	2.134
Upper Bound	2.776	2.875	2.745	2.794	2.854
All Points within Lower and Upper Chauvenet's Criterion Bound					
Mean	2.505	2.510	2.504	2.502	2.505
St Dev	0.087	0.091	0.097	0.091	0.091
No. Pts	39	39	39	39	156

Table B6
Radial Sr-Wave Velocity Log for Boring WDH2 Core Samples

Depth (m)	Sr-Wave Velocity, km/s				All Orientations
	0 deg	45 deg	90 deg	135 deg	
0.00	1.935	--	1.752	2.146	
0.15	2.482	2.421	2.508	2.409	
0.30	2.547	2.520	2.476	2.433	
0.46	2.324	2.730	2.363	2.533	
0.61	2.560	2.533	2.587	2.560	
0.76	2.482	2.501	2.607	2.533	
0.91	2.520	2.482	2.445	2.560	
1.22	2.630	2.680	2.717	2.665	
1.37	2.644	2.465	2.441	2.535	
1.52	2.509	2.568	2.602	2.687	
1.68	2.644	2.484	2.529	2.497	
1.83	2.522	2.562	2.630	2.562	
1.98	2.630	2.658	2.651	2.623	
2.90	2.497	2.503	2.435	2.680	
3.05	2.459	2.555	2.509	2.673	
3.20	2.602	2.747	2.609	2.630	
3.35	2.548	2.623	2.702	2.548	
3.51	2.465	2.503	2.509	2.522	
3.66	2.658	2.602	2.568	2.717	
3.81	2.595	2.568	2.623	2.609	
3.96	2.467	2.537	2.625	2.597	
4.11	2.597	2.590	2.632	2.625	
4.27	2.653	2.697	2.583	2.543	
4.42	2.712	2.604	2.618	2.742	
4.57	2.550	2.383	2.583	2.524	
4.72	2.517	2.556	2.604	2.570	
4.88	2.492	2.625	2.570	2.498	
5.03	2.558	2.572	2.525	2.647	
5.18	2.506	2.481	2.532	2.493	
5.33	2.468	2.558	2.565	2.525	
5.49	2.506	2.626	2.512	2.532	
5.64	2.585	2.519	2.450	2.512	
5.79	2.551	2.592	2.551	2.512	
5.94	2.556	2.543	2.524	2.639	
6.10	2.442	2.543	2.632	2.550	
6.25	2.517	2.604	2.604	2.570	
6.40	2.682	2.576	2.675	2.590	
6.55	2.543	2.563	2.556	2.576	
6.71	2.697	2.742	2.611	2.689	
6.86	2.530	2.788	2.682	2.366	
All Points					
Mean	2.535	2.574	2.547	2.561	2.554
St Dev	0.125	0.088	0.151	0.105	0.12
No. Pts	40	39	40	40	159
Chauvenet's Criterion					
Tau	2.498	2.489	2.498	2.498	2.953
Lower Bound	2.223	2.355	2.17	2.299	2.2
Upper Bound	2.847	2.793	2.924	2.823	2.908
All Points within Lower and Upper Chauvenet's Criterion Bound					
Mean	2.55	2.574	2.568	2.571	2.566
St Dev	0.08	0.088	0.079	0.082	0.082
No. Pts	39	39	39	39	156

Table B7
Radial P-Wave Velocity Log for Boring WDH3 Core Samples

Depth (m)	P-Wave Velocity, km/s				All Orientations
	0 deg	45 deg	90 deg	135 deg	
1.98	4.670	4.692	4.561	4.604	
2.13	4.583	4.692	4.499	4.593	
2.29	4.292	4.448	4.302	4.349	
2.44	4.572	4.551	4.349	4.428	
2.59	4.737	4.572	4.438	4.418	
2.74	4.438	4.520	4.715	4.359	
2.90	4.302	4.246	4.468	4.359	
3.05	4.250	4.373	4.373	4.335	
3.20	4.422	4.442	4.364	4.383	
3.35	4.393	4.463	4.483	4.288	
3.51	4.344	4.556	4.316	4.269	
3.66	4.641	4.483	4.463	4.535	
3.81	4.483	4.413	4.524	4.545	
3.96	4.524	4.364	4.514	4.754	
4.11	4.493	4.422	4.503	4.577	
4.27	4.473	4.514	4.731	4.463	
4.42	4.288	4.535	4.453	4.473	
4.57	4.178	4.152	4.364	4.269	
4.72	4.493	4.403	4.577	4.473	
4.88	4.463	4.503	4.556	4.598	
5.03	4.545	4.620	4.545	4.493	
5.18	4.494	4.610	4.525	4.474	
5.33	4.365	4.424	4.394	4.326	
5.49	4.346	4.484	4.414	4.326	
5.64	4.621	4.546	4.588	4.643	
5.79	4.206	4.298	4.374	4.346	
5.94	4.298	4.384	4.197	4.384	
6.10	4.414	4.494	4.355	4.414	
6.25	4.188	4.197	4.355	4.261	
6.40	4.252	4.525	4.394	4.206	
6.55	4.355	4.317	4.075	4.384	
6.71	4.414	4.494	4.444	4.307	
6.86	4.414	4.317	4.444	4.444	
7.01	4.643	4.621	4.484	4.424	
7.16	4.444	4.336	4.505	4.355	
7.16	4.298	4.346	4.484	4.233	
7.32	4.317	4.424	4.414	4.326	
7.47	4.434	4.536	4.474	4.394	
7.62	4.484	4.557	4.424	4.494	
7.77	4.505	4.632	4.384	4.404	
7.92	4.505	4.454	4.588	4.365	
8.08	4.224	4.394	4.336	4.307	
All Points					
Mean	4.424	4.461	4.446	4.414	4.436
St Dev	0.138	0.124	0.120	0.120	0.126
No. Pts	42	42	42	42	168
Chauvenet's Criterion					
Tau	2.515	2.515	2.515	2.515	2.970
Lower Bound	4.077	4.149	4.144	4.112	4.062
Upper Bound	4.771	4.773	4.748	4.716	4.810
All Points within Lower and Upper Chauvenet's Criterion Bound					
Mean	4.424	4.461	4.455	4.406	4.436
St Dev	0.138	0.124	0.106	0.108	0.126
No. Pts	42	42	41	41	168

Table B8
Radial Sa-Wave Velocity Log for Boring WDH3 Core Samples

Depth (m)	Sa-Wave Velocity, km/s				All Orientations
	0 deg	45 deg	90 deg	135 deg	
1.98	2.635	2.533	2.495	2.514	
2.13	2.489	2.553	2.514	2.533	
2.29	2.363	2.219	2.335	2.421	
2.44	2.553	2.386	2.439	2.427	
2.59	2.657	2.607	2.421	2.369	
2.74	2.439	2.533	2.495	2.380	
2.90	2.189	2.335	2.501	2.214	
3.05	2.498	2.454	2.337	2.424	
3.20	2.504	2.485	2.485	2.543	
3.35	2.504	2.466	2.549	2.354	
3.51	2.448	2.610	2.442	2.448	
3.66	2.590	2.549	2.603	2.583	
3.81	2.610	2.388	2.479	2.498	
3.96	2.576	2.442	2.523	2.811	
4.11	2.485	2.530	2.624	2.603	
4.27	2.549	2.460	2.617	2.530	
4.42	2.377	2.530	2.543	2.543	
4.57	2.659	2.448	2.549	2.430	
4.72	2.510	2.460	2.583	2.596	
4.88	2.485	2.498	2.510	2.583	
5.03	2.645	2.681	2.583	2.569	
5.18	2.583	2.537	2.590	2.556	
5.33	2.667	2.485	2.424	2.537	
5.49	2.524	2.570	2.563	2.448	
5.64	2.604	2.653	2.689	2.667	
5.79	2.355	2.412	2.473	2.424	
5.94	2.360	2.406	2.406	2.436	
6.10	2.455	2.284	2.461	2.505	
6.25	2.653	2.389	2.461	2.436	
6.40	2.294	2.537	2.537	2.511	
6.55	2.294	2.401	2.537	2.430	
6.71	2.550	2.511	2.424	2.436	
6.86	2.412	2.524	2.550	2.639	
7.01	2.524	2.576	2.289	2.395	
7.16	2.448	2.517	2.550	2.467	
7.16	2.412	2.305	2.349	2.563	
7.32	2.604	2.689	2.550	2.524	
7.47	2.566	2.570	2.498	2.537	
7.62	2.418	2.570	2.343	2.424	
7.77	2.537	2.537	2.530	2.576	
7.92	2.550	2.597	2.583	2.563	
8.08	2.389	2.517	2.479	2.418	
All Points					
Mean	2.499	2.494	2.498	2.497	2.497
St Dev	0.112	0.102	0.087	0.101	0.100
No. Pts	42	42	42	42	168
Chauvenet's Criterion					
Tau	2.515	2.515	2.515	2.515	2.970
Lower Bound	2.217	2.237	2.279	2.243	2.200
Upper Bound	2.781	2.751	2.717	2.751	2.794
All Points within Lower and Upper Chauvenet's Criterion Bound					
Mean	2.507	2.501	2.498	2.496	2.497
St Dev	0.102	0.093	0.087	0.078	0.095
No. Pts	41	41	42	40	166

Table B9
Radial Sr-Wave Velocity Log for Boring WDH3 Core Samples

Depth	Sr-Wave Velocity, km/s				All
(m)	0 deg	45 deg	90 deg	135 deg	Orientations
1.98	2.657	2.527	2.520	2.635	
2.13	2.614	2.657	2.553	2.540	
2.29	2.476	2.501	2.508	2.495	
2.44	2.594	2.464	2.489	2.527	
2.59	2.664	2.642	2.464	2.464	
2.74	2.573	2.540	2.580	2.540	
2.90	2.398	2.421	2.560	2.501	
3.05	2.491	2.510	2.536	2.498	
3.20	2.617	2.448	2.562	2.562	
3.35	2.530	2.479	2.576	2.460	
3.51	2.510	2.689	2.576	2.517	
3.66	2.645	2.603	2.645	2.674	
3.81	2.674	2.596	2.576	2.510	
3.96	2.696	2.498	2.631	2.852	
4.11	2.523	2.562	2.652	2.681	
4.27	2.596	2.610	2.667	2.576	
4.42	2.498	2.583	2.466	2.549	
4.57	2.536	2.562	2.652	2.400	
4.72	2.517	2.510	2.718	2.659	
4.88	2.562	2.631	2.562	2.638	
5.03	2.674	2.764	2.631	2.624	
5.18	2.646	2.625	2.485	2.576	
5.33	2.667	2.530	2.543	2.537	
5.49	2.517	2.576	2.570	2.492	
5.64	2.667	2.667	2.682	2.719	
5.79	2.485	2.543	2.570	2.473	
5.94	2.517	2.550	2.412	2.467	
6.10	2.550	2.505	2.734	2.563	
6.25	2.389	2.406	2.492	2.492	
6.40	2.442	2.675	2.511	2.597	
6.55	2.511	2.479	2.401	2.576	
6.71	2.505	2.618	2.418	2.448	
6.86	2.590	2.550	2.689	2.590	
7.01	2.667	2.653	2.498	2.543	
7.16	2.550	2.570	2.570	2.604	
7.16	2.038	2.237	2.537	2.505	
7.32	2.530	2.653	2.604	2.550	
7.47	2.682	2.632	2.556	2.537	
7.62	2.583	2.675	2.537	2.604	
7.77	2.646	2.646	2.556	2.653	
7.92	2.604	2.556	2.639	2.511	
8.08	2.406	2.611	2.442	2.436	
All Points					
Mean	2.553	2.566	2.561	2.557	2.559
St Dev	0.116	0.094	0.081	0.086	0.094
No. Pts	42	42	42	42	168
Chauvenet's Criterion					
Tau	2.515	2.515	2.515	2.515	2.97
Lower Bound	2.261	2.33	2.357	2.341	2.28
Upper Bound	2.845	2.802	2.765	2.773	2.838
All Points within Lower and Upper Chauvenet's Criterion Bound					
Mean	2.566	2.574	2.561	2.549	2.562
St Dev	0.083	0.079	0.081	0.073	0.079
No. Pts	41	41	42	41	165

Table B10
Radial P-Wave Velocity Log for Boring WDH4 Core Samples

Depth (m)	P-Wave Velocity, km/s				All Orientations
	0 deg	45 deg	90 deg	135 deg	
1.07	4.037	3.988	3.940	3.825	
1.22	4.227	4.060	4.146	4.245	
1.37	4.338	4.190	4.043	4.310	
1.52	4.211	4.333	4.352	4.257	
1.68	4.219	4.228	4.255	4.255	
1.83	4.249	4.461	4.314	4.133	
1.98	4.554	4.401	4.575	4.295	
2.13	4.752	4.684	4.857	4.729	
2.29	4.267	4.277	4.324	4.212	
2.44	4.249	4.177	4.267	4.258	
2.59	4.372	4.362	4.372	4.295	
2.74	4.471	4.333	4.249	4.277	
2.90	4.391	4.324	4.343	4.502	
3.05	4.333	4.286	4.295	4.352	
3.20	4.646	4.701	4.560	4.446	
3.35	4.467	4.657	4.679	4.602	
3.51	4.701	4.570	4.679	4.602	
3.66	4.735	4.560	4.613	4.668	
3.81	4.549	4.539	4.679	4.804	
3.96	4.456	4.668	4.679	4.735	
4.11	4.497	4.387	4.592	4.436	
4.27	4.928	4.903	4.761	4.855	
4.42	4.831	4.738	4.761	4.693	
4.57	4.749	4.563	4.439	4.390	
4.72	4.595	4.459	4.439	4.500	
4.88	4.584	4.649	4.682	4.693	
5.03	4.380	4.371	4.380	4.167	
5.18	4.380	4.371	4.322	4.400	
5.33	4.355	4.424	4.215	3.883	
5.49	4.454	4.424	4.346	4.307	
5.64	4.536	4.424	4.414	4.424	
5.79	4.766	4.298	4.326	4.505	
5.94	4.567	4.525	4.346	4.665	
6.10	4.434	4.444	4.567	4.424	
6.25	4.434	4.610	4.424	4.546	
6.40	4.347	4.386	4.386	4.318	
6.55	4.367	4.367	4.386	4.465	
6.71	4.396	4.300	4.357	4.357	
6.86	4.300	4.590	4.569	4.465	
7.01	4.262	4.019	4.272	4.645	
7.16	4.300	4.281	4.309	4.235	
7.32	4.137	4.290	4.208	4.496	
All Points					
Mean	4.448	4.420	4.422	4.421	4.428
St Dev	0.199	0.196	0.201	0.223	0.203
No. Pts	42	42	42	42	168
Chauvenet's Criterion					
Tau	2.515	2.515	2.515	2.515	2.970
Lower Bound	3.948	3.927	3.916	3.860	3.825
Upper Bound	4.948	4.913	4.928	4.982	5.031
All Points within Lower and Upper Chauvenet's Criterion Bound					
Mean	4.448	4.420	4.422	4.435	4.431
St Dev	0.199	0.196	0.201	0.205	0.199
No. Pts	42	42	42	41	167

Table B11
Radial Sa-Wave Velocity Log for Boring WDH4 Core Samples

Depth (m)	Sa-Wave Velocity, km/s				All Orientations
	0 deg	45 deg	90 deg	135 deg	
1.07	2.255	2.303	2.133	2.147	
1.22	2.369	2.244	2.416	2.265	
1.37	2.397	2.560	2.397	2.553	
1.52	2.388	2.454	2.442	2.331	
1.68	2.433	2.594	2.482	2.482	
1.83	2.447	2.616	2.503	2.509	
1.98	2.568	2.516	2.665	2.387	
2.13	2.637	2.582	2.595	2.568	
2.29	2.336	2.370	2.459	2.241	
2.44	2.423	2.325	2.325	2.314	
2.59	2.465	2.435	2.535	2.336	
2.74	2.503	2.325	2.376	2.459	
2.90	2.447	2.435	2.453	2.602	
3.05	2.478	2.453	2.484	2.503	
3.20	2.512	2.592	2.585	2.572	
3.35	2.599	2.592	2.565	2.408	
3.51	2.612	2.506	2.551	2.558	
3.66	2.605	2.585	2.572	2.605	
3.81	2.558	2.538	2.640	2.669	
3.96	2.301	2.599	2.647	2.605	
4.11	2.592	2.481	2.468	2.373	
4.27	2.708	2.678	2.587	2.566	
4.42	2.664	2.715	2.693	2.520	
4.57	2.152	2.527	2.003	2.250	
4.72	2.520	2.409	2.547	2.594	
4.88	2.600	2.553	2.501	2.635	
5.03	2.628	2.230	2.281	2.220	
5.18	2.392	2.416	2.352	2.514	
5.33	2.289	2.383	2.461	2.257	
5.49	2.406	2.377	2.505	2.372	
5.64	2.563	2.430	2.424	2.461	
5.79	2.473	2.300	2.366	2.294	
5.94	2.704	2.550	2.667	2.576	
6.10	2.343	2.461	2.436	2.498	
6.25	2.625	2.590	2.401	2.550	
6.40	2.493	2.344	2.431	2.431	
6.55	2.525	2.499	2.538	2.425	
6.71	2.402	2.474	2.462	2.361	
6.86	2.551	2.518	2.544	2.640	
7.01	2.505	2.344	2.544	2.449	
7.16	2.449	2.474	2.493	2.344	
7.32	2.578	2.480	2.419	2.551	
All Points					
Mean	2.488	2.473	2.475	2.452	2.472
St Dev	0.125	0.115	0.133	0.134	0.126
No. Pts	42	42	42	42	168
Chauvenet's Criterion					
Tau	2.515	2.515	2.515	2.515	2.970
Lower Bound	2.174	2.184	2.141	2.115	2.098
Upper Bound	2.802	2.762	2.809	2.789	2.846
All Points within Lower and Upper Chauvenet's Criterion Bound					
Mean	2.496	2.473	2.495	2.452	2.475
St Dev	0.114	0.115	0.098	0.134	0.121
No. Pts	41	42	40	42	167

Table B12
Radial Sr-Wave Velocity Log for Boring WDH4 Core Samples

Depth (m)	Sr-Wave Velocity, km/s				All Orientations
	0 deg	45 deg	90 deg	135 deg	
1.07	2.370	2.405	2.364	2.341	
1.22	2.477	2.335	2.471	2.387	
1.37	2.368	2.409	2.403	2.469	
1.52	2.485	2.583	2.491	2.418	
1.68	2.527	2.514	2.445	2.458	
1.83	2.471	2.609	2.582	2.497	
1.98	2.637	2.548	2.673	2.509	
2.13	2.755	2.630	2.732	2.725	
2.29	2.429	2.459	2.429	2.376	
2.44	2.529	2.478	2.370	2.393	
2.59	2.548	2.568	2.516	2.535	
2.74	2.609	2.393	2.447	2.582	
2.90	2.542	2.382	2.568	2.644	
3.05	2.509	2.478	2.484	2.529	
3.20	2.487	2.626	2.592	2.633	
3.35	2.619	2.605	2.487	2.512	
3.51	2.626	2.551	2.640	2.669	
3.66	2.691	2.683	2.759	2.683	
3.81	2.647	2.683	2.662	2.855	
3.96	2.519	2.728	2.647	2.751	
4.11	2.619	2.558	2.605	2.538	
4.27	2.628	2.715	2.649	2.607	
4.42	2.685	2.768	2.642	2.547	
4.57	2.292	2.324	2.250	2.489	
4.72	2.580	2.547	2.587	2.580	
4.88	2.600	2.737	2.614	2.715	
5.03	2.427	2.324	2.308	2.386	
5.18	2.573	2.489	2.427	2.501	
5.33	2.461	2.103	2.467	2.418	
5.49	2.524	2.505	2.524	2.461	
5.64	2.524	2.436	2.524	2.485	
5.79	2.682	2.094	2.467	2.436	
5.94	2.550	2.653	2.485	2.618	
6.10	2.418	2.597	2.505	2.543	
6.25	2.646	2.604	2.530	2.550	
6.40	2.612	2.487	2.512	2.544	
6.55	2.493	2.487	2.584	2.512	
6.71	2.474	2.558	2.564	2.413	
6.86	2.612	2.551	2.661	2.647	
7.01	2.468	2.367	2.551	2.525	
7.16	2.558	2.598	2.437	2.493	
7.32	2.449	2.480	2.402	2.690	
All Points					
Mean	2.541	2.515	2.525	2.540	2.530
St Dev	0.098	0.148	0.111	0.114	0.119
No. Pts	42.000	42	42	42	168
Chauvenet's Criterion					
Tau	2.515	2.515	2.515	2.515	2.970
Lower Bound	2.295	2.143	2.246	2.253	2.177
Upper Bound	2.787	2.887	2.804	2.827	2.883
All Points within Lower and Upper Chauvenet's Criterion Bound					
Mean	2.547	2.536	2.525	2.532	2.536
St Dev	0.091	0.117	0.111	0.104	0.109
No. Pts	41.000	40	42	41	166

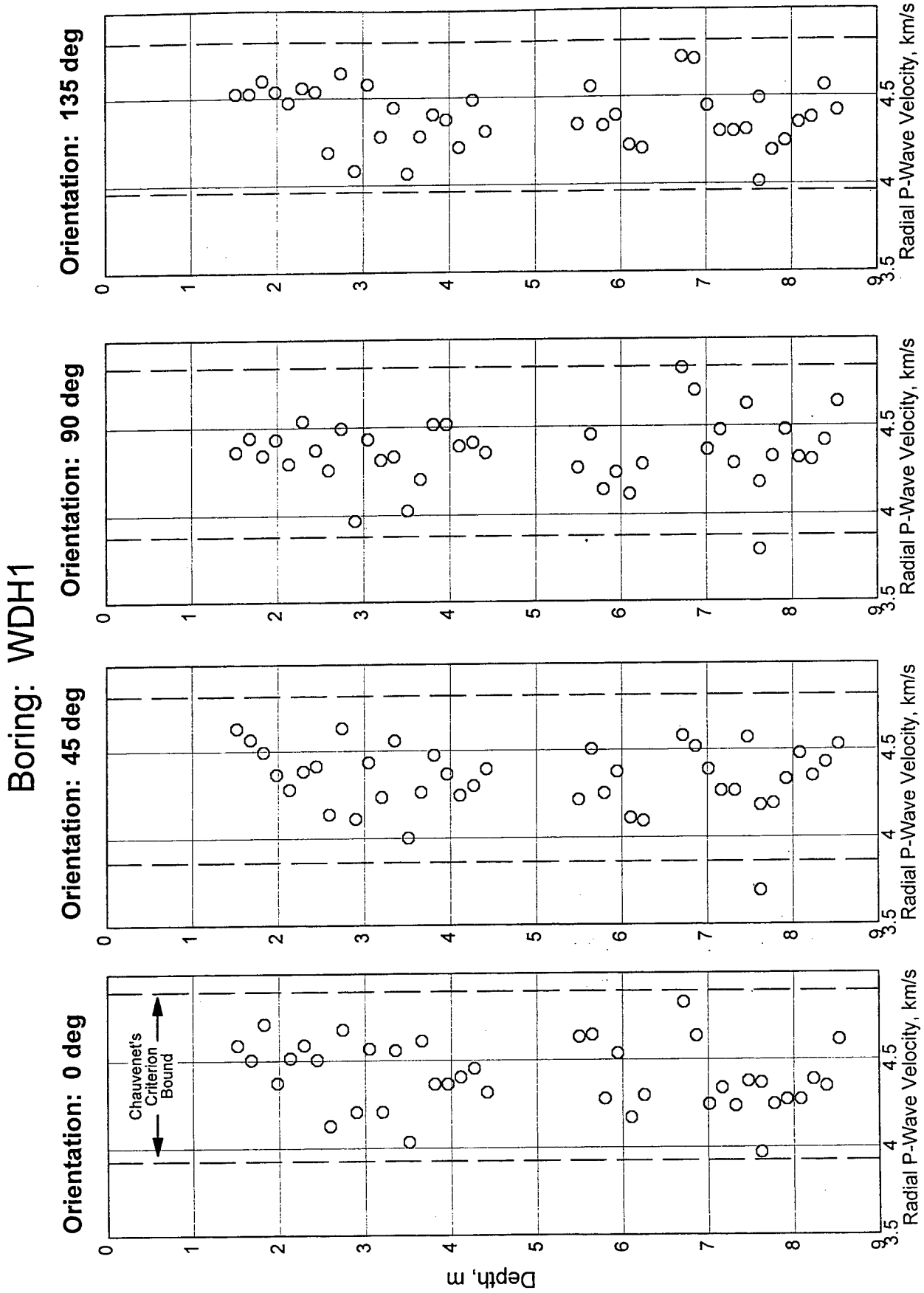
Boring: WDH1
Orientation: 0 deg
Orientation: 45 deg
Orientation: 90 deg
Orientation: 135 deg
Chauvenet's Criterion Bound
Depth, m
Radial P-Wave Velocity, km/s
0
1
2
3
4
5
6
7
8
9
3.5
4
4.5

Boring: WDH1

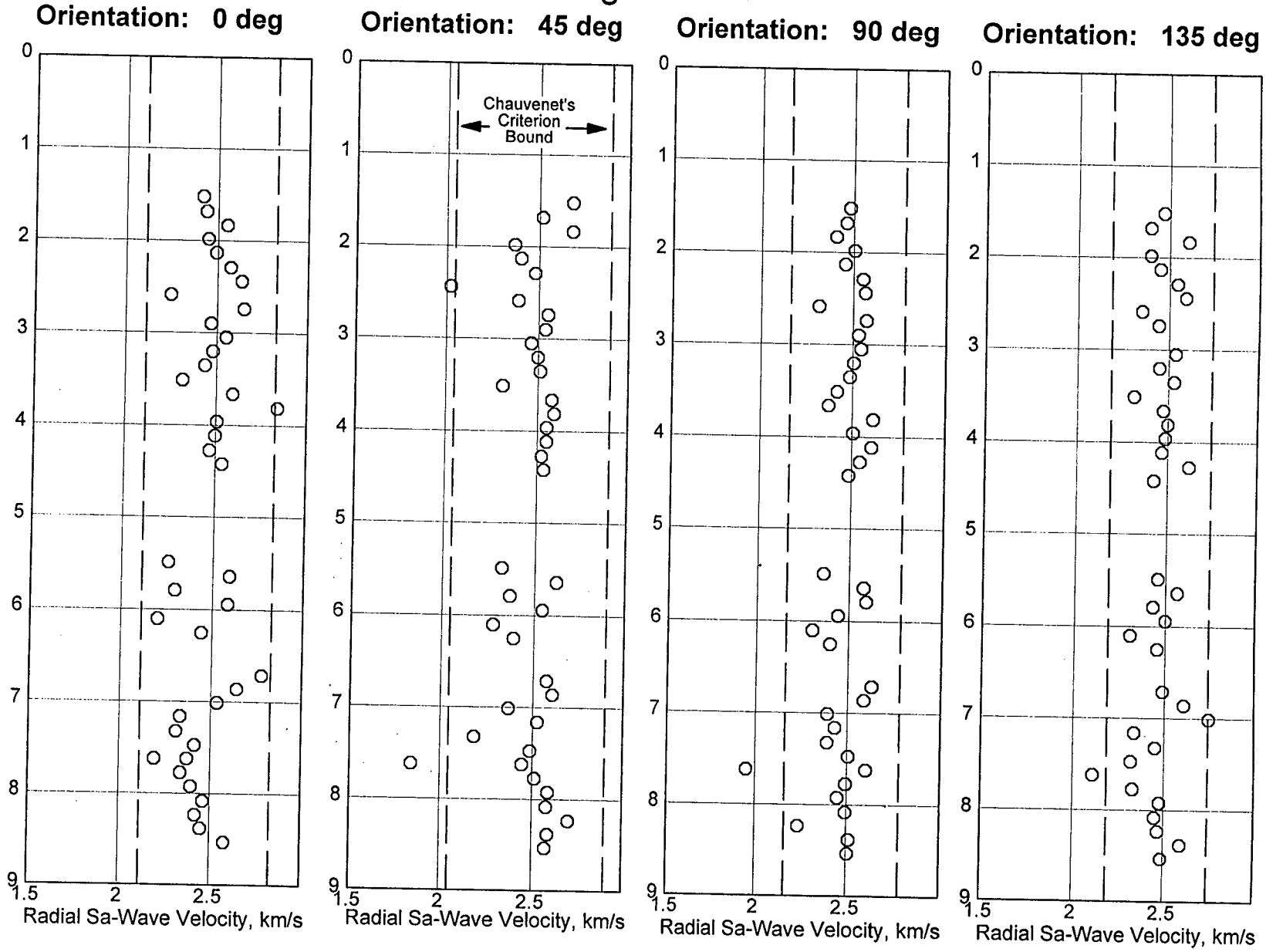
Orientation: 0 deg
Orientation: 45 deg
Orientation: 90 deg
Orientation: 135 deg
Chauvenet's Criterion Bound
Depth, m
0
1
2
3
4
5
6
7
8
9
1.5
2
2.5
Radial Sa-Wave Velocity, km/s

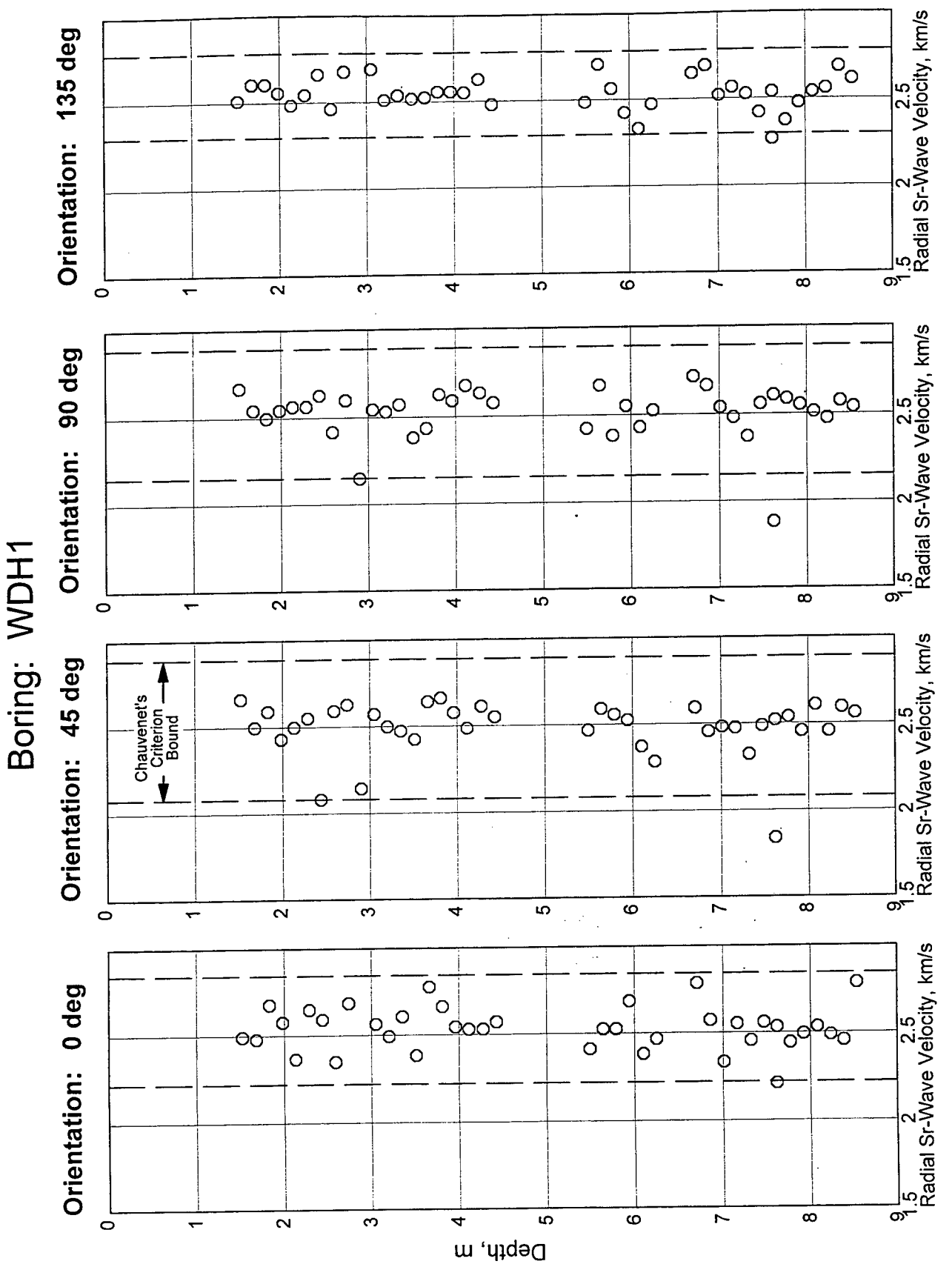
Boring: WDH1
Orientation: 0 deg
Orientation: 45 deg
Orientation: 90 deg
Orientation: 135 deg
Chauvenet's Criterion Bound
Depth, m
Radial Sr-Wave Velocity, km/s
0
1
2
3
4
5
6
7
8
9
1.5
2
2.5

Boring: WDH2

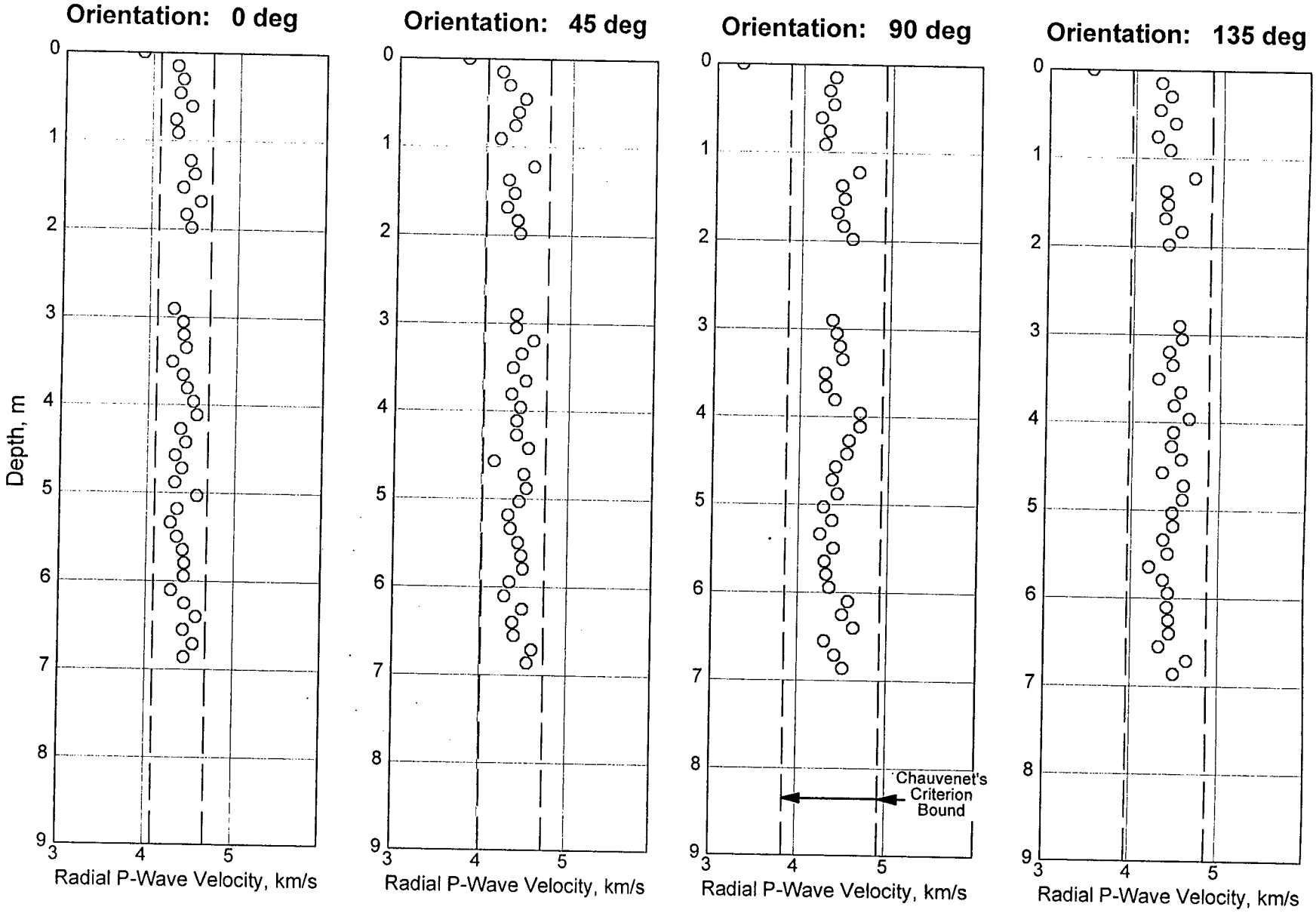
Orientation: 0 deg
Orientation: 45 deg
Orientation: 90 deg
Orientation: 135 deg
Depth, m
0
1
2
3
4
5
6
7
8
9
3
4
5
Radial P-Wave Velocity, km/s
Chauvenet's Criterion Bound

Boring: WDH2

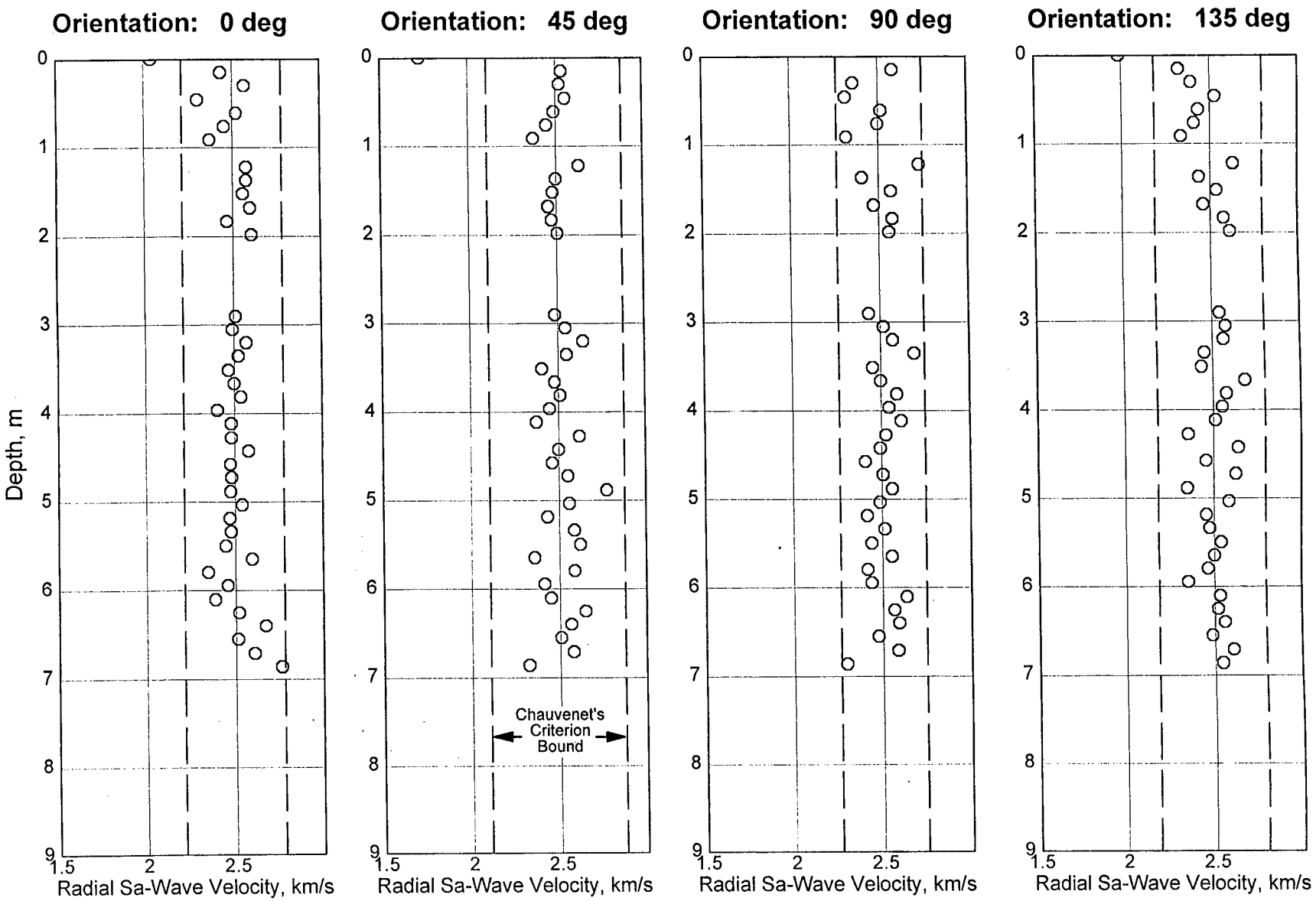
Orientation: 0 deg
Orientation: 45 deg
Orientation: 90 deg
Orientation: 135 deg
Depth, m
0
1
2
3
4
5
6
7
8
9
1.5
2
2.5
Radial Sa-Wave Velocity, km/s
Chauvenet's Criterion Bound

Boring: WDH2

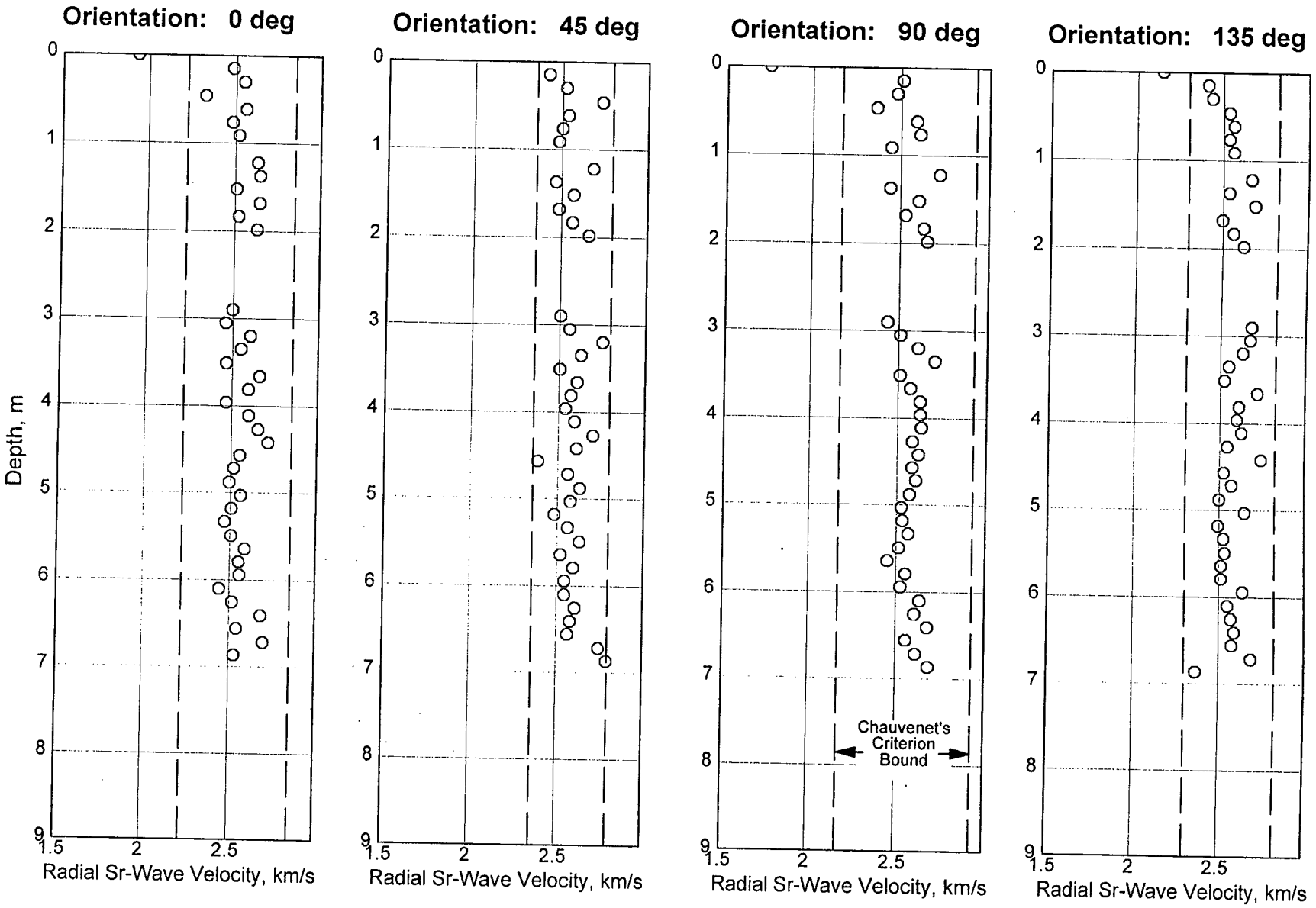
Orientation: 0 deg
Orientation: 45 deg
Orientation: 90 deg
Orientation: 135 deg
Depth, m
0
1
2
3
4
5
6
7
8
9
1.5
2
2.5
Radial Sr-Wave Velocity, km/s
Chauvenet's Criterion Bound

Boring: WDH3

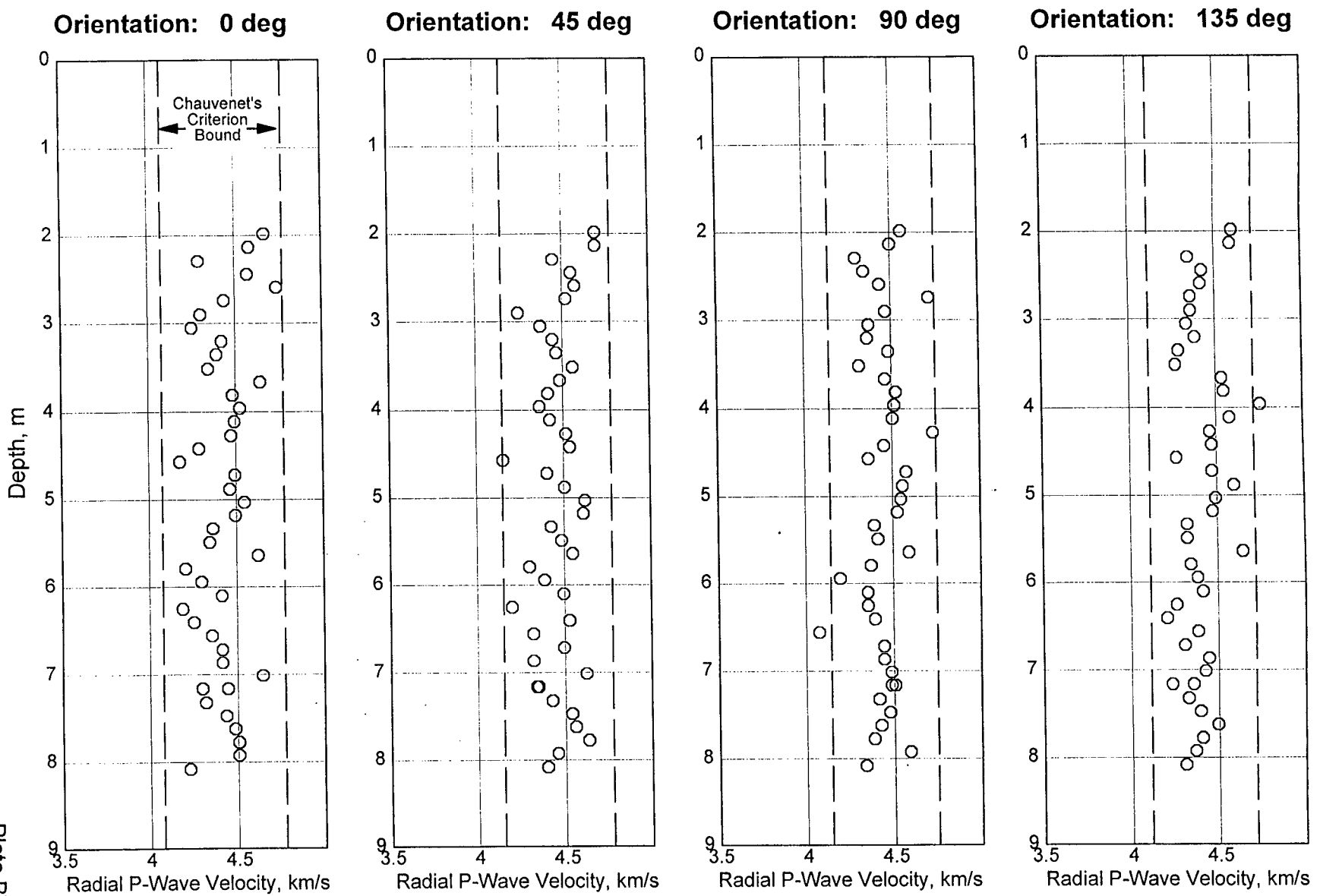
Orientation: 0 deg
Orientation: 45 deg
Orientation: 90 deg
Orientation: 135 deg
Chauvenet's Criterion Bound
Depth, m
0
1
2
3
4
5
6
7
8
9
3.5
4
4.5
Radial P-Wave Velocity, km/s

Boring: WDH3

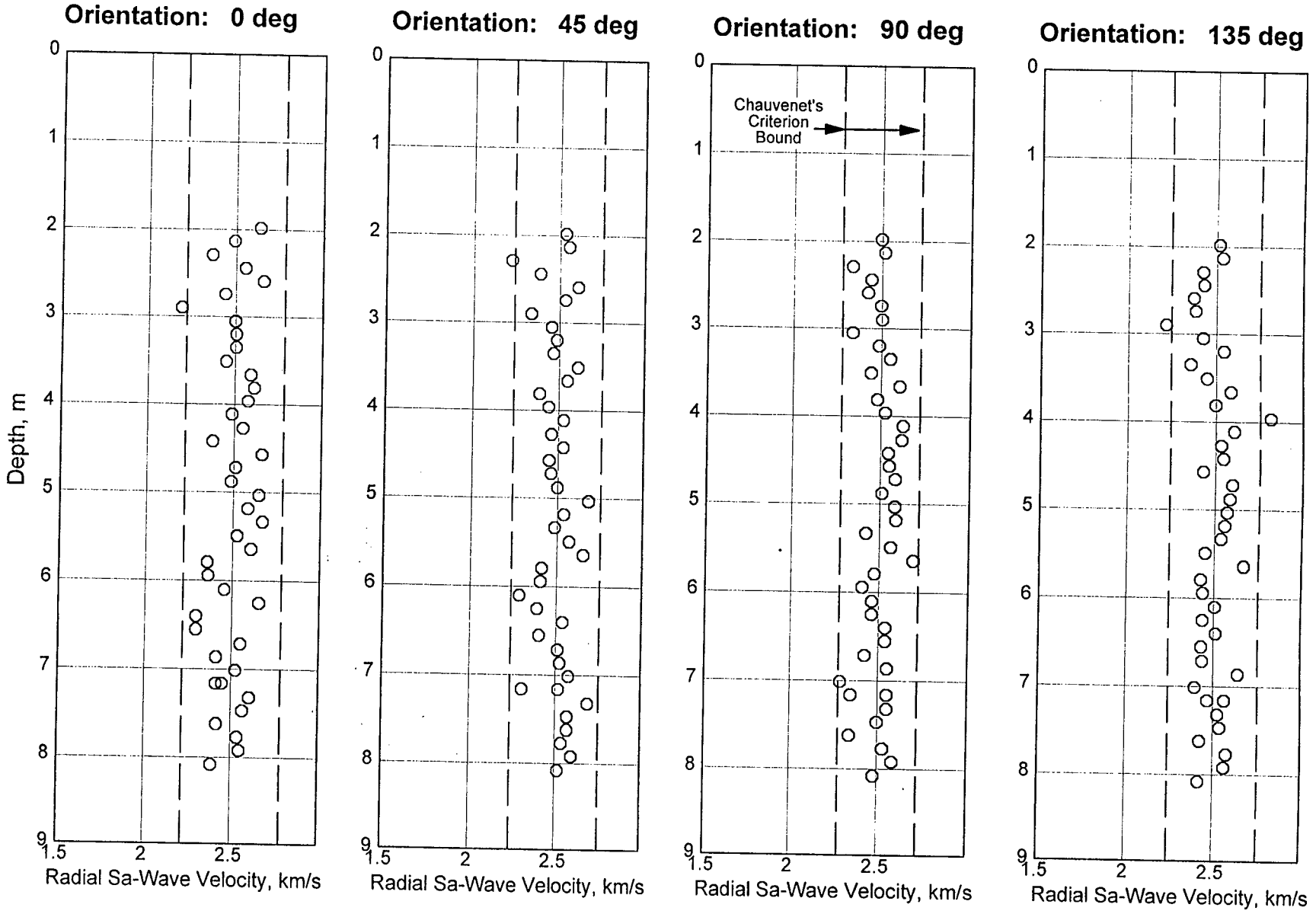
Orientation: 0 deg
Orientation: 45 deg
Orientation: 90 deg
Orientation: 135 deg
Chauvenet's Criterion Bound
Depth, m
0
1
2
3
4
5
6
7
8
9
1.5
2
2.5
Radial Sa-Wave Velocity, km/s

Boring: WDH3

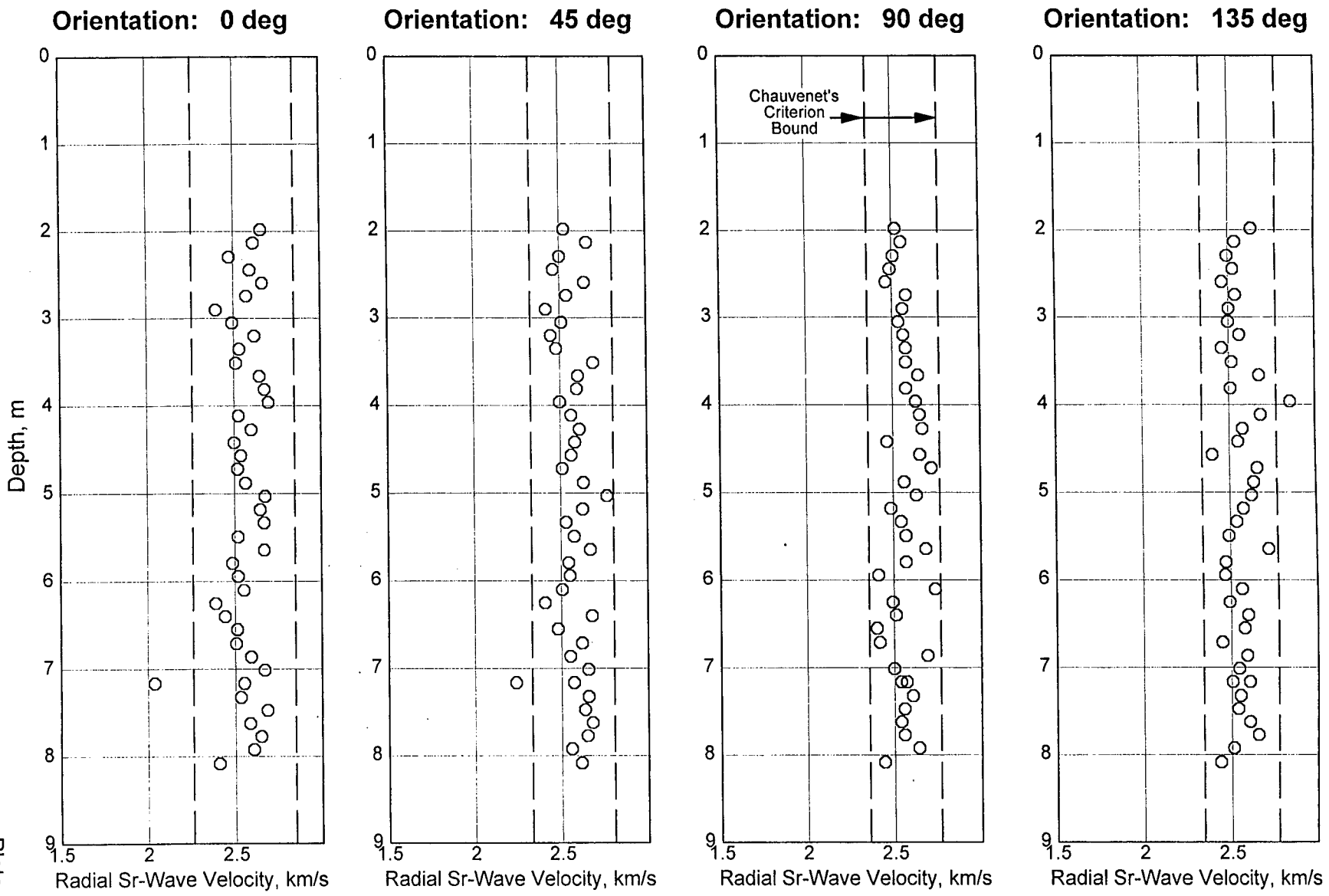
Orientation: 0 deg
Orientation: 45 deg
Orientation: 90 deg
Orientation: 135 deg
Chauvenet's Criterion Bound
Depth, m
0
1
2
3
4
5
6
7
8
9
1.5
2
2.5
Radial Sr-Wave Velocity, km/s

Boring: WDH4

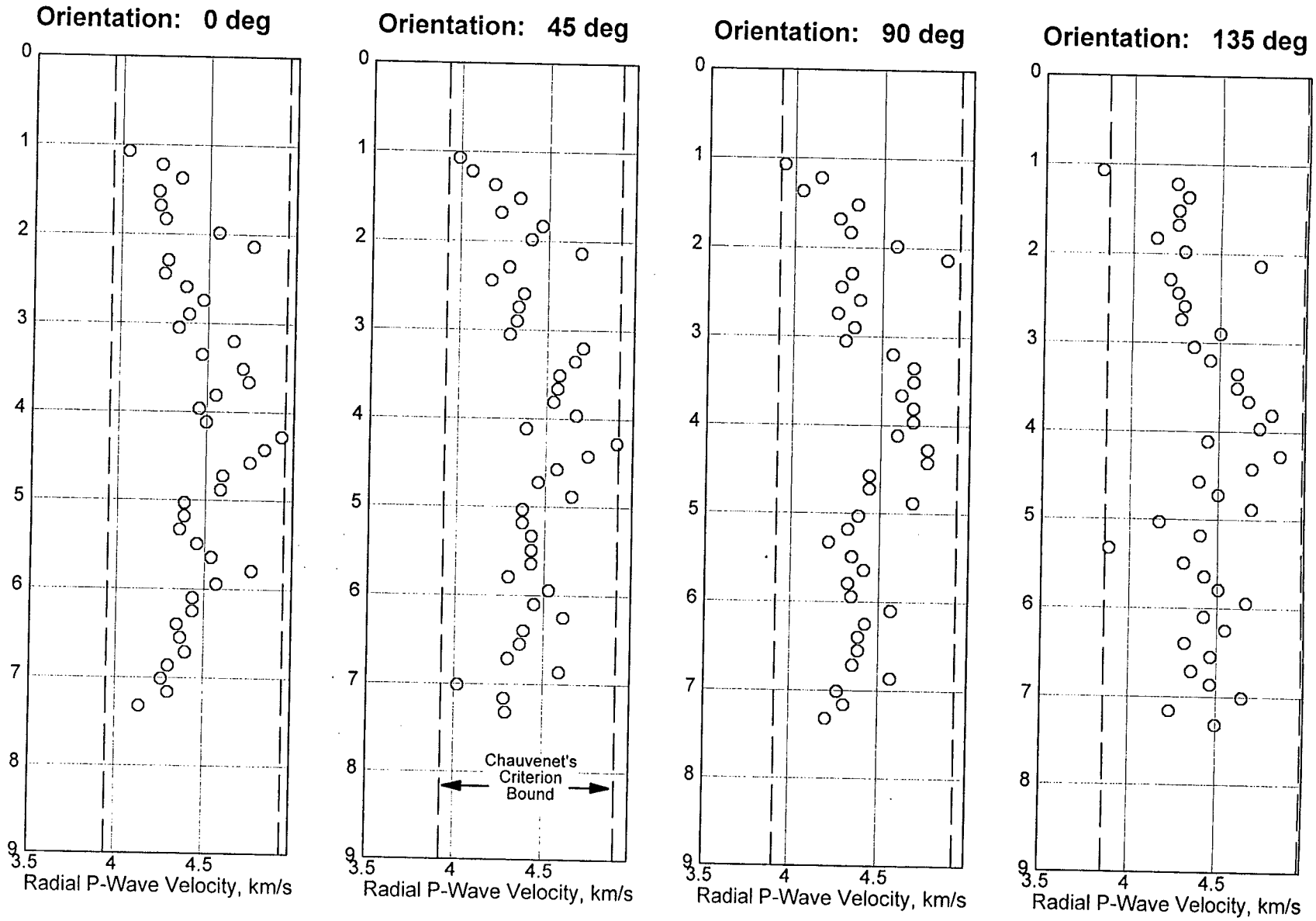
Orientation: 0 deg
Orientation: 45 deg
Orientation: 90 deg
Orientation: 135 deg
Depth, m
0
1
2
3
4
5
6
7
8
9
3.5
4
4.5
Radial P-Wave Velocity, km/s
Chauvenet's Criterion Bound

Boring: WDH4

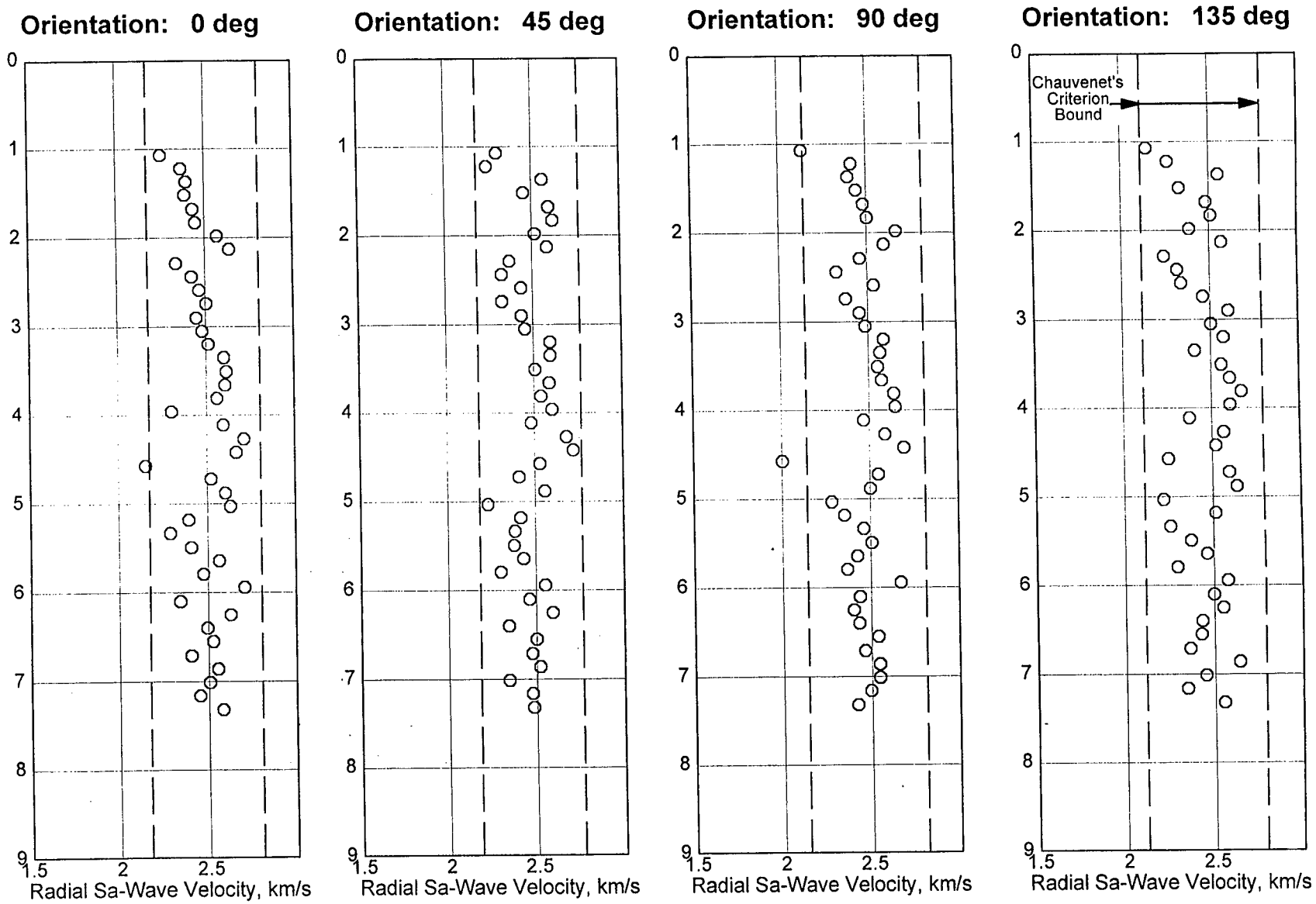
Orientation: 0 deg
Orientation: 45 deg
Orientation: 90 deg
Orientation: 135 deg
Chauvenet's Criterion Bound
Depth, m
0
1
2
3
4
5
6
7
8
9
1.5
2
2.5
Radial Sa-Wave Velocity, km/s

Boring: WDH4

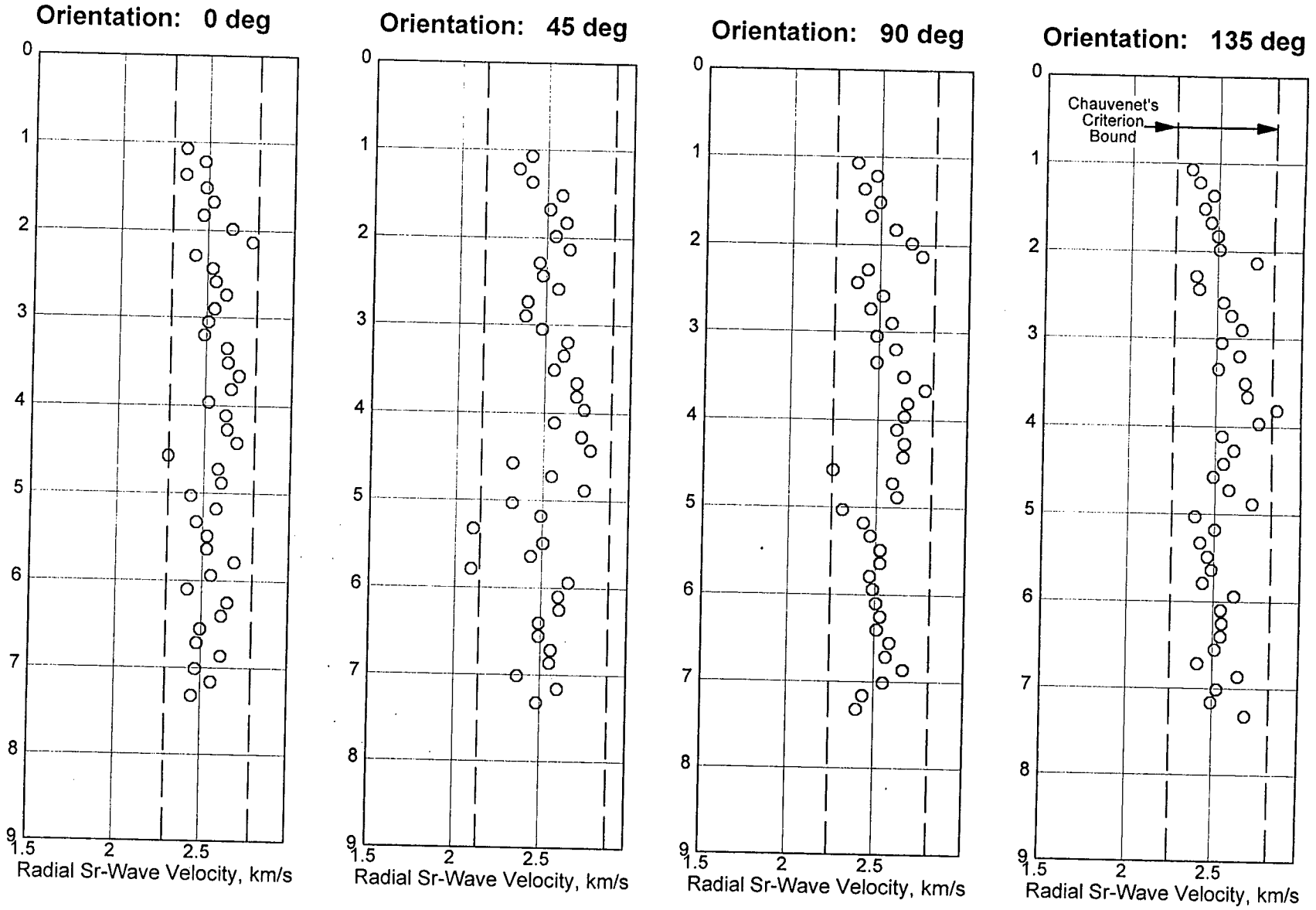
Orientation: 0 deg
Orientation: 45 deg
Orientation: 90 deg
Orientation: 135 deg
Chauvenet's Criterion Bound
Depth, m
0
1
2
3
4
5
6
7
8
9
1.5
2
2.5
Radial Sr-Wave Velocity, km/s

REPORT DOCUMENTATION PAGE

Form Approved
OMB No. 0704-0188

1.AGENCY USE ONLY *(Leave blank)*

2.REPORT DATE
May 1998

3.REPORT TYPE AND DATES COVERED
Report 1 of a series

4.TITLE AND SUBTITLE
Roller-Compacted Concrete (RCC) Dams; Report 1, Laboratory Characterization of RCC Cores from Elk Creek Dam, Trail, Oregon

5.FUNDING NUMBERS

6.AUTHOR(S)
Mark L. Green, Billy D. Neeley, Paul A. Reed, Clayton T. Amundson

7.PERFORMING ORGANIZATION NAME(S) AND ADDRESS(ES)
U.S. Army Engineer Waterways Experiment Station
3909 Halls Ferry Road, Vicksburg, MS 39180-6199
U.S. Army Engineer District, Portland, Geotechnical Engineering Branch,
333 SW-First Avenue, Portland, OR 97208-2946

8.PERFORMING ORGANIZATION REPORT NUMBER
Technical Report SL-98-4

9.SPONSORING/MONITORING AGENCY NAME(S) AND ADDRESS(ES)
U.S. Army Corps of Engineers
Washington, DC 20314-1000

10.SPONSORING/MONITORING AGENCY REPORT NUMBER

11.SUPPLEMENTARY NOTES
Available from National Technical Information Service, 5285 Port Royal Road, Springfield, VA 22161.

12a.DISTRIBUTION/AVAILABILITY STATEMENT
Approved for public release; distribution is unlimited.

12b.DISTRIBUTION CODE

13.ABSTRACT *(Maximum 200 words)*

This report documents the results from a laboratory mechanical property investigation of large-diameter, roller-compacted concrete (RCC) core samples obtained from the main Elk Creek Dam, Trail, Oregon. The test matrix included 10 unconfined compression tests, 13 unconfined tension (direct pull) tests, 8 triaxial compression tests, 16 direct shear tests, and 7 splitting tensile strength tests. Eight of the direct shear tests and six of the unconfined tension tests were performed for the purpose of characterizing the strength properties of the interfaces between the RCC lifts. All tests were performed quasi-statically on air-dry specimens of the RCC. In addition, an extensive suite of nondestructive pulse velocity tests were performed on the cores to assess the degree of anisotropy in the RCC. This included numerous P-(compression), Sa-(shear waves vibrating in the axial plane), and Sr-(shear waves vibrating in a radial or cross-axis plane) wave speed determinations measured radially through the core with propagation directions oriented 0, 45, 90, and 135 deg from the right-abutment side of the dam core. Axial P- and Sa-wave velocities were determined for each mechanical property test specimen prior to being mechanically deformed.

14.SUBJECT TERMS
Direct shear
Mechanical property tests
Roller-compacted concrete
Splitting tensile strength
Triaxial compression
Ultrasonic wave velocity
Unconfined compression
Unconfined tension

15.NUMBER OF PAGES
148

16.PRICE CODE

17.SECURITY CLASSIFICATION OF REPORT	18.SECURITY CLASSIFICATION OF THIS PAGE	19.SECURITY CLASSIFICATION OF ABSTRACT	20.LIMITATION OF ABSTRACT
UNCLASSIFIED	UNCLASSIFIED		